CONCRETE CARBONATION PREDICTION FOR VARYING ENVIRONMENTAL EXPOSURE CONDITIONS

Rakesh Gopinath

Thesis presented in fulfilment of the requirements for the degree of

DOCTOR OF PHILOSOPHY

Faculty of Engineering and the Built Environment
Department of Civil Engineering
UNIVERSITY OF CAPE TOWN

February 2020

CAPE TOWN

DECLARATION

I, Rakesh Gopinath, hereby declare that the work on which this thesis is based is my original work (except where acknowledgements indicate otherwise) and that neither the whole work nor any part of it has been, is being, or is to be submitted for another degree in this or any other university. I authorise the University to reproduce for the purpose of research either the whole or any portion of the contents in any manner whatsoever.

Signed by candidate

Signature: Date: **09 February 2020**

Rakesh Gopinath

ABSTRACT

The Durability Index (DI) approach has been developed in South Africa, in order to improve the durability performance of reinforced concrete structures. The DI approach is based on durability index tests, which are linked to transport mechanisms related to particular deterioration processes (Alexander et al., 1999a). Carbonation of concrete is governed, inter alia, by the microstructure and the transport characteristics of the concrete. A carbonation model with permeability coefficient (k) from the Oxygen Permeability Index (OPI) test as the key material variable was developed by Salvoldi (2010) using accelerated carbonation test data. The main aim of this research is to further develop the carbonation model by adopting the modelling framework of Salvoldi (2010) using natural carbonation data.

For the experimental work, a total 48 different concrete mixes were produced by with different water:binder ratios (w/b), cement types, cement extender (addition) type and curing regime. The OPI test was conducted on all the concretes, and their corresponding permeability coefficients were determined. A set of 48 concrete specimens were exposed to five different sites for natural carbonation, and carbonation depths were measured periodically. Based on the modelling framework of Salvoldi (2010) and using the natural carbonation data between 150-850 days, a model predicting the depth of natural carbonation was developed. However, in the case of concrete exposed to rain, drying/wetting is a major factor influencing the rate of carbonation. Therefore, the carbonation model was further modified taking into account the influence of drying/wetting cycles, by coupling it with a moisture model. For the development of the moisture model, the concrete specimens were exposed to a laboratory environment maintained at constant temperature and relative humidity (RH). The internal RH of the concrete specimens at varying depth was measured at different time intervals. Based on the measured RH data, the moisture model was also developed with ‘k’ from the OPI test as the key input parameter. The moisture model was then coupled with the carbonation model developed. This provides an integrated and powerful solution for predicting carbonation of concrete both sheltered and exposed to rain by using only one main material input parameter ‘k’, which is one of the major contributions of this research.

SUMMARY

The deterioration of concrete structures by environmental actions has become a great concern for those involved in engineering design and maintenance. In most cases, corrosion of the reinforcing steel in the concrete is the main cause of deterioration affecting the durability performance of the structures. The alkaline environment of the concrete normally protects the reinforcing steel by passivating it, i.e. maintaining it in a passive state. However, the protection offered by the concrete can be compromised by aggressive agents that penetrate the cover concrete and de-passivate the steel with time. Apart from chloride ingress, the diffusion of carbon dioxide (CO_2) into concrete is one of the major factors responsible for the depassivation of steel, which can then be followed by corrosion provided there is the presence of sufficient oxygen and moisture.

There is a need from both industry and academia not only to understand and diagnose the process of carbonation of concrete, but also to adequately model it. Most of the carbonation models currently available predict the depth of carbonation based on constant humidity or moisture conditions. The influence of varying weather conditions (i.e. drying/wetting cycles) is typically not taken into consideration in predicting the progressive depth of carbonation. However, prediction of carbonation based on such an approach may be conservative or non-conservative, depending on the prevailing moisture condition which influences the rate of carbonation. The main aim of this research is therefore to develop a carbonation model that is sensitive towards the influence of varying weather conditions.

In South Africa, an existing carbonation prediction model is available, based on an empirical power relationship between concrete permeability and carbonation depth in concretes with selected binder types (Alexander et al., 2007). The advantage of such an approach is that the permeability coefficient can be quantified, since it is an output of the Oxygen Permeability Index (OPI) test, which is a Durability Index (DI) test developed in South Africa for performance-based durability design and specification. The OPI test provides an engineering measure of the resistance of cover concrete to gaseous transport for varying constituent material properties, and accounts for concrete construction parameters such as mixing, placing, compaction, finishing and curing practices (Beushausen and Alexander, 2009).

A further South African carbonation model for concrete, drawing on the model discussed above, and also based on the oxygen permeability coefficient as the key material variable, but also taking into account the effect of relative humidity (RH) on diffusion and carbonation, was

developed by Salvoldi (2010) using accelerated carbonation test data. The strategy of the present research includes developing a carbonation model by adopting the modelling framework of Salvoldi (2010) for natural carbonation. This model was developed using experimental results of carbonation tests conducted under natural conditions for different exposures and for concretes with different binder types. Finally, the carbonation prediction model for concrete was further modified by coupling it with the modelling of the moisture content in concrete, in order to take into account the influence of drying/wetting cycles.

For the experimental program, different concrete specimens were prepared using twelve different concrete mixes with various cement types and cement extenders (additions), such as CEM I 52.5 N, CEM II B-L 42.5 N, low calcium fly ash (FA) at 30% replacement, and ground granulated blast furnace slag (GGBS) at 50% replacement by mass. The water content in all the mixes was kept constant at 170 L/m^3, with water:binder ratios (w/b) of 0.45, 0.55 and 0.65. The slumps for all the mixes were maintained in the range of 90-120 mm. Four different practice-relevant curing regimes were adopted in order to achieve a wide range of concrete microstructures in the critical surface (cover) zone. The scope of the research was limited to exposure conditions in South Africa. The concrete specimens were exposed to natural carbonation in two different cities in South Africa, namely Cape Town and Johannesburg. The choice of the cities was based on the difference in their environmental conditions. The average annual temperature and RH in Cape Town were 19°C and 68% respectively; whereas, for Johannesburg the annual average annual temperature and RH were 19°C and 50% respectively. Another major difference in environmental conditions between the two cities relates to the rainfall patterns and associated drying/wetting cycles. Johannesburg is drier and generally experiences fewer drying/wetting cycles compared to Cape Town.

In the current research, different sets of 48 specimens (with twelve different mixes × four different curing conditions) were cast and exposed to natural carbonation with and without shelter from rain in Cape Town and Johannesburg. One additional set of specimens was exposed to natural carbonation in an enclosed parking garage in Cape Town where the ambient CO_2 concentrations are higher compared to the general natural environment. The depths of natural carbonation were measured at different intervals. The OPI test was also part of the experimental program and was conducted on the 48 different concretes at the age of 28 days.

The experimental results reflect similar observations found in literature and coincide with the trends observed in previous studies. The OPI test results successfully reflected the influence of

curing and w/b, in that significant differences were observed depending on these variables. With all factors remaining the same, an increase in w/b and/or poor curing conditions result in lower OPI values, indicating higher permeability. Lower permeabilities were observed when cement was replaced with cement additions (especially GGBS) in combination with standard 28-day water curing. On the contrary, permeability increased when cement was replaced with extenders with other curing regimes (i.e. poor curing conditions). Similar trends of variation in permeability as for the cement additions were observed in concrete with ground limestone addition in the cement (CEM II B-L 42.5 N).

The depths of natural carbonation were measured at different intervals on specimens exposed at different locations. The tests results after approximately 1000 days of exposure reflected the influence of exposure conditions, w/b, curing conditions, etc. The depth of carbonation was observed to be higher with an increase in w/b and with poor curing conditions. Specimens that were exposed to rain showed lower rates of carbonation when compared to specimens sheltered from rain, both in Cape Town and Johannesburg. The reduction in the rate of carbonation was interpreted to be a result of the saturation of concrete pores with water due to rain, thereby hindering the diffusion of CO_2.

Using carbonation depth data between 150-850 days of natural carbonation, and OPI test results (at 28 days after casting), a carbonation depth prediction model was developed, based on the principle of Fick's laws of diffusion and by adopting the modelling framework of Salvoldi (2010). The amount of carbonatable material, required as a parameter in the model, was taken as the quantity of calcium hydroxide after 28 days of curing, calculated based on the concrete mix proportions, binder type, curing condition, and oxide composition of the binder. Using the experimental data, a correlation between the CO_2 diffusion coefficient and the permeability coefficient from the OPI test was developed. After deriving the model variables (carbonatable material and diffusion coefficient) using the earlier age carbonation data, the carbonation model was validated based on the experimental data of carbonation depth after 1000 days of natural carbonation. At this stage the comparison of the predicted depth of carbonation and experimental results showed that the model was able to predict the depth of carbonation with good precision for specimens which were sheltered from rain, but was not able to address the influence of rain, i.e. drying/wetting cycles.

The carbonation model was thus further modified taking into account the influence of drying/wetting cycles, by coupling it with a moisture model, and adopting Bakker's approach

(Bakker, 1988). According to Bakker (1988), in a drying/wetting cycle, concrete will carbonate during the drying period. During the wetting period (t_w), the concrete is assumed to be saturated instantaneously and the carbonation ceases completely for the entire duration of wetting. During the drying period (t_d) of the subsequent cycle, the carbonation will proceed once the drying depth of the concrete reaches the depth of carbonation at the end of the previous cycle. Thereafter, the concrete will continue to carbonate for the rest of the drying period. The vapour diffusion coefficient of the moisture model was expressed in a novel way in terms of the permeability coefficient based on the OPI measurements. Taking into account the rainfall data of Cape Town and Johannesburg, a drying/wetting cycle with drying (t_d) and wetting (t_w) periods of 3.5 days per week each ($t_d + t_w = 7$ days) was adopted for Cape Town and a wetting period of two days per week was adopted for Johannesburg. Thereafter the model was validated using carbonation data measured after 1000 days of exposure for natural carbonation.

In summary, a carbonation model to predict the time-dependent depth of carbonation of concrete, exposed to or sheltered from rain, was developed, with the unique feature of using the oxygen permeability coefficient as the key integrating variable, governing both carbonation rate and drying/wetting rates. This permits the model to be used directly in performance-based approaches to durability prediction. The end of service life of reinforced concrete structure is generally considered as the time when the carbonation front reaches the level of reinforcement steel (i.e., when the passive layer is destroyed). However, moisture must be present for actual corrosion to take place. Hence the service life prediction model developed in this work towards carbonation-induced corrosion initiation can be further refined to predict the service life of concrete structures, with the onset of the corrosion reaction as the limit state with moisture as a prerequisite. Furthermore, the deterministic output of the models contrasts with the fact that concrete properties, moisture movement and corrosion processes are inherently variable, and therefore the numerical model can be further developed into a probabilistic service life prediction model.

ACKNOWLEDGEMENTS

I would like to express my sincere gratitude to my supervisor Professor Mark Alexander for his guidance and continuous support during my tenure as a PhD student. The expectations and the goodwill he conferred on me have always been a constant source of motivation to achieve higher goals. Working with him as a PhD student was a fulfilling experience. His knowledge, integrity, commitment and gentleness have been an inspiration to me.

I also like to thank my co-supervisor Professor Hans Beushausen, for his technical support and motivation both personally and academically. I am truly grateful for all the opportunities he has identified and guided me towards, and the experience that I have derived therefrom.

To be a part of the Concrete Materials and Structural Integrity Research Unit (CoMSIRU) was an amazing experience and I would like to acknowledge the friendship and support of my fellow colleagues.

I would also like to acknowledge with gratefulness the financial support over the period of this work received from CoMSIRU and from the University of Cape Town (UCT)

The staff of the civil engineering laboratory and workshop at UCT will always have a special place in my heart for all the efforts they have put in towards the successful completion of my experimental work. I would like to express my sincere gratitude to all of the lab staff for their assistance. I am also grateful to the administrative staff in the Faculty of Engineering & the Built Environment at UCT for their help and support in fulfilling the administrative requirement towards my PhD studies.

Finally, I am indebted to my parents and my life partner for their continuous support, love and encouragement that they have given me throughout the completion of this research work.

Above all, I thank the Almighty, without the blessings of whom this would not be a success.

TABLE OF CONTENTS

LIST OF FIGURES

LIST OF TABLES

LIST OF ABBREVIATIONS AND SYMBOLS

Abbreviations

RC	Reinforced Concrete
SLP	Service Life Prediction
CO_2	Carbon Dioxide
DI	Durability Index
OPI	Oxygen Permeability Index
CH	Calcium Hydroxide
RH	Relative humidity
PC	CEM I 52.5 N
LS	CEM II B-L 42.5 N
w/b	Water:binder Ratios
GGBS	Ground Granulated Blast Furnace Slag
$CaCO_3$	Calcium Carbonate
CSH	Calcium Silicate Hydrates
C_3S	Tricalcium Silicate
C_2S	Dicalcium Silicate
c/s	Calcium to Silica
CCI	Chloride Conductivity Index
TGA	Thermogravimetric Analysis
NRUS	Nonlinear Resonant Ultrasound Spectroscopy
SHG	Second Harmonic Generation
ToW	Time of wetness

Symbols

m	Mass of CO_2 (m^2/s)
D	Diffusion coefficient (m^2/s),
c	CO_2 concentration at the concrete surface (mol/m^3),
c_i	CO_2 concentration at the carbonation front (mol/m^3)
A1	Penetrated area
t	Time (s)
x	Carbonation depth
a.	Carbonatable material (mol/m^3)

[k]	Molar concentration of compound ‘k’
F_i	Degree of hydration of compound ‘i’
P_j	Degree of reactivity of compound ‘j’
C	Calcium oxide,
S.	Silica
A	Alumina
F_i	Degree of hydration
t_c	Duration of the curing regime in days.
T	Temperature (K)
R	Universal gas constant (J/K/mol)
E_a	Average activation energy
H_S	RH modification factor
D_{de}	Eeffective dry diffusion coefficient of concrete (m^2/s)
K	Permeability coefficient (m/s)
t_w	Wetting period
t_d	Drying period
Xm	Maximum depth of carbonation
A	Rate of carbonation or carbonation co-efficient
B	Rate of drying or drying coefficient.
D_v	Vapour diffusion coefficient (m^2/s)
λ	Drying front coefficient
p_{vs}	Saturated vapour pressure (Pa)
h_s	Relative humidity at gas–liquid interface
h_0	Relative humidity at the concrete surface (ambient relative humidity)
M_V	Molar mass of vapour (kg/mol)
ρ_l	Density of water (kg/m^3)
$t_{e(n)}$	Total effective time of carbonation at the end of ‘n’ drying/wetting cycles

CHAPTER 1: INTRODUCTION

1.1 BACKGROUND

Reinforced concrete (RC) structures, in general, experience deterioration depending on their interactions with the service environment. The main cause of deterioration of RC elements or structures is identified as the ingress of various ions, liquids and gases from the environment (especially chlorides or carbon dioxide), resulting in depassivation of the reinforcing steel in concrete, followed by corrosion of the steel. Durability design of RC structures is generally concerned with ensuring the ability of the concrete to resist the penetration of aggressive agents during its intended service life.

Carbonation-induced corrosion occurs in many concrete structures, particularly those which are exposed to carbon dioxide-rich environments. The carbon dioxide (CO_2) from the atmosphere diffuses into the capillary pores of concrete and combines with pore water, forming carbonic acid, which reacts with the dissolved alkali hydroxide in the pore solution, forming carbonates. Since the concentration of calcium hydroxide is higher than other compounds in the in pore solution, the reaction of carbon dioxide with calcium hydroxide predominates. This chemical reaction of CO_2 with the products of cement hydration is called carbonation and as a consequence of this reaction, the pH of the concrete pore solution drops from between 12.5 - 13.5, to a value of about 8.3 in the carbonated zones. This reduction in the alkalinity makes the protective oxide layer on the embedded steel unstable and renders the steel susceptible to corrosion (Saetta et al., 1993; Steffens et al., 2002).

The deterioration of RC structures due to carbonation-induced corrosion mainly involves two phases, namely the initiation phase (or period) (t_i) and the propagation phase (or period) (t_p) (Tuutti, 1982; Parrott, 1996; Raupach, 2006; Chun, 2004; Otieno et al., 2011), as shown in Figure 1.1. The initiation phase is characterized by the development and propagation of the carbonation front until it reaches the reinforcement, followed by reduction in the alkalinity of the concrete resulting in the depassivation of the reinforcing steel. The propagation phase reflects the corrosion of the depassivated steel, followed by the expansion of the corrosion products, resulting in cracking and spalling of the cover concrete. However, performance-based durability design of RC structures is based on service life conventionally defined by the end of the corrosion initiation period (Sirivivantnanon, 2001) (a conservative approach in some cases),

and the depassivation of steel is generally considered as the end of the initiation phase in most service life prediction (SLP) models.

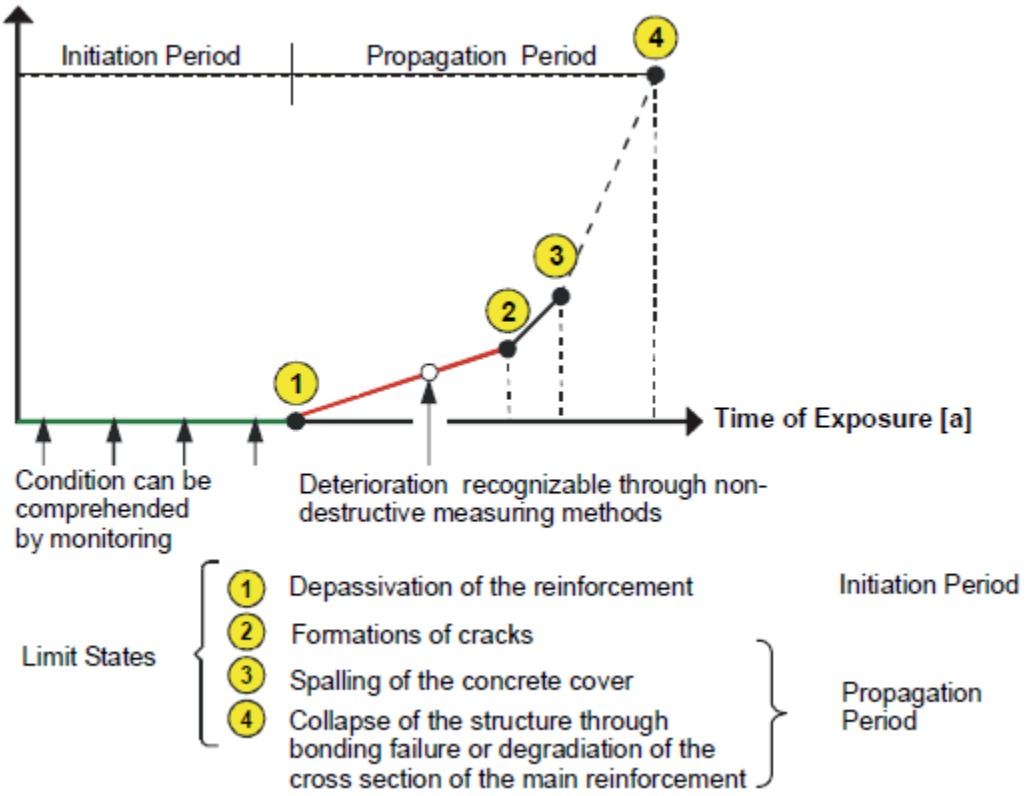

Figure 1.1 Phases in the service life of RC structures (fib Model Code for Service-life Design, 2006)

The focus of the present research is to predict the corrosion initiation phase in the SLP model for carbonation-induced corrosion, taking into account the moisture condition and moisture transport in the concrete. The South African SLP model for carbonation-induced corrosion initiation is an semi-empirical model based on a power relationship between carbonation depths and permeability of concrete, which is an output of one of the Durability Index (DI) tests developed in South Africa (Mackechnie and Alexander, 2002; Alexander et al., 2007).

In South Africa, Durability indexes (DIs) have been adopted as engineering measures of the potential resistance of the concrete cover to the transport mechanisms of gaseous diffusion, water absorption and chloride diffusion. The DIs were derived in association with three different tests, namely; the chloride conductivity test, where chloride ion resistance is important; the oxygen permeability test to establish carbonation resistance; and a sorptivity test to examine the efficiency of curing of concrete using water absorption (Alexander et al., 1999a; Alexander et al., 2017). With these indexes, together with service life prediction models, a

performance specification can be established. A performance-based approach measures properties of the concrete pertinent to the degradation mechanism and thus establishes its performance, as opposed to a prescriptive approach that specifies limiting values for the concrete mix design, such as a minimum cement content and maximum w/c ratio, according to the exposure environment (Alexander et al., 2017).

In South Africa, an existing carbonation model has been used, based on a power relationship between permeability and measured carbonation depths in concretes with certain binders (Alexander et al., 2007). The advantage of such an approach is that the permeability coefficient is an output of the Oxygen Permeability Index (OPI) test, which is one of the DI tests developed in South Africa for performance-based durability design and specification. The OPI test provides an engineering measure of the resistance of cover concrete to gaseous transport for varying constituent material properties, and accounts for concrete construction variables such as mixing, placing, compaction, finishing and curing practices (Beushausen and Alexander, 2009). Apart from the influence of diffusivity and permeability of the concrete on carbonation, concrete chemistry also plays an important role in carbonation and hence needs to be considered in the model. Therefore it is important to develop a carbonation model for different exposures and for concretes with different binders based on natural carbonation data, and to couple it with a moisture model, in order to take into account the influence of drying/wetting cycles.

1.2 RESEARCH SIGNIFICANCE

Much of the South African concrete infrastructure, due to a relatively harsh environment in certain areas, coupled with inadequate attention toward durability with regard to both design and construction, has experienced premature deterioration. The main cause of deterioration is related to reinforcement corrosion induced by the ingress of chlorides and carbon dioxide. Apart from structures directly exposed to the marine environment, most infrastructures are prone to carbonation-induced corrosion. The carbonation of calcium hydroxide (CH) and other hydration products in concrete i.e., their reaction with the atmospheric CO_2 that diffuses through the pores of the concrete, results in the reduction in the pH of concrete followed by the depassivation of the thin corrosion-protection layer on the steel surface (Neville, 2007; Ballim et al., 2009). Corrosion may start when the protective layer is destroyed, and then propagates in the presence of oxygen and water. Protection of reinforcement against carbonation-induced corrosion can be achieved by selecting the cover depth and mix design for the cover concrete,

such that the carbonation front will not reach the reinforcing bar surface within the expected service life of the structure. This can be achieved by developing a quantitative model which predicts the carbonation depth in terms of the exposure conditions, and the variations in mix design. Therefore it is necessary to develop a performance-based model for the prediction of the carbonation of concrete that can be applied for various environments, and which incorporates differences in mix designs, and accounts for concrete construction variability.

Several models predicting the rate of carbonation have been developed by different researchers (Parrott, 1987; Ballim, 1994, Saetta et al., 1995; Bary and Sellier, 2004). A carbonation model based on the oxygen permeability coefficient as the key material variable, and taking into account the effect of cement chemistry and relative humidity (RH) on diffusion and carbonation, was developed at the University of Cape Town by Salvoldi (2010), using accelerated carbonation test data for concrete specimens subjected to standard 28 days of water curing. However the durability of reinforced concrete in terms of carbonation also depends on the aggressiveness of the environment, which is related to drying/wetting cycles. The most favourable exposure condition for carbonation to progress relates to between 50 to 70% RH (Richardson, 2002; Neville, 2007). A reduction in the rate of carbonation is experienced when concrete is exposed to drying/wetting cycles (rain) (Houst and Wittmann, 2002; Leemann et al., 2017). Salvoldi's model does not account of the influence of the drying/wetting cycles. Therefore, a carbonation model coupled with a moisture model has to be developed in order to predict the service life of concrete structures in terms of carbonation-induced corrosion initiation more realistically. The main aim of the present research is to develop a carbonation model by adopting the modelling framework of Salvoldi (2010), extend and expand this model for natural carbonation for different exposures and for concretes with different binders and curing conditions; and to couple it with a moisture model, in order to take into account the influence of drying/wetting cycles. Such an approach is necessary and effective from a sustainability point of view since the prognosis of the condition and behaviour of a structure is an important basis for effective service life management.

1.3 OBJECTIVES AND AIMS OF RESEARCH

The following are the main aims of this research:

1. To critically review the existing carbonation models and to develop a new model or upgrade the existing model based on natural carbonation data, taking into account

all the important parameters and relevant conditions; with the oxygen permeability coefficient (k) from OPI test as the key prediction parameter.

2. To develop and integrate a moisture model into the carbonation model in order to take into account the influence of drying/wetting cycles (influence of rain).

The research will also focus on addressing the following objectives and primary questions:

- Past research has come up with a number of carbonation models with various theories and based on different assumptions. Hence it is necessary to critically review these models and assess their shortcomings (if any).

- The moisture content in concrete is a critical parameter affecting the carbonation of concrete. This research will explore how the influence of moisture (in terms of relative humidity) can be accommodated in the carbonation model.

- The drying/wetting cycles affect the moisture transport in concrete and hence have an effect on the carbonation process. Therefore it is important to understand the influence of the drying/wetting cycles on carbonation of concrete and to incorporate this in the model.

- The different combinations and replacement percentages of cementitious binders and extenders affect the degree of carbonation. Hence it is necessary to incorporate these effects in the model in terms of the change in microstructure and quantity of carbonatable materials.

- How the influence of curing and different methods of curing (which influence the OPI) affect the development of the carbonation front with respect to the microstructure and carbonatable materials also needs to be studied.

1.4 SCOPE AND LIMITATIONS OF RESEARCH

Carbonation of concrete in RC structures is influenced by factors related to exposure conditions (extrinsic) and concrete properties (intrinsic). Hence the accuracy of the model developed will greatly depend on how selectively and rationally these factors are taken into account. This can be achieved by understanding the effect of individual factors affecting carbonation and corrosion, and simultaneously considering them to fully describe carbonation-induced

corrosion. However this is not realistic with the current state of knowledge, technology and time frame. The research will therefore be based on the following scope and limitations:

- Environmental conditions such as temperature, RH, and precipitation (rainfall) have major impact on the rate of carbonation. South Africa is a country with a total area of 1.2 x 10^6 square kilometres and a coast line of about 2800 km. The local environmental conditions are different for coastal and inland areas. This is due to the variation in the climatic conditions which govern the temperature, RH and precipitation (rainfall). To take these variations into account in the model, two cites with different climatic condition were chosen for the experimental programme for carbonation, namely Cape Town and Johannesburg. Cape Town climate is characterised by cool, wet winters and hot, dry summers, whereas Johannesburg experiences cold, dry winters and hot summers with mainly short precipitation periods (Alexander et al., 2007). This difference in climatic conditions, which is representative of much of South African climatic conditions, results in different rates of carbonation, and the model developed will be sensitive to these variations. The details of site location and the local environmental conditions where the concrete specimens were exposed on site for natural carbonation are presented in Chapters 3 and 5.

- The environmental CO_2 concentration is another factor which influences the rate of carbonation. A detailed investigation on the impact of the CO_2 concentration was not conducted for the current research. For the natural carbonation study, the variation in the CO_2 concentration was limited to that of the ambient CO_2 concentrations of Cape Town and Johannesburg, as well as a site location with higher CO_2 concentration, being a parking garage in Cape Town. Details are presented in Chapters 3 and 5.

- The model development will be based on with oxygen permeability coefficient (k) from the OPI test as the key input parameter. The experimental programme was designed to achieve OPI values for concrete ranging from about 9.2 - 10.9, which covers the range of concrete typically used in industry. This wide range of OPI values was achieved by varying the concrete binder types (CEM I 52.5 N (PC), 30/70 PC/fly ash, 50/50 PC/GGBS and CEM II B-L 42.5 N (LS)) and water:binder ratios (w/b) (0.45, 0.55 and 0.65). Along with varying the binder content and w/b,

four different curing regimes were adopted in order to achieve OPI in the above-mentioned range. The curing regimes include standard 28-day water curing, one-day curing in the mould, and curing by covering with plastic for seven days. Curing by means of coatings or curing compounds or steam curing was not adopted in this research. The details of the materials used, mix proportion and curing regime adopted are given in Chapter 3.

- The carbonation model developed in this research is intended to predict the rate of carbonation of typical 'normal' construction concretes with different binders and subjected to different environmental conditions.

- The carbonation model will be developed based on the initial natural carbonation data with oxygen permeability from the OPI test as the key variable. Model validation will be done using the natural carbonation data from the same specimens after 1000 days of natural exposure for carbonation, and also based on natural carbonation data for South African conditions from another independent research from the literature.

1.5 THESIS OUTLINE

The thesis is presented in six chapters. A brief summary of each chapter is given below.

Chapter 1: This chapter provides detailed introduction of the real-life problem which is the basis of this thesis. The significance of this research is also highlighted in this chapter. The aims and objectives as well as the scope and limitation of the current research are listed. Finally a brief outline of the thesis is presented in this chapter.

Chapter 2: A literature review on the mechanism of carbonation in concrete, and the factors which influence the process of carbonation, are discussed this chapter. A detailed summary of on the different transport mechanisms and details of the Durability Index approach and its links to carbonation of concrete are also provided. Finally a review on the existing carbonation models and details of various test methods to assess the degree of carbonation are given.

Chapter 3: In this chapter, detailed description are given of the various materials such as cement, cement extenders (i.e. additions), their proportions used, and curing regime adopted for the current research. It also provides a detailed summary of the different test and

measurement techniques used in this research, such as compressive strength test, Oxygen Permeability Index (OPI) test, measurement of moisture profiles and carbonation. Details of the different site locations where the concrete specimens were exposed for natural carbonation and the environmental conditions of each site are also documented in this chapter.

Chapter 4: The test results from the experimental programme adopted are presented in Chapter 4. Detailed discussion of the OPI test results as well as natural and accelerated carbonation test results are given. The influence of curing and environmental conditions on OPI and carbonation are highlighted. Furthermore, the results from moisture profile measurement are presented and discussed.

Chapter 5: This chapter deals with the development of the carbonation model. The basic principle of carbonation modelling and the derivation of carbonation models is detailed and the assumptions made for the derivation are emphasised. The summary of the variables of the carbonation models and their correlation with the test results are given (correlation between diffusion coefficient and permeability coefficient based on OPI test). Thereafter, refining of the carbonation model to incorporate the influence of drying/wetting cycles using a moisture model is presented. Finally the validation of the carbonation model using long-term natural carbonation data is also provided in this chapter.

Chapter 6: A summary of the carbonation model developed to predict the natural carbonation of concrete, and the limitations of the model, are presented in this chapter. Conclusions and future recommendations from the current research are also provided.

CHAPTER 2: LITERATURE REVIEW

2.1 BACKGROUND

The durability of concrete is a major factor governing the success of concrete in terms of its service life. The deterioration of concrete in service may be the result of a variety of physical and chemical processes. In reinforced concrete, the most serious deterioration mechanism is that of the corrosion of the reinforcing steel. This can result from a number of causes. For example, the carbonation of concrete results in the reduction in the alkalinity of the concrete surrounding the reinforcing steel thereby depassivating the steel and making it prone to corrosion. The carbonation of concrete is a complex physico-chemical process and hence a clear understanding of the factors affecting carbonation is needed in order to predict carbonation and its effects on the service life.

Though several models exist to predict the influence of carbonation on service life, based on different approaches, the development of new generation concretes (new materials, mix designs, high performance concretes) makes it difficult to predict and validate future behaviour of concrete structures. Advances in research are beginning to extend the definition and scope of service life from the corrosion initiation phase, to include the corrosion propagation phase (Otieno 2014). During recent decades, the evolution of service life concepts has led to new and innovative ways to define and calculate service life of RC structures in corrosion-aggressive environments. The modern performance and reliability-based service life design methodology for structures has been adopted and implemented in both new designs and in re-design of existing structures.(Alexander et al., 2008; Alexander et al., 2017)

In this chapter a detailed review of the mechanism of carbonation along with the factors, both internal and external, which influence the rate/process of carbonation is presented. The various transport mechanisms in concrete that enable the carbonation of concrete and the test methods to characterize them are also summarised. The difference between accelerated and natural carbonation processes, and the effectiveness of use of accelerated carbonation tests in predicting the carbonation under natural conditions is also discussed. Thereafter, a brief discussion of different test methods used to measure the degree or extent of carbonation in concrete is also presented. Finally the state-of-the-art of carbonation models highlighting the advantages and disadvantages, and identifying the gaps that needs to be accommodated in future models, is addressed.

2.2 CARBONATION OF CONCRETE

The carbonation of concrete is a physico-chemical process where the carbon dioxide (CO_2) in the atmosphere reacts with hydration products in the concrete to form calcium carbonate ($CaCO_3$) and other secondary products such as silica gel. The process of carbonation involves gaseous, dissolved and solid reactants. The solids that react with CO_2 include not only calcium hydroxide (CH), but also calcium silicate hydrates (CSH) and the un-hydrated cement constituents such as tricalcium silicate (C_3S) and dicalcium silicate (C_2S) (Papadakis et al., 1989; Papadakis et al., 1991b). The different stages of the carbonation process can be described by the following chemical reactions (Ihekwaba et al, 1996):

$$H_2O + CO_2 \rightleftharpoons 2H^+ + CO_3^{2-} \quad 2.1$$

$$Ca(OH)_2 + 2H^+ + CO_3^{2-} \longrightarrow CaCO_3 + 2H_2O \quad 2.2$$

Reaction with CSH

$$CSH + 3CO_2 \longrightarrow (3CaCO_3 \,.\, 2SiO_2 \,.\, 3H_2O) \quad 2.3$$

Reaction with residual unhydrated cement compounds

$$C_3S + 3CO_2 + vH_2O \longrightarrow SiO_2 \,.\, vH_2O + CaCO_3 \quad 2.4$$

$$C_2S + 2CO_2 + vH_2O \longrightarrow SiO_2 \,.\, vH_2O + 2CaCO_3 \quad 2.5$$

The above reaction will occur depending upon the pH of the pore solution below which the hydrated cement phase is unstable as shown in Table 2.1. CH and CSH are the hydrated cement phases which will undergo carbonation first. However the carbonation of CSH depends on the calcium to silica ratio (c/s). For c/s below 1.85, carbonation of CSH only take place once all the CH at that level is depleted (Visser, 2014).

Table 2.1 Stability of cement phases at different pH (Visser, 2014)

Stage	pH	Stable Phases
1 (non-carbonated)	>12.6	CH, CSH (C/S > 1.8 or at high comon iron effect), Monosulphate (AFm), Ettringite (AFt)
2	11.6 - 12.6	CSH (C/S < 1.8), AFm, Aft
3	10.5 - 11.6	CSH (C/S < 1.05), Aft, Aluminium Hydroxide $Al(OH)_3$
4	10.0 - 10.5	CSH (C/S < 0.85), $Al(OH)_3$, Ferric Hydroxide $Fe(OH)_3$
5 (fully carbonated	<10	Silica ($SiO_{2)}$ with some Calcium Oxide (CaO), $Al(OH)_3$, $Fe(OH)_3$

The process of carbonation is considered as a front which travels into the concrete as shown in Figure 2.1 (Ballim et al., 2009). However a semi carbonated zone separating the fully carbonated and uncarbonated concrete has been observed by many researchers (Thiery et al., 2007; Ji et al., 2014). Deterioration of RC concrete mostly associated with the change in pH of concrete, therefore the carbonation progression can be idealised as front as indicated by Salvoldi (2010). Carbonation results in the reduction in alkalinity of the pore solution thereby leading to the depassivation of the steel in contact with the carbonation zone. The water released during the chemical reaction makes the carbonation process self-sustaining, but can be limiting to the increasing difficulty for the carbon dioxide to penetrate into the depth of the concrete (Richardson, 2002).

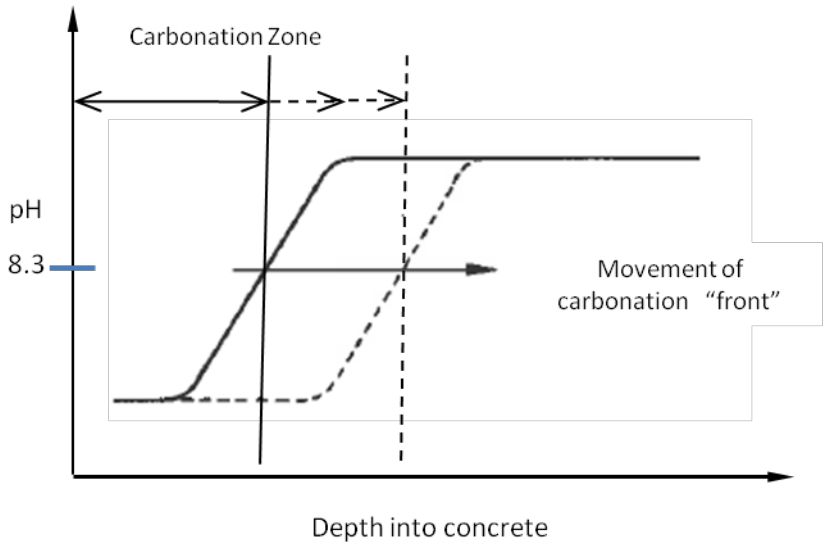

Figure 2.1 Representation of development of carbonation 'front' in concrete (Ballim et al., 2009)

The physico-chemical processes that occur during concrete carbonation are complex and depend on many variables including permeability, porosity, chemical composition of the concrete, CO_2 concentrations, and very importantly relative humidity. The step-wise process as proposed by Papadakis et al. (1991a) is as follows and takes place in the concretes pores:

- The chemical reactions from which carbonatable materials are produced, i.e. the cement hydration reactions
- The diffusion of CO_2 in the gaseous phase
- The dissolution of CO_2 in the pore water
- The dissolution of $Ca(OH)_2$ in the pore water
- The diffusion of $Ca(OH)_2$ in the aqueous phase from uncarbonated to carbonated areas
- The reaction between dissolved CO_2 and $Ca(OH)_2$
- The reaction of gaseous CO_2 with solid carbonatable materials (hydrated and unhydrated)
- The reduction of pore volume due to the solid products of carbonation
- The condensation of water vapour on the walls of the pores

The rate of carbonation of concrete is mainly controlled by the ingress of carbon dioxide into the concrete pore system. This implies that if transport of aggressive agents such as CO_2 into concrete is limited, then the durability of the concrete structure is enhanced. The transport of aggressive agents can be mitigated by first understanding the mechanisms of penetration of aggressive agents into concrete. Penetrability – being a general term - involves a number of transport processes (or mechanisms), namely the diffusion of ions/gases under a concentration gradient, permeation of a solution under a hydrostatic head, and the capillary absorption of liquids (Muigai, 2008), among others. The major driving mechanism in the case of carbonation is diffusion of CO_2, which in turn depends on the diffusivity of concrete. Fick's first law of diffusion has been used to describe the depth of carbonation and hence is the basis of the majority of the carbonation models. Measuring diffusion is usually a difficult process; at the same time there are techniques available that can measure permeability of concrete on site and

in the laboratory. The research done by Parrot (1996) shows that the carbonation depth can be related to the air permeability. In South Africa, durability indexes (DIs) (see Section 2.4) have been adopted to characterise the transport mechanisms of concrete. The oxygen permeability index (OPI) test is used in the case of identifying the carbonation resistance of concrete.

There is no standard test method to measure carbonation depth, but several publications (for example CPC-18 (1988)) discuss different methods. The most commonly accepted method is the phenolphthalein test, where the freshly broken concrete surface is sprayed with 1% or 2% phenolphthalein solution. The concrete surface with pH is more than 9 turns pink, whereas the fully carbonated surface where the pH is less than 8, remains colourless. Even though the phenolphthalein test fails to identify the partially carbonated areas, it is widely accepted as an indicator of the extent of carbonation due to its simplicity and ease of use. Also the pH indication can be used as a tool towards durability, since as the corrosion initiation of steel reinforcement is caused by the depassivation of steel resulting from the reduction in pH due to carbonation.

2.3 FACTORS AFFECTING CARBONATION

By examining the physico-chemical mechanism of carbonation, the factors which affect the carbonation depth, apart from time, can be categorised as environmental factors (extrinsic) and concrete properties (intrinsic).

2.3.1 Environmental Factors

Relative humidity (RH): The ambient RH at the exposure site influent the rate of drying of concrete and hence the internal relative humidity. The most favourable humidity condition for carbonation to progress is in the range of 50 to 70 % RH (Verbeck, 1958; Saetta et al., 1995; Richardson, 2002; Neville, 2007) The above-mentioned range of RH can be attributed to the fact that at lower RH, the concrete pores dry out and there is not enough water for the dissolution of CO_2 and hence the carbonation process is slowed or stopped. On the other hand, at higher RH the pores are completely filled with water, which restricts the diffusion of CO_2 further inside the concrete.

CO_2 gas diffusivity: The CO_2 gas diffusivity in concrete depends on the degree of saturation, and the pore structure of concrete. Gas diffusivity of concrete decreases by increasing the degree of saturation due to the effect of pore blocking. The degree of saturation and pore

structure of concrete also can change the gas diffusivity in concrete. Different preconditioning before the start of a carbonation test can change the degree of saturation and pore structure of concrete (Bahador and Jong, 2006).

Carbon dioxide concentration: The partial pressure of CO_2 affects the diffusion rate and reaction rate of carbonation, since the diffusion is a concentration gradient-driven transport of CO_2 (Salvoldi, 2010). However the change in CO_2 concentration will not change the carbonation reactions, rather it will increase or decrease the reaction process by varying the rate of transport of CO_2 to the pore air – pore solution interface (Visser, 2014)

Temperature: Small variation in ambient temperature in do not have major effect on the rate of carbonation. However, the dissolution and degree of saturation of various cementitious compounds can be affected by the change in temperature. For example, at lower temperature, the dissolution of CH and CO_2 is higher resulting in more CH molecules to take part in reaction; on the contrary, the rate of reaction will be slower at lower temperature (Van Balen and Van Gemert, 1994). On the other hand with increase in temperature, the activation energy and hence the diffusivity of CO_2 will increase. In general regions with similar RH, elevated temperature such as 30-40°C results in higher rate of carbonation when compared to lower temperatures such as 18-25°C. On the other hand the effect of elevated temperature on increasing the carbonation rate is compromised by the presence low RH (Ekolu, 2018)

2.3.2 Concrete Properties

Microstructure: The carbonation of concrete mainly depends on the microstructure of the cover concrete, since the transport rates for the ingress of various ions depend on the microstructure of the concrete. The microstructure depends upon many factors: the w/b ratio, the paste content, cement content, binder type, degree of hydration, aggregate type, aggregate content, water content, quality of mix constituents, and concrete practice variables such as mixing, transportation, placing, compacting, curing etc; each of these has a direct or indirect influence on microstructure. The pore structure seems to be refined because of the carbonation of concrete due to the formation of calcium carbonate during carbonation. However studies show that concrete with blast furnace slag shows a higher capillary porosity in the carbonated area which may be due to the reaction of carbon dioxide with hydration products other than CH resulting in carbonation shrinkage which further facilitates the CO_2 ingress (Gruyaert et al., 2013)

Chemical composition: the carbonation of concrete depends on the chemical composition of the concrete, which in turn depends on the concrete mix constituents such as cement and binder type and quantity. Carbonation also depends on the degree of degree of hydration in the case of cement and degree of pozzolanic activity in the case of binders with cement extenders. The amount of carbonatable materials; which is the hydrated and unhydrated cement phase is responsible for the increase and decrease of rate of carbonation. Studies shows that at higher CO_2 concentration (>3%), both unhydrated as wel as the hydrated cement phase such a CSH gel, CH, ettringite will carbonate; whereas at ambient CO_2 concentration, mainly CH undergo carbonation (Castellote et al., 2009). The lower the CH content, the higher the carbonation rate (Younis et al., 2011). However a comparative study by Borges et al. (2012) on blended cement paste with blast furnace slag and pulverised fuel ash (fly ash) showed that, even for pastes with same amount of CH, the carbonation rate varies. This shows that CH is not the only parameter that governs the extent of carbonation in a cement/concrete matrix system and the variation can also be attributed due to the difference in permeability and porosity in the system.

Cement extenders: Studies have shown that cement extenders such as fly ash and blast furnace slag have negative impacts on carbonation resistance of concrete with partial cement replacements with these materials. (Thomas et al., 1992; Papadakis, 2000; Neville 2007; Gonen and Yazicioglu, 2007). For the same replacement level, the carbonation resistance of both cement paste and concrete with blast furnace slag is superior to that of cement paste and concrete with fly ash; due to the denser and refined microstructure of paste/concrete with blast furnace slag and also due to the presence of higher CH content with the respect to fly ash concrete (Hui-sheng et al., 2009; Borges et al., 2012). Another study showed that an increase in blast furnace slag content in concrete increases the depth of carbonation, which can be attributed to the reduced CH content and increase in permeability (Gruyaert et al., 2013). On the other hand, the incorporation of silica fume has beneficial effects towards carbonation of concrete, as studies have shown a reduction in carbonation depth of concrete with silica fume when compared to the reference concrete (Gonen and Yazicioglu, 2007)

Curing: Curing has a major role in the progression of carbonation in concrete, since it governs the composition (development of CH) and the microstructure of the concrete. In general, rate of carbonation decreases with increase in the duration of moist curing (Parrot, 1996; Thomas et al., 1992). Studies showed that prolonged curing (up to 90 days) increases carbonation resistance in the case of blended cement concrete with blast furnace slag (Gruyaert et al., 2013).

Even in the case of normal water curing, the resistance towards carbonation is observed to improve with increase in extent of curing (Sisomphon and Franke, 2007). The specimens were less porous and more resistant to carbonation when cured under water (when compared to uncured concrete), and this was more noticeable for the mixtures with the lower clinker contents. A reduction in 20-50% of carbonation depth was observed in specimens cured under water when compared to uncured specimens due to reduction in porosity because of extended cement hydration during water curing (Younsi et al., 2011)

2.4 DURABILITY INDEX (DI) APPROACH.

Durability of a reinforced concrete structure, which is its ability resist deterioration during its service life. However the cases of premature deterioration RC structure resulting in substantial amount of repair and maintenance, is increasing in a fast rate. The durability related problem varies with the structure and its environment. Most of the durability problems are associated with the corrosion of the reinforcement steel rather than the deterioration of the concrete itself. For example the structures exposed in marine environment experience reinforcement corrosion because of the chlorides when compared to the structures in inland where CO_2 concentration is higher and carbonation is the cause of reinforcement corrosion. Therefore the durability issues associated with a RC structure is mostly depended on the exposure environment and the material parameters of the cover concrete as shown in Figure 2.2

Traditional approach towards dealing with the durability of concrete structure was to relate it with the compressive strength. However this approach is not suitable as the effects of factors which governs durability (such as permeability) of concrete have a different effect on the strength of concrete. For example, no correlation between the compressive strength and the permeability was observed by Nganga et al. (2013), based on measurements from RC structures. Furthermore, taking into wide range of binder and manufacturing process used in concrete construction, compressive strength cannot be used as a representation of durability (Alexander et al., 2017). Nevertheless the compressive strength was used to correlate the durability performance of concrete structure for decades with reasonable success, where the concrete compressive strength test acted as an “index” test which characterizes the intrinsic potential of concrete to resist the applied stresses (Alexander et al., 2017).

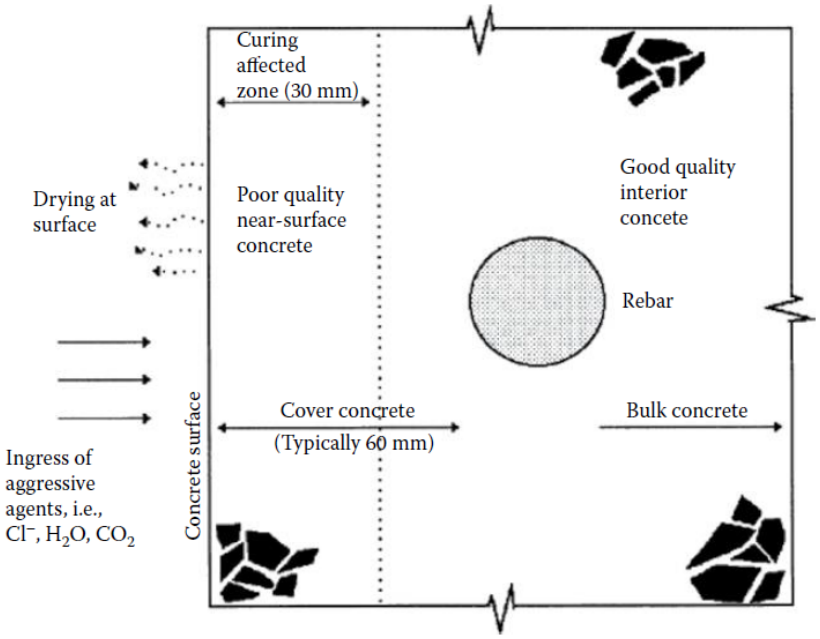

Figure 2.2 Interaction of environment and the material parameters on cover concrete (Alexander et al., 2017)

DI approach is also based on similar indexing methodology. Corrosion of the reinforcing steel is the major durability problem associated with the RC structures, which is governed by the quality of the cover concrete. Therefore it is necessary to characterise the quality of the cover concrete using parameters that influence the deterioration process of the concrete. The strength parameter may not be the true reflection of the quality of cover concrete as it represent the overall response of the material towards stress. Whereas the cover concrete is largely affected by the construction practice such as initial curing etc. and also by the environmental parameters leading towards subsequent deterioration process. The deterioration process are linked with the transport mechanism like gaseous and ionic diffusion, water absorption etc. These parameters act as a "durability indicator" and are able to provide information on the resistance of the material to the deterioration mechanism (Alexander et al., 1999a). This approach can be adopted to a wide range to durability problems. A series of durability index test is needed where each durability index test is linked to a certain transport mechanism related to a particular deterioration process. In South Africa, three durability index test were developed to characterise the cover concrete based on the transport mechanisms related to durability; Oxygen Permeability Index (OPI) test for permeation, Chloride Conductivity Index (CCI) test for diffusion and Water Sorptivity for absorption. The suggested range of durability classification based on the above three test as per Alexander et al. (1999a) is given in Table 2.2

Table 2.2 Range of durability classification based on DI tests (Alexander et al. (1999a)

Durability Class	OPI (log scale)	Sorptivity (mm/√h)	Conductivity (mS/cm)
Excellent	>10	<6	<0.75
Good	9.5 - 10	6.0 - 10.0	0.75 - 1.50
Poor	9.0 - 9.5	10.0 - 15.0	1.50 - 2.50
Very poor	<9.0	>15	>2.50

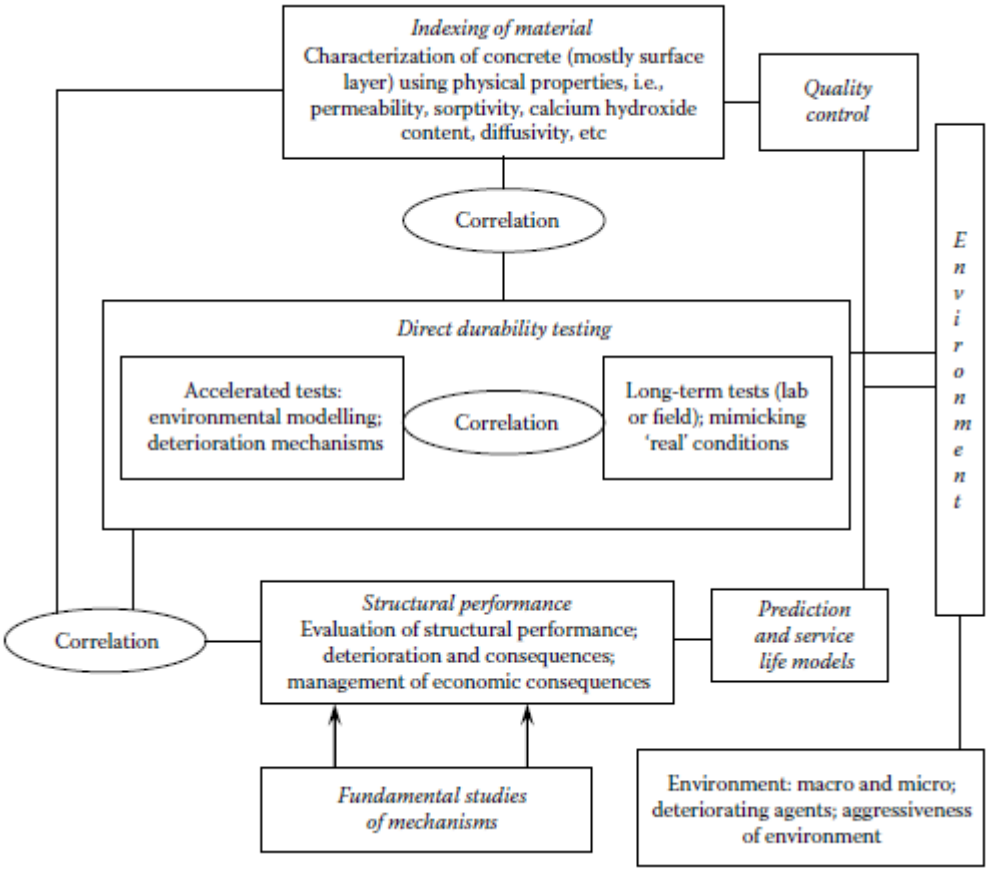

Figure 2.3 A framework for durability index design and specifications for concrete (Alexander et al., 2017)

The material index based on these test represents the quality of the cover concrete and are sensitive to the material type, concrete manufacturing process and environmental factors such as type and degree of curing etc. These material indexes can also be used as "proxies" which indicates the long-term durability performance. These durability indexes are then be correlated with the results of actual durability test both accelerated as well as long term measurements, for example; chloride penetration testing, carbonation testing, sulphate resistance testing etc. A framework for durability index design and specifications for concrete was developed

(Alexander et al., 2017) as shown in Figure 2.3 indicating the interaction and link between the material indexing, direct durability testing and long term durability performance of RC structures.

2.5 TRANSPORT MECHANISM IN CONCRETE

Transport properties of concrete are very important in predicting the durability of concrete, as the process of carbonation and other deterioration mechanisms are related to the ability of fluids or ions to move through the concrete microstructure. The movement of fluids, ions or molecules of aggressive species both in liquid and gaseous form (for example CO_2 and moisture in the case of carbonation) primarily depends on the penetrability of the concrete. The penetrability of the concrete can be broadly defined as the degree or extent to which the concrete permits the transport of gases, liquids, or ionic species through its pore structure. Moreover, the concrete microstructure and the permeability of the cement paste, especially at the interface with aggregate particles has a predominant influence on the permeability of concrete (Alexander and Mindess, 2005). Mechanisms such capillary action, flow under a concentration gradient, and flow under pressure, are involved in fluid and ion movement through concrete and are characterised by material properties such as sorptivity, diffusivity and permeability respectively (Richardson, 2002). However, carbonation of concrete relies mostly on the mechanism of diffusion, which can be linked to permeation, covered in detail in the following section along with their inter-relationship.

2.5.1 Diffusion

Diffusion can be defined as the transfer of mass from regions of higher concentration to regions of lower concentration by the random motion of free molecules or ions of the diffusing substance. The rate of mass transfer through a unit area of a section (F) is proportional to the concentration gradient (dc/dx) and the diffusion coefficient D (m^2/s), and is stated in Fick's first law.

$$F=-D\frac{dc}{dx} \qquad 2.6$$

Where,

F = mass flux (g/m^2s)
m = mass of substance flowing (g)
t = time (s)

A = area (m^2)

D = diffusion coefficient (m^2/s)

c = concentration (g/m^3)

x = distance (m)

The diffusion coefficient (D) characterises the transport ability of a given substance by a solid. In many cases, this is superimposed by mechanisms other than random motion of molecules, such as the flow of condensed gas along the pores, or saturated or non-saturated capillary flow. The moisture may also flow as the diffusion of water vapour in porous solids (Rose, 1965). In spite of these additional transport mechanisms, which exist in most cases, Fick's law of diffusion can be applied to quantify the multiple transport phenomena (Bazant and Najjar, 1972).

The diffusion coefficient (D), is influenced by a number of factors such as the local concentration (c) of the free ions and molecules, the location (x) in the case of non-homogenous solids, time (t) in the case of ageing materials, and also by temperature (T) (Kropp et al., 1995). In the case of transient diffusion processes, the change of concentration in a unit volume with time is referred to as Fick's second law of diffusion, and can be expressed as shown below

$$\frac{\partial c}{\partial t} = \frac{\partial}{\partial x}\left(D\frac{\partial c}{\partial x}\right) \qquad 2.7$$

Where, D is theoretically a constant, or a function of different variables

Due to the chemical interaction or physical adsorption from mass forces, the diffusing substance may be partially immobilized, which is taken into account using a sink term s

$$\frac{\partial c}{\partial t} = \frac{\partial}{\partial x}\left(D\frac{\partial c}{\partial x}\right) - s \qquad 2.8$$

The binding capacity of the penetrated material may be a variable of different parameters and may depend on the local concentration of the diffusing substance, temperature and also the changes of the penetrated material (Kropp et al., 1995).

2.5.2 Permeation

Permeation can be described as the flow of liquids or gases caused by the pressure head through the saturated pore structure. Permeability is therefore the measure of the extent by which fluids can be transported by permeation. However the concrete microstructure, the moisture condition of the material, and the characteristics of the permeating fluid influence the permeability.

(Ballim et al, 2009). The coefficient of permeability represents the material characteristics, and can be determined experimentally. Based on the viscosity of the flowing medium and also depending on the pore structure of the permeating medium, the flow can be either laminar or turbulent flow, where the volume transported is not proportional to the pressure head. In the case where the fluid is gas, depending on the compressibility and viscosity of the gas, for laminar flow the coefficient of permeability can be expressed as follows (Kropp et al., 1995).

$$k=\eta\times\frac{Ql}{tA}\times\frac{2p}{(p_1-p_2)(p_1+p_2)} \qquad 2.9$$

Where,

k = coefficient of permeability (m^2)

η = viscosity of the gas (Ns/m^2)

Q = volume of gas flowing (m^3)

L = thickness of penetrated section (m)

A = penetrated area (m^2)

P = pressure at which volume Q is measured (N/m^2)

P_1 = pressure at entry of gas (N/m^2)

P_2 pressure at exit of gas (N/m^2)

t = time (s)

Since the permeability coefficient represents the material characteristics, it can be used to characterise the concrete microstructure, and therefore to predict some of the durability mechanisms of concrete such as carbonation (Ballim et al, 2009). Ballim (1994) developed a test method to characterise concrete microstructure based on the principle of permeation using a falling head permeameter. The permeability coefficient is calculated based on the D'Arcy equation for the flow of fluids through porous media, presented by Alexander et al. (1999a) based on Ballim (1994), and is shown below.

The D'Arcy equation for permeation can be expressed as

$$\frac{\partial m}{\partial t}=\frac{-k}{g}\frac{\partial P}{\partial z} \qquad 2.10$$

Where,

$\partial m/\partial t$ = rate of mass flow per unit cross-sectional area

$\partial P/\partial z$ = pressure gradient in the direction of flow

k = coefficient of permeability

g = acceleration due to gravity

For a gas, mass is related to volume V and pressure P by the following equation

$$m = \frac{\omega V P}{R\theta} \qquad 2.11$$

Where,

ω = molecular mass of permeating gas

θ = absolute temperature

R = Universal gas constant

The change in total mass of stored gas in time ∂t is

$$\frac{\partial m}{\partial t} = \frac{\omega V}{R\theta} \cdot \frac{\partial P}{\partial t} \qquad 2.12$$

For a test specimen of cross-sectional area A, measured normal to the direction of flow, and thickness d; Equation (2.10) can be rewritten as follow

$$\frac{\partial m}{\partial t} = \frac{-k}{g}\frac{PA}{d} \qquad 2.13$$

Hence,

$$\frac{\omega V}{R\theta} \cdot \frac{\partial P}{\partial t} = \frac{-k}{g}\frac{PA}{d} \qquad 2.14$$

Rearranging,

$$\frac{-\omega V g d}{R\theta k A} \cdot \frac{\partial P}{P} = \partial t \qquad 2.15$$

Integrating,

$$\frac{-\omega V g d}{R\theta k A} \cdot \ln(P) = t + \text{constant} \qquad 2.16$$

At t=0, P = P_0, therefore,

$$\text{constant} = \frac{\omega V g d}{R\theta k A} \cdot \ln(p_0) \qquad 2.17$$

Substituting in Equation (2.16)

$$t = \frac{\omega V g d}{R\theta k A} \cdot \ln\frac{P_0}{P} \qquad 2.18$$

Rearranging,

$$k = \frac{\omega V g d}{RA\theta t} . \ln \frac{P_0}{P} \qquad 2.19$$

2.5.3 Relation between Permeability and Diffusion

With respect to the durability of concrete, diffusion tends to be the dominant transport mechanism, whether it is transport of chlorides in the case of fully submerged structures in sea water, or transport of oxygen to the steel surface in reinforced concrete structures, both governed mainly by diffusion. The transport of CO_2 in concrete, which is the main driving mechanism for the process of carbonation, is also based on diffusion. However, determining diffusion experimentally is not easy and few test methods are available (example Papadakis et al. (1991a), Jung et al. (2011)). On the other hand, permeation, based on a pressure head, can be used to predict the diffusion of concrete especially with respect to the carbonation of concrete. Different test methods exist to determine the permeations characteristics of concrete, such as the Cembureau permeability test (Kollek 1989), Torrent permeability test (Torrent 1992), and the South African oxygen permeability index (OPI) test (Alexander et al., 1999).

The flow of liquids, gases and ions in a specific concrete pore structure may be inter-related as the flow process occurs in the same pore system. Nilsson and Luping (1995), established a theoretical relationship between permeability and the diffusion coefficient as follows. For a small single straight pore with radius r embedded within a concrete matrix with cross-section A, with the assumption that Hagen–Poiseuille's law can be applied to small pores; Permeability coefficient (k) can be expressed as follows:

$$k = \frac{\pi r^4}{8A} \qquad 2.20$$

Similarly the diffusion coefficient for the same pore can be expressed as fraction of the diffusion coefficient in a bulk fluid. Therefore the diffusion coefficient (D) can be expressed as follows:

$$D = D_0 \times \frac{\pi r^2}{A} \qquad 2.21$$

Where, D_0 is the diffusion coefficient through a bulk liquid. Since the flow occurs through the same pore of radius r, Equation (2.20) and (2.21) can be combined to form

$$k = \frac{A}{8\pi D_0^2} \times D^2 \qquad 2.22$$

The effective radius of the pores may vary due to different flow mechanisms, cracks, different fluids and substances being transported. Hence Equation (2.22) can be generalised as follows

$$k = \text{constant} \times D^{b} \qquad 2.23$$

However the parameter b depends on the transported substance as well as the friction and tortuosity of the pore structure. Based on limited experimental data, the values of b depending on the permeating and diffusing substance by Nilsson and Luping (1995), are as shown in Table 2.3 below.

Table 2.3 Values of parameter b based on experimental data (Nilsson & Luping, 1995)

Substance in permeation	Substance in diffusion	b
Water	Water vapour	1.8
Gas	Gas	1.0
Water	Ions	1.5

In order to improve the durability performance of reinforced concrete structures in South Africa, a ‘‘Durability Index’’ approach has been developed as discussed in Section 2.4. The approach is based on developing different test methods to measure the transport related properties of cover concrete in an attempt to characterise the concrete microstructure and its sensitivity towards material, constructional, and environmental factors. Each durability index test is based on a particular transport mechanism relevant to a specific deterioration process. (Alexander et al., 2008; Ballim et al., 2009) For example the South African OPI test is a durability index test based on the permeation, and can be used to address the deterioration mechanism such as carbonation concrete. The OPI test is summarised in Chapter 3 and further details regarding the test procedure and apparatus can be obtained from UCT Durability Index Testing Procedure Manual (Ver 4.5.1, April 2018) and Alexander et al., (1999). A comparative study shows that the OPI test gives good correlation with other internationally accepted permeability test methods (Cembureau permeability test, Torrent permeability test etc.) in spite of the difference in preconditioning of specimens, application of pressure, specimens size, test duration etc.; the OPI test method was able to detect the differences in w/b ratio, binder type, and curing condition (Beushausen and Alexander, 2008).

Salvoldi et al. (2015), based on accelerated carbonation studies, observed a correlation between diffusion and permeability coefficient (obtained from the OPI test) similar to Equation (2.23) as shown in Figure 2.4. However the correlation is based on the accelerated carbonation test and the range of permeability is limited as his research was only based on 28 days water cured specimens and hence the concretes under study had dense microstructures.

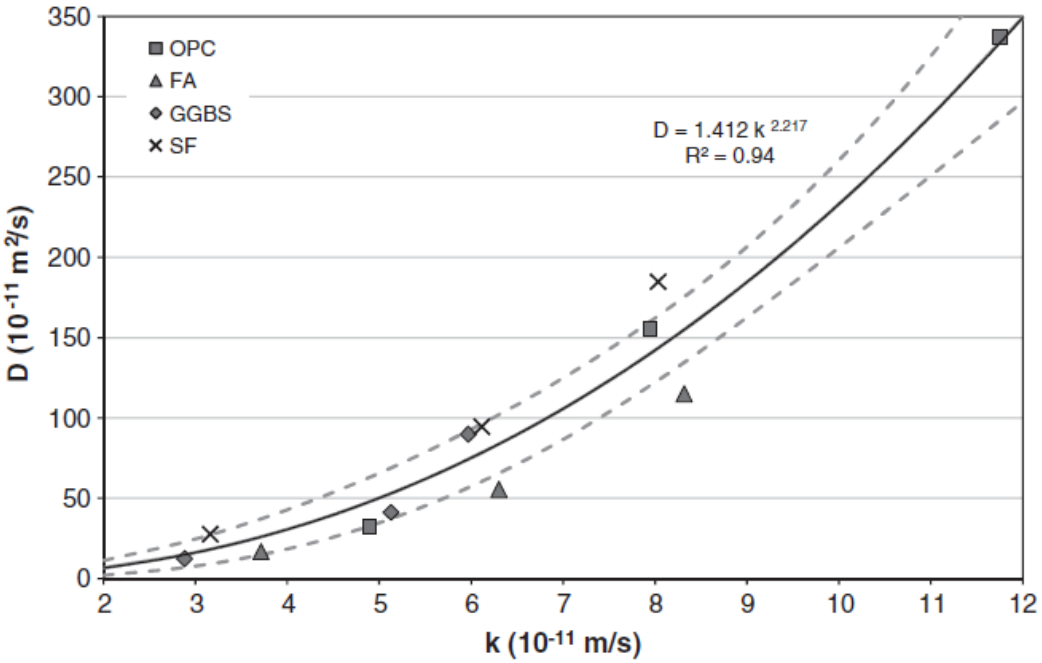

Figure 2.4 Correlation between diffusion and permeability coefficient (Salvoldi et al, 2015)

The OPI test is a relevant test method to address the deterioration mechanism of carbonation of concrete. Firstly the output of the test give in site on the extent by which the aggressive species can transport through the concrete and secondly the test method is sensitive to material factors such as choice of material and mix proportions etc.; construction factors such as placing, degree of compaction, curing techniques; and environmental factors. OPI test also bale to assess the micro voids and cracks, presence of bleed voids and channels, and the degree of interconnectedness of the pore structure which influence the permeability of concrete (Ballim et al., 2009). Studies done by Mackechnie and Alexander (2002) shows good correlation between the OPI values recorded at 28 days and the depth of carbonation under natural conditions as shown in Figure 2.5. Hence OPI test can be used an important tool to represent the diffusion process in concrete carbonation and to develop service life prediction models based on carbonation induced corrosion.

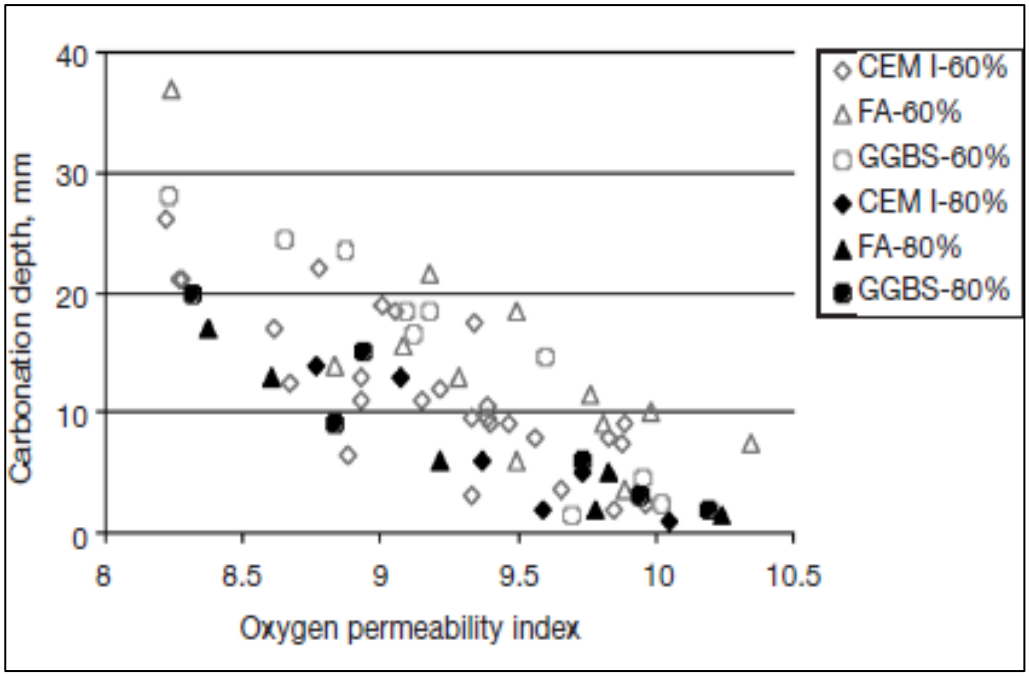

Figure 2.5 Correlation between carbonation depth and OPI (Mackechnie and Alexander, 2002)

2.6 ACCELERATED AND NATURAL CARBONATION

Carbonation of concrete as discussed previously is a physico-chemical mechanism whereby CO_2 from the atmosphere diffuses into concrete and reacts with the compounds of concrete forming calcium carbonate. Since the concentration of CO_2 in the atmosphere is very low, of the order of 0.03–0.04% by volume (Sisomphon and Franke, 2007), and depending on the moisture condition of the concrete, the reaction is very slow and will take years to reach the depth of reinforcement steel. In order to study carbonation, such as the effect of different compositions, the rate of carbonation etc., the process of carbonation is usually accelerated by exposing concrete to higher CO_2 concentrations. Different guidelines recommend different conditions for accelerated carbonation testing. For example, fib Model Code for Service-life Design (2006), recommends a constant temperature of 20°C ± 2°C, relative humidity of 65% ± 5%, and CO_2 concentration of 2% ± 0.1% with a preconditioning for 21 days in standardised laboratory condition (temperature of 20°C ± 2°C, relative humidity of 65% ± 5%). By contrast, the Chinese standard GBJ82-85 recommends CO_2 concentration of 20% ± 3%, relative humidity of 70% ± 5% and a constant temperature of 20°C ± 5°C (Hui-sheng et al. 2009). Different CO_2 concentrations have been used by different researches for conducting accelerated carbonation tests in the range of 1% (Bernal et al, 2012), 2% (Visser, 2012), 3% (Sisomphon

and Franke, 2007), 5% (Sanjuan et al., 2003), 10% (Gruyaert et al., 2013), 50% (Thiery et al., 2007), 100% (Sanjuan et al., 2003) etc.

Studies show that the mechanism of carbonation differs from that of natural carbonation when subjected to higher CO_2 concentration. Castellote et al. (2009) observed that at CO_2 concentration above 3%, the calcium silicate hydrate gel (CSH) is completely carbonated, whereas in the case of natural carbonation, CSH was not completely carbonated, but rather observed to be present at a lower calcium to silica ratio. Similar dependency of CO_2 concentration on CSH carbonation was also observed by Hyvert et al. (2010). Contradictory to the above observation, Visser (2014) concluded that high concentration of CO_2 will not change the carbonation process as the reactions are instantaneous at the reaction front. Rather the effect of high CO_2 concentration will be in terms of faster transport of CO_2 molecules at the air-solution interface in the pores, thereby increasing the reaction rate. Visser et al, (2012) point out that the discrepancy in the rate of carbonation between accelerated and natural carbonation can be due to the amount of water produced during the accelerated carbonation. A large amount of water is released, both from the reaction with calcium hydroxide (CH) and from other hydrates (Sanjuan et al., 2003; Mier et al., 2007) especially in the case of dense concrete with large amount of CH. Hence for the carbonation front to proceed further, the water needs to dry out. Therefore, the progression of drying front can be the dominating factor rather than the diffusion of CO_2 particularly in the case of low permeable materials (fib Model Code for Service-life Design, 2006; Visser, 2012) during accelerated carbonation.

A further drawback of accelerated carbonation is the decrease in pH of the pore solution as observed in alkali-activated binders by Bernal et al. (2012), and coating of CH crystals with calcium carbonate ($CaCO_3$) (Thiery et al., 2007), thereby reducing the buffering capacity of CH. Visser (2014) also indicated the possibility of back-diffusion of CH during natural carbonation based on the investigation of Saeki et al. (1991). As a result, massive precipitation of $CaCO_3$ near the concrete surface may occur thereby slowing the diffusion of CO_2. Such a phenomenon is lacking when the process of carbonation is accelerated, and as a result there will be differences in test results between natural and accelerated carbonation.

The above facts bring into question the feasibility of accelerated carbonation testing to predict natural carbonation. However, the correlation between accelerated and natural carbonation, depending on the CO_2 concentration used in the accelerated carbonation, has been studied. The accelerated carbonation using 5% CO_2 was observed to be 3.9 times (Borges et al., 2012) and

5 times (Sanjuan et al., 2003) faster than natural carbonation at 50-60% relative humidity. Assuming constant gas diffusivity and CO_2 binding capacity, Sisomphon and Franke (2007) proposed the following relation between natural and accelerated carbonation co-efficient

$$\frac{k_{acc}}{k_{env}} = \frac{\sqrt{c1_{acc}}}{\sqrt{c1_{env}}} \qquad 2.24$$

Where k_{acc} and k_{env} are the carbonation coefficients from the accelerated carbonation and natural carbonation, and $c1_{acc}$ and $c1_{env}$ are the CO_2 concentration during accelerated carbonation testing and in natural conditions respectively. A similar approach was also adopted by other researchers to evaluate the rate of natural carbonation from accelerated carbonation test results. (Salvoldi, 2010; Borges et al., 2012). A comparison of the carbonation rate ratio obtained from various literature with the theoretically achieved values as per Equation (2.24) summarised by (Sisomphon and Franke, 2007) is shown in Table 2.4.

Table 2.4 Comparison of ratio of carbonation rates: experimental vs theoretical (Sisomphon and Franke, 2007)

References	$c_{1\ acc}$ (%)	Long term exposure conditions	(k_{acc}/k_{env}) measured	(k_{acc}/k_{env}) theoretical
Dhir et al. (1989)	4.0	Outdoor/sheltered	8.06	10.69
Khunthongkeaw et al. (2006)	4.0	City/sheltered	8.96	10.69
	4.0	City/non-sheltered	10.25	10.69
Ohga and Nagataki (1989)	7.0	Indoor	13.62	14.14
Chin (1991)	7.0	Outdoor/sheltered	14.37	14.14
	12.0	Outdoor/sheltered	19.44	18.51
	18.0	Outdoor/sheltered	20.46	22.68

2.7 MEASUREMENT OF CARBONATION

The conventional method of determining the depth of carbonation is using the phenolphthalein test as specified by the fib Model Code for Service-life Design (2006), and as per RILEM Recommendations (CPC-18, 1988). The methodology behind the test is to determine the carbonation depth by determining the change in pH using phenolphthalein indicator. On complete carbonation, the pH of the concrete pore water reduces from ca. 12.5 to ca. 8.5 (Ballim et al., 2009) and the application of phenolphthalein indicator on the freshly cut/broken surface turns the non-carbonated area pink leaving the completely carbonated area colourless. The carbonation front progression was also determined using other indicators with different

pH thresholds (Jung et al., 2003). Phenolphthalein test only provides information on the state of alkalinity of concrete, and hence the carbonation profile or extent of carbonation cannot strictly be identified. Chemical analysis makes it possible to quantity the mineralogical phases of carbonated or uncarbonated concrete (Villain et al., 2007; Ji et al., 2014)

Other more sophisticated test methods are also used to determine the carbonation profile for concrete, such as powder x-ray diffraction analysis. In this method, X-rays from a Cu source are bombarded on a powdered specimens at different angles, following Bragg's law, and the X-ray diffraction analytical spectra was obtained. The relative diffraction peaks of $CaCO_3$ and CH in the X-ray diffraction analytical spectra were compared, and depending on the intensity distribution and presence of $CaCO_3$ and CH peaks, the concrete specimens are classified as carbonated, partially carbonated and fully carbonated (Chang and Chen, 2006) (see Figure 2.6)

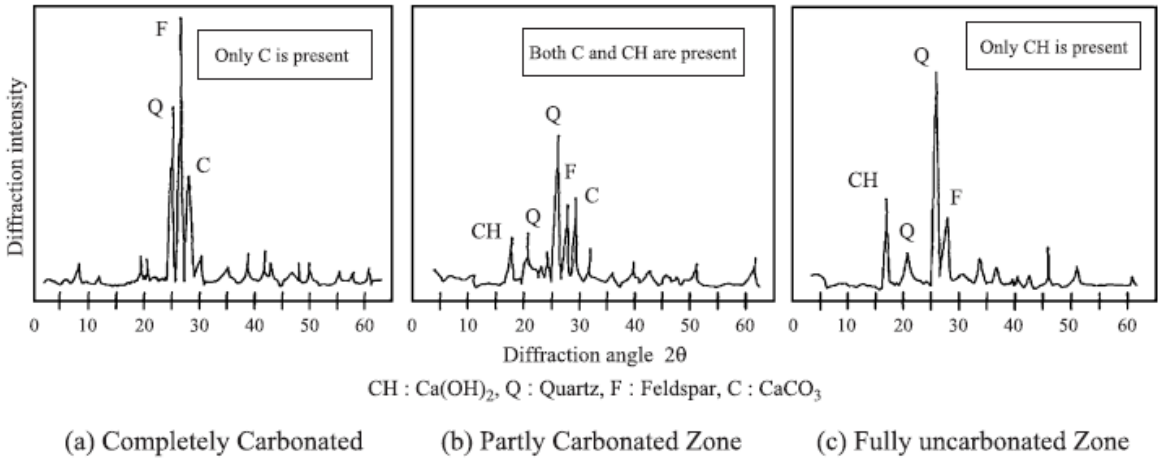

Figure 2.6 X-ray diffraction spectra of concrete specimens indicating the extent of carbonation (Chang and Chen, 2006)

Thermogravimetric analysis (TGA) is another method that can be used to determine the carbonation of concrete by quantifying the calcite and portlandite contents. This uses a thermal analyser provided with a furnace with heating capacity ranging from room temperature to ca. 1500°C. For the determination of the carbonation profile, the powdered concrete/mortar samples from different depths are obtained and heated to 1150°C at the rate of 10°C per minute. The mass variation of the sample with temperature is monitored and the calcite and portlandite contents are calculated from the TGA curve (Villain and Platret, 2006); as each component has a characteristic temperature range of decomposition as shown in Table 2.5.

Table 2.5 Temperature range of decomposition of hydrates and carbonates (Villain & Platret, 2006)

Field	Temperature range	Decomposition of hydrates or carbonaed products
1	25 to 430 °C	Free and adsorbed H_2O, H_2O from C-S-H, AFt, AFm, gypsum, and CO_2 adsorbed in C-S-H
2	430 to 520 °C	H_2O from portlandite $Ca(OH)_2$
3	520 to 620 °C	OH^- from structure of hydrates, structure H_2O or CO_2 from vaterite, and C-S-H carbonation
4	650 to 720 °C	CO_2 from calcite of carbonation
5	720 to 900 °C	CO_2 from calcite of aggregates
6	900 to 1150 °C	Other structural H_2O

*For heating rate of 10 °C/minute.

The carbonation profile of concrete can also be determined using Gamma-ray measurement or Gammadensimetry, whereby the density variation of concrete is determined, since the carbonation of concrete results in a change in density of the concrete. Gammadensimetry is a non-destructive method following Lambert's law and is based on the absorption of gamma photons emitted from a radioactive source of Caesium by the material under investigation. This method is also used to measure the porosity and drying profile of concrete (Villain and Platret, 2006; Villan and Thiery 2006). Other non-destructive techniques such as Nonlinear Resonant Ultrasound Spectroscopy (NRUS) (Bouchaala et al. 2011), and second harmonic generation (SHG) technique in nonlinear Rayleigh surface waves (Kim et al., 2016) have also been adopted to characterise carbonation in concrete.

As discussed above, a variety of test methods and techniques are available to determine carbonation profiles or the depth of carbonation of concrete. However, the choice of method depends on the output as each method has its own advantages, disadvantages and range of precision. Villain and Platret (2006) did a comparative study between TGA, Gammadensimetry and the phenolphthalein test, and observed that the test results of the more sophisticated methods are comparable but slightly more than those from the phenolphthalein test (see Figure 2.7). The difference in test results can be attributed to the fact that the carbonation depth using TGA and Gammadensimetry is based on the CH and $CaCO_3$ and represents the depth at which

the $CaCO_3$ is completely absent, whereas the carbonation depth using the phenolphthalein test is based on change in pH.

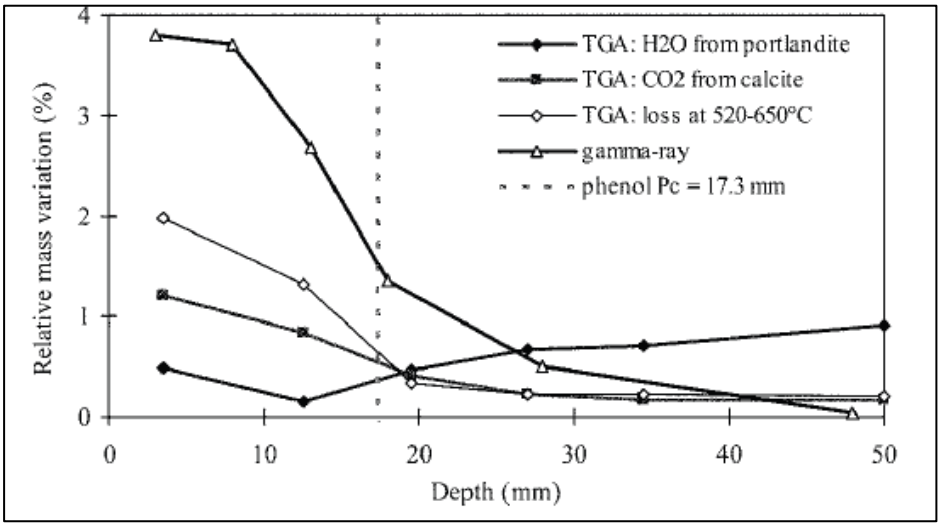

Figure 2.7 Carbonation profile using TGA, Gammadensimetry and Phenolphthalein test (Villain and Platret, 2006)

Table 2.6 Comparison of carbonation depth tests (Salvoldi, 2010)

Test	**Advantages**	**Disadvantages**
Phenolphthalein	• easy, quick, cheap • minimal expertise required • only one plane of fracture needed	• not exact measurement • can be incorrect due to acids, unhydrated cement • semi-destructive
XRD	• gives a qualitative depth and width of the carbonation front	• expensive • destructive • needs considerable expertise • time consuming • samples at different depths needed
Chemical Analysis	• quantitative measurement	• expensive • destructive • needs considerable expertise • time consuming • samples at different depths needed
TGA	• quantitative measurement	• expensive • destructive • needs considerable expertise • samples at different depths needed • disagreement amongst researchers of exact temperature ranges
Gammadensimetry	• non destructive • quantitative	• a baseline measurement is required (i.e. before carbonation)

A detailed comparison of various test methods summarising the advantage and disadvantages of different test methods to assess the carbonation of concrete is as shown in Table 2.6. However, as indicated by Salvoldi (2010) and Bernal et al. (2014), since the pH identification from the phenolphthalein test corresponds to pH at which depassivation of reinforcement steel occurs, the phenolphthalein test can be adopted as an easy, reproducible and practical test method to determine the carbonation depth of concrete.

2.8 CARBONATION MODELS

A number of carbonation models have been developed to predict the depth of carbonation. However, the models found in literature were developed based on different approaches towards modelling, taking into account different factors such as environmental conditions, material properties etc. In general, all the carbonation models can be categorised as Empirical models, Semi-empirical models, and Numerical models.

Empirical models (Parrott, 1987; Ballim, 1994) are easy to use and are developed based on a specific set of experimental data. These models provide good prediction of carbonation depth within the range of material properties and exposure conditions used in deriving the model. However these models will not be able to accommodate variations in mix design, chemical composition of cement, change in quantity of carbonatable material, variation of curing conditions, change in microstructure of concrete, influence of variation in humidity condition etc. Hence the empirical models will not provide accurate prediction of carbonation depth when adopted for other systems different from the original concrete for which the empirical relationship was established.

On the other hand, numerical models developed to predict carbonation (Saetta et al., 1995; Bary and Sellier, 2004) are based on the reaction-diffusion of CO_2, moisture, temperature etc. These are scientifically sound models and are based on proper theoretical understanding of the carbonation process. However, some assumption of initial conditions, approximation of functions and definition of parameters via empirical means is done, resulting in residual errors. In other cases, numerical and iterative methods such as the finite element or finite difference methods are needed to solve these models. Hence these models are not practically easy to use as they require accurate and large input parameters to compute carbonation depths, apart from calibration with experimental results. (Salvoldi et al., 2010; Ta et al., 2016)

Semi-empirical models have the advantage of a theoretical base, and parameters influencing the system are simplified by making assumptions and deriving empirical relationships (Bakker, 1988; Papadakis et al., 1992). Any changes in the mix design, cement compositions, microstructure and RH will be accounted for and hence these models can be adopted to predict the depth of carbonation of different types of concrete. However, the accuracy of the models depend on how well the system is defined based on the set of parameters of the models, and the ability of each parameter to accommodate the variation and their influence on the carbonation process.

In general the carbonation of concrete follows a square root-time relationship. A number of empirical models have been developed based on the square root-time concept, defined by the expression

$$x = A\sqrt{t} \qquad 2.25$$

Where x is the depth of carbonation (mm), A the carbonation coefficient (mm/year$^{1/2}$) (characteristic of the exposure environment and the type of concrete) and t the time (year).

Ballim and Lampacher (1996) proposed an empirical model based on their research on reinforced concrete structures in Johannesburg. They observed a square root relationship as shown in Equation (2.25) and proposed the carbonation coefficient as, A = 3.67 mm/year$^{1/2}$. However, while the proposed model gives a good representation of the rate of carbonation in the Johannesburg area in South Africa, it may not be able to predict the depth of carbonation precisely in other localities in South Africa. This is observed by Alexander et al. (2007) based on the studies conducted by Yam (2004) in different localities in South Africa, who proposed different rate of carbonation for different localities with respect to strength as shown in Table 2.7. It was also observed that the proposed model deviates for the square root-time form for some of the localities. The difference in the carbonation rate and the deviation from the square root-time form may be due to the different environmental conditions to which the concrete is exposed.

Table 2.7 90th Percentile carbonation prediction models for exposed conditions at different localities in South Africa (Alexander et al., 2007)

Locality	Strength grade	Prediction Model
Cape Peninsula	Grade 20	$d_c = 5.94\ t^{0.4}$
	Grade 30	$d_c = 3.48\ t^{0.4}$
	Grade 40	$d_c = 2.95\ t^{0.4}$
Durban (1970-1982)	Grade 25	$d_c = 7.01\ t^{0.4}$
	Grade 35	$d_c = 5.53\ t^{0.4}$
	Grade 45 (sheltered)	$d_c = 4.38\ t^{0.4}$
Durban (1956-1964)	Grade 25	$d_c = 4.18\ t^{0.4}$
Johannesburg	Grade 30	$d_c = 5.00\ t^{0.5}$
	Grade 35	$d_c = 4.65\ t^{0.5}$

On a fundamental platform, the most common approach towards carbonation modelling is based on the solution to Fick's law and mass balance equations, which can be reduced to a square root-time form. Different approaches are adopted in order to define the rate of carbonation. Some of the models use the inverse effective carbonation resistance of concrete, determined using accelerated carbonation test (fib Model Code 2010, 2012). Other models relates diffusion coefficient to the rate of carbonation (Tuutti, 1982; Papadakis et al., 1989). Another approach is based on the gas permeability coefficient (Parrot, 1994; Salvoldi, 2010). Based on a unique approach, Castellote and Andrade (2008) developed a carbonation model which uses the principles of the "unreacted-core" system and depth of carbonation as a function of diffusion coefficient of carbon dioxide through the carbonated layer.

2.8.1 Carbonation Models with Inverse Effective Carbonation Resistance of Concrete as Key Parameter

The inverse effective carbonation resistance of concrete is a parameter which take into account the influence of the concrete quality on the carbonation depth. It can be assessed through direct test methods such as accelerated carbonation tests. It can also be determined from the existing database and literature if the concrete composition is known. In the case of existing structures, inverse effective carbonation resistance of concrete can be obtained based on the measured carbonation depth (Guiglia and Taliano, 2013). A carbonation model based on inverse effective carbonation resistance of concrete is proposed in fib Model Code 2010 (2012) as follows.

$$X_c(t)= \sqrt{2.k_e.\ k_c.R^{-1}_{NAC,0}.\ C_s}\ .\ W(t).\ \sqrt{t} \qquad 2.26$$

Where Xc(t) is the carbonation depth (mm), t is the time (year), k_e is the environmental function, k_c is the execution transfer parameter which takes into account the influence of the curing, Cs is the CO_2-concentration (kg_{CO2}/m^3), W(t) is the weather function and $R^{-1}_{NAC,0}$ is the inverse effective carbonation resistance of concrete, $(mm^2/year)/(kg_{CO2}/m^3)$, under natural conditions (NAC).

The inverse carbonation resistance of concrete under accelerated conditions $R^{-1}_{ACC,0}$ was determined based on accelerated test on concrete specimens with the same composition as that of the design mix and are subjected to the curing regime adopted on site for that project. Since the inverse carbonation resistance under accelerated carbonation varies significantly from the natural condition, a regression parameter which takes into account the influence of the accelerated carbonation test method and error term to compensate the inaccuracies which may occur during the accelerated carbonation test method was introduced. Therefore the inverse effective carbonation resistance determined using accelerated carbonation testing can be related with $R^{-1}_{NAC,0}$ using the following expression

$$R^{-1}_{NAC,0}= k_t.\ R^{-1}_{ACC,0}+ \varepsilon_t \qquad 2.27$$

Where, $R^{-1}_{ACC,0}$ is the inverse carbonation resistance of concrete in an accelerated test under laboratory conditions, kt is the test-method factor (average value: 1.25), ε_t is the error term (average value: 315.5 $(mm^2/year)/(kg_{CO2}/m^3)$). In the case of existing structures, the inverse effective carbonation resistance of concrete can be obtained indirectly by measuring the carbonation depth on the existing structure.

The weather function W(t) is introduced to take into account the influence of rainy days (rainy day is defined by a minimum amount of precipitation of 2.5 mm per day) and its capability to wet the surface based on the average distribution of the wind direction during rain events. This is because in the event of rain, wetting of the concrete will result in the saturation of pores thereby preventing the progression of carbonation.

The carbonation model as per fib Model Code 2010 (2012) is complex and takes into account a large number of parameters to define the carbonation depth. On the other hand, the model prediction will be based on the accelerated carbonation test results. The adaptability or use of

accelerated carbonation test results for natural carbonation is debatable as discussed in the Section 2.6. However the model addresses this issue and provides correlation to convert the inverse effective carbonation resistance based on accelerated tests to values in natural conditions. Nevertheless the correlation is based on limited research work and the adaptability of such a correlation to different test methods and environmental conditions is questionable. Even though the model introduces a weather function to incorporate the influence of rainfall on the carbonation process, the model is not capable of addressing drying/wetting cycles.

2.8.2 Carbonation Models with Compressive Strength as Key Parameter

Compressive strength is a major parameter used to characterise the concrete and often used as proxy to represent the durability. Based on the extensive investigation of carbonation on RC structures (for abutments, piers and tunnels), Guiglia and Taliano (2013) proposed a simplified carbonation model with 28-day compressive strength as the key parameter. The experimental investigation was on about 1350 compression tests on concrete specimens (cores) extracted from the structures and were in the range of 20-50 N/mm2. The model developed was a simplified form of the carbonation model proposed in fib Model Code 2010 (2012); based on compressive strength and RH, as shown below.

$$x_c(t) = 163 \sqrt{k_e \, f_{cm}^{-2.1}} \; \sqrt{t} \qquad 2.28$$

$$x_c(t) = 203 \sqrt{k_e \, f_{cm}^{2.1}} \; \sqrt{t} \qquad 2.29$$

Where, f_{cm} is the 28 day mean compressive strength (N/mm^2), t is the age of the structure in years and k_e is the environmental function depends on RH expressed as follows.

$$k_e = \left\{ \left[1 - \left(\frac{RH_{real}}{100} \right)^5 \right] / \left[1 - \left(\frac{65}{100} \right)^5 \right] \right\}^{2.5} \qquad 2.30$$

Later, Ekolu (2018) developed a carbonation model with 28 day compressive strength as the key parameter and taking into account of the influence of RH, outdoor exposure condition (whether sheltered or unsheltered), CO_2 concentration. The carbonation model as per Ekolu (2018) is as follows.

$$d_{(f,t)} = e_h e_s e_{co} \, cem\left(F_{c(t)}\right)^g \sqrt{t} \qquad 2.31$$

Where, e_h and e_s are the environmental factors for RH and shelter respectively as given below.

$$e_h=16\left(\frac{RH-35}{100}\right)\left(1-\frac{RH}{100}\right)^{1.5} \quad \text{for } 50\% \leq RH \leq 80\% \qquad 2.32$$

$$e_s=\begin{cases} 1.0 \text{ for sheltered outdoor exposure} \\ f_c^{0.2} \text{ for unsheltered outdoor exposure} \end{cases} \qquad 2.33$$

Where f_c is 28 day strength. e_{co} is the environmental factor to take into account the influence of the varying CO_2 ,concentration as given below.

$$e_{co}=\begin{cases} \alpha f_c^r \text{ for } 20<f_c<60 \text{ MPa} \\ 1.0 \text{ for } f_c \geq 60 \text{ MPa} \end{cases} \qquad 2.34$$

Where, α and r ate the correction factors for natural carbonation under varied CO_2 concentration depending on the 28 day strength as given below. 'cem' and 'g' are the factors which depends on the type and proportion of the cementitious material used in the concrete. $F_{c(t)}$ is the parameter which represent the growth rate of compressive strength based on the compressive strength (day or long term) and time. However the model over predicts the carbonation rate for concrete with compressive strength less than 20 MPa and hence the model is only applicable for the carbonation prediction of concrete with strength more than 20 MPa

Both the above mentioned model (Guiglia and Taliano, 2013 and Ekolu, 2018) were based on compressive strength as the key parameter. However the carbonation is a physico-chemical process whereby the CO_2 in the atmosphere diffuse though the concrete pore structure reacts with hydration products in the concrete. The mechanism of carbonation mainly depends on the transport properties and the chemical composition of concrete. Hence, predicting carbonation based on compressive strength as a key parameter is not a suitable approach (as discussed in Section 2.4), as the concrete with the same strength have different chemical compositions and transport characteristic

2.8.3 Carbonation Models with Diffusion Coefficient as Key Parameter

As discussed earlier in this chapter, diffusion is a key mechanism for carbonation of concrete. A number of models have been developed based on the diffusion coefficient as a major parameter. Tuutti (1982) developed a model incorporating diffusion coefficient as a key parameter in the carbonation model. Tuutti's model as discussed in Galan and Andrade (2009) is based on the square root-time relationship. The carbonated zone is assumed to be defined by a sharp front and the CO_2 is assumed to react with the solid phases such that the concentration of CO_2 is assumed to be zero beyond the carbonation front. The model developed is as shown below.

$$\frac{C_s}{C_x}=\sqrt{\pi}.\left(\frac{x/\sqrt{t}}{2.\sqrt{D}}\right).exp\left(\frac{x^2/t}{4.D}\right).erf\left(\frac{x/\sqrt{t}}{2.\sqrt{D}}\right) \quad 2.35$$

Where, C_s is the CO_2 environmental concentration (kmol/m^3), C_x is the CO_2 concentration bound in the concrete (kmol/m^3), x is the carbonation depth (m), t is the time (s) and D is the CO_2 diffusion coefficient (m^2/s).

Diffusion is assumed to take place in a non-stationary state and the diffusion coefficient D is constant and varies only as a function of concrete humidity content. The change in diffusion coefficient due to change in microstructure because of carbonation is not accounted for. A prescriptive approach was used for the estimation of the CO_2 diffusion coefficient using diagrams for O_2 effective diffusion coefficient as a function of the water/cement ratio and the relative humidity (RH) for different type of cements and w/c ratio. Since the moisture content of the concrete is the determining parameter for CO_2 and O_2 diffusion, a satisfactory relative measure of the CO_2 diffusion coefficient can be obtained from the diagrams and is the basis of the assumption (Galan and Andrade, 2009)

Later, Papadakis et al. (1989) proposed a model which is based on the physiochemical process of carbonation. The modelling was based on the assumption that the concrete is initially macroscopically uniform, but structural changes induced due to carbonation, such as change in porosity and pore surface area, need to be considered. Another assumption was that when the porosity is uniform and steady, the liquid water saturation is at equilibrium with the external relative humidity regardless of the amount of H_2O produced or consumed by the chemical reactions (Papadakis et al., 1989). The second assumption shows that the model is not able to take into account the variation of external relative humidity (RH), and therefore the material's hydric state (dry or wet). The carbonation depth in the Papadakis model is as follows.

$$X = \sqrt{\frac{2D^c_{co2}[CO_2]}{[CH]+3[CSH]+3[C_3S]+2[C_2S]}} \quad 2.36$$

Where, $[CO_2]$ is the gaseous concentration of CO_2 (mol/m^3), [CH], [CSH], $[C_3S]$ and$[C_2S]$ is the initial concentration of calcium hydroxide, calcium silicate hydrates, tricalcium silicate and dicalcium silicate respectively (mol/m^3) and D^c_{CO2} is the carbon dioxide diffusion coefficient in the carbonated zone. Based on the experimental data from diffusion test and accelerated carbonation test, Papadakis et al. (1991a) put forward the following empirical formula to estimate the carbon dioxide diffusion coefficient

$$D^{c}_{CO2} = 1.64.10^{-6} \Phi^{c\ 1.8} (1\text{-}RH)^{2.2} \quad 2.37$$

Taking into account the effects of drying/wetting cycles, Bakker (1988) proposed a model based on the assumption that the carbonation only takes place if the concrete is dry enough for the diffusion of CO_2 to take place (ie., not saturated and RH between 50 % to 70 % RH (Richardson, 2002; Neville, 2007)) and the carbonation proceeds as a sharp front following a square root of time relationship as shown below (adopted from Galan and Andrade (2009))

$$x_n = A \sqrt{t_{eff,n}} \quad 2.38$$

Where, t_{eff} is the effective carbonation time which is the sum of the dry periods minus the time it takes to dry out the concrete. According to the model, the maximum depth of carbonation depends on the drying capacity of the concrete since the wetting is assumed to be instantaneous and carbonation will not proceed until the concrete is dry again at the carbonation front. The schematic representation of the Bakker model is shown in Figure 2.8 and the effective carbonation time is presented in Equation (2.39) (adopted from Galan and Andrade (2009)).

$$t_{eff,n} = \left[t_{d1} + t_{d2} - \left(\frac{x_1}{B}\right)^2 + t_{d3} - \left(\frac{x_2}{B}\right)^2 + \cdots\cdots + t_{dn} - \left(\frac{x_{n-1}}{B}\right)^2 \right] \quad 2.39$$

Equation (2.39) can be rewritten as follows

$$t_{eff,n} = \sum_{i=1}^{n} t_{di} - \left[\frac{x_{ci-1}}{B}\right]^2 \quad 2.40$$

Where, A and B are the carbonation and drying rate respectively.

$$A = \sqrt{(2D_c/a).(c_1 - c_2)} \quad 2.41$$

$$B = \sqrt{(2D_v/b).(c_3 - c_4)} \quad 2.42$$

In Figure 2.8, x_n is the carbonation depth after the nth cycle (m), D_c is the CO_2 diffusion coefficient at a given moisture distribution in the pores (m^2/s), t_{dn} is the length of the n^{th} period (s), c_1-c_2 is the CO_2 concentration difference between air and the carbonation front (kg/m^3) and a is the amount of alkaline substance in the concrete (kg CaO/m^3), D_v is the effective diffusion coefficient for water vapour at a given moisture distribution in the pores (m^2/s), b is the amount of water vapour to evaporate from the concrete (kg/m^3) ,and c_3-c_4 is the difference in water vapour concentration at the drying front and outside the concrete (kg/m^3)

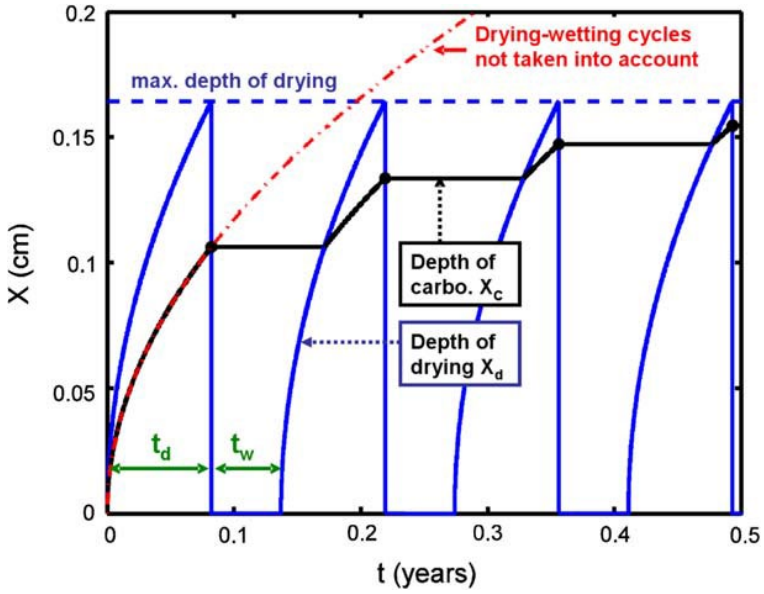

Figure 2.8 Schematic representation of Bakkers model (Thiery et al., 2012)

All the models discussed above adopt diffusion coefficient as the major parameter. However for Tuutti's model, the coefficient is adopted based on a prescriptive approach and the influence of humidity variation is not taken into account. The Papadakis model has a more fundamental approach, based on the physicochemical process of carbonation, and can take into account the variation in chemical composition of the concrete. However, the diffusion coefficient is related to the porosity of concrete which is not the best way to representation of the penetrability of concrete. Also the proposed correlation of diffusion coefficient with porosity is based on the accelerated carbonation test which may have serious implications on the accuracy of the model in predicting the depth of carbonation in natural conditions. Yet again, the models do not accommodate the variation in humidity condition due to the drying/wetting cycles, resulting in overestimation of the depth of carbonation as shown in Figure 2.8. This shortcoming has been rectified by the Bakker model where the influence of drying/wetting cycles has taken into consideration.

2.8.4 Carbonation Models with Permeability Coefficient as Key Parameter

In most of the carbonation prediction models, the diffusion coefficient is related to capillary porosity of the cover concrete which is estimated from the concrete strength, gravimetric analysis or by using empirical relations. Hence, the geometric aspects of pore structure such as the pore size distribution, tortuosity and connectivity are not taken into consideration. However Parrot (1994) proposed a carbonation model taking into consideration the above-mentioned

complexities, where the carbon dioxide diffusion coefficient is represented by the air permeability of the cover concrete. The proposed model is as follows.

$$D = a\, k^{0.4}\, t_i^{n} / c^{0.5} \qquad 2.43$$

Where, k (in units of 10^{-16} m^2) is the air permeability of cover concrete and depends on the relative humidity, r% in the cover concrete

$k = m\, k_{60}$

$m = 1.0$ if $r < 60$

$m = 1.6 - 0.00115\, r - 0.0001475\, r^2$ if $r > 60$

n = power exponent that is close to 0.5 for indoor exposure but decrease as the relative humidity rises above 70% to account for the slower rates of carbonation observed under wetter conditions.

$n = 0.5$ if $r < 70$

$n = 0.02536 + 0.01785\, r - 0.0001623\, r^2$ if $r > 70$

Where, c is the calcium oxide content in the hydrated cement matrix of the cover concrete in kg/m^3 of cement matrix, a is the coefficient that which is assigned a value of 64 based on the available published data. However the variation of atmospheric carbon dioxide concentration is not taken into account.

A similar approach to predict the depth of carbonation, by representing the diffusion coefficient based on the oxygen permeability of cover concrete, was developed by Salvoldi (2010). The oxygen permeability was estimated experimentally as per the UCT Durability Index Testing Procedure Manual (Ver 4.5.1, April 2018). The carbonation model developed by Salvoldi (2010) is as follows

$$x = \sqrt{\frac{2 D_{dry}\, c\beta}{a}} \times \sqrt{t_e} \qquad 2.44$$

Where, 'x' is the depth of carbonation, 'c' is the ambient carbon dioxide concentration (mol/m^3), β is the relative humidity factor, 'a' is the amount of carbonatable material in the concrete matrix (mol/m^3) and D_{dry} is the effective dry diffusion coefficient and is calculated from the oxygen permeability k

$$D_{dry} = \left(1.4 \times \left(\frac{k}{10^{-11}}\right)^{2.2}\right) \times 10^{-11} \qquad 2.45$$

The effective time (t_e) of carbonation over the service life of the concrete, which is based on the 'time of wetness' ToW (defined as the number of days with rainfall more than 2.5 mm per year), is adopted from the fib Model Code 2010 (2012) and calculated as follows

$$t_e = t_{SL} \times (1 - ToW/365) \quad 2.46$$

Where, t_{SL} is the design life of the structure given in years

The carbonation model proposed by Salvoldi (2010) is based on Papadakis model (Papadakis et al., 1989), and representing diffusion coefficient as a function of permeability coefficient. Such an approach is beneficial as the OPI test has been used for durability specifications in South Africa over an extended period, and its application in durability performance prediction has been discussed in Section 2.4. However, like the Papadakis model, the correlation of permeability coefficient with the diffusion coefficient is based on accelerated carbonation test results, and hence the model's accuracy is questionable as discussed earlier. Also, the data set do not cover the wide spectrum of concrete microstructure, since the model is based on concrete cured at 28 days. Even though Salvoldi's model accounts for the effect of RH and takes into account rainfall or wetting, the model does not cater for the effect of drying cycles on the carbonation process. Therefore a carbonation model taking into account the influence of drying/wetting cycles using natural carbonation data for an extensive range of concretes, with coefficient of permeability from OPI test as a key parameter, needs to be developed.

2.9 SUMMARY

A detailed review on the mechanism of carbonation in concrete and the factors which influence the process of carbonation is presented in in this chapter. The various transport mechanisms by which the aggressive agents move through the concrete pore structure were studied, and the interrelationship of different mechanisms highlighted. Carbonation is a slow process and hence accelerated carbonation studies are done to understand the behaviour of concrete during carbonation, and to be able to predict long-term carbonation under natural conditions. However, the literature show contradictory views on the difference between accelerated and natural carbonation processes, and does not significantly support prediction of natural carbonation based on accelerated studies. A detailed summary of different test procedure used to measure the degree of carbonation, and certain existing carbonation modes are also presented in this chapter. Different approaches towards carbonation modelling by adopting various assumptions and correlations can be observed in the literature. However, a comprehensive

model efficiently addressing all the parameters influencing the mechanism of carbonation that can be adopted for South African conditions is still lacking. In South Africa, durability indexes have been widely used towards performance-based durability specifications and design. Studies show good correlation of carbonation depth with OPI, and attempts have been made to develop carbonation models with the durability index of OPI as a key parameter, based on accelerated carbonation studies. Nevertheless, the influence of variation in moisture due to drying/wetting cycles and the effect on carbonation is not addressed. Hence a carbonation model with OPI as one of the key variables which can address the variation in microstructure due to material, constructional and environmental factors and the influence of drying/wetting cycles needs to be developed. This is presented in the following chapters along with the experimental programme adopted for the current research.

CHAPTER 3: EXPERIMENTAL PROGRAMME AND DETAILS

3.1 INTRODUCTION

The principal mechanism of carbonation of concrete, and the influence of various factors including cement extenders on the rate of carbonation, were explained in the previous chapter. A detailed comparison of the various models predicting the depth of carbonation was done, and drawbacks of the current models and the scope of further research were also pointed out. Though carbonation is a long-term process, certain environmental conditions (especially the moisture conditions) and material characteristics can affect the rate of carbonation. However it is evident that most service life prediction models rely on the depth of carbonation reaching the level of the steel as the limit state for carbonation-induced corrosion. The presence or absence of moisture, which has a major role both in terms of carbonation and corrosion, is seldom taken into consideration.

A number of variables are associated with different carbonation models. In order to understand a model and to validate the suitability of a model, a range of experimental or in situ data is necessary. Consequently, the main objective of this chapter is to discuss the experimental techniques that were used in the present work for characterising the variables involved, and which were required to validate the model that was adopted and developed for the current research.

In this chapter, the material constituents used in the research are first detailed, followed by the description of the various tests. The strength of the concrete was obtained by preparing concrete specimens as per SANS 5861-3:2006 and thereafter conducting the standard compressive strength test as per SANS 5863:2006. The permeability characteristics of different concrete mixes with different combinations of curing conditions were measured using the Oxygen Permeability Index (OPI) test according to SANS-3001-CO3-1&2. Accelerated and natural carbonation tests were done to obtain the depth of carbonation at different ages. In order to measure the moisture profile of the concrete, a modification of the method used by Parrott (1988) was adopted.

3.2 MATERIALS AND SPECIMEN DETAILS

A number of concrete mixes with different combinations of cement extenders and a range of w/b ratios under varying curing conditions, analogous to the concrete used in industry, were designed for the present research. The materials used in the concretes were:

- Cement of types CEM I 52.5 N and CEM II B-L 42.5 N, the normal EN 52 grade cement and EN 42 grade cement respectively, with CEM II B-L 42.5 N containing a moderate content of limestone (chemical composition, see Table 3.1). The choice of the cements was on the basis that CEM I 52.5 N was a widely-used cement for many structures in the South African construction industry. CEM II B-L 42.5 N is a limestone-based cement with a lower carbon footprint.

- The fine aggregate used was a blend of dune sand and granite crusher sand at a ratio of 40:60, which is commonly used in industry

- Coarse aggregate used was crushed granite of nominal maximum size 13 mm. Aggregate size of 13 mm was chosen (opposed to commonly used 19 mm aggregate) in order to get more data point (higher mortar content along the cross sectional area) for carbonation depth measurements. Furthermore, the coarse aggregate content was kept constant 1000 kg/m^3 for all the mixes in order to avoid the influence of aggregate content on test results. The selection of granite for both coarse and fine aggregate was to avoid any other form of chemical reaction (e.g. alkali silica reaction etc.) of aggregate with cement, since the granite is chemically 'inert'.

- The cement extenders (also known as cement additions, sourced in South Africa): low calcium fly ash at 30% replacement and ground granulated blast furnace slag (GGBS) at 50% replacement by mass (chemical composition, see Table 3.1), are the most economical and widely used form of cement extenders in South Africa.

- The water content in all the mixes was kept constant at 170 L/m^3 (in order to study the influence of binder content on test results) with w/b ratios of 0.45, 0.55 and 0.65 (the w/b of majority of the concrete mixes used in the construction industry are in this range). Details of the mix constituents and proportions of the mixes are shown in Table 3.2. A total of twelve different concrete mixes were developed, using three

different w/b and four different binder combinations. In Table 3.2 the concrete mixes are labelled based on the binder combination of the mix - PC (CEM I 52.5 N only), FA (70% CEM I 52.5 N + 30% fly ash), GS (50% CEM I 52.5 N + 50% GGBS) and LS (CEM II B-L 42.5 N only); and the corresponding number indicated the w/b ratio in percentage terms. For example PC-55 refers to the concrete mix with CEM I 52.5 N binder and w/b of 0.55; whereas, GS-45 refers to the concrete mix with a binder combination of 50% CEM I 52.5 N and 50% GGBS with a w/b of 0.45.

- Superplasticizer (SP) (Sika ViscoCrete10 - details see Appendix A) at varying dosage for each mix was used in order to maintain the slump in the range of 90-120 mm.

Table 3.1 Chemical composition of cement (tested at PPC Montague Gardens, Cape Town)

Composition		**CEM I 52.5 N**	**CEM II B-L 42.5 N**	**Fly ash**	**GGBS**
		% by weight			
Calcium oxide (CaO)		63.20	61.60	4.79	34.80
Silica (SiO_2)		20.20	18.00	52.80	36.40
Alumina (Al_2O_3)		4.03	3.92	31.80	12.70
Iron oxide (Fe_2O_3)		3.19	3.05	3.09	0.80
Magnesia (MgO)		0.91	2.26	1.06	7.52
Sulphur anhydrite (SO_3)		2.64	1.61	0.62	2.50
Phosphorus pentoxide (P_2O_5)		0.15	0.04	0.00	0.05
Manganese (III) oxide (Mn_2O_3)		0.10	0.46	0.05	0.92
Titanium dioxide (TiO_2)		0.24	0.34	1.62	0.82
Total loss on ignition		4.08	8.43	0.80	0.86
Total chloride content (Cl)		0.01	0.00	0.00	0.02
Available alkali	Na_2O	0.18	0.08	0.32	0.40
	K_2O	0.67	0.22	1.78	1.94
Total		**99.60**	**100.01**	**98.73**	**99.73**

Table 3.2 Concrete mix proportions

Mix Designation	CEM I 52.5N	FA (30%)	GGBS (50%)	CEM II B-L 42.5 N	Crusher Sand	Dune sand	13mm Granite	Water	w/b
	(kg/m^3)								
PC-45	377	0	0	0	511.8	341.2	1000	170	0.45
FA-45	264	113	0	0					
GS-45	188.5	0	188.5	0					
LS-45	0	0	0	377					
PC-55	309	0	0	0	552.6	368.4	1000	170	0.55
FA-55	216	93	0	0					
GS-55	154.5	0	154.5	0					
LS-55	0	0	0	309					
PC-65	262	0	0	0	580.8	387.2	1000	170	0.65
FA-65	183	79	0	0					
GS-65	131	0	131	0					
LS-65	0	0	0	262					

The mixing of concrete and the fabrication of specimens was done at the concrete laboratory of the University of Cape Town (UCT), Cape Town and also at the concrete laboratory of the University of the Witwatersrand (Wits), Johannesburg. The choice of two laboratories was due to the curing regimes adopted. The mixing of concrete and the fabrication of all the concrete specimens which were subjected to the curing regime 'Curing-D' (see Table 3.5), were done at the concrete laboratory of Wits. The curing regime 'Curing-D' represents 'harsh' curing conditions (details see below), achieved by exposing the specimens to outdoor natural environment sheltered from rain (20-22°C and 50-55% RH, see details below), on the roof of the Hillman Engineering Building, Wits, Johannesburg (-26.192209, 28.029418). The rest of the concrete specimens used in this research (subjected to the curing regimes Curing-A, Curing-B and Curing-C) were fabricated in the concrete laboratory of UCT. The casting at UCT for each concrete mix was done in three batches (namely Batch-a, Batch-b and Batch-c), due to the smaller capacity of the concrete mixer (50 liters). The mixing of concrete, fabrication of specimens and the curing were done in the following sequence:

- The cement and the aggregates were dry-mixed in a pan mixer of 50 litres capacity for 1 minute.

- This was followed by adding water corresponding to 80% of the total water content and continuing mixing for another 1 minute.

- Finally the SP was added along with the remaining 20% of the water and then mixed for two further minutes. The SP dosage was increased in small increments until the target slump in the range of 90-120 mm was achieved, which is determined as per SANS 5862-1:2006 (details of SP dosage used in different concrete mix is given in Table 3.3).

- The concrete was then filled in the moulds in layers of about 50 mm thickness and compaction was done using a table vibrator for a period of two minutes, and finally the top surface was levelled using a trowel. Moulds of four different sizes and materials used are shown in Table 3.4.

- Four different curing regimes as shown in Table 3.5 were adopted to achieve OPI values in the range of 9.0-10.8 at 28 days after casting. Curing-A is the standard 28 days water curing in a water bath maintained at a temperature of 23 - 25°C. Curing-B and Curing-D were adopted to replicate harsh curing practice on site, where the demoulding was done after one day of casting and the concrete was left to cure in air. In the case of Curing-B the specimens were stored in a laboratory environment (concrete laboratory of UCT; 20-22°C and 60-70% RH) after 1 day of casting till 28 days. For Curing-D, the specimens were exposed to outdoor natural environment sheltered from rain subjected to large variation in RH conditions, unlike the laboratory environment. The specimens were stored on the roof of Hillman Engineering Building, Wits, Johannesburg (-26.192209, 28.029418), after one day of casting, where the average RH is in the range of 50-55%. Curing-C was designed to replicate moderate curing practice where the concrete was cured for 7 days using plastic sheeting. For Curing-C, after 1 day of casting, the specimens were covered with plastic sheeting for 6 days and thereafter the specimens were stored in a laboratory environment (concrete laboratory of UCT; 20-22°C and 60-70% RH) until 28 day after casting.

Table 3.3 SP dosage and slump achieved for the different concretes

Mix Designation	Dosage range (% by weight of cement)	Slump range (mm)
PC-45	0.2-0.66	90-120
FA-45	0.2-0.45	
GS-45	0.68-0.88	
LS-45	0.34-0.43	
PC-55	0.18-0.36	
FA-55	0.13-0.78	
GS-55	0.49-1.02	
LS-55	0.3-0.45	
PC-65	0.13-0.60	
FA-65	0.08-0.91	
GS-65	0.43-1.05	
LS-65	0.21-0.55	

Table 3.4 Dimensions of concrete specimens and the material used for the moulds.

Material used for the mould	**Dimensions of the cast specimen**	**Use of the cast specimen**
Rigid Rubber	100x100x100 mm	Compressive strength test
Wood	100x100x200 mm	Carbonation test
Steel	100x100x500 mm	Carbonation test/Oxygen permeability index test
Combination of wood and polyvinyl chloride (PVC)	100x100x150 mm	Moisture profile measurement

Table 3.5 Curing regimes adopted

Curing Designation	Details of curing conditions
Curing-A	Curing in water bath maintained at a temperature of 23 - 25°C (until 28 days after casting)
Curing-B	1 day in moulds, then in air inside lab (until 28 days after casting at 20-22°C and 60-70% RH)
Curing-C	1 day in moulds, 6 days covered by plastic then in air inside lab (until 28 days after casting at 20-22°C and 60-70% RH)
Curing-D	1 day in moulds, then kept in an outdoor sheltered environment (until 28 days after casting at 20-22°C and 50-55% RH).

3.3 TESTING

3.3.1 Compressive Strength

The compressive strength of concrete is an indicator of the strength performance of concrete during its serviceable life and is characteristic of the particular concrete mix. In the present research, the compressive strength was determined on all concretes prepared as described in Section 3.2. The determination of compressive strength was carried out in accordance with SANS 5863:2006. In the present research, nine cubes per mix were cast (three cubes per testing age) and cured in a water bath maintained at a temperature of 23 - 25°C for 28 days. The testing was performed at ages of 3, 28 and 90 days using a manually-operated Amsler hydraulic compression testing machine. Each compressive strength result corresponds to an average of the determinations from three specimens.

3.3.2 Oxygen Permeability Index Test

The oxygen permeability index (OPI) test was done as per the UCT Durability Index Testing Procedure Manual (Ver 4.5.1, April 2018) (SANS-3001-CO3-1&2). The specimens were obtained from beams of dimension 100x100x500 mm, made from twelve different mixes with different curing regimes as explained in Section 3.2. Each test specimen consisted of a 70 ± 2 mm diameter, 30 ± 2 mm thick concrete disc. The specimens were acquired by coring the beam perpendicular to the casting direction at the ages of 28 days and 90 days. 5 mm slices on either end of the core were cut off and discarded to avoid any wall effect. From the remaining core, two concrete discs of required thickness (30 ± 2 mm) were cut, one from each end, and the rest of the core was discarded. For the OPI test, four specimens were needed and were obtained from two cores of the same beam as discussed above.

Directly after cutting, the specimens were conditioned by placing them in an oven at 50 ± 2°C for 7 days ± 4 hours. This was followed by cooling the specimens to 23 ± 2 °C in the desiccator for a period of no less than 2 hours and no longer than 4 hours. The specimen was then placed and clamped on the top of the test chamber and the testing was commenced by introducing oxygen gas in the test chamber of the OPI testing apparatus (see Figure 3.1). The test chamber was initially maintained at a pressure of 100 ± 5 kPa and the subsequent pressure drop with time was noted. The D'Arcy coefficient of permeability was then calculated for each specimen from the data obtained. The OPI is expressed as the average of the negative log of the coefficients of permeability of the specimens (details of the test and calculation: see UCT Durability Index Testing Procedure Manual (Ver 4.5.1, April 2018) and SANS-3001-CO3-1&2.

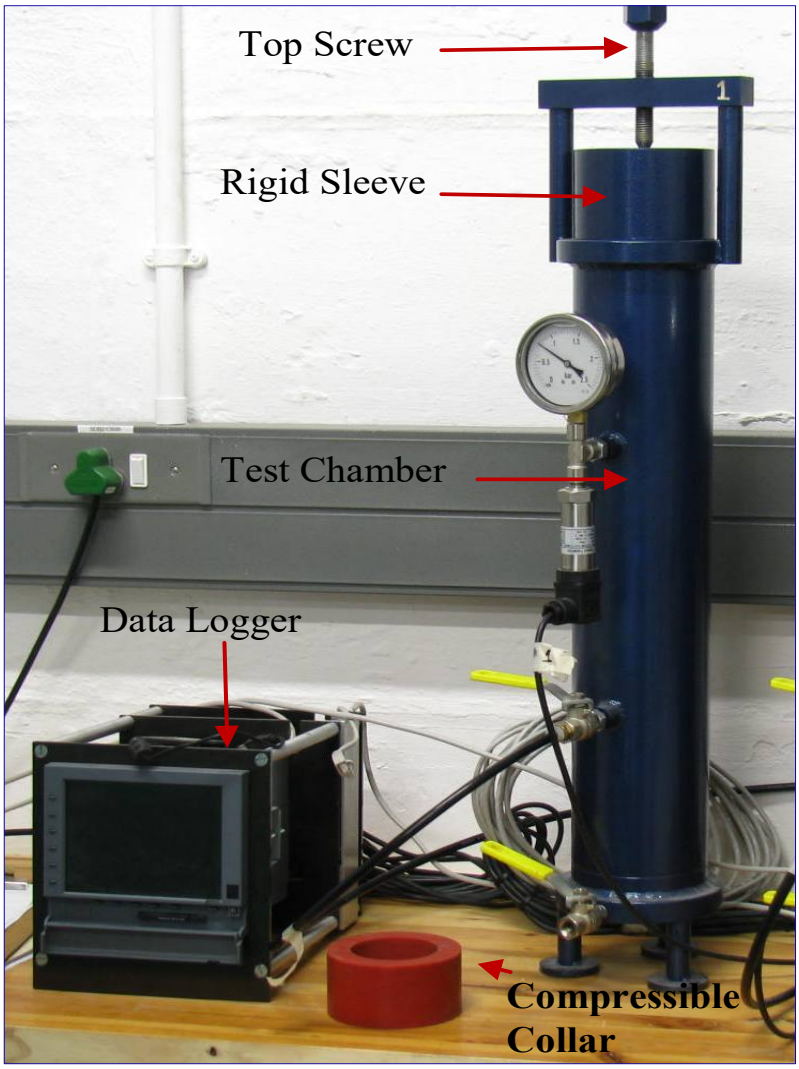

Figure 3.1 Oxygen Permeability Index test apparatus

3.3.3 Moisture Profile Measurement

A variety of techniques are available for moisture profile measurements. In the current research, the moisture condition of concrete was expressed in terms of relative humidity (RH), using a modified version of the method used by Parrott (1988). The RH measurement was done on concrete prisms of dimensions 100x100x150 mm cast using a specially designed mould which contained seven removable steel pins, 7 mm diameter and 80 mm long, with a PVC collar 20 mm diameter and 16 mm long at one end (which was embedded in the concrete after casting) as shown in Figure 3.2 and Figure 3.3. The pins were arranged parallel to each other and at a distance of 4, 8, 12, 20, 30, 50 and 80 mm from the bottom of the mould as shown in Figure 3.3. Once the concrete hardened, the steel pins were removed by unthreading them from the PVC collar, leaving a cavity of 7 mm diameter and 80 mm long inside the concrete. The specimens were then demoulded and the cavity sealed off by inserting a silicon button (with a small slit in the middle) in the collar and covered with a hollow PVC cap as shown in Figure 3.4. The opening of three cavities can be seen in Figure 3.4, the opening of the remaining four cavities are on the opposite face of the same specimen (see Figure 3.2). The specimens were subjected to different curing conditions as shown in Table 3.5. For the specimens cured in the water bath, the steel pins were inserted back into the specimen after demoulding till the end of curing period. Thereafter the surface of the specimen was coated with epoxy except the bottom face in the casting direction. This was done to ensure that moisture and water vapour movement took place unidirectionally (see Figure 3.4).

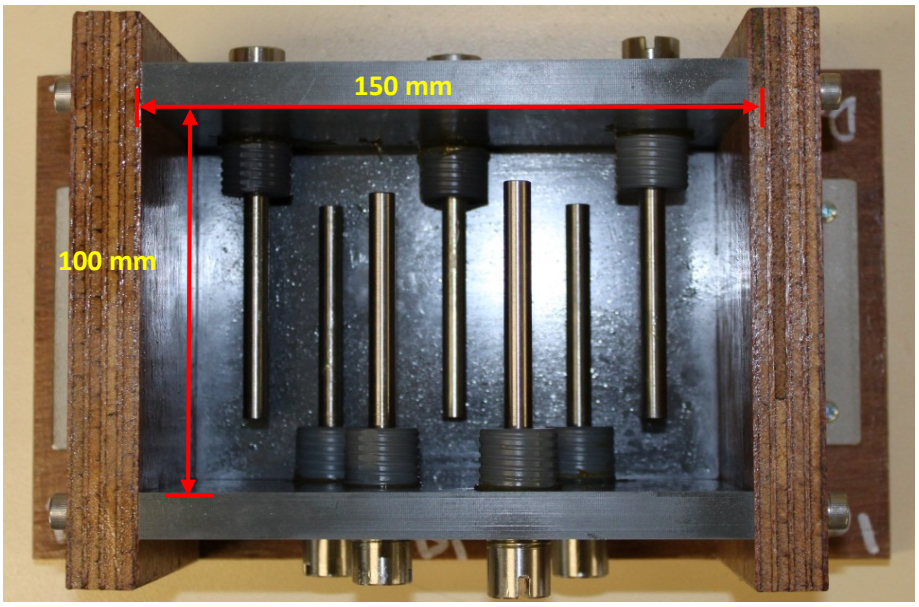

Figure 3.2 Plan View of mould used for casting concrete specimens for moisture measurement

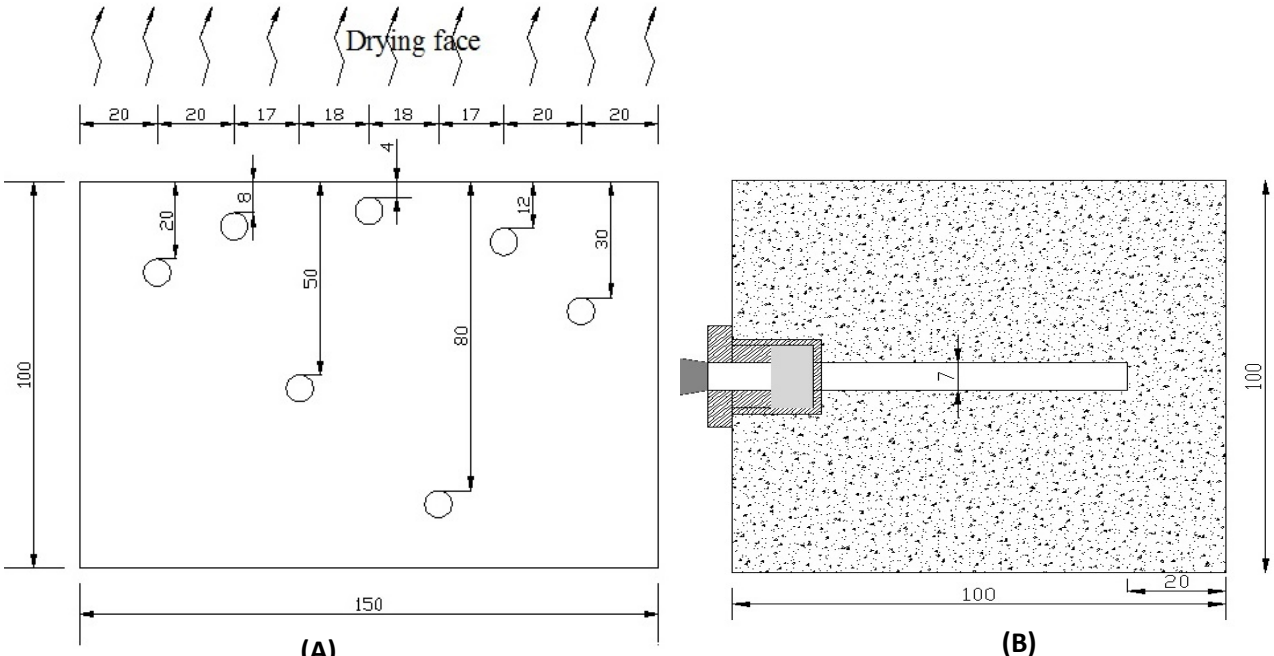

Figure 3.3 Arrangement of cavities in concrete prism (A) Elevation, (B) Cross-section through cavity

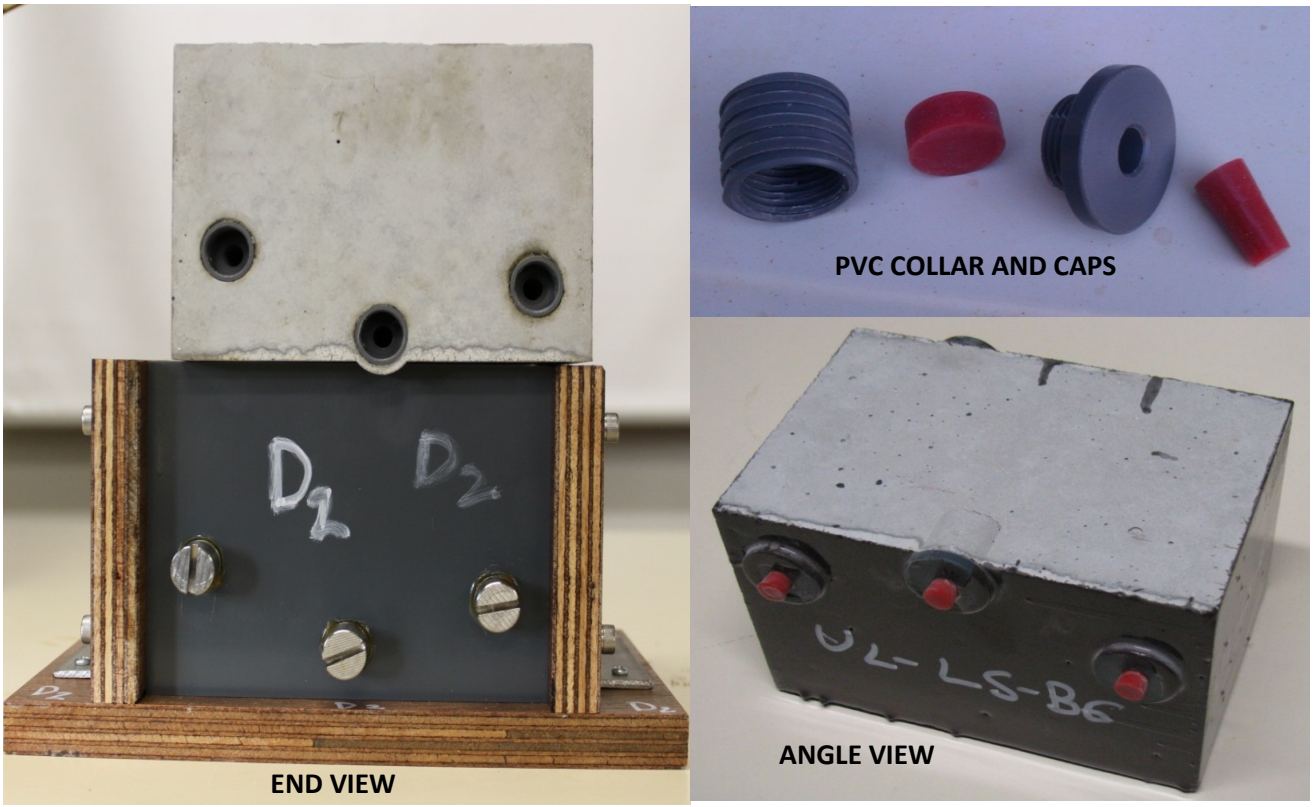

Figure 3.4 Specimen for moisture measurement after demoulding and epoxy coating

In the current research, six sets of 48 specimens (with twelve different mixes × four different curing conditions, see Table 3.2 and Table 3.5) were cast as described above, for humidity measurements, and exposed at six different site locations as described in Table 3.6. The site locations were selected to accommodate a range of environmental conditions. As discussed in Chapter 1, two localities with different climatic conditions, namely Cape Town and Johannesburg, were chosen. Cape Town climate is characterised by cool, wet winters and warm, dry summers whereas Johannesburg experiences cold, dry winters and warm summers with mainly short precipitation periods (Alexander et al., 2007). The two localities provide very different climatic conditions especially in terms of precipitation, and hence provide a general overview of the extent of variation of climatic condition in South Africa. The different exposure conditions adopted for the experimental programme in this research were as follows

- Exposed to outdoor environment and (mainly winter) rain (on UCT Upper Campus, Cape Town, and Wits East Campus, Johannesburg (details in Table 3.6))
- Exposed to outdoor environment but sheltered from rain (on UCT Upper Campus, Cape Town, and Wits East Campus, Johannesburg (details in Table 3.6))
- Exposed to indoor environment (parking garage of Cavendish Square shopping centre, Claremont, Cape Town - with average environmental conditions of 22°C, 60% RH)
- Exposed to indoor laboratory environment (UCT concrete laboratory with average environmental conditions of 20°C and 50% RH)

After coating the specimens with epoxy (on the non-exposed surfaces), the initial moisture readings at different depths from the exposed surface were taken. The measurement was done using a 5 mm diameter humidity probe (HC2-P05 from Rotonic Measurement Solutions with measurement range: -40 to 85°C / 0 to 100 % RH) attached to a digital hygrometer (HygroPalm 23-A from Rotonic Measurement Solutions with measurement range: -10 to 60°C / 0 to 100 %RH) as shown in Figure 3.5. After the initial measurement was taken, the specimens were exposed at the six different sites as described in Table 3.6. The specimens from each site were transported back to the lab after field exposure, and the RH measurement was done in lab

conditions. After the RH measurements, the specimens were returned to their respective locations and the process repeated for all sites at appropriate intervals.

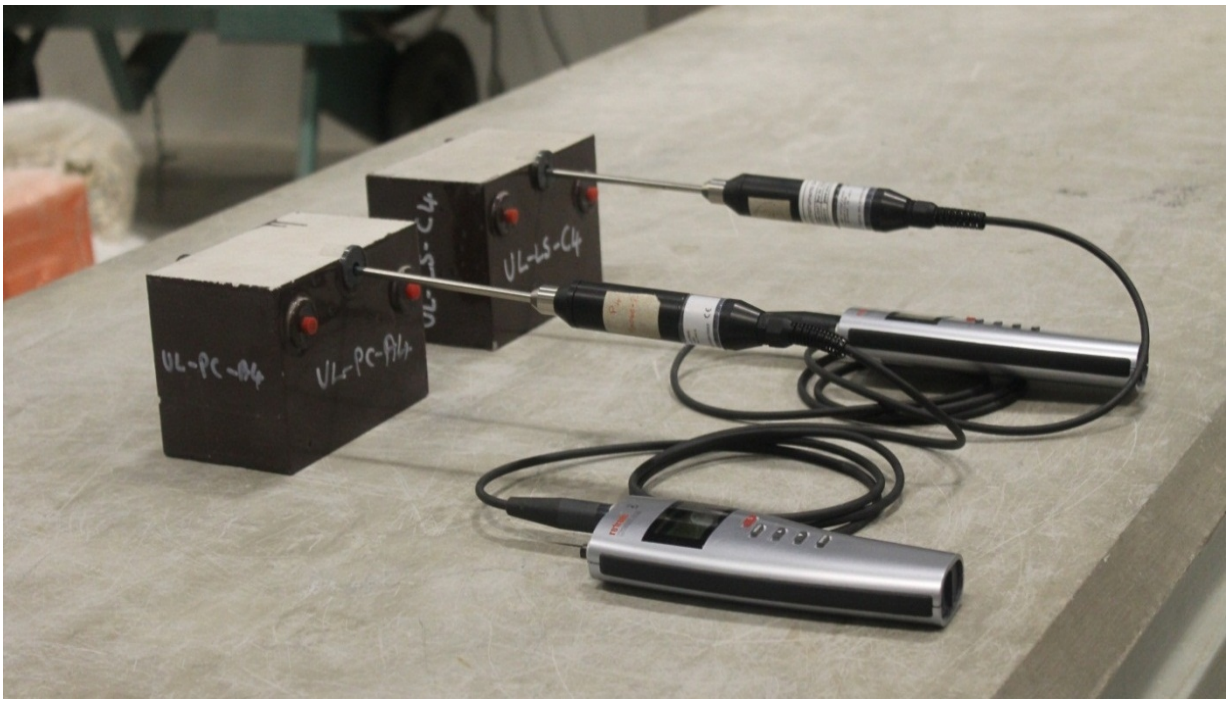

Figure 3.5 Moisture measurement using humidity probe and digital hygrometer

3.3.4 Carbonation – Natural Conditions

The natural carbonation test was conducted on prisms of dimensions 100x100x200 mm. Similar to the moisture measurement specimens, five sets of 48 specimens (with 12 different mixes × 4 different curing conditions, see Table 3.2 and Table 3.5) were cast. A beam of 100x100x500 mm was cast and the specimens were subjected to different curing conditions as shown in Table 3.5. At the end of the curing period, specimens of dimensions 100x100x200 mm were cut from the 100x100x500 mm beam. The surface of the specimen was coated with epoxy except the two opposite faces perpendicular to the casting direction. This was done to allow bi-directional carbonation front progression from two opposite faces perpendicular to the casting direction (see Figure 3.6). After coating the specimen with epoxy, the specimens were exposed at the different sites (see Table 3.6), without any preconditioning.

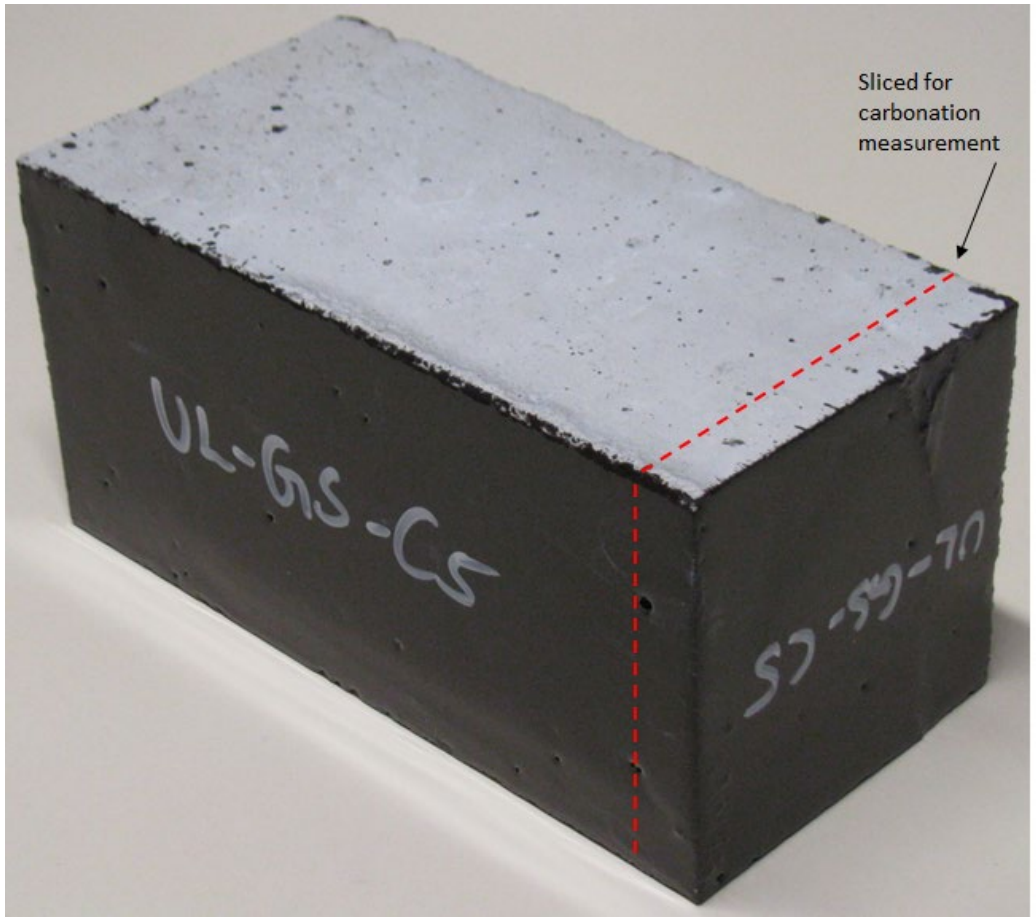

Figure 3.6 Specimen for carbonation test after epoxy coating

Table 3.6 Site locations for carbonation and moisture measurements.

Site Designation	Location	Site condition	Specimens on site
ME	Roof of Menzies building, UCT, Cape Town (-33.958662, 18.460060)	Exposed to outdoor environment and rain with average environmental conditions of 19°C, 68% RH and CO_2 concentration of 358 ppm)	
MS	Roof of Menzies Building, UCT, Cape Town (-33.958662, 18.460060)	Exposed to outdoor environment but sheltered from rain with average environmental conditions of 19°C, 68% RH and CO_2 concentration of 358 ppm)	

Table 3.6 continued…

Site Designation	Location	Site condition	Specimens on site
WE	Roof of Hillman Building, Wits University, Johannesburg (-26.192209, 28.029418)	Exposed to outdoor environment and rain with average environmental conditions of 19°C, 50% RH and CO_2 concentration of 272 ppm)	
WS	Roof of Hillman Building, Wits, Johannesburg (-26.192209, 28.029418).	Exposed to outdoor environment but sheltered from rain with average environmental conditions of 19°C, 50% RH and CO_2 concentration of 272 ppm)	

Table 3.6 continued…

Site Designation	Location	Site condition	Specimens on site
CD	Cavendish Square Parking garage, Claremont, Cape Town. (-33.980243, 18.463574)	Exposed to indoor environment (parking garage) with average environmental conditions of 22°C, 60% RH and CO_2 concentration of 550 ppm)	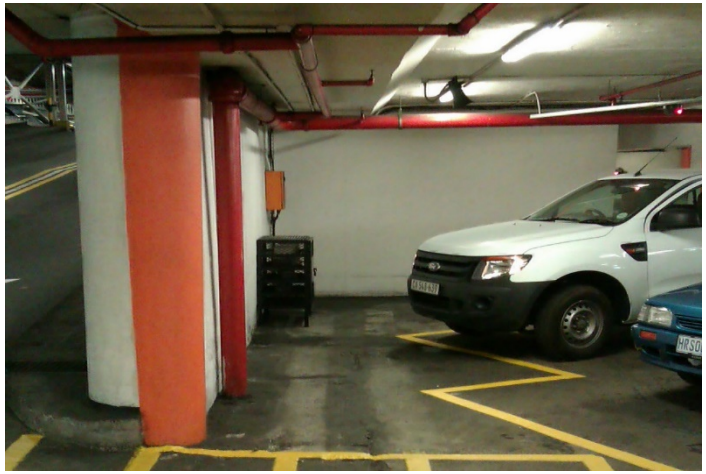
UL	UCT Concrete Laboratory (-33.958804, 18.459149)	Exposed to indoor laboratory environment (average values of 20°C and 50% RH).	

3.3.5 Test for Depth of Carbonation

Carbonation depth was measured using Phenolphthalein indicator. The specimens from site were transported back to the lab, and the carbonation depth measurement was done in lab conditions. The carbonation depth was measured by applying a 1% solution of Phenolphthalein in a mixture of water and alcohol, on the freshly cut surface of 15 mm thick slices removed from the specimens as shown in Figure 3.6. Although some literature is in disagreement with the approach of cutting concrete specimen for Phenolphthalein test due to the possible contamination of cut surface during the cutting process, necessary precaution was taken in this study by thoroughly washing the cut surface. The application of Phenolphthalein solution on the freshly cut surface causes the un-carbonated area change its colour to pink whereas the carbonated area remains colourless (or unchanged) as shown in Figure 3.7. The depth of colourless area from the exposed surface of the specimen was measured using a Vernier Calliper. A minimum of six readings was taken on each side and the average of the twelve readings was recorded as the depth of carbonation. Afterwards, the freshly cut surface was resealed with epoxy and allowed to dry for one day in laboratory conditions (site UL). The specimens were then returned to their respective locations (or re-introduced to the carbonation chamber in the case of accelerated carbonation) and the process repeated for all sites.

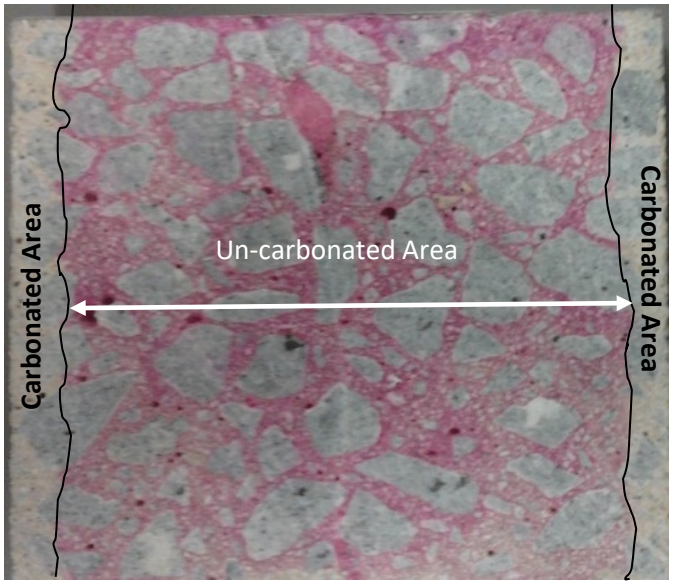

Figure 3.7 Concrete cross-section after applying phenolphthalein

3.4 CLOSURE

This chapter highlighted the characteristics of the material components and the mix proportions and curing conditions adopted for the research. Cement types CEM I 52.5 N and CEM II B-L 42.5 N, 13 mm crushed granite coarse aggregate, a blend of dune sand and granite crusher as fine aggregate, and w/b ranging from 0.45 to 0.65 were adopted in the current research. The choice of the materials and the mix proportions were based on availability and common usage in the South African construction industry.

Four different curing regimes were adopted; representing good quality standard curing in controlled laboratory conditions, to poor quality site curing, and also with the aim of achieving a broad range of concrete permeability and carbonation rates. The methodology used for the determination of permeability was also emphasised in this chapter.

The method used for the determination of moisture profiles of the concrete, along with a comprehensive explanation of the experimental techniques used to study the carbonation of concrete both in natural and accelerated conditions, was detailed. Six different site locations were described, with two outdoor locations exposed to rain, two outdoor locations sheltered from rain, and two indoor locations - one a parking garage and the other a standard laboratory condition. The choice of the site locations was based on the aim to cover all the key environmental conditions pertaining to carbonation of concrete.

CHAPTER 4: EXPERIMENTAL RESULTS AND DISCUSSION

4.1 INTRODUCTION

Carbonation of concrete is influenced by a number of factors, both internal and external, and hence a detailed experimental programme covering all the aspects was needed to understand the inter-relationship of these factors. Therefore, an experimental programme taking into account the key factors affecting the process of carbonation on a wide range of concretes used in general practice was designed for this research. The previous chapter detailed the experimental programme, emphasising the materials used, their characteristics, mix proportions, and curing regimes adopted. Furthermore, the different test methods adopted for determining strength, permeability and depth of carbonation were also explained.

This chapter presents the detailed test results of all the experiments summarised in Chapter 3. The carbonation model will be developed in Chapter 5, based on the experimental data, focusing mostly on the permeability coefficient and depth of carbonation under natural conditions. For the experimental programme, a total of twelve different concrete mixes were developed, using three different w/b and four different binder combinations. Concrete mix proportions and the mix designations were given in Table 3.2. The characterisation of the concretes used in this research in terms of oxygen permeability index was done, and is presented in this chapter. The compressive strength of all the concrete mixes at 3, 28 and 90 day are given. Finally, the test results of carbonation depth of specimens exposed at different locations under natural and accelerated conditions are presented and discussed along with the moisture profile data of concrete specimens exposed to different environmental conditions.

4.2 COMPRESSIVE STRENGTH

Compressive strength test results are shown in Figure 4.1 (except for LS-45, LS-55, LS-65 due to shortage of cement). Each compressive strength result corresponds to an average of results from three specimens and the error bars represent ± 1.0 standard deviation. Detailed test results are given in Appendix B. The test results show the influence of strength with age. As expected, all the specimens gained strength with time irrespective of the mix proportions and w/b. This can be attributed to the on-going cement hydration and pozzolanic reactions. It can be observed from Figure 4.1 that, with increase in w/b, the strength gain decreases, irrespective of the age of testing and concrete mix.

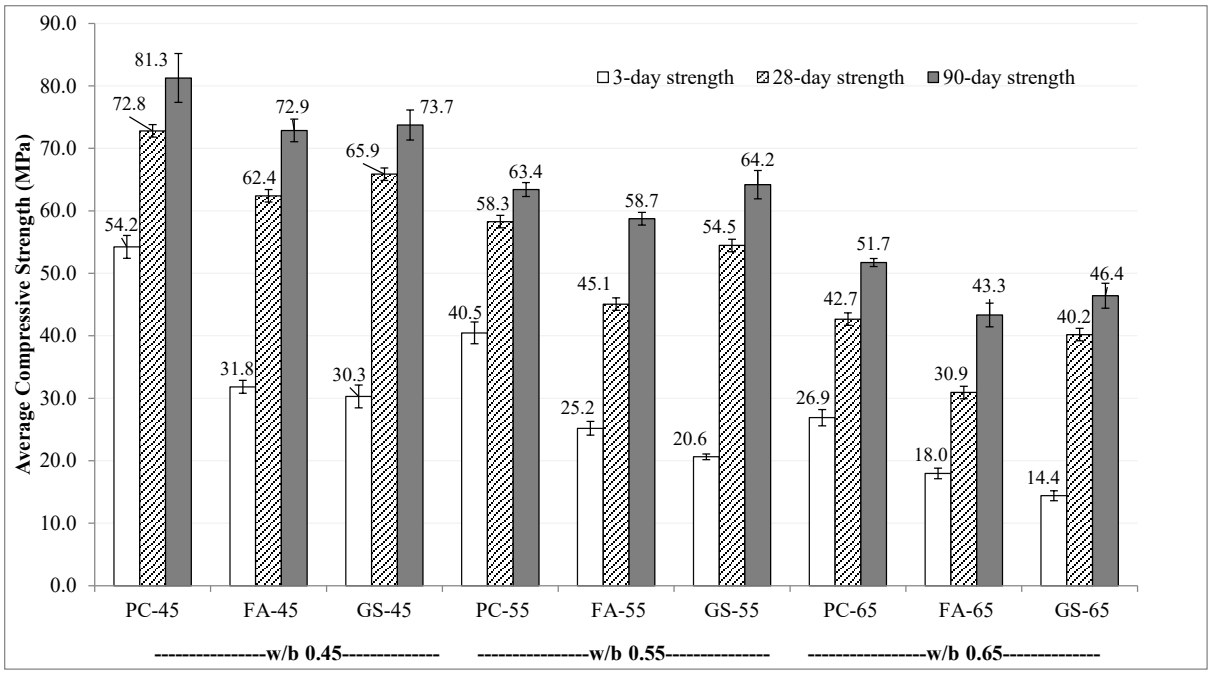

Figure 4.1 Compressive strength results at 3, 28 and 90 days

The compressive strength gain over 3 time periods is shown in Figure 4.2. In general the strength gain of concrete mixes having cement extenders (mixes such as FA and GS) is greater in the later time periods, compared to the concrete mixes with Portland cement only (PC).

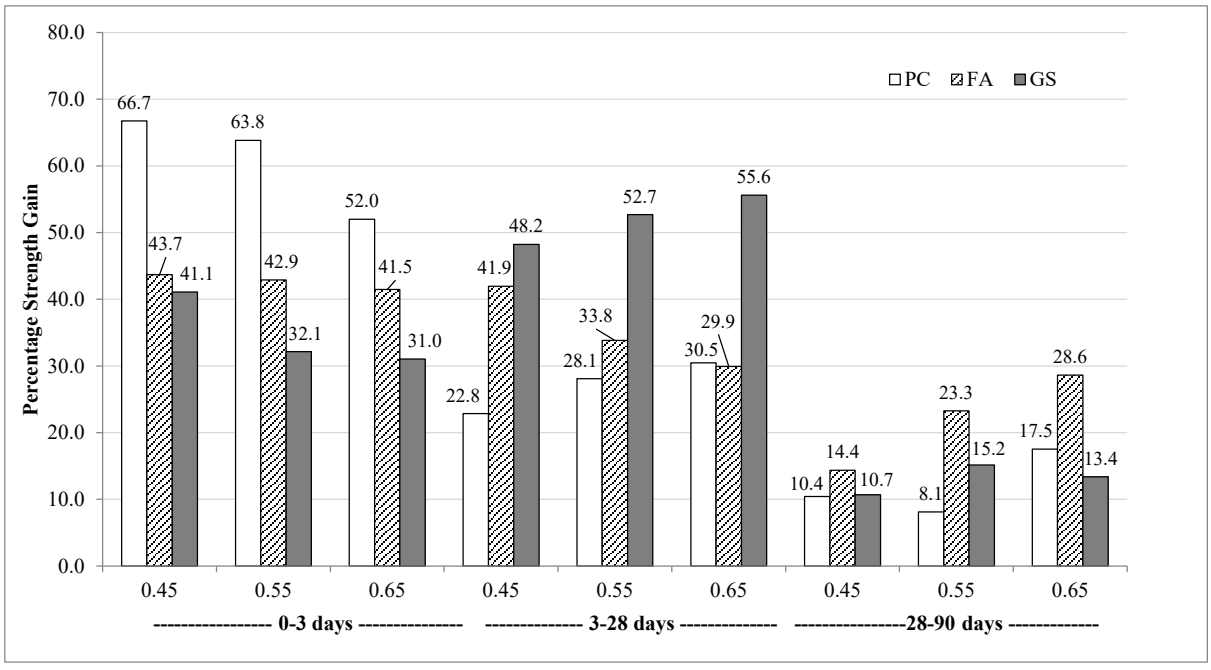

Figure 4.2 Comparison of compressive strength gain over 3 time periods (% of 28-day strength)

Figure 4.2 shows that PC concrete achieve more than 50% of its final strength within the first three days irrespective of the w/b. For the concrete with fly ash and GGBS the strength gain in the first three days was between 30-40% of its final strength. It can also be observed that the strength gain of FA and GS concrete from 3-28 days was higher when compared to PC concrete. Such an increase in strength gain with time can be attributed to longer term hydration and pozzolanic reactions of the FA and GS concrete. Furthermore, the strength gain continues for the FA concrete at later age from 28-90 days, which indicates the continued pozzolanic reaction of the FA concrete.

4.3 OXYGEN PERMEABILITY INDEX

The oxygen permeability index (OPI) test results on concrete specimens at 28 days after casting are shown in Figure 4.3. The test results of the individual specimens and their corresponding statistical variation are presented in detail in Appendix C.

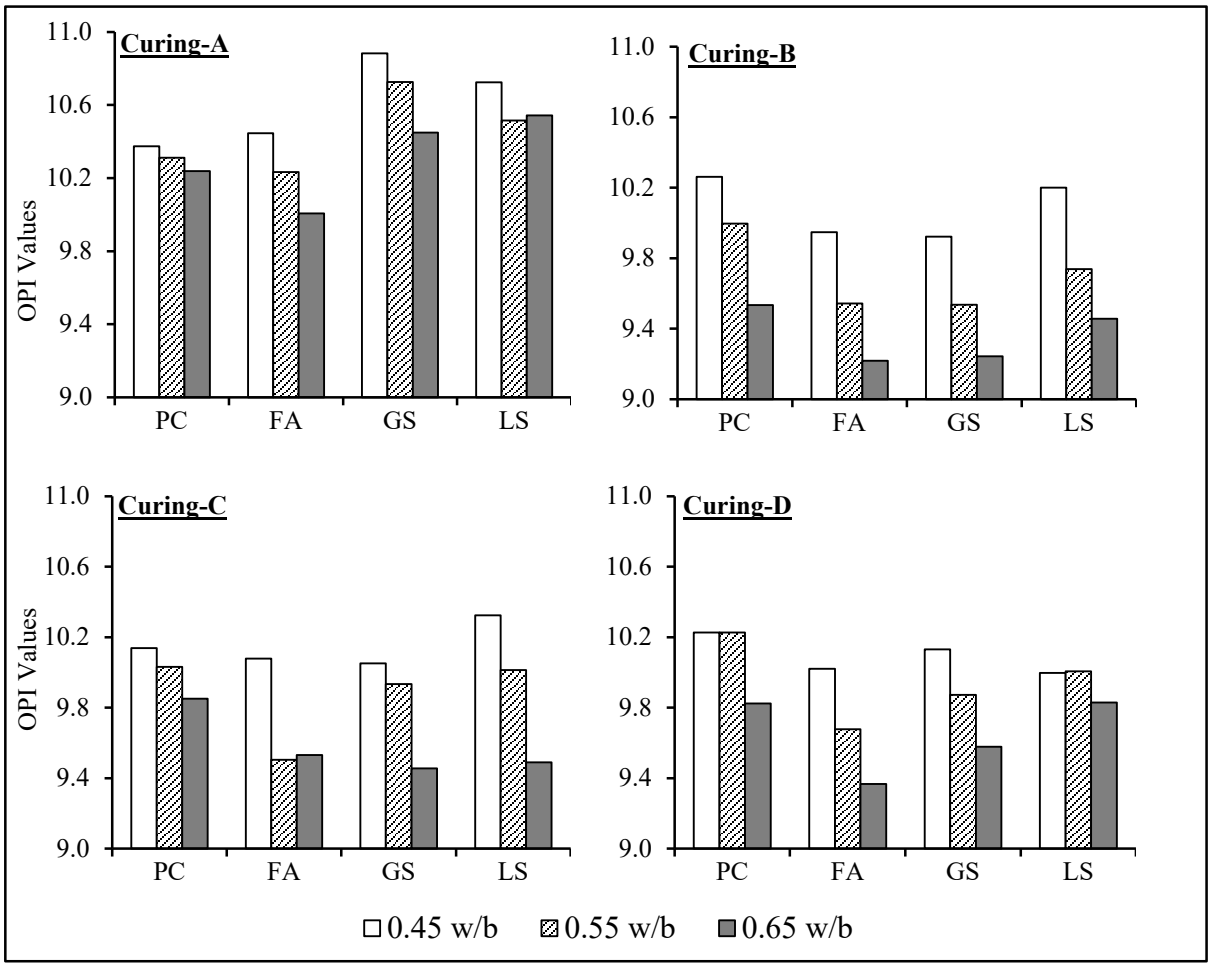

Figure 4.3 OPI test result of concrete at 28 days after casting, subject to different curing regimes

4.3.1 Effect of w/b on Concrete Permeability

The test results clearly show the influence of w/b on concrete permeability. It is evident from Figure 4.3 that the OPI reduces as the w/b increases, irrespective of the concrete mix and curing conditions. Since the OPI test measures the coefficient of permeability (k) of the concrete, and the OPI value represents the negative logarithm of the k value, a higher OPI value indicates a lower permeability coefficient. Therefore, it can be generalised that with an increase in w/b, the permeability of concrete increases (see Figure 4.4). This can be attributed to the increase in porosity and interconnectivity of the pore structure due to an increase in w/b. A similar observation of decrease in OPI values (i.e. an increase in permeability) with increase in w/b was also observed by other researchers such as Salvoldi (2010), and Alhassan (2014).

4.3.2 Effect of Curing on Concrete Permeability

From Figure 4.3, specimens subjected to Curing-A, the OPI values are higher for specimens made of FA (with 0.45 w/b) and GS concrete when compared to the PC concrete irrespective of w/b. This is expected as the use of cement extenders tends to generate a denser microstructure because of further hydration and pozzolanic activity. Similar trends were also observed by other researchers (Ballim et al., 2009; Salvoldi, 2010; Alhassan, 2014). For all the concrete specimens with Curing-A, for the same w/b, the GS concrete shows the lowest permeability, i.e. the highest OPI values. A similar trend of higher OPI value for concrete with GGBS was also observed by Salvoldi (2010). The lower permeability coefficient of GS concrete can also be due to the denser microstructure.

The influence of curing on the permeability of concrete can be assessed based on Figure 4.4. It can be clearly observed that the specimens which were subjected to standard water curing (Curing-A) show better permeability characteristics as a dense microstructure was developed due to good hydration as discussed above, and this is reflected in terms of lower k values. On the other hand, the outcome of poor curing conditions (Curing-B), where the specimens were only cured for one day in the mould and then exposed in the laboratory condition is reflected in Figure 4.4. It can be observed that all the specimens subjected to Curing-B show higher k (or lower OPI) value. It can be observed that all the specimens subjected to Curing-B show higher k (or lower OPI) values indicating higher permeability (see Figure 4.3 and Figure 4.4). This can be attributed to the poor microstructure developed because of inadequate conditions for cement hydration.

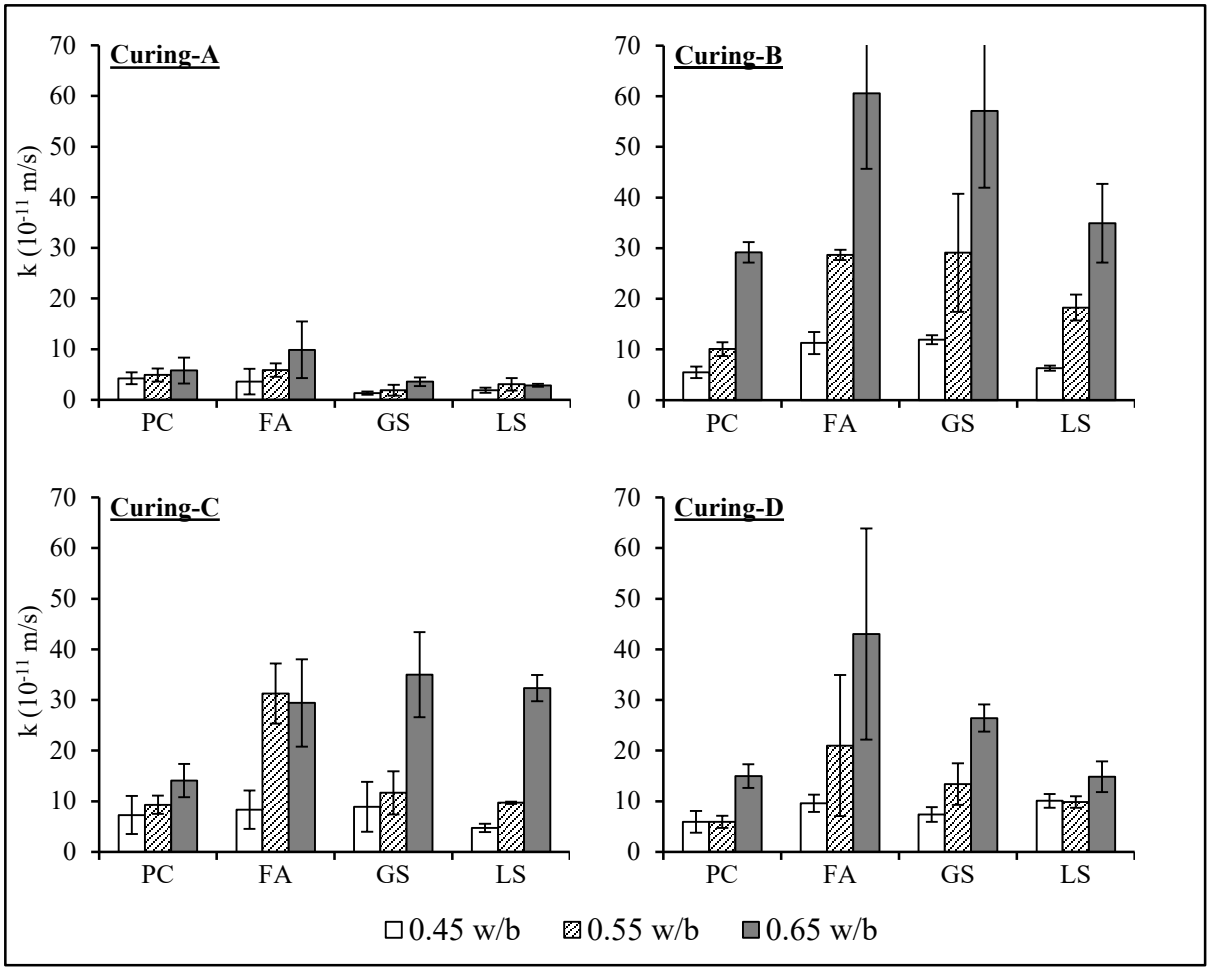

Figure 4.4 Coefficient of permeability (k, m/s) from OPI test result of concrete at 28 days after casting, subject to different curing regime

However, in terms of permeability, the specimens with Curing-C show better performance when compared to the specimens with Curing-B. The reduction in permeability of specimens with Curing-C was due to the better curing conditions offered by this particular curing regime where the specimens were covered with plastic for six days before exposing to the laboratory conditions. This resulted in more favourable conditions for the cement hydration, and development of a denser microstructure. Regarding Curing-D – an outdoor environment - it can be observed that the permeability of specimens lie in between the performance of specimens subjected to Curing-B and Curing-C, even though Curing-B and Curing-D are similar. This can be attributed to the variation in climatic conditions as the specimens subjected to Curing-D are exposed to the natural environment where variation in temperature and RH is uncontrolled and variable. Hence, in general it can be summarised that, with respect to the curing regimes adopted, the permeability of concrete increases in the order of Curing-A, (Curing-C or Curing-D) and Curing-B. Similar trends of increase in permeability or reduction

in OPI depending on the curing were noted in previous studies by other researchers (Krook, 1995; Martin, 2012).

A comparison of the OPI values of specimens subject to Curing-B, Curing-C and Curing-D versus the OPI values of specimens subject to Curing-A is given in Figure 4.5 to Figure 4.8. It can be observed that all the data points are below the 45° line indicating that OPI values of concrete specimens subjected to Curing-A is higher when compared to the concrete subjected to other curing regime. The above observation once again emphasis the better performance of 28 days standard water curing (Curing-A) in the development of denser microstructure as discussed above. It can also be seen from Figure 4.5 to Figure 4.8 that the variation of OPI values with respect to the curing regime is more profound for the FA and GS concrete (concrete mixes with cement extenders) when compared to the PC concrete

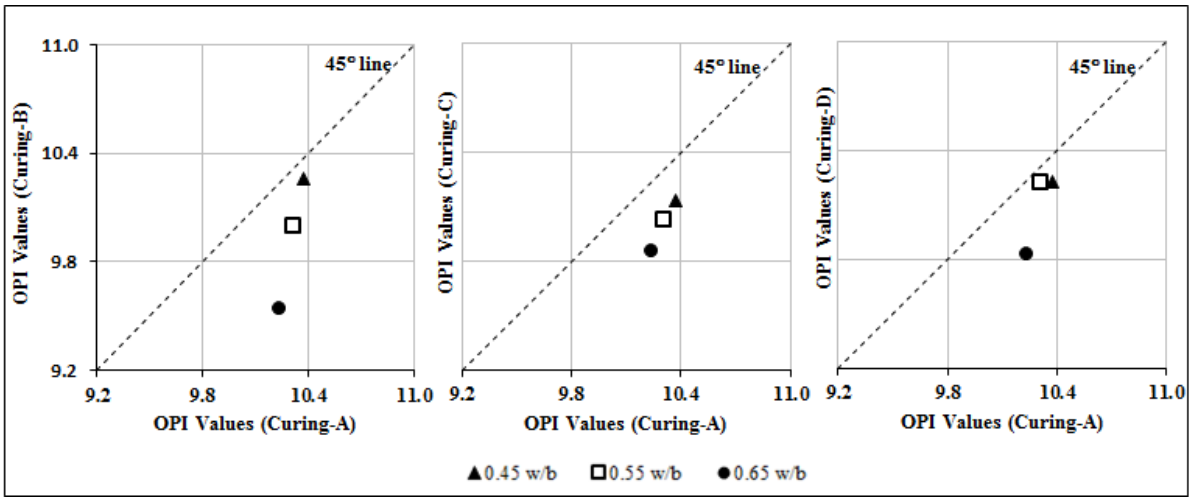

Figure 4.5 OPI values of PC concrete: (Curing-B, Curing-C and Curing-D) vs Curing-A

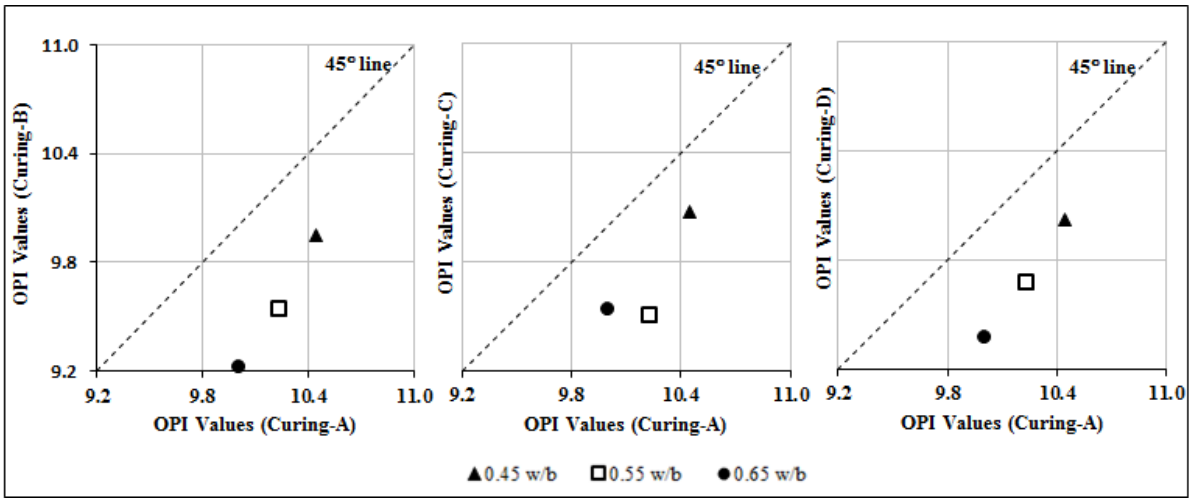

Figure 4.6 OPI values of FA concrete: (Curing-B, Curing-C and Curing-D) vs Curing-A

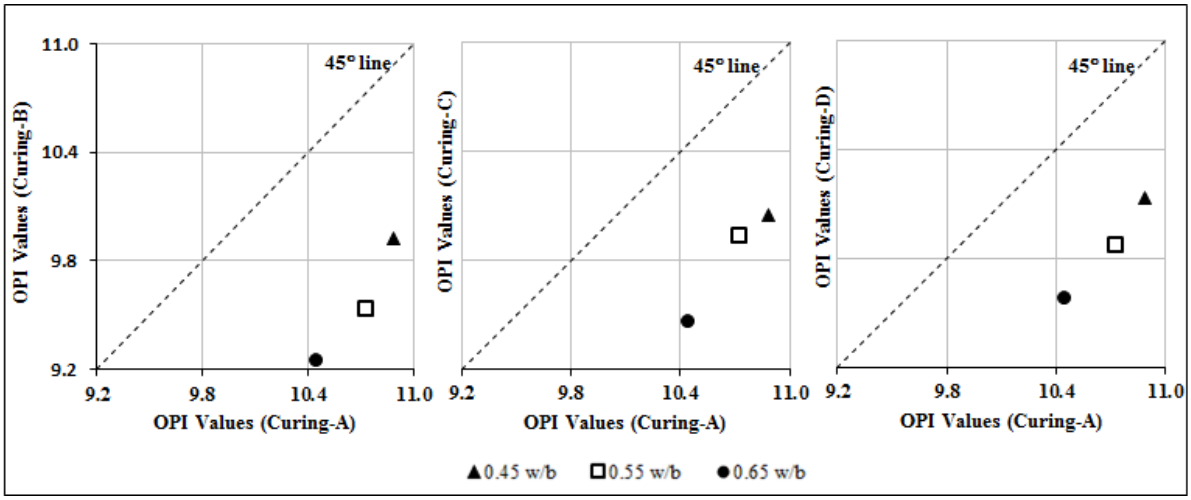

Figure 4.7 OPI values of GS concrete: (Curing-B, Curing-C and Curing-D) vs Curing-A

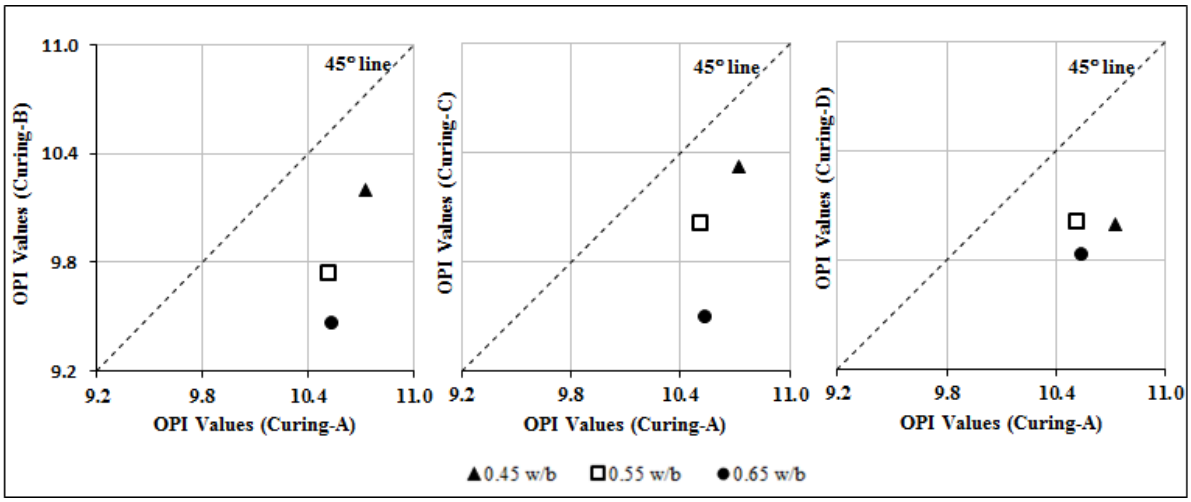

Figure 4.8 OPI values of LS concrete: (Curing-B, Curing-C and Curing-D) vs Curing-A

4.3.3 Effect of Binder Type on Concrete Permeability

A comparison of the OPI values of specimens made of FA, GS and LS concrete versus PC concrete for all the four curing regimes is given in Figure 4.9 to Figure 4.12. As discussed above, curing has a major influence on the permeability performance of concrete, especially in the case of concrete with cement extenders. Improved permeability performance of FA and GS concrete over PC concrete was mainly observed in the case of 28 days standard water curing (Curing-A) (see Figure 4.9). On the other hand, from Figure 4.10 to Figure 4.12 it can be seen that all the data points are below the 45° line indicating that for same w/b ratio, the OPI values of FA and GS concrete were observed to be lower than the PC concrete for all curing other than Curing-A. A similar trend of reduction in OPI with poor curing was also observed by Martin (2012).

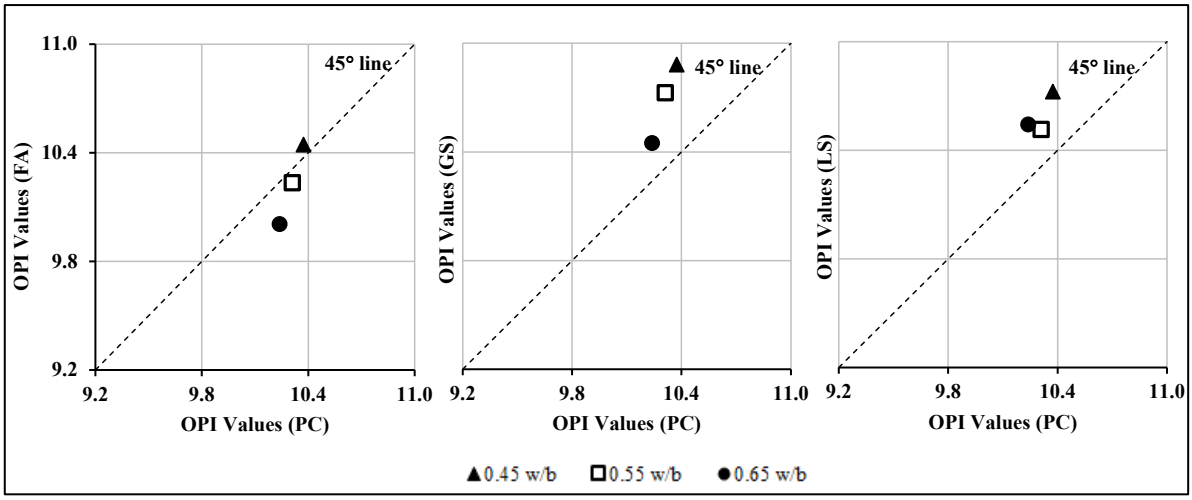

Figure 4.9 OPI values of specimens with Curing-A: (FA, GS and LS) vs PC concrete

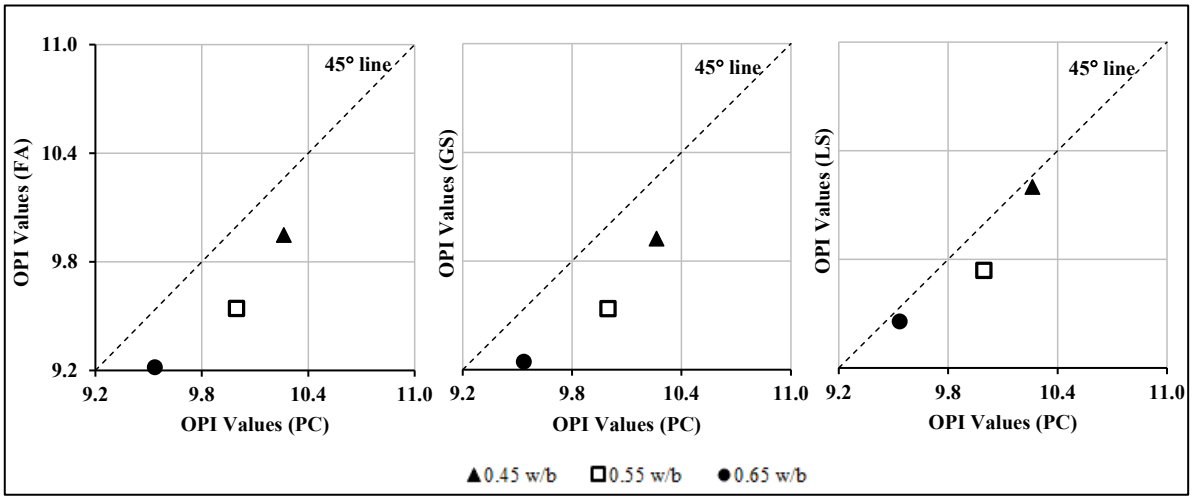

Figure 4.10 OPI values of specimens with Curing-B: (FA, GS and LS) vs PC concrete

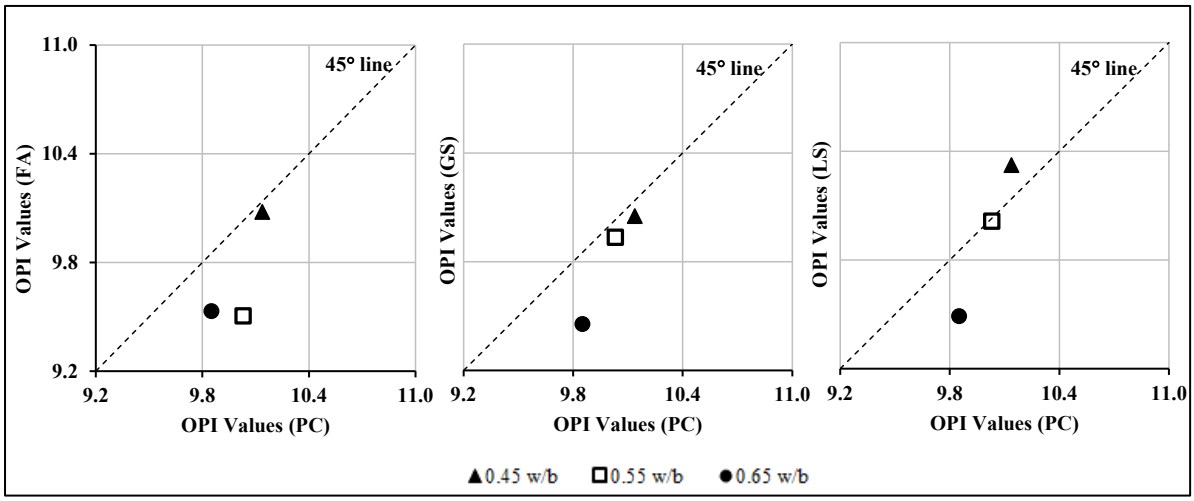

Figure 4.11 OPI values of specimens with Curing-C: (FA, GS and LS) vs PC concrete

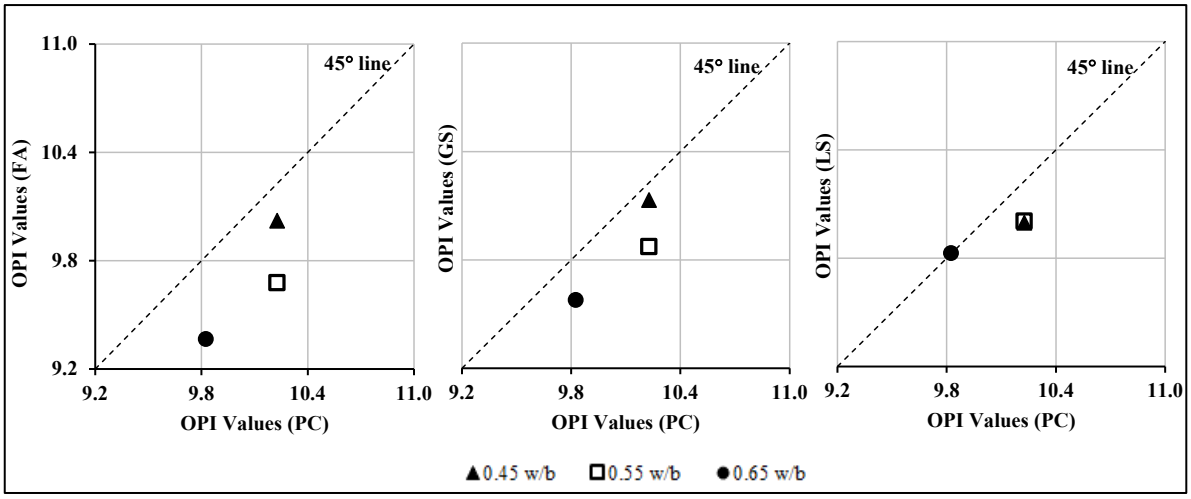

Figure 4.12 OPI values of specimens with Curing-D: (FA, GS and LS) vs PC concrete

Similar to the GS concrete, a better permeability performance of concrete with cement containing limestone (CEM II B-L 42.5 N) (denoted as LS) can be observed when subjected to Curing-A (see Figure 4.3, Figure 4.8 and Figure 4.9). This would need further investigation, as the refining in microstructure may be due to the fine filler effect because of the presence of limestone. However, studies conducted with limestone cement (CEM II A-L 42.5 N), did not showed large differences in permeability when compared to Portland cement; rather a lower value of OPI (higher permeability) for limestone cement was noted (Githachuri, 2010; Githachuri and Alexander, 2013). The difference in observation of the test result from the literature can be due to the variation in the limestone content in the cement used in both studies, as the cement CEM II B-L 42.5 N used in this research has higher percentage of limestone when compared to the cement CEM II A-L 42.5 N used in Githachuri and Alexander (2013). The difference in OPI can also be due to the difference in fineness of the limestone used in respective cement. On the other hand, similar to FA and GS concrete, for same w/b the OPI values of LS concrete was also found to be lower when compared to the PC concrete when subjected to Curing-B, C and D (Figure 4.10 to Figure 4.12), once again indicating the importance of curing.

4.4 CARBONATION DEPTH RESULTS

The influence of concrete mix proportions, w/b, curing regime and environmental conditions on the rate of carbonation was studied and is presented below. Five sets, each of 48 concrete prisms of dimensions 100x100x200 mm (with 12 different mixes × four different curing conditions, see Table 3.2 and Table 3.5) were cast and exposed at five different sites (see Table

3.6). All the concrete specimens were exposed to natural carbonation at the end of the curing regime and without any preconditioning. The specimens were allowed to carbonate under natural environmental conditions and the depths of carbonation were measured at frequent intervals. Details of the specimen preparation and the carbonation depth measurement are presented in Section 3.3.4 and Section 3.3.5. Carbonation results measured at different times and the progression of carbonation depth with time are presented in Appendix D.1–D.10. Carbonation depths after 1000 days (i.e. 1000 ± 2 days) of exposure to different natural environments are shown in Figure 4.13 to Figure 4.17. Each data point is an average of 12 measurements.

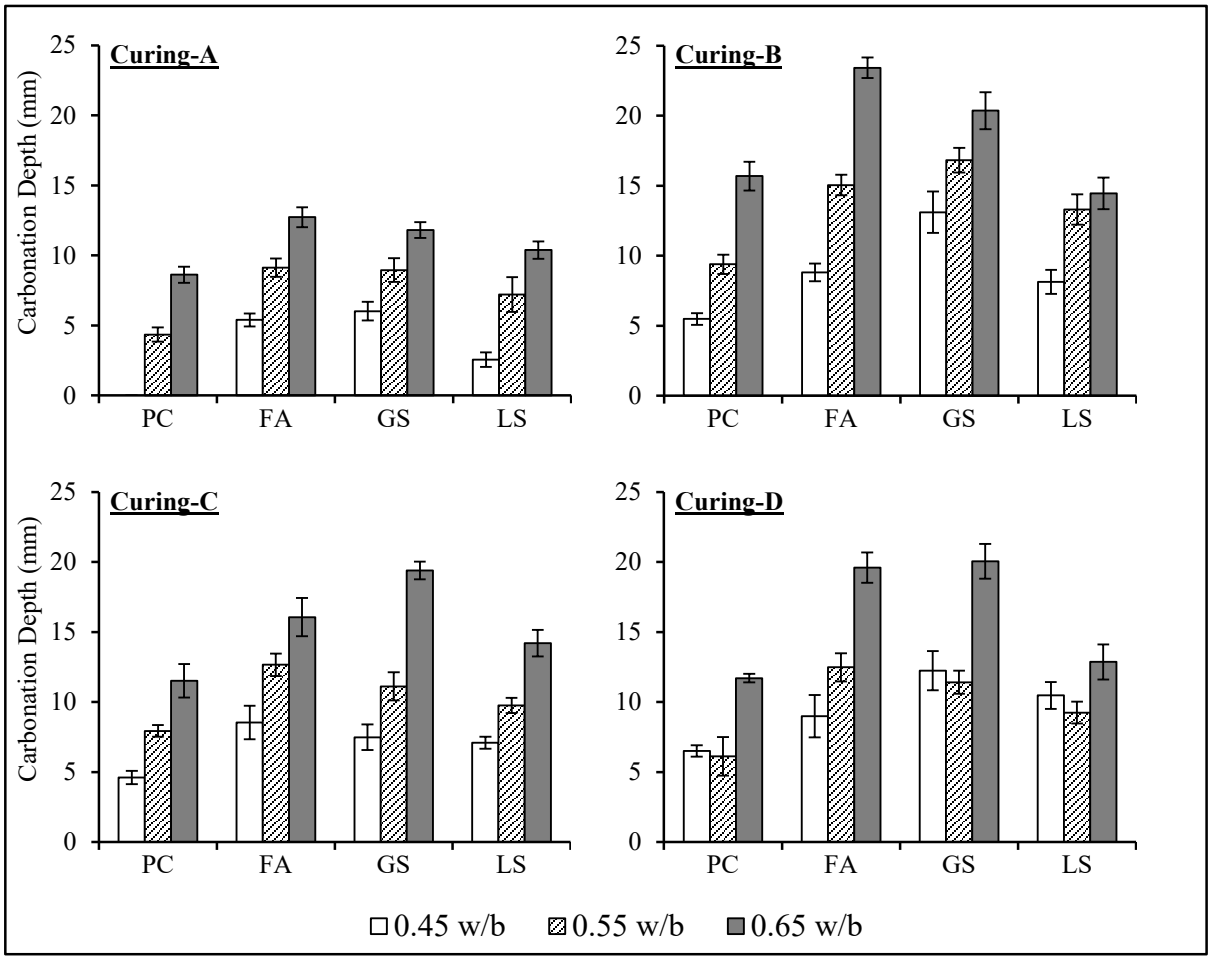

Figure 4.13 Carbonation depth after 1000 days of exposure at site CD

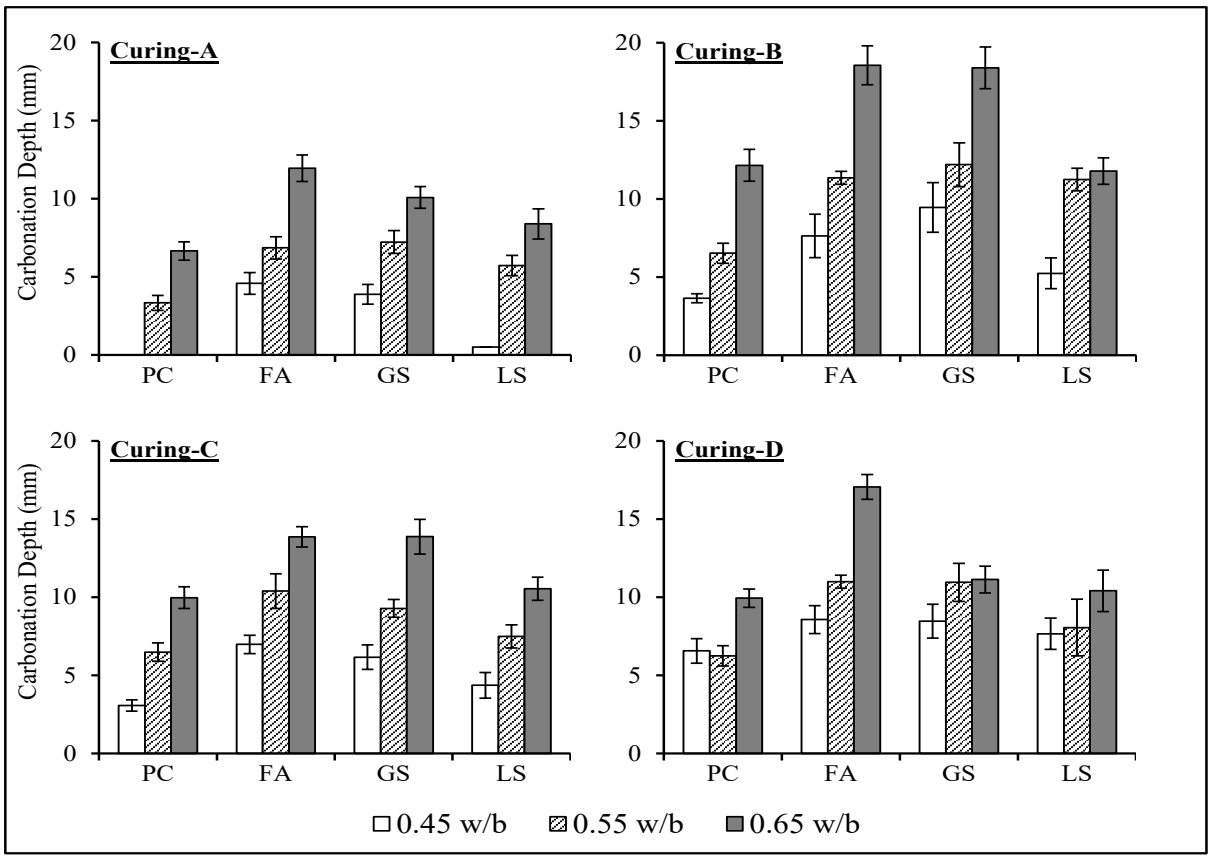

Figure 4.14 Carbonation depth after 1000 days of exposure at site MS

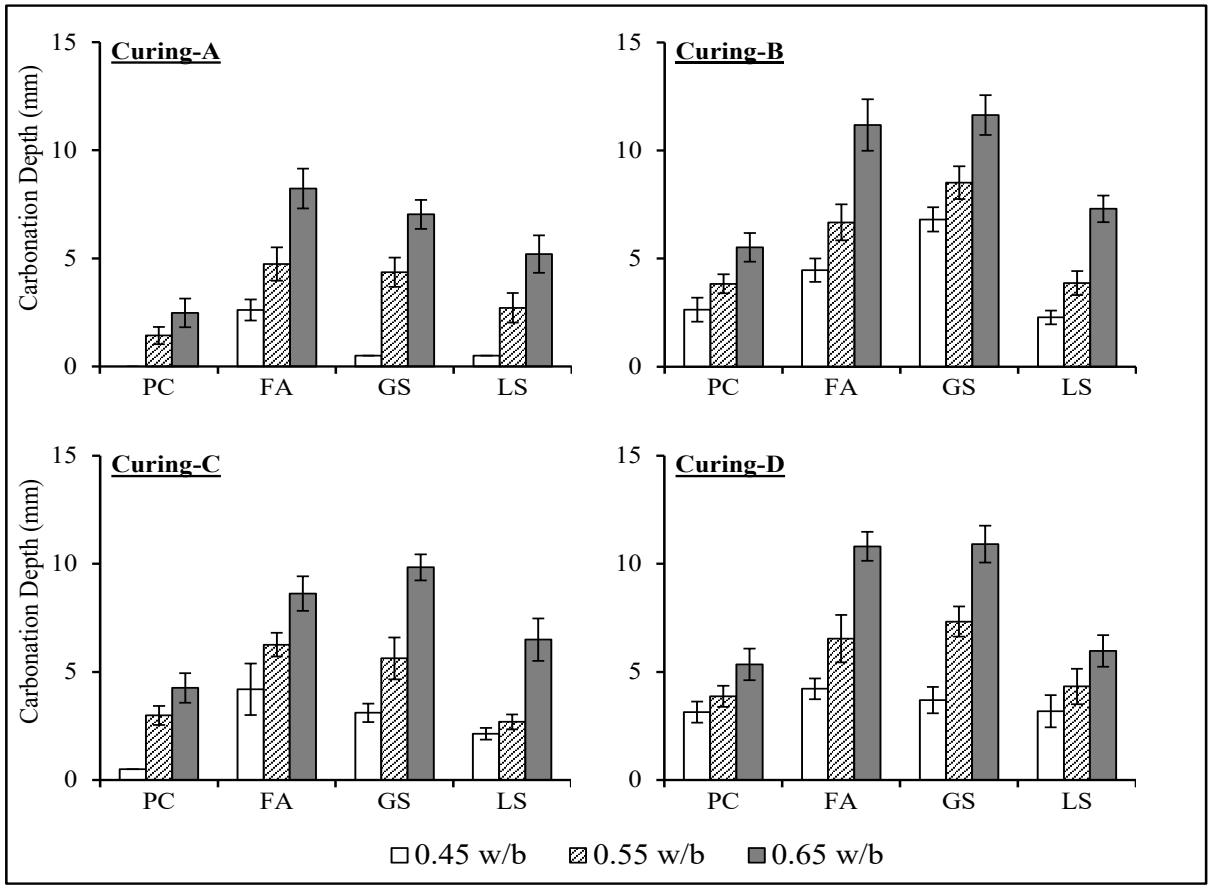

Figure 4.15 Carbonation depth after 1000 days of exposure at site ME

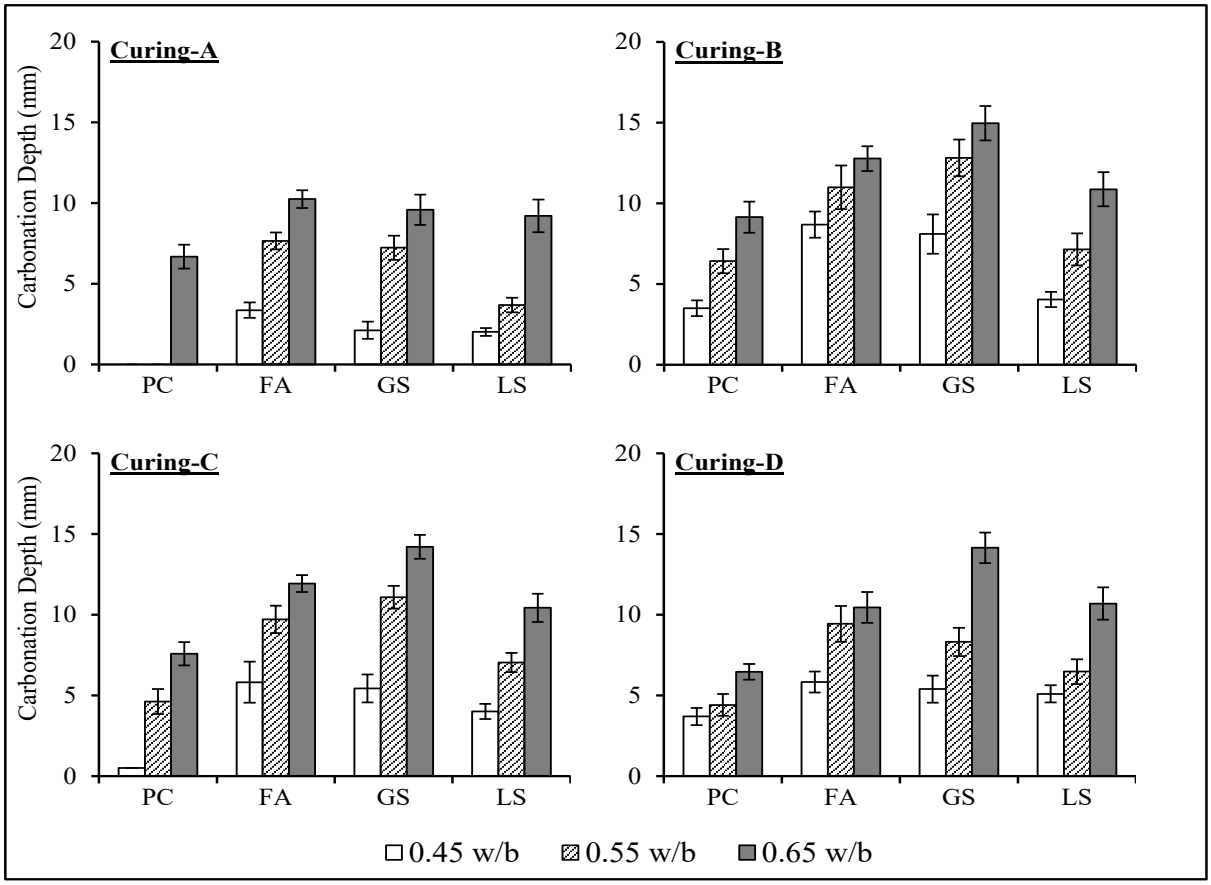

Figure 4.16 Carbonation depth after 1000 days of exposure at site WS

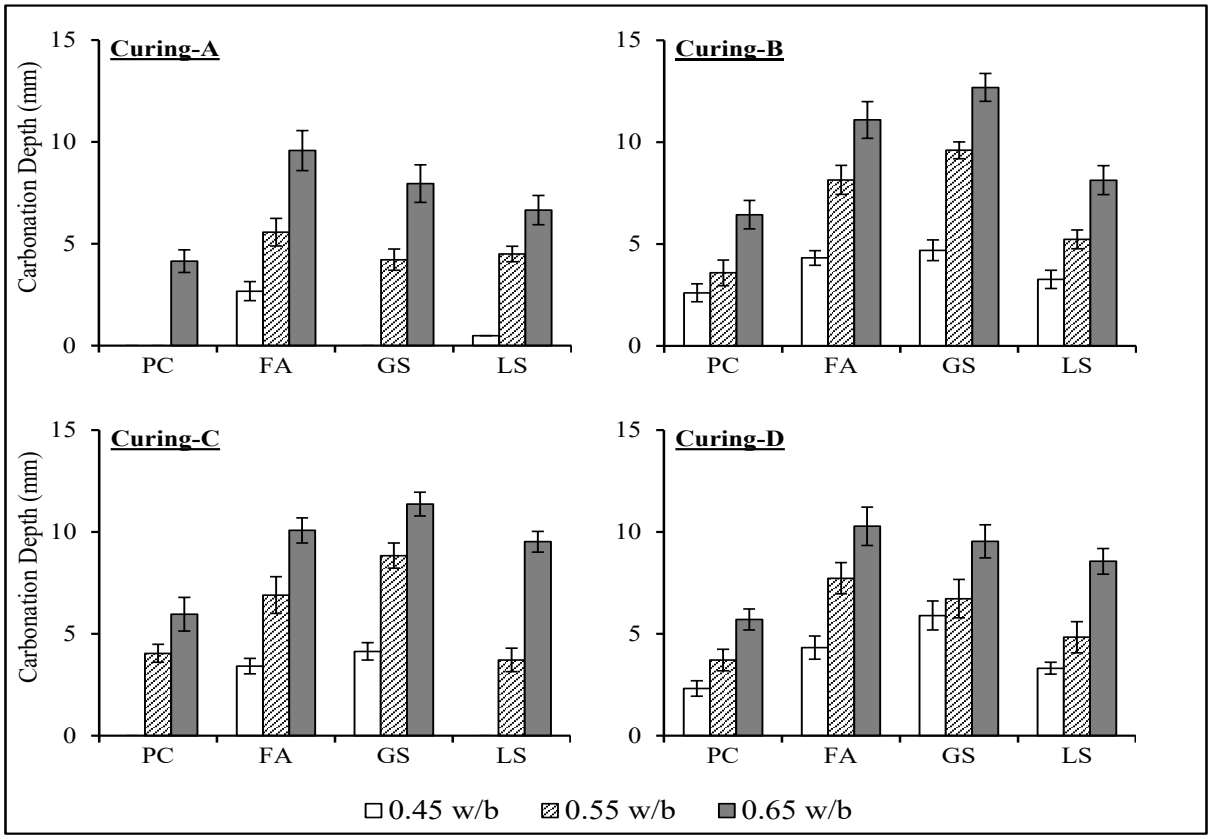

Figure 4.17 Carbonation depth after 1000 days of exposure at site WE

4.4.1 Effect of w/b on Concrete Carbonation

From the test results presented in Figure 4.13 to Figure 4.17, it is seen that for the same concrete mix, with increase in w/b the rate of carbonation increases irrespective of the exposure site. This is in good agreement with the OPI results discussed in the previous section. Hence, it can be inferred that the increase in w/b makes the concrete more porous and penetrable, which favours the transport of CO_2 inside the concrete, resulting in a higher carbonation rate. Furthermore, an increase in w/b implies lower binder content (and hence lower amount of carbonatable material), since the water content was kept constant in the mixes. Therefore the increase in carbonation rate with increase in w/b is also due to the lower resistance offered by the carbonatable material towards the progression of the carbonation front. Hence the increase in carbonation rate with increase in w/b is due to the combined action of the above two phenomenon and similar observations were found by other researchers (Houst and Wittmann, 1994; Sulapha et al., 2003; Khunthongkeaw et al., 2006; Salvoldi, 2010; Alhassan, 2014; Zhao et al., 2016).

4.4.2 Effect of Curing on Concrete Carbonation

The influence of curing was also evident from the results (see Figure 4.13 to Figure 4.17), as the carbonation depths were observed to be higher for poorly cured concrete. The carbonation rates increase in the order of Curing-A, (Curing-C or Curing-D) and Curing-B, A similar trend was observed in the case of OPI test results where the permeability of concrete increased in the above order. This behaviour can be attributed to the coarser microstructure, and also less calcium hydroxide (CH) formation due to lesser degree of hydration (because of poor curing). The lower CH results in increasing the rate of carbonation, since CH is one of the major hydrated cement phases which undergoes carbonation reaction (as discussed in Section 2.2) or in essence buffers the progression of the carbonation front.

A comparison of the carbonation depths of concrete specimens subject to Curing-B, Curing-C and Curing-D versus the concrete specimens subject to Curing-A, for all the concrete specimen, after 1000 days of exposure at the site CD is given in Figure 4.18 to Figure 4.21 and for exposure at site ME, MS, WE and WS is given in Appendix D.11.

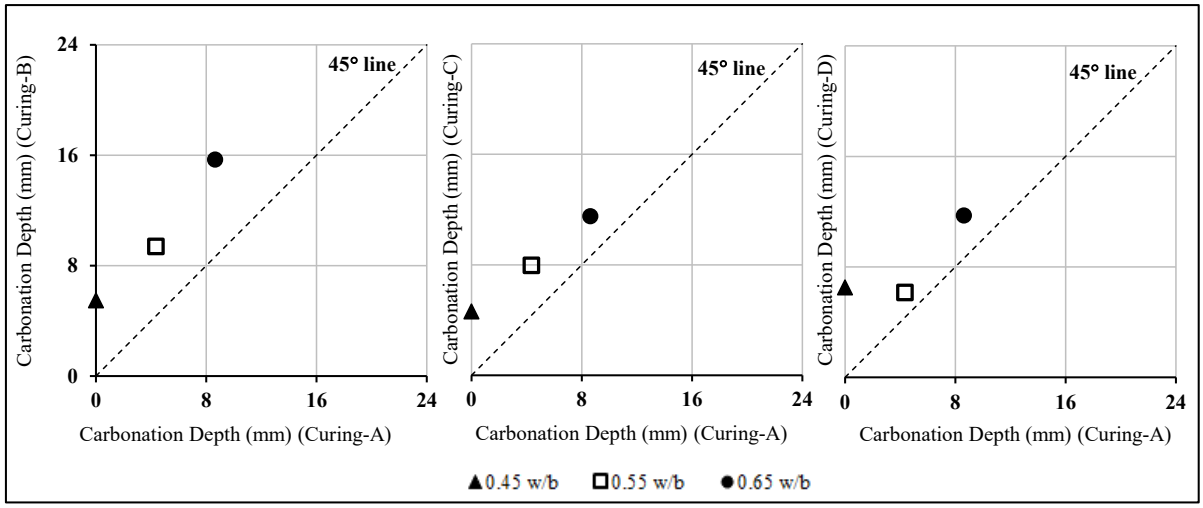

Figure 4.18 Carbonation depth of PC concrete after 1000 days of exposure at CD: (Curing-B, Curing-C and Curing-D) vs Curing-A

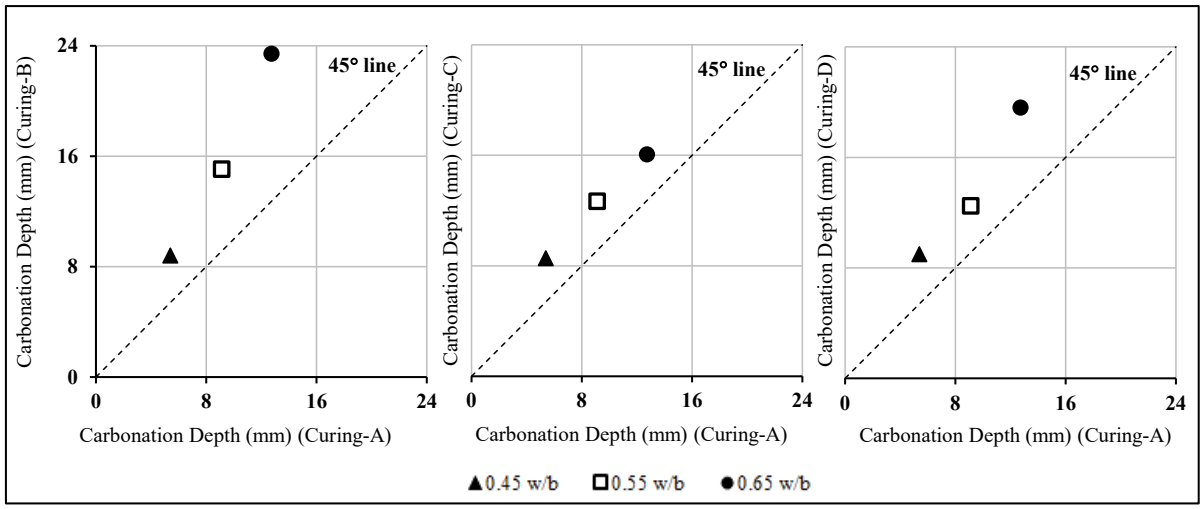

Figure 4.19 Carbonation depth of FA concrete after 1000 days of exposure at CD: (Curing-B, Curing-C and Curing-D) vs Curing-A

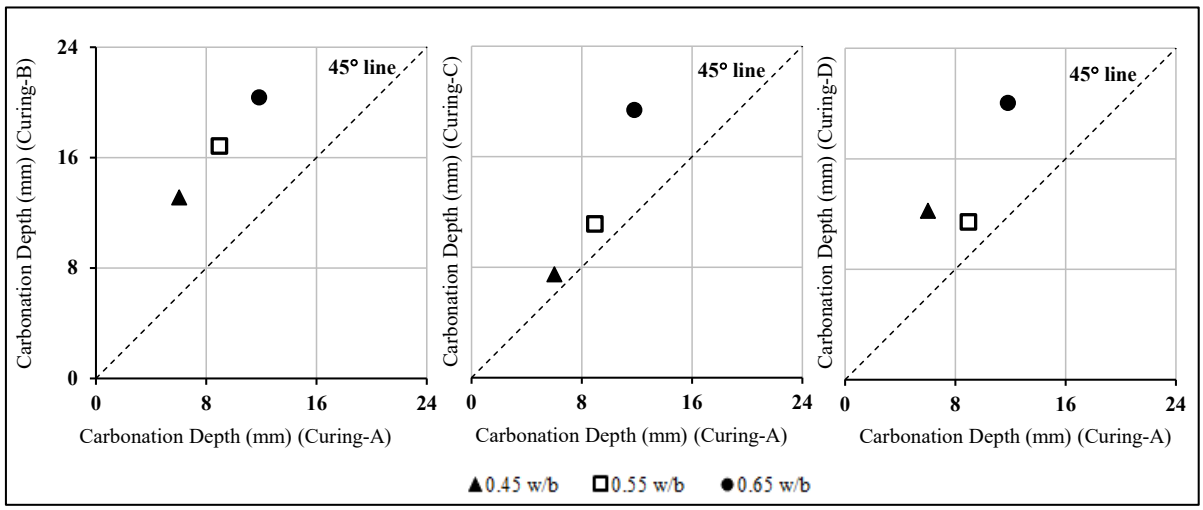

Figure 4.20 Carbonation depth of GS concrete after 1000 days of exposure at CD: (Curing-B, Curing-C and Curing-D) vs Curing-A

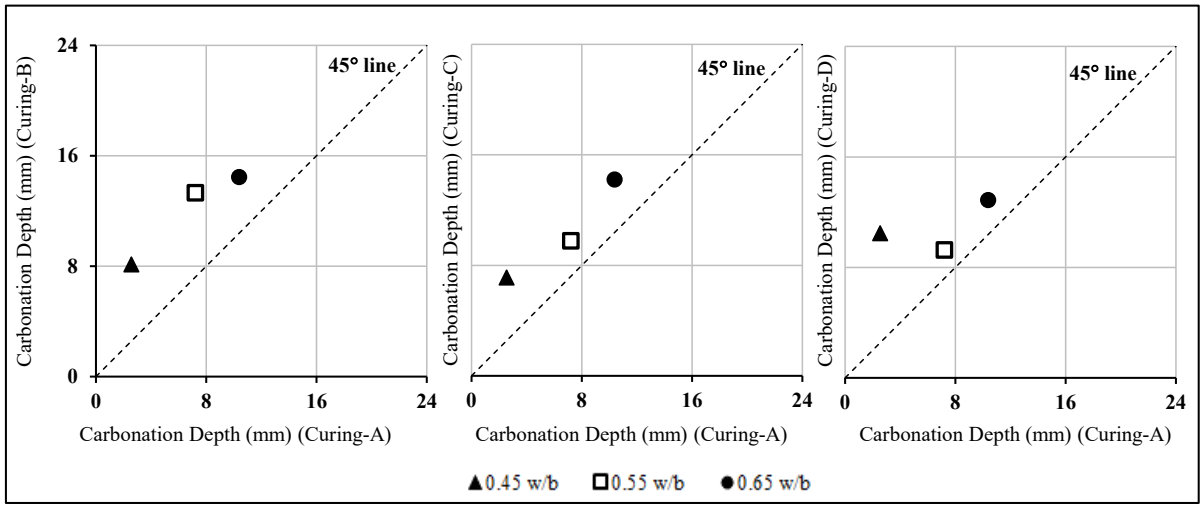

Figure 4.21 Carbonation depth of LS concrete after 1000 days of exposure at CD: (Curing-B, Curing-C and Curing-D) vs Curing-A

Figure 4.18 to Figure 4.21 indicate the influence of 28 days standard water curing in reducing the rate of carbonation. It can be observed that all the data points are above the 45° line indicating a higher carbonation depth after 1000 days of exposure for specimens which were subjected to Curing-B, Curing-C and Curing-D, when compared to those specimens subjected to Curing-A. Similar observation was given by Younsi et al. (2011), where a reduction of 20-50% of carbonation depth was observed in samples cured under water when compared to uncured samples. The influence of Curing-A in reducing the rate of carbonation was also observed in the case of specimens exposed to sites ME, MS, WE and WS (details, see Appendix D.11). The improvement of carbonation resistance with water curing was also validated by other researchers (Sisomphon and Franke, 2007; Sanjuan et al., 2018)

4.4.3 Effect of Binder Type on Concrete Carbonation

In order to assess the influence of cement extenders and the use of limestone cement (CEM II B-L 42.5 N) on the rate of carbonation of concrete, a comparison of carbonation depth of concrete specimens made with FA, GS and LS concrete versus the carbonation depth of concrete specimens made of PC concrete, for all the concrete specimens, after 1000 days of exposure at the site CD, is given in Figure 4.22 to Figure 4.25 below.

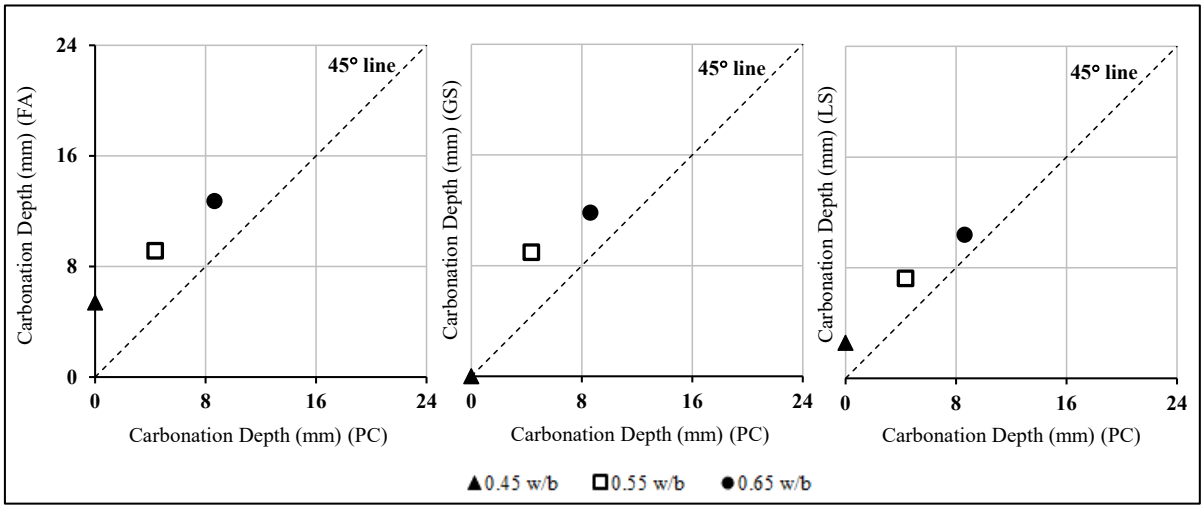

Figure 4.22 Carbonation depth of specimens with Curing-A, after 1000 days of exposure at site CD: (FA, GS and LS) vs PC concrete

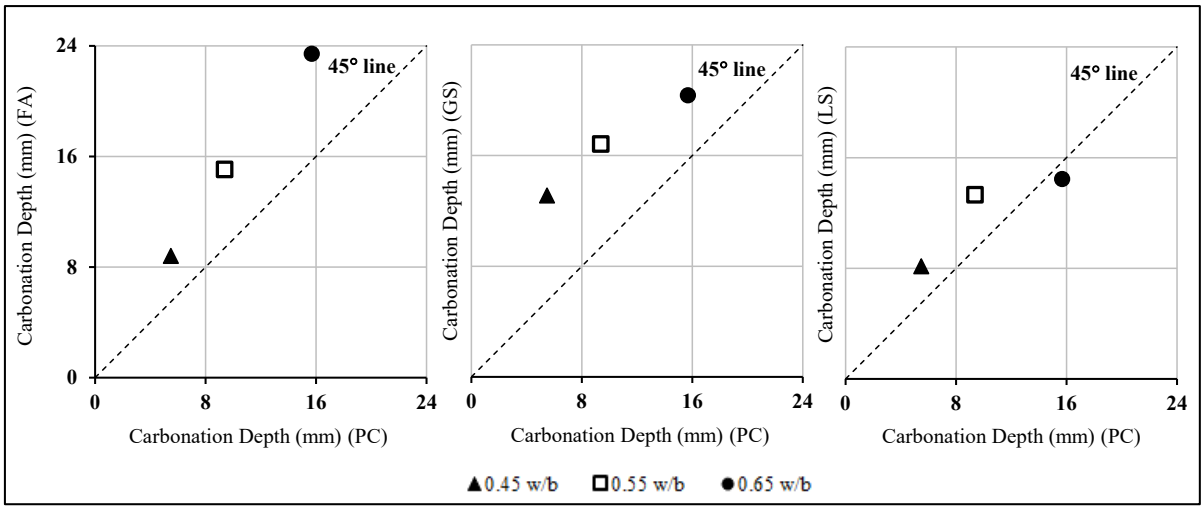

Figure 4.23 Carbonation depth of specimens with Curing-B, after 1000 days of exposure at site CD: (FA, GS and LS) vs PC concrete

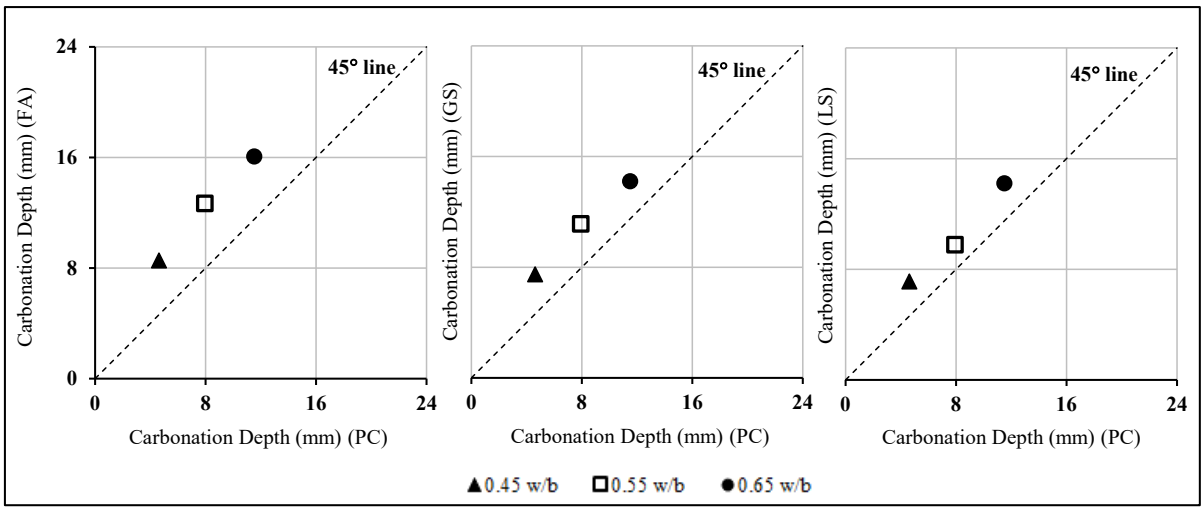

Figure 4.24 Carbonation depth of specimens with Curing-C, after 1000 days of exposure at site CD: (FA, GS and LS) vs PC concrete

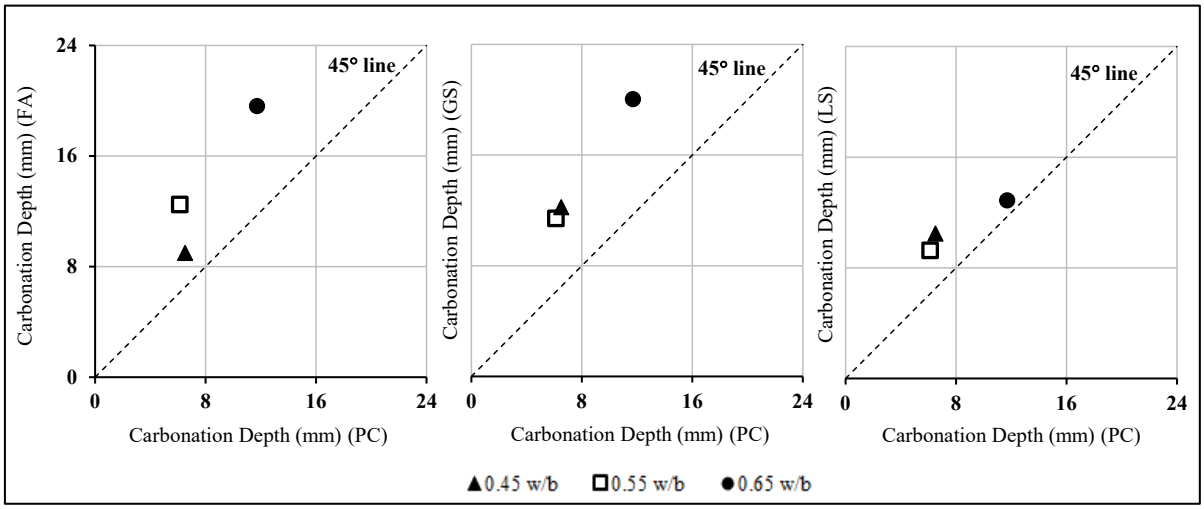

Figure 4.25 Carbonation depth of specimens with Curing-D, after 1000 days of exposure at site CD: (FA, GS and LS) vs PC concrete

It can be observed from Figure 4.22 to Figure 4.25 that all the data points (except LS-65, curing-B) are above the 45° line indicating that the rate of carbonation of PC concrete is lower than that of FA, GS and LS concrete, irrespective of the w/b and curing regime adopted. A similar trend was also observed in the case of specimens exposed at the site ME, MS, WE and WS (details, see Appendix D.12). The reduced rate of carbonation of PC concrete can be attributed to the presence of higher carbonatable material which will buffer the progression of the carbonation front, when compared to FA, GS and LS concrete. Similar trends of reduction in the rate of carbonation of concrete with Portland cement with respect to the concrete with cement extenders was also observed by other researchers (Papadakis, 2000; Khunthongkeaw et al. (2006) Gonen and Yazicioglu, 2007; Gruyaert et al., 2013; Zhao et al., 2016).

However the beneficial effect of reduction in permeability of concrete with cement extenders, indicating a denser pore structure when subjected to Curing-A (see Figure 4.9), does not seem to be have a positive impact with respect to carbonation. This can be due to the reduction in carbonatable material in the case of FA and GS concrete when compared to PC concrete due to the lower Portland cement content, for the same w/b. In addition to the lower Portland cement content, the reduction in carbonatable material can also be due to the pozzolanic reaction as in the case of FA concrete. When compared to concrete specimens subjected to Curing-B and Curing-C, this effect is observed to be higher with Curing-A, since the pozzolanic activity is higher in the case of FA concrete because of better hydration and curing conditions. This phenomenon as evidently perceived from Figure 4.22 to Figure 4.25, where the percentage increase of carbonation depth of concrete with cement extenders with respect to the PC concrete is higher for concrete subjected to Curing-A, despite their lower permeability as

discussed in the previous section. It can be inferred that, along with permeability, the quantity of carbonatable material is also a governing factor affecting the rate of carbonation (Borges et al., 2012; Alhassan, 2014).

In the case of LS concrete, trends similar to those of the concretes with cement extenders was observed. The reduction in permeability because of the curing-A (see Figure 4.9) is not observed to be advantageous in reducing the carbonation rate (see Figure 4.22), and the percentage increase in carbonation depth is observed to higher. This can be justified due to the lower buffering capacity of the LS concrete as the clinker quantity of the cement used for LS concrete is lower that of the PC concrete. Again for the same w/b, LS concrete shows similar trends to those of blended cement concrete both in terms of permeability and carbonation in comparison with PC concrete. As can be seen from Figure 4.22 to Figure 4.25, the rate of carbonation of LS concrete is higher when compared to PC concrete for the same w/b irrespective of the curing conditions (except LS-65, curing-B), but lower than the concrete with cement extenders.

4.4.4 Effect of Environmental Factors on Concrete Carbonation

Bakker (1988) addressed the influence of drying/wetting cycles on the carbonation rate, where a reduction in progress of the carbonation was indicated until the concrete is dry enough after the wetting cycle. Similar variation of the rate of carbonation was observed in the current research. Comparison of carbonation depths of concrete specimens sheltered from rain (site MS) versus the carbonation depths of concrete specimens exposed to rain (site ME) are presented in Figure 4.26 to Figure 4.29. Similarly, the comparison of the concrete specimens exposed at site WS (specimens sheltered from rain) versus site WE (specimens exposed to rain) are given in Figure 4.30 to Figure 4.33.

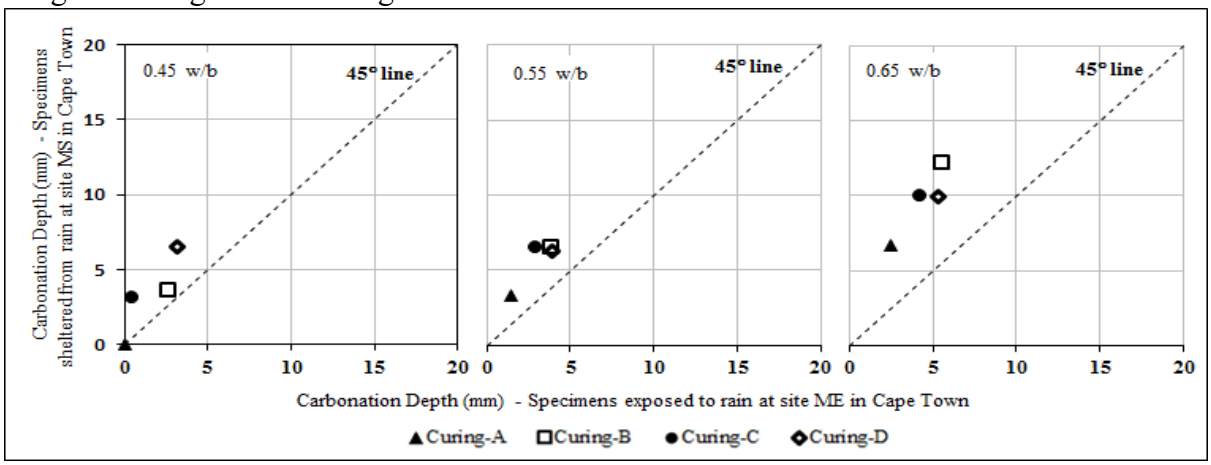

Figure 4.26 Carbonation depth of PC concrete specimens after 1000 days of exposure at site MS vs site ME

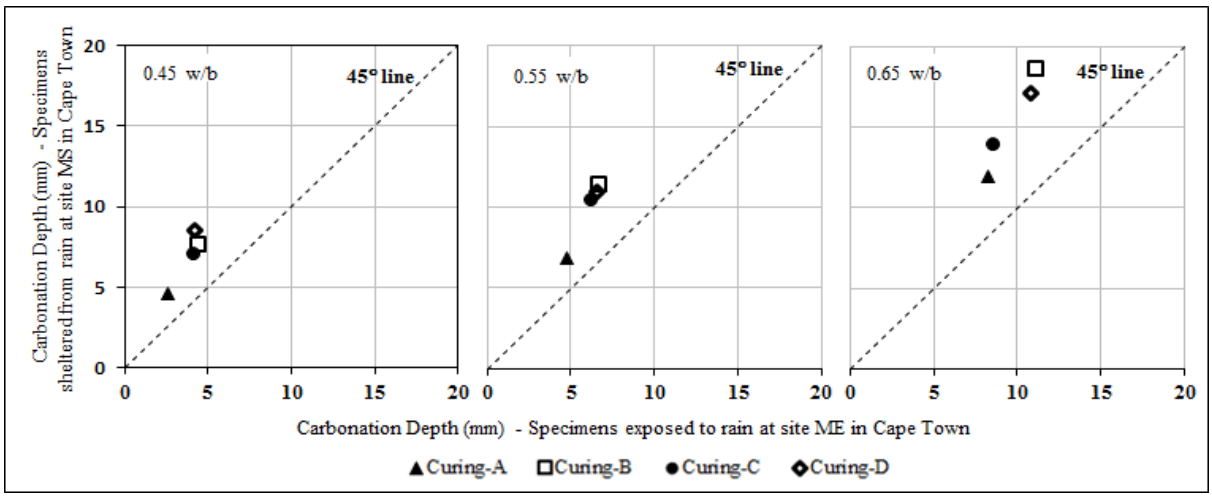

Figure 4.27 Carbonation depth of FA concrete specimens after 1000 days of exposure at site MS vs site ME

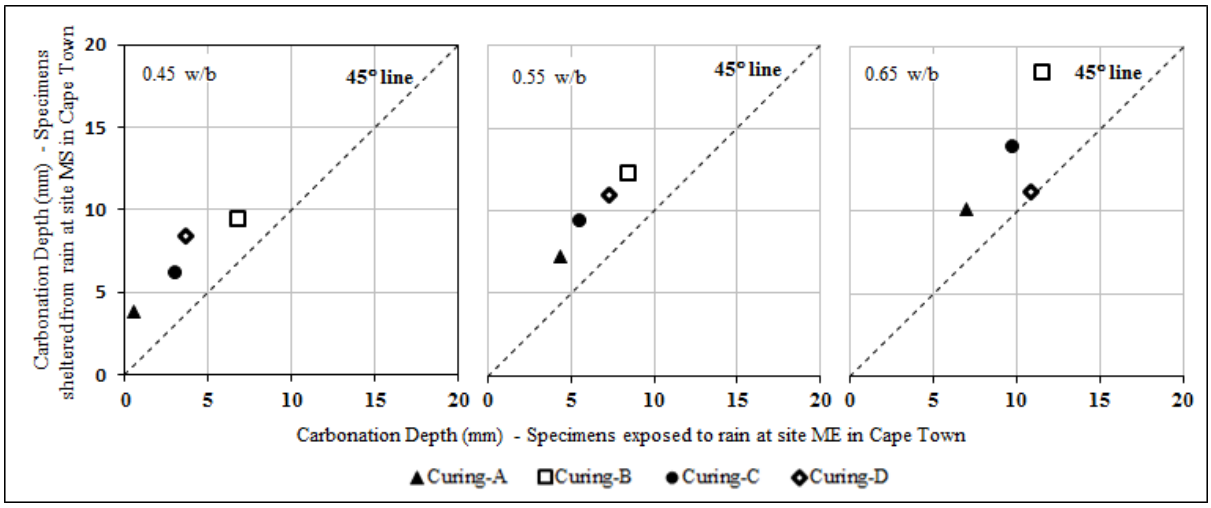

Figure 4.28 Carbonation depth of GS concrete specimens after 1000 days of exposure at site MS vs site ME

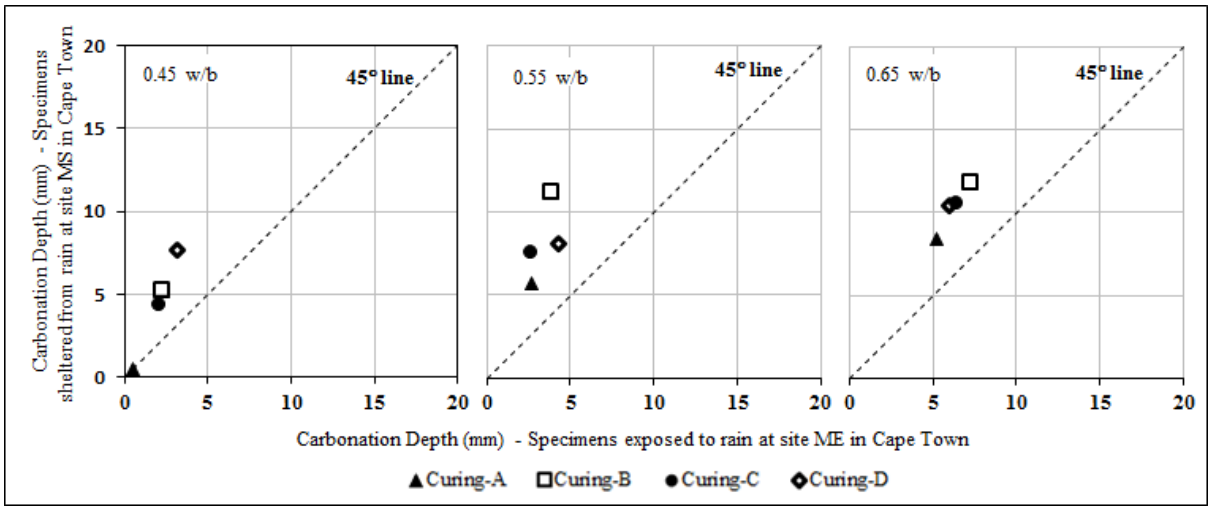

Figure 4.29 Carbonation depth of LS concrete specimens after 1000 days of exposure at site MS vs site ME

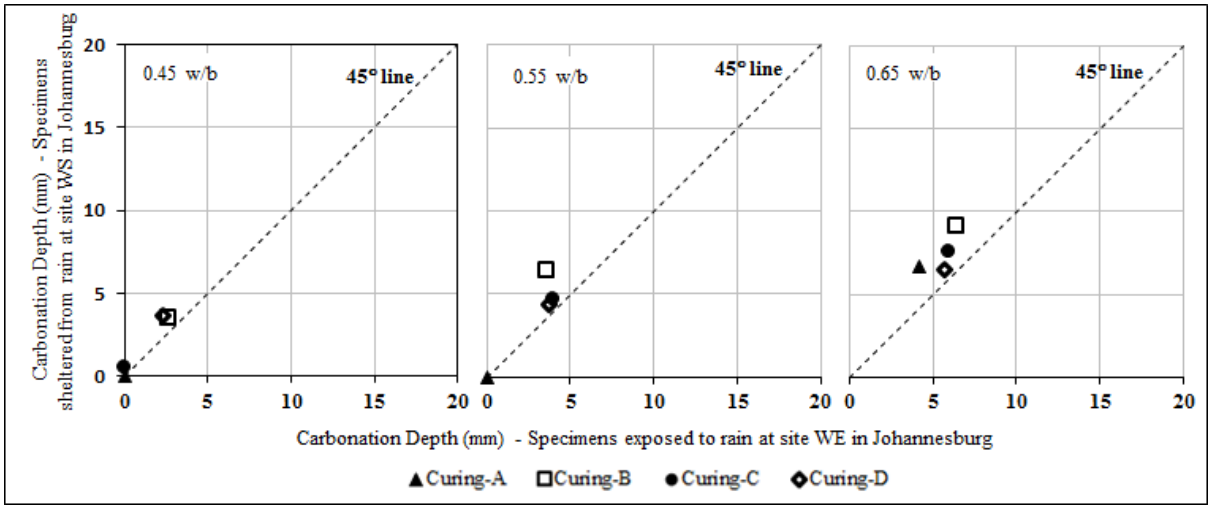

Figure 4.30 Carbonation depth of PC concrete specimens after 1000 days of exposure at site WS vs site WE

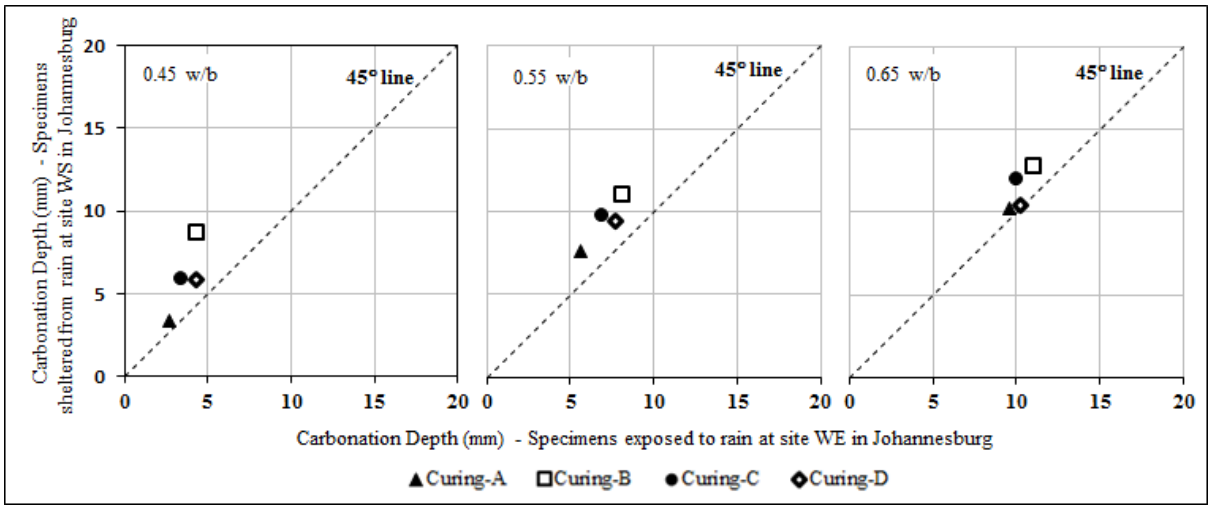

Figure 4.31 Carbonation depth of FA concrete specimens after 1000 days of exposure at site WS vs site WE

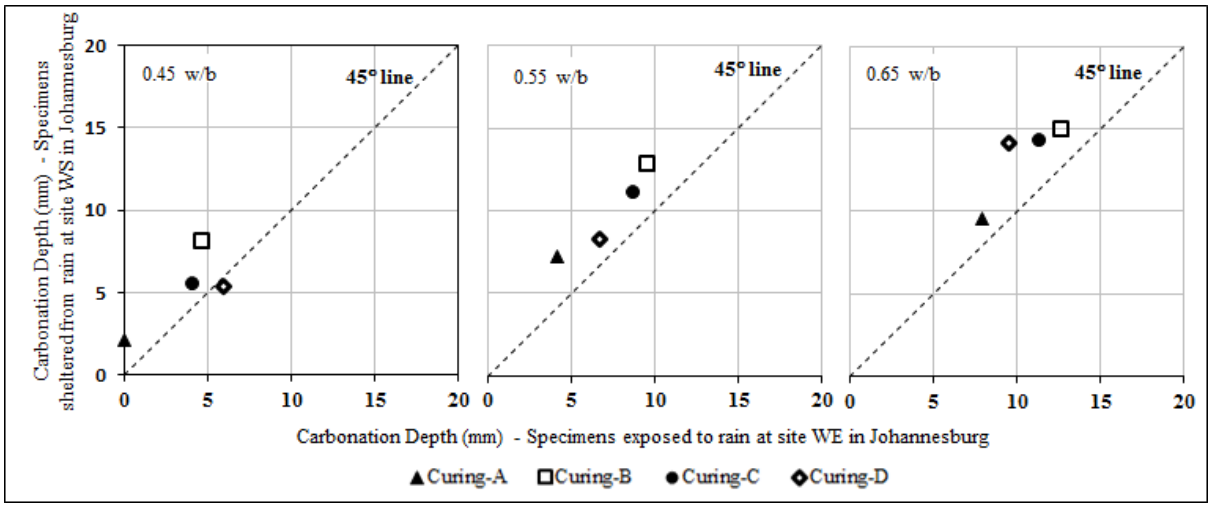

Figure 4.32 Carbonation depth of GS concrete specimens after 1000 days of exposure at site WS vs site WE

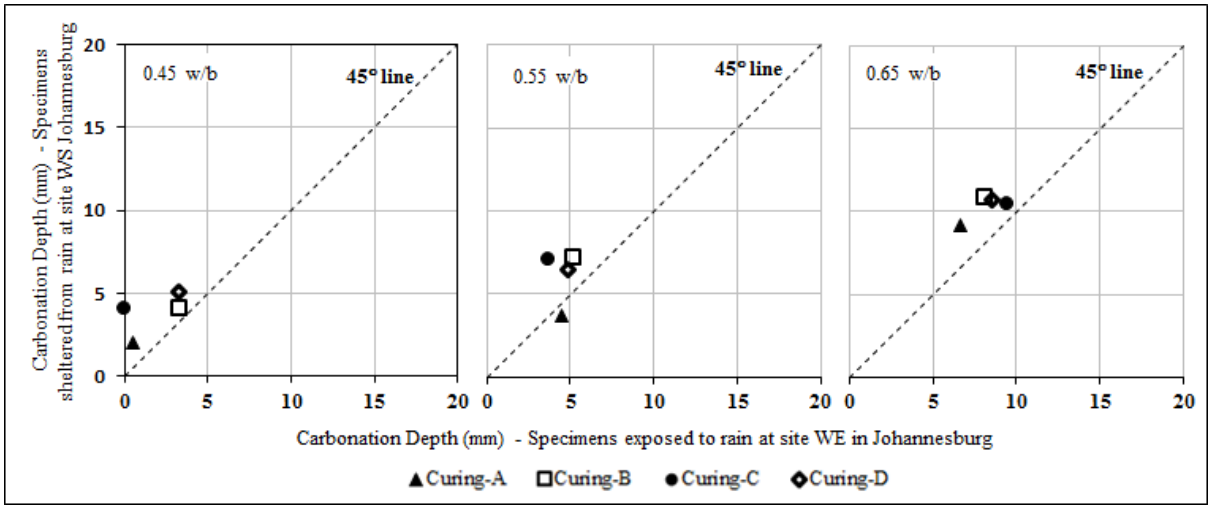

Figure 4.33 Carbonation depth of LS concrete specimens after 1000 days of exposure at site WS vs site WE

The test results shows that for all the concrete (except site WE, GS-45 curing-D; LS-55 curing-A) exposed to rain (site ME and WE), the depth of carbonation after 1000 days is lower than their paired samples which were sheltered from rain at the same location (site MS and WS). This clearly points out the influence of drying/wetting cycles on the carbonation rate, as the concrete pores were saturated with water due to rain (wetting cycle) and the diffusion of CO_2 was hindered until the concrete dries out after the rain (during drying cycle). Similar observations of reduction in the rate of carbonation of concrete specimens when exposed to rain were already documented in literature (Parrott, 1987; Houst and Wittmann, 2002; Leemann et al., 20616; Ekolu, 2018). From Figure 4.26 to Figure 4.33, it can also be observed that the difference in rate of carbonation of the specimens exposed at site ME and MS is higher than the difference in rate of carbonation of the specimens exposed at site WE and WS. This can be attributed to the higher number of rainy days in the site ME and MS in Cape Town (site MS is sheltered from rain) when compared to the site WE and WS in Johannesburg (site WS sheltered from rain). The average number of days of rainfall per annum in Cape Town is 124 days (based on three years of rainfall data from weather station around five kilometres from the site ME and MS; details in Appendix E); whereas the average number of days with rainfall per annum in Johannesburg is 89 days (based on three years of rainfall data from weather station around seven kilometres from the site WE and WS; details in Appendix E). Therefore, the concrete specimens exposed to site ME will be wet for longer periods of time when compared to the site WE, preventing progression of the carbonation front. Therefore it can be inferred that not only exposure to rain, but also the extent of rainfall, also have a major

influence on the rate of carbonation of concrete and hence the weather condition of the exposure site also dictates the progression of carbonation of concrete.

To gauge the influence of CO_2 concentration on the rate carbonation, a comparison of carbonation depths of concrete specimens sheltered from rain (site MS, CO_2 concentration 358 ppm) versus the carbonation depths of concrete specimens exposed in a parking garage (site CD, CO_2 concentration 550 ppm) are presented in Figure 4.34 to Figure 4.37

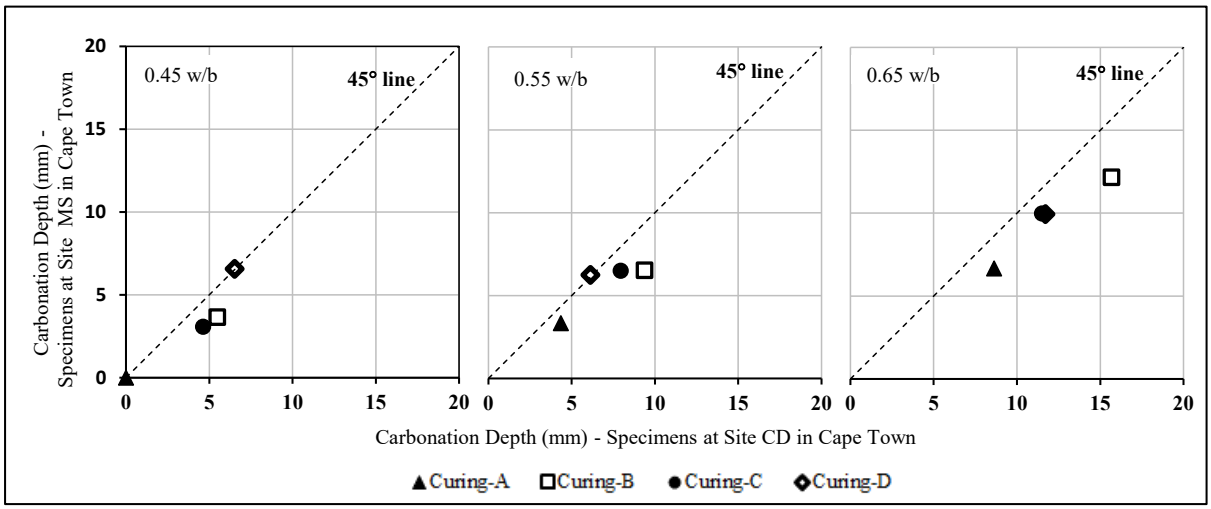

Figure 4.34 Carbonation depth of PC concrete specimens after 1000 days of exposure at site MS vs site CD

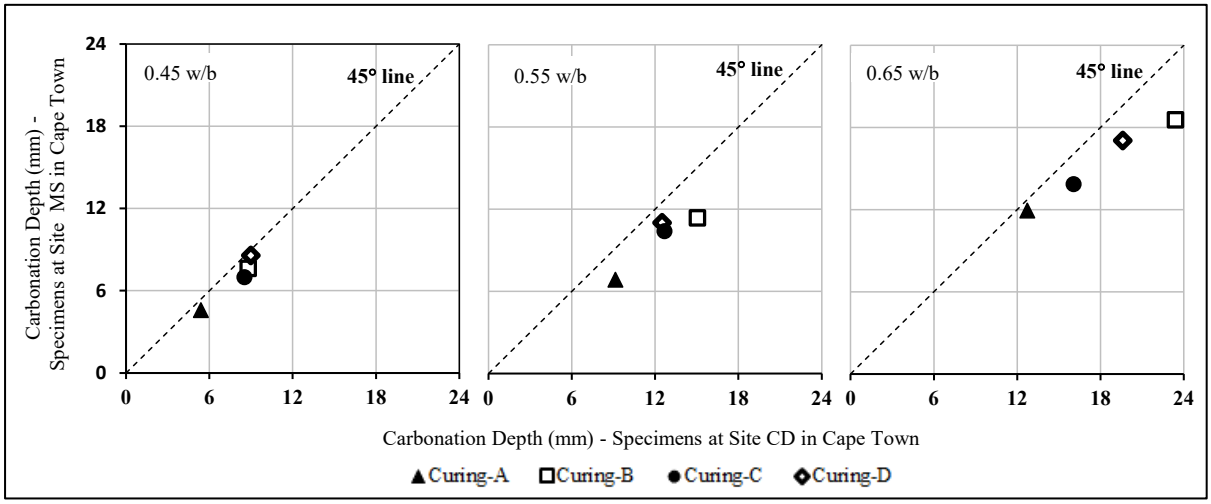

Figure 4.35 Carbonation depth of FA concrete specimens after 1000 days of exposure at site MS vs site CD

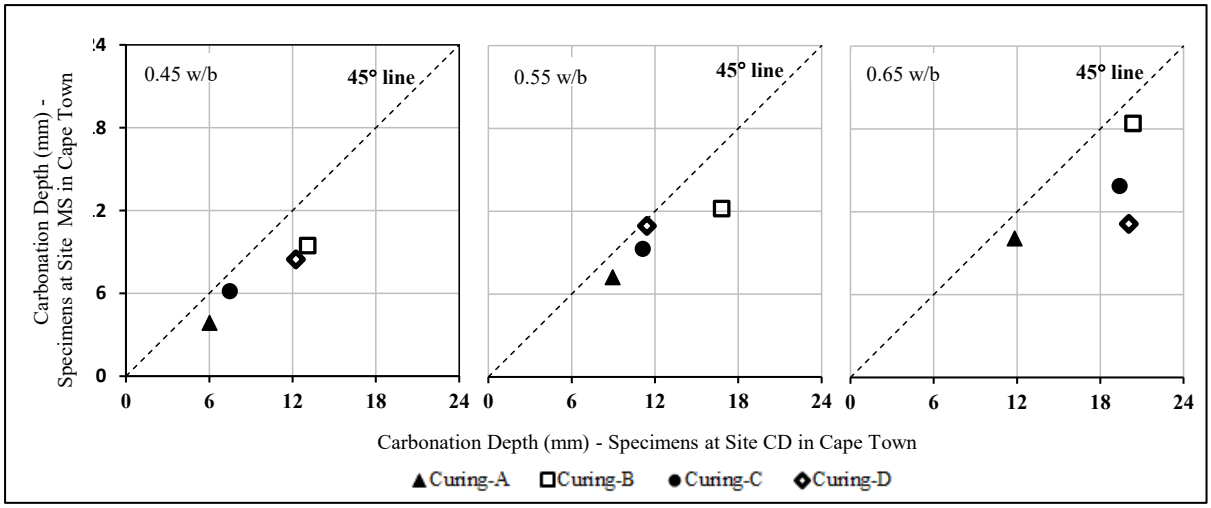

Figure 4.36 Carbonation depth of GS concrete specimens after 1000 days of exposure at site MS vs site CD

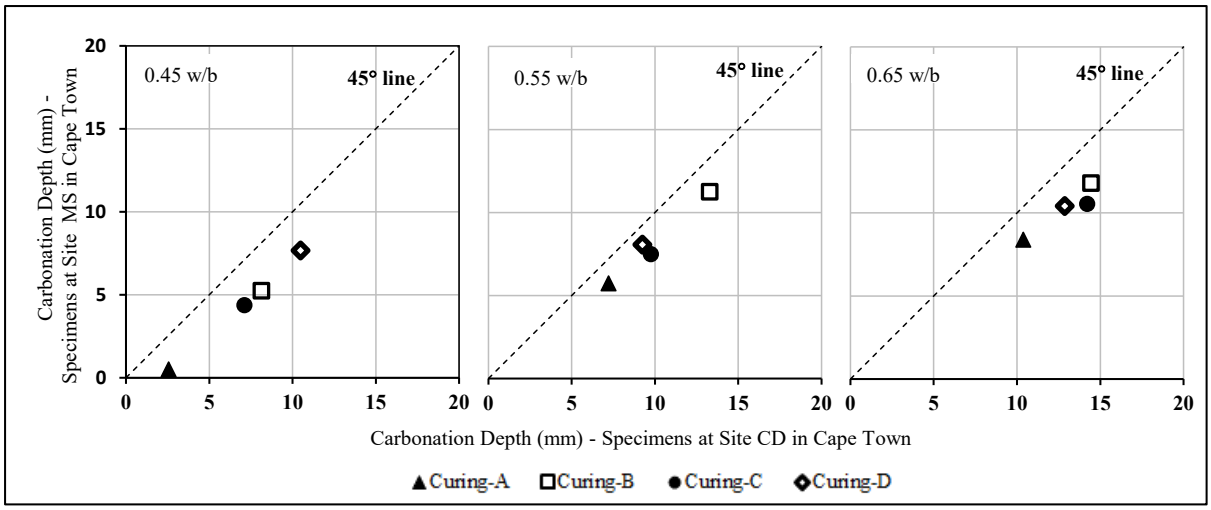

Figure 4.37 Carbonation depth of LS concrete specimens after 1000 days of exposure at site MS vs site CD

The environmental factors such as RH, temperature and CO_2 concentration influence carbonation process, and the difference in rate of carbonation between the site MS and CD is due to the combined effect of RH, temperature and CO_2 concentration. However, the difference in RH and temperature of site MS and CD is negligible when compared to when compared to the CO_2 concentration. Therefore the predominant factor which affect the rate of carbonation between the site MS and CD is CO_2 concentration. Influence of CO_2 concentration on the rate carbonation is clearly depicted in Figure 4.34 to Figure 4.37 It can be observed that all the data points are below the line of equality indicating that rate of carbonation of concrete specimens exposed at site CD is higher than those exposed at site MS. This can be attributed due to the higher CO_2 concentration of the site CD with respect to site MS; which results in the increased

carbonation process. Similar trend of increase in rate of carbonation with increase in CO_2 concentration was also observed by other researchers (Yoon et al., 2007; Visser, 2014).

4.5 MOISTURE PROFILE MEASUREMENTS

The moisture condition of concrete (internal RH) has a major influence on the rate of carbonation, as the carbonation reaction mostly takes place at a certain range of internal RH (50%-70%) of concrete. The influence of concrete mix proportions, w/b, curing regime and environmental conditions on the internal RH condition was studied based on the experimental programme as described in Section 3.3.3. The experimental method adopted was a modified version of the method used by Parrott (1988), and the moisture condition of concrete was expressed in terms of relative humidity (RH). A total of 48 specimens (with twelve different mixes × four different curing conditions, (see Table 3.2 and Table 3.5) were cast for the RH measurements and were exposed to the natural environment at the sites ME, MS, WE and WS (details see Table 3.6) along with the concrete specimens used for carbonation measurements.

Another set of 48 specimens was exposed to controlled environmental conditions in the laboratory, where the temperature and RH were maintained at 20-22°C and 50% respectively. Examples of the drying or RH profile development with time and their variation with respect to depth from the surface of exposure for concrete specimen subjected to Curing-A and Curing-B is shown Figure 4.38 to Figure 4.41

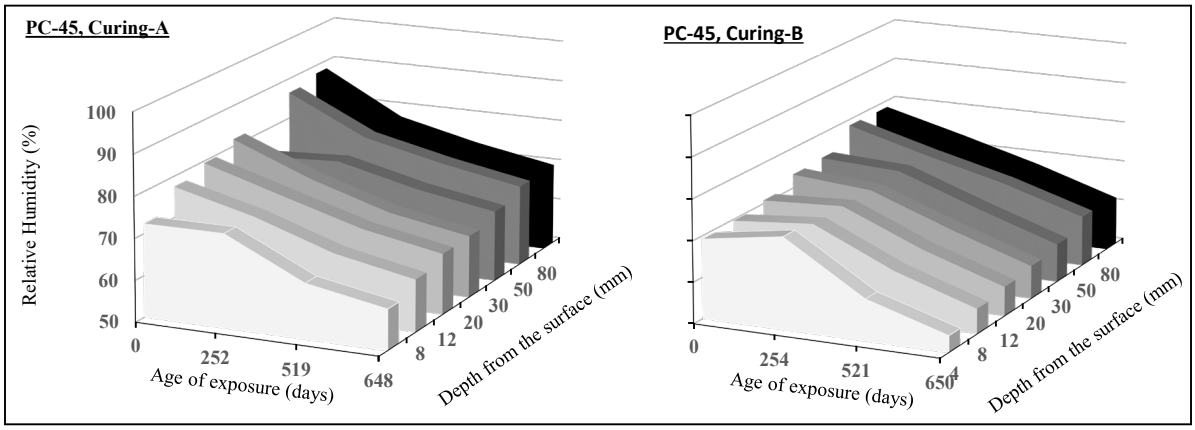

Figure 4.38 RH profile development with time of PC concrete specimens exposed to 20-22°C and 50% RH (0.45 w/b; Curing-A and Curing-B)

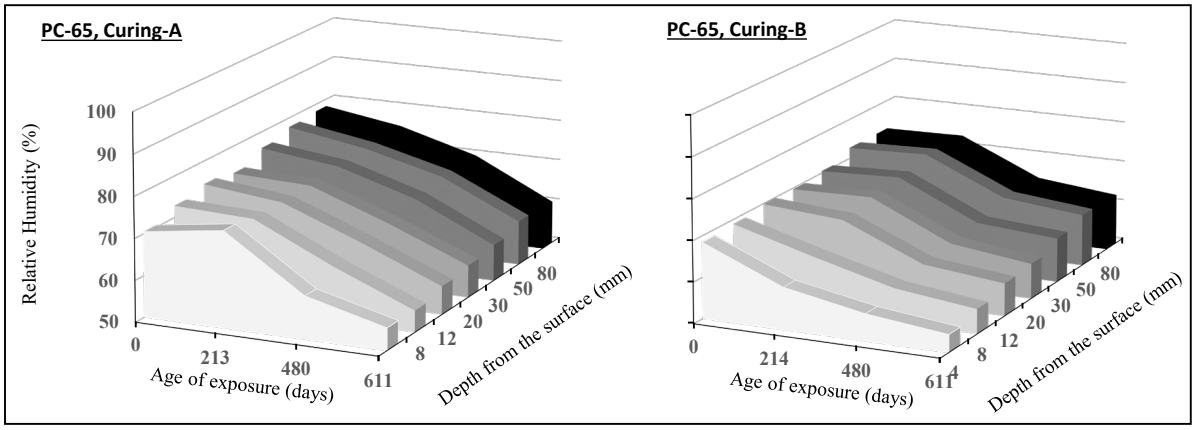

Figure 4.39 RH profile development with time of PC concrete specimens exposed to 20-22°C and 50% RH (0.65 w/b; Curing-A and Curing-B)

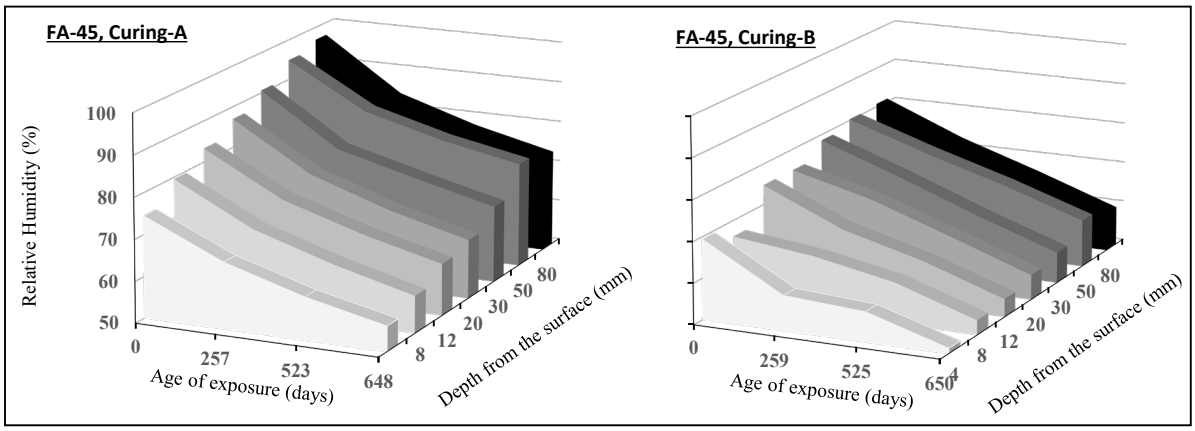

Figure 4.40 RH profile development with time of FA concrete specimens exposed to 20-22°C and 50% RH (0.45 w/b; Curing-A and Curing-B)

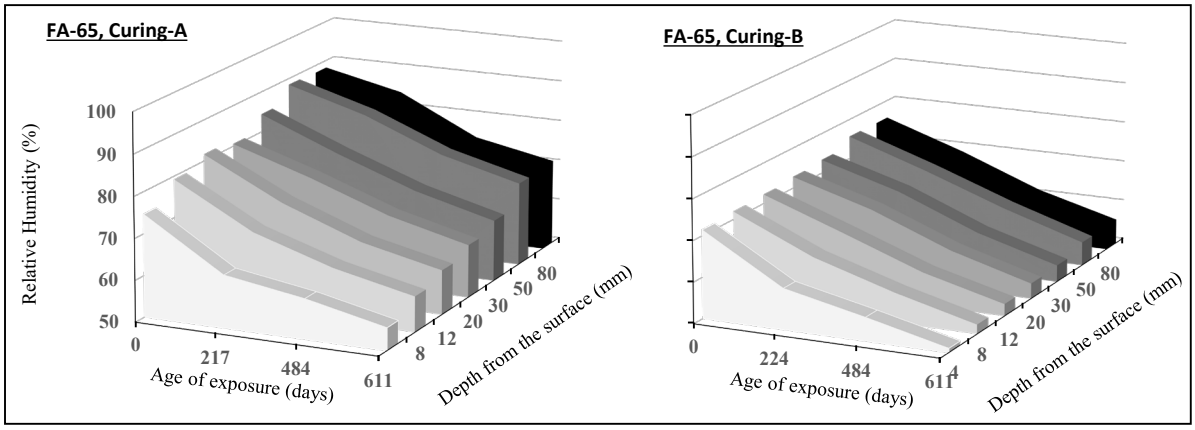

Figure 4.41 RH profile development with time of FA concrete specimens exposed to 20-22°C and 50% RH (0.65 w/b; Curing-A and Curing-B)

4.5.1 Effect of w/b and Curing on Rate of Drying of Concrete

The influence of w/b and curing condition on the rate of drying can be observed from Figure 4.38 to Figure 4.41. The concrete specimens subjected to poor curing conditions (Curing-B) tend to dry faster. For the same curing condition the drying rate increases with increase in w/b. Furthermore, it can be inferred that the surface layer of the concrete is more sensitive towards drying and the rate of drying is diminished for the deeper layers of concrete. In order to establish the general trends and variations of RH with respect to change in w/b, binder type, curing etc. on the rate of drying, a comparison of RH profiles of the concrete specimens measured after 16-20 months of unidirectional drying are presented in Figure 4.42 to Figure 4.45 (same marker is used to indicate the day of drying and curing regime). Since the casting and moisture measurements was done in batches, the exposure period of each specimen is different and in the range (480-600 days).

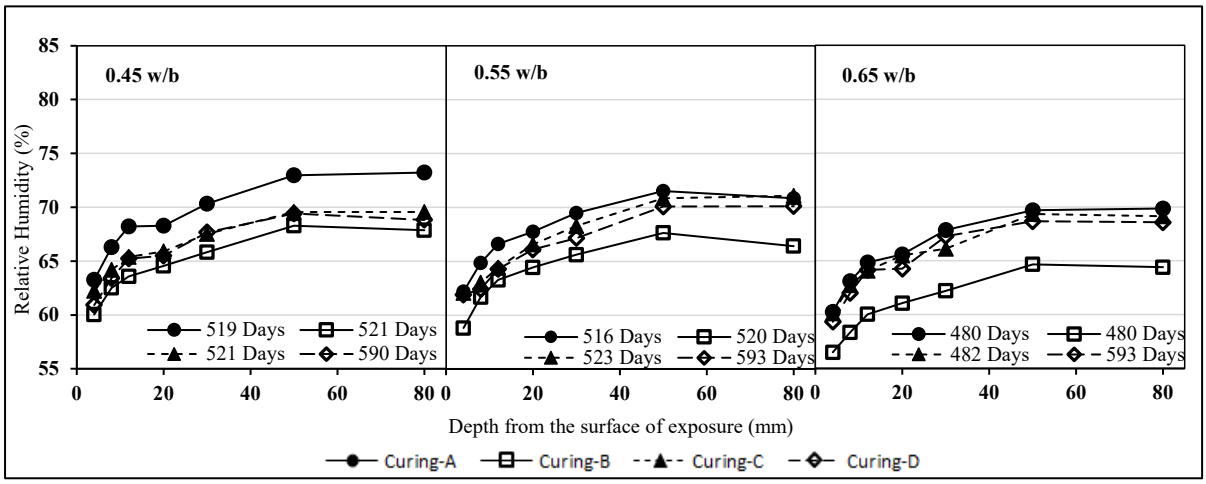

Figure 4.42 RH profile of PC concrete specimens exposed to 20-22°C and 50% RH

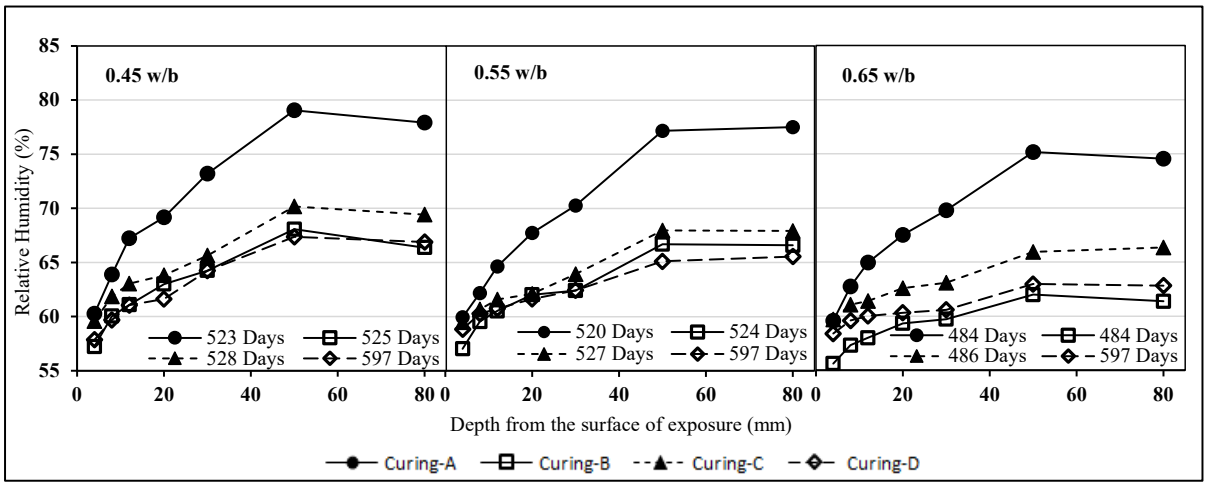

Figure 4.43 RH profile of FA concrete specimens exposed to 20-22°C and 50% RH

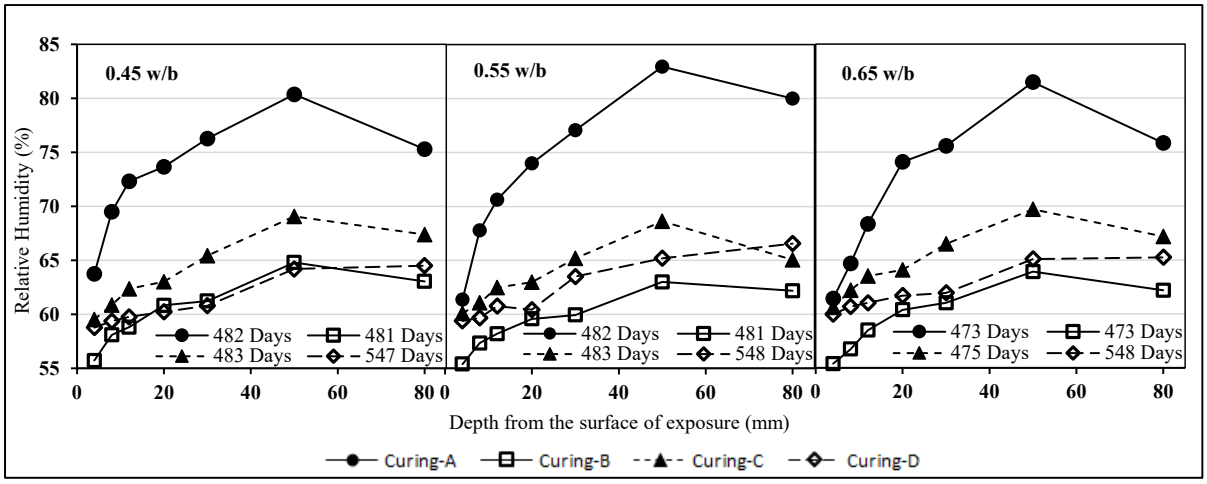

Figure 4.44 RH profile of GS concrete specimens exposed to 20-22°C and 50% RH

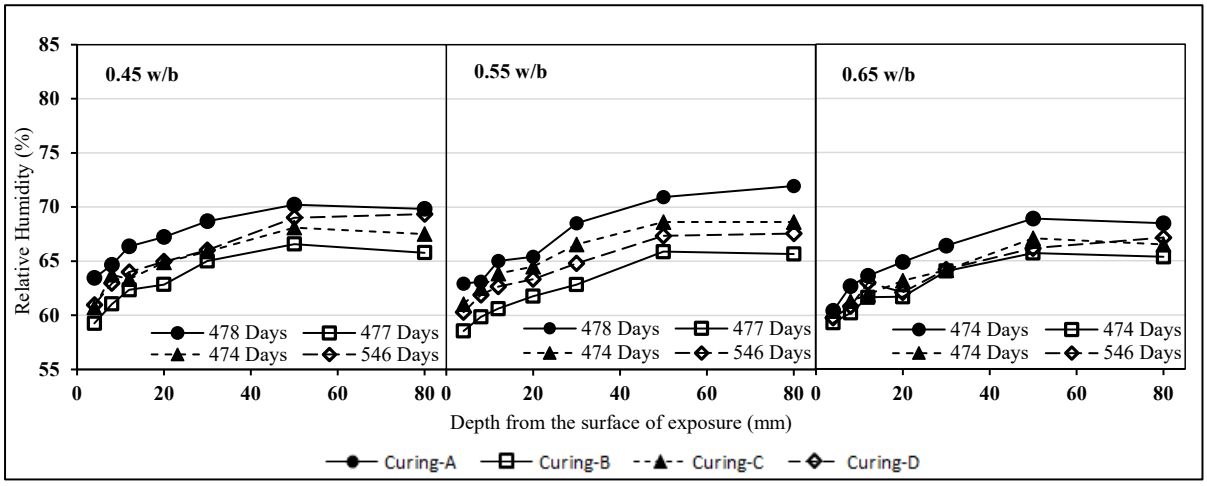

Figure 4.45 RH profile of LS concrete specimens exposed to 20-22°C and 50% RH

It can be observed from Figure 4.42 to Figure 4.45 that the w/b influences the rate of drying, as the internal RH of the concrete was observed to be lower as the w/b increases. The increase in the rate of drying of concrete with increase in w/b can be attributed to the coarser pore structure of concrete with higher w/b. This observation is in agreement with the OPI results, where a higher permeability was observed with increase in w/b. Hence the increase in rate of carbonation with increase in w/b can be due to the combined effect of faster drying and higher permeability. The influence of curing can also be observed from Figure 4.42 to Figure 4.45. Irrespective of the concrete type and the w/b, concrete specimens subjected to Curing-A experience the lowest drying rate, and specimens subjected to Curing-B experience the highest drying rate. Again, this is due to the refinement of pore structure from the better curing conditions of the 28 days standard water curing (Curing-A). Similar trends was also observed in the case of OPI results where the specimens with Curing-A experience higher OPI values (see Figure 4.3). The combined effect of poor drying rate and lower permeability of concrete specimens subjected to Curing-A was reflected in the carbonation results (see Figure 4.13 to Figure 4.17). It can also be observed that in all cases

presented in Figure 4.42 to Figure 4.45, specimens subjected to Curing-B experience the highest rate of drying, higher than the specimens subjected to Curing-D, which are exposed for drying for a longer duration (in the range of 546 to 597 days) when compared to specimens subjected to other curing regimes. This clearly shows the effect of poor curing conditions (Curing-B) on the drying rate of concrete.

In the case of concrete subjected to Curing-B, the specimens with cement extenders such as fly ash and GGBS showed higher drying rate as the internal RH were observed to be lower when compared to the specimens made of PC and LS concrete. On the other hand, when subjected to Curing-A, the specimens with fly ash and GGBS showed slower drying rate when compared to the PC or LS concrete specimens. This reduction in rate of drying of concrete with fly ash and GGBS when compared to PC concrete and when subjected to 28 days standard curing was also observed by Parrott (1988), and can be attributed due to the finer pore structure developed due to better curing conditions (Parrott, 1988; Leemann et al., 2015). The above observation is in accordance with the OPI test results where the OPI values of FA and GS concrete were higher that the PC and LS concrete when subjected to Curing-A, due to the development of a denser microstructure. From the above results, it can also be inferred that the variation in microstructure because of curing (Curing-A and Curing-B), resulting in slower and faster rate of drying respectively, is more pronounced in the case of concrete with fly ash and GGBS when compared to PC and LS concrete. The impact of variation in microstructure with curing was also reflected in the OPI test results (predominantly for concrete with fly ash and GGBS) as discussed in Section 4.3.2

4.5.2 Effect of Environmental Factors on Internal RH of Concrete

The exposure conditions or the environmental factors is one of the major factor which influence internal humidity as well as the rate of drying of concrete, which in turn effects the rate of carbonation. In order to understand the influence of variation in environmental conditions on the internal RH of concrete, a comparison of the internal RH (after long term exposure) of concrete specimens subjected to Curing –A and Curing-B and exposed to the site ME and MS is given in Figure 4.48 to Figure 4.55. Typical example of the difference in development of drying or RH profile with time for the site ME and MS is given in Figure 4.46 and Figure 4.47

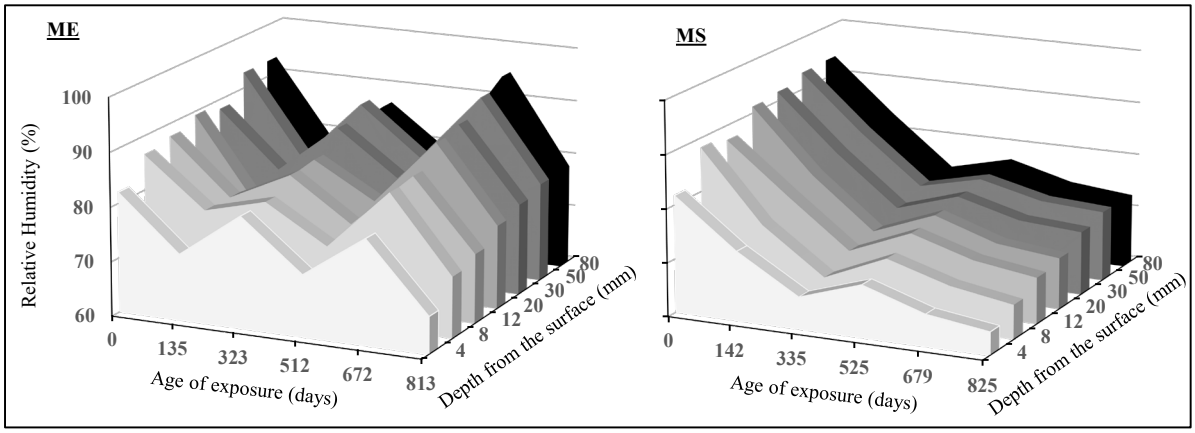

Figure 4.46 RH profile development with time of concrete specimen exposed to site ME and MS (PC-45, Curing-A)

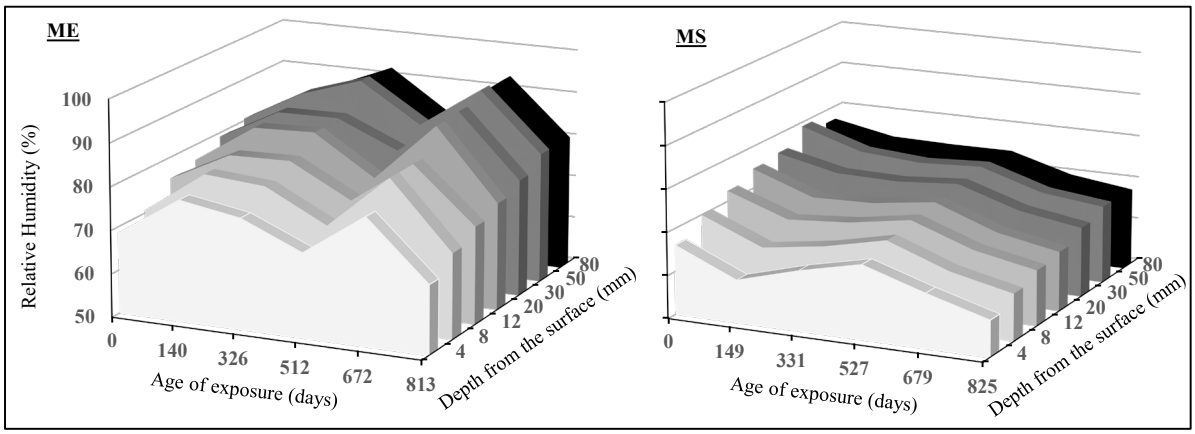

Figure 4.47 RH profile development with time of concrete specimen exposed to site ME and MS (PC-45, Curing-B)

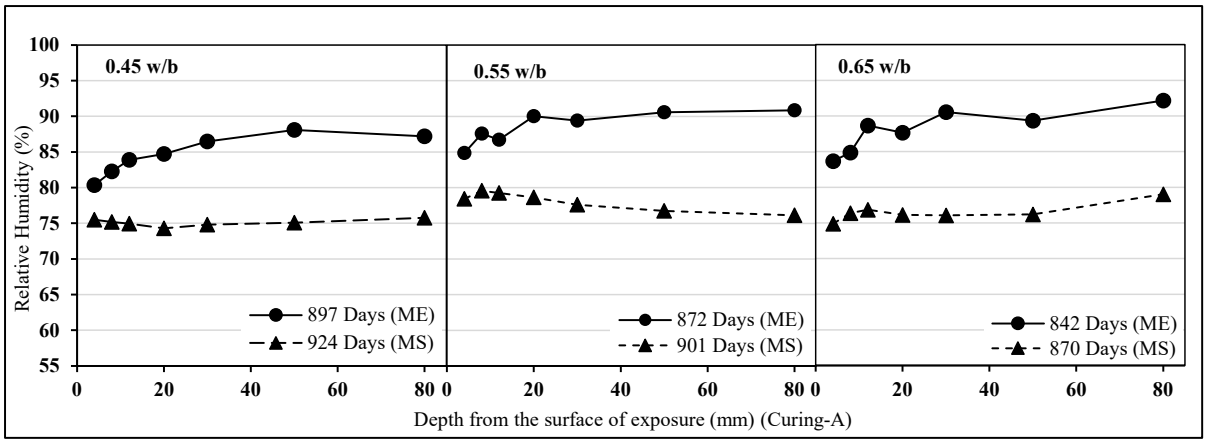

Figure 4.48 RH profile of PC concrete specimens exposed to site ME and MS (Curing-A)

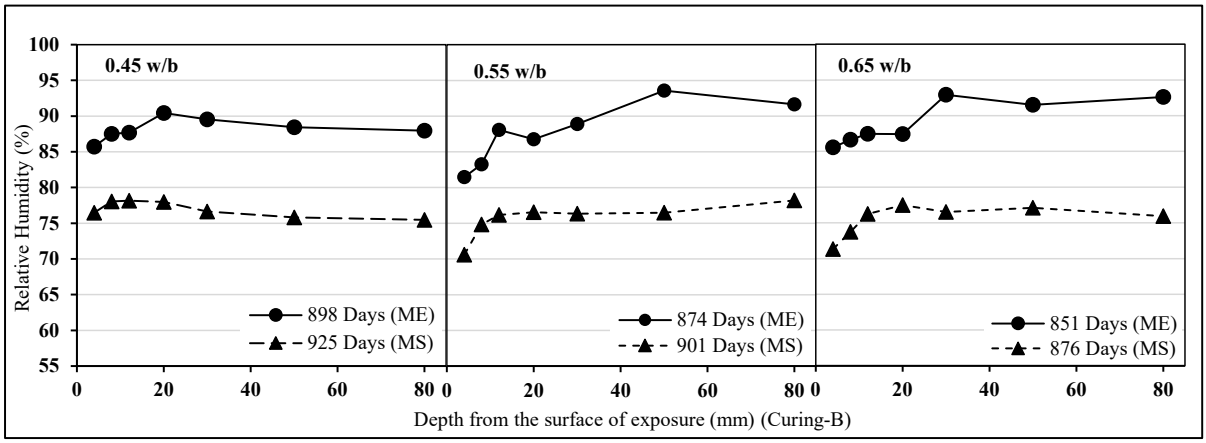

Figure 4.49 RH profile of PC concrete specimens exposed to site ME and MS (Curing-B)

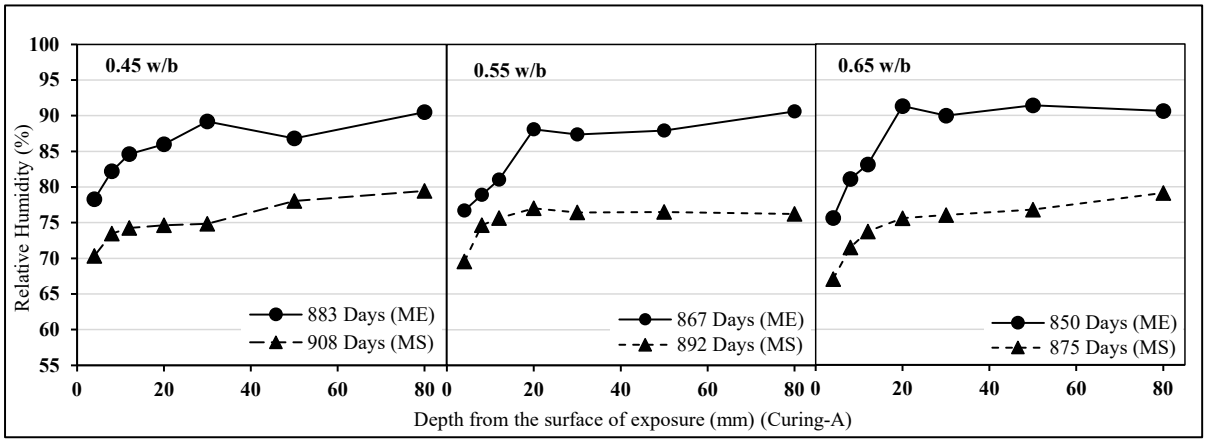

Figure 4.50 RH profile of FA concrete specimens exposed to site ME and MS (Curing-A)

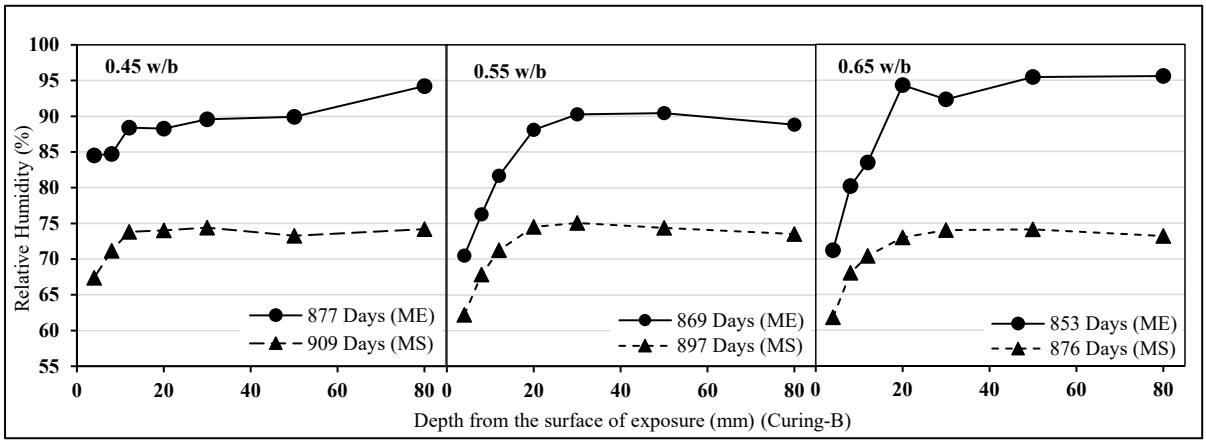

Figure 4.51 RH profile of FA concrete specimens exposed to site ME and MS (Curing-B)

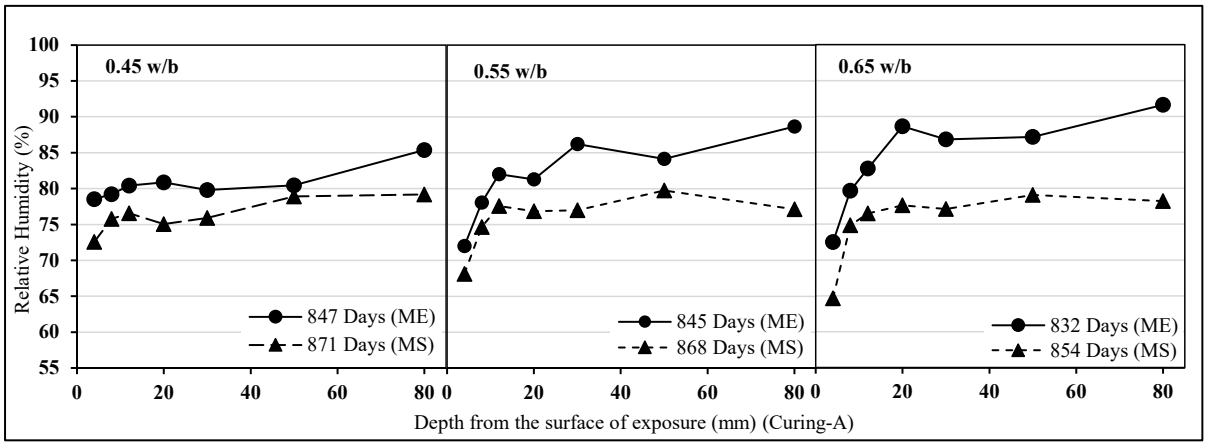

Figure 4.52 RH profile of GS concrete specimens exposed to site ME and MS (Curing-A)

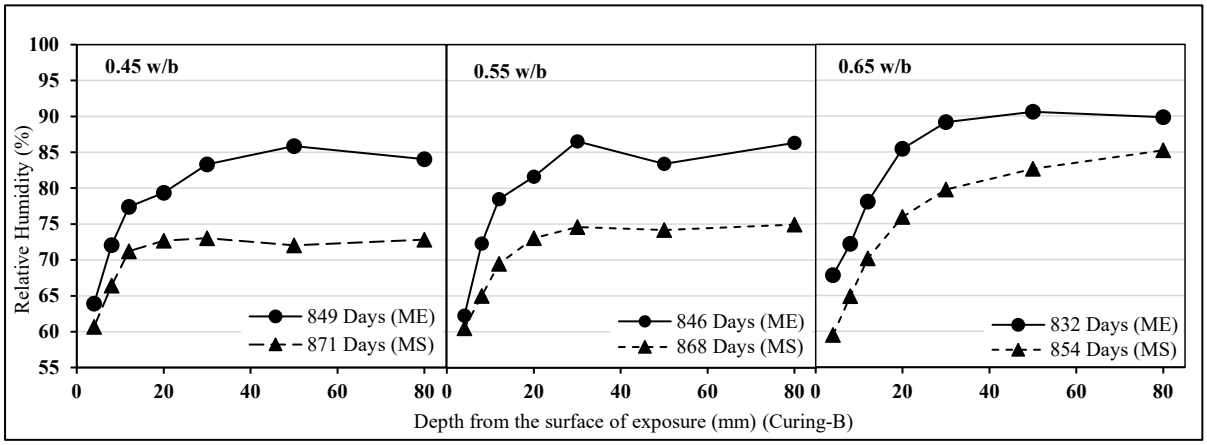

Figure 4.53 RH profile of GS concrete specimens exposed to site ME and MS (Curing-B)

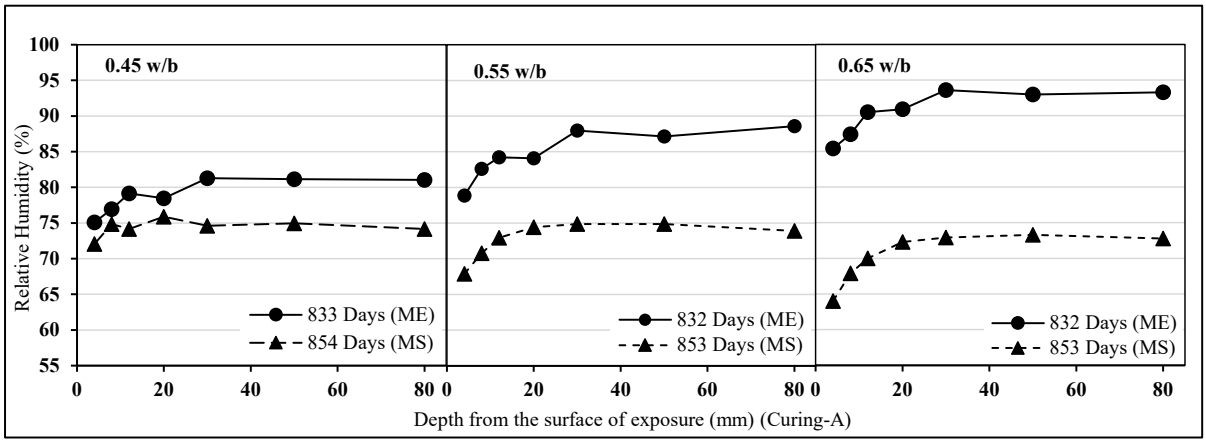

Figure 4.54 RH profile of LS concrete specimens exposed to site ME and MS (Curing-A)

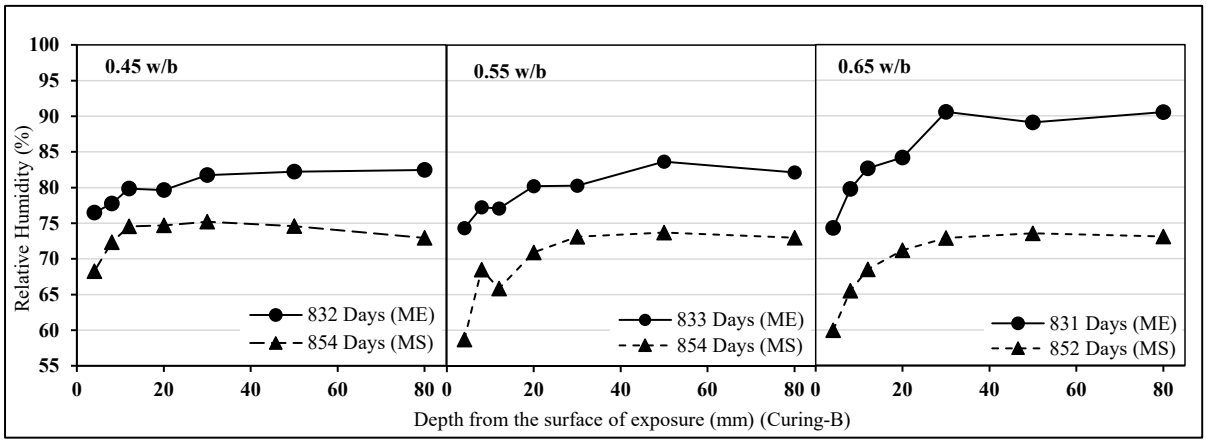

Figure 4.55 RH profile of LS concrete specimens exposed to site ME and MS (Curing-B)

The influence of drying/wetting cycles and rain on the rate of drying or RH profile development can be clearly visible from Figure 4.46 and Figure 4.47. The internal RH of the specimens exposed at site ME fluctuates with time, which can be attributed due to the exposure of these specimens to alternate wet and drying period. Whereas in the case of specimens exposed at site MS, RH continuously depreciates with time. As discussed earlier in the case of specimens exposed at controlled RH and temperature, the drying rate is higher in the case of Curing-B. Similar trend can be observed in the case of specimens at MS with Curing-B. However, contradictory to this, the internal RH profile after long-term exposure period (830-920 days) at site ME (see Figure 4.48 to Figure 4.55) shows slightly higher internal RH for specimens subjected to Curing-B than Curing-A. This can be due to the fact that the internal RH measurement was done just after the wetting period, as the specimens subjected to Curing-B can absorb and release RH at a faster rate. In general, from the above RH results (Figure 4.48 to Figure 4.55) of specimens exposed at sites ME and MS, it can be inferred that the internal RH of the specimens exposed to rain is higher than that of the internal RH of specimens sheltered from rain, irrespective of the w/b, mix proportions or curing regime adopted. The above observation corresponds with the carbonation depth measurement where the depth of carbonation was observed to be lower in the case of specimens exposed to rain when compared to the specimens sheltered from rain. The higher internal RH of unsheltered specimens reduce the rate of diffusion of CO_2 resulting in lower rates of carbonation. Therefore, it can be concluded that the drying/wetting cycles or rainfall have a major influence on the rate of progression of the carbonation front. Similar trends of higher internal RH for specimen exposed to rain (site ME) were also observed in the case of specimens subjected to Curing-C and Curing-D when exposed to site ME and MS; also for site WE and WS for all curing regimes (details, see Appendix F).

4.6 GENERAL DISCUSSION

Carbonation of concrete in general is effected by a number of internal and external parameters. Therefore, in order to predict the carbonation of concrete, it is essential to understand the effects of these parameters on carbonation and their interrelationships. Three major experimental test regimes were adopted in this research, namely: permeability test, moisture or RH profile measurements, and measurements of depth of carbonation. The test results provide an insight to the influence of major parameters such as w/b, curing condition, binder type, and environmental conditions on the rate of carbonation

Carbonation of concrete in general increases with an increase in w/b, irrespective of the binder type or curing condition. This correlates to the compressive strength results, where the compressive strength declines with increase in w/b. The major reason for both these phenomena is the development of a less dense, more porous microstructure with an increase in w/b, resulting in higher permeability. This is confirmed by the OPI test results, where a lower OPI value indicating higher permeability was observed with an increase in w/b. The development of a more permeable microstructure with an increase in w/b makes is easier for the CO_2 to enter the concrete and react with the carbonatable components, which results in a higher carbonation rate. Furthermore, the increase in w/b enhances the drying process as observed from the RH profile measurements, creating a favourable condition for carbonation reaction to take place. The increase in w/b ratio (for a fixed water content) also means a reduction in binder content in the concrete mix. The reduction in binder content further reduces the amount of carbonatable material in concrete, resulting in faster progression of carbonation. Therefore it is important to understand that the increase in the rate of carbonation with an increase in w/b is the combined effect of different phenomena, and not just related to the reduction in strength.

Curing is another major factor which has a direct impact on the rate of carbonation, since extended curing promotes the development of a denser microstructure. Out of the four curing regimes adopted in this research, the 28-day standard water curing (Curing-A) results in the highest resistance towards carbonation, and Curing-B results in the lowest. This is in agreement with the OPI test results where a lower permeability coefficient was observed for Curing-A specimens. However the effect of curing on the microstructure development is more pronounced in the case of concretes with cement extenders such as fly ash and slag. The difference in permeability between concrete subjected to Curing-A and Curing-B is

significantly higher in the case of concrete with cement extenders, compared to PC and LS concrete. Furthermore, specimens subjected to Curing-A retain moisture or RH more effectively due to the development of denser microstructure with finer pores, which can be observed from the moisture profile measurements. This makes the transport of CO_2 into the concrete more constricted due to the presence of moisture, in addition to the resistance related to the lower permeability, resulting in lower rates of carbonation. In contrast, with Curing-B, the drying rate is higher resulting in favourable moisture conditions for carbonation. Therefore it is important to incorporate curing specifications at the design stage and implement strict quality control for curing practices during construction. However, since the OPI test can characterise the influence of curing and w/b, the results from the OPI test can be used as an essential parameter for durability specifications and for carbonation modelling, as adopted in the current research.

Cement extenders are often used in construction in order to reduce the clinker content in concrete, thereby reducing the carbon footprint and also to make use of industrial by-products. The use of cement extenders in concrete with proper curing (Curing-A) has the advantage of reduced permeability over PC concrete, as discussed above. Similar to the permeability, the drying rate is also lower for concrete with cement extenders when subjected to Curing-A. Consequently the resistance to carbonation is expected to be higher than that of PC concrete. However, contradictory to the above the carbonation resistance of concrete with cement extenders was observed to be lower irrespective of w/b or curing condition. This phenomenon is due to the reduction in the amount of carbonatable material in the case of concrete with cement extenders. In the case of LS concrete the permeability performance is similar to that of concrete with cement extenders and the drying rate corresponds to that of PC concrete, but is slightly higher. However the rate of carbonation is higher when compared to PC concrete due to the lower clinker content in LS concrete. Therefore, with respect to carbonation, the amount of carbonatable material, which depends on the binder content of the concrete, is a critical parameter, since the carbonatable material buffers the progression of the carbonation front.

The environmental condition is another factor which creates a major impact on the rate of carbonation. The rate of carbonation depends on the internal RH, and conditions favourable for carbonation are in the range of 50 - 70% RH. However, the internal RH is altered due to environment factors such as rain or drying/wetting cycles, which is reflected in the RH profile of concrete specimens exposed to rain (site ME). Consequently, the internal RH is increased

and/or the pores become partially saturated during the wetting period. The increase in RH or saturation of pores stifles the carbonation reaction, until such time when the internal RH of the pores drops to conditions favourable for carbonation. However, in the case of concrete sheltered from rain, the carbonation process is continuous (even though a slight fluctuation in internal RH can be observed due to changes in environmental RH), resulting in a higher rate of carbonation, when compared to samples exposed to rain in the same location. Therefore, other than the intrinsic properties such as w/b, curing conditions and binder type; the environmental conditions also influence the rate of carbonation and need to be accounted for in the development of the carbonation model or durability design specifications, towards addressing the issue of carbonation-induced corrosion.

4.7 SUMMARY

The test results presented above (especially the OPI test results) clearly depict the variation in microstructure and transport properties of concrete and their effect on carbonation with respect to changes in w/b, mix proportions, curing conditions, etc. The test results represent a large range of permeability coefficient values, and corresponding depths of carbonation along with internal RH data; which represents a broader data set covering the majority of types of concrete used in normal construction. The experimental results reflect similar observations found in literature and coincide with the trends observed in previous studies. Taking into account the above factors, the test results seems to be a representative and useful data set and can be adopted for the development of the carbonation model, which is presented in the next chapter.

CHAPTER 5: CONCRETE CARBONATION MODELLING

5.1 BACKGROUND

The mechanism of carbonation and the factors which influence the rate of carbonation have been detailed in the previous chapters. A detailed understanding of the various carbonation models, the approach towards the model development and their shortcomings were presented in Chapter 2. This was followed by the development of a systematic experimental programme to address and analyse the different factors and their interrelationship for a range of concretes used in normal construction. The experimental outcomes were carefully analysed and their interrelationships identified.

In this chapter, the detailed framework of the proposed carbonation model is outlined. The basic derivation of the carbonation model, based on Fick's law, is presented. The correlation of different parameters are derived based on the experimental results from this research, or obtained from the literature. Also, the methodology adapted from the literature for the calculation of certain parameters of the model, especially the amount of carbonatable material, is presented. The influence of drying/wetting cycles on the rate of carbonation is addressed, and the carbonation model developed is modified accordingly by developing a correlation between the permeability coefficient obtained from the OPI test and the vapour diffusion coefficient. Finally, the carbonation model is validated using the carbonation data obtained after approximately 1000 days of exposure under different natural environmental conditions, and also using carbonation data from literature.

5.2 BASIC PRINCIPLES OF CARBONATION MODELLING

Carbonation of concrete as discussed in the previous chapters is a physico-chemical process where, at the simplest level, the CO_2 from the atmosphere diffuses through the pore structure of concrete and reacts with the carbonatable materials to form calcium carbonate. Hence, the rate of carbonation depends on the ingress of CO_2 through the concrete pore system, with the concentration gradient of CO_2 between the external environment and the interior of the concrete as the driving force. The carbonation process can be idealised using Fick's first law of diffusion. According to this, the amount of CO_2 diffusing through a concrete layer can be demonstrated as per Kropp (1995) as follows:

$$dm = -D A_1 \frac{c-c_i}{x} dt \quad 5.1$$

Where m = mass of CO_2 (m^2/s) D = diffusion coefficient (m^2/s), c = CO_2 concentration at the concrete surface (mol/m^3), c_i = CO_2 concentration at the carbonation front (mol/m^3), A_1= penetrated area, t = time (s) and x = carbonation depth (m).

The amount of CO_2 needed to carbonate the carbonatable material 'a' (mol/m^3) is given by

$$dm = a A_1 dx \quad 5.2$$

Therefore, Equation (5.1) can be rewritten as follows

$$-a A_1 dx = -D A_1 \frac{c-c_i}{x} dt \quad 5.3$$

Integrating Equation (5.3) and considering that the CO_2 concentration at the carbonation front is much lower than that in the environment (close to zero, making c_i effectively equal to zero), the carbonation depth (x) from the concrete surface at time t can be expressed as

$$x = \sqrt{\frac{2Dc}{a}} \times \sqrt{t} \quad 5.4$$

Similar approaches towards carbonation prediction were adopted by other researchers in the past (Kropp, 1995; Audenaert, 2007; Sisomphon and Franke, 2007; Salvoldi 2010). However Equation (5.4) is derived based on the assumption that the diffusion coefficient is a material property and is constant throughout the material. This assumption is not true during the entire service life of the structure, as the diffusion coefficient 'D' may vary due to the change in RH and the moisture condition of the concrete from factors such as rainfall. The carbonation of concrete itself results in a change in diffusion coefficient because of the formation of $CaCO_3$ which densifies the pore structure.

Another assumption in the derivation of Equation (5.4) is that the process of carbonation is idealised as a front which travels into the concrete, separating the non-carbonated material from the carbonated material (Ballim et al., 2009). The existence of a transition zone where the concrete is observed to be partially carbonated has been established by other researchers (Thiery et al., 2007; Ji et al., 2014). However, as indicated by Salvoldi et al. (2010), it is the pH that is critical to concrete deterioration by way of reinforcement corrosion, rather than the change in concentration of carbonatable material. According to the standard Pourbaix diagrams at 25˚C, the reinforcing steel corrodes at pH values less than 9 under appropriate humidity

conditions. Therefore for the purposes of modelling, carbonation progression will be idealized as a front, and the Phenolphthalein test can be adopted to measure the depth of carbonation which separates the area where pH values are less than 8.2 from the rest of the concrete which is not carbonated.

Finally, the amount of carbonatable material is assumed to be constant throughout the concrete matrix. This is reasonably true after an adequate period of hydration (i.e. several months or years), although in the near-surface layers where hydration may be less, this will not entirely hold. Equation (5.4) is regarded as the initial step towards the development of a carbonation model. The factors and assumptions influencing the model need to be addressed, and the variables need to be defined or modified accordingly. This is discussed below.

5.3 VARIABLES OF THE CARBONATION MODEL

The basic principle of the carbonation model and the derivation of the generic form of the model has been discussed in the previous section. The main variables of the carbonation model, such as the environmental parameters, carbonatable materials, and the diffusion coefficient, are defined and the factors affecting these variables are discussed in this section.

5.3.1 Environmental Parameters

The environmental parameters influencing the carbonation of concrete were taken as rainfall, relative humidity (RH), temperature, and CO_2 concentration, rainfall etc. The rain fall data for three consecutive years was collected from weather station in Cape Town around five kilometres from the site ME and MS, as well as from Johannesburg around seven kilometres from the site WE and WS; details in Appendix E. RH, temperature, and CO_2 concentration were measured for all five sites (ME, MS, WE, WS, CD) chosen for this research, as mentioned in Table 3.6. These five sites represented a reasonable cross-section of different environments encountered in Cape Town and Johannesburg. Only one set of measurements was taken for the two sites ME and MS, since they are adjacent to each other, with the site MS providing shelter from rain to the concrete samples. The same applies for the sites WE and WS. A separate set of measurement was taken for the site CD which is located in a parking garage under sheltered condition as discussed in Table 3.6. The average monthly values of RH, temperature and CO_2 for the sites ME, MS and CD for a span of two years is shown in Figures 5.1 and 5.2. The mean values shown in Figure 5.1 and Figure 5.2 are the average of data measured at 20 minute intervals for two years. Figure 5.3 represents the average monthly values of RH, temperature

and CO_2 for twelve months, for the locations WE and WS; the data were adopted from Alhassan (2014), since the same location was adopted for the current research.

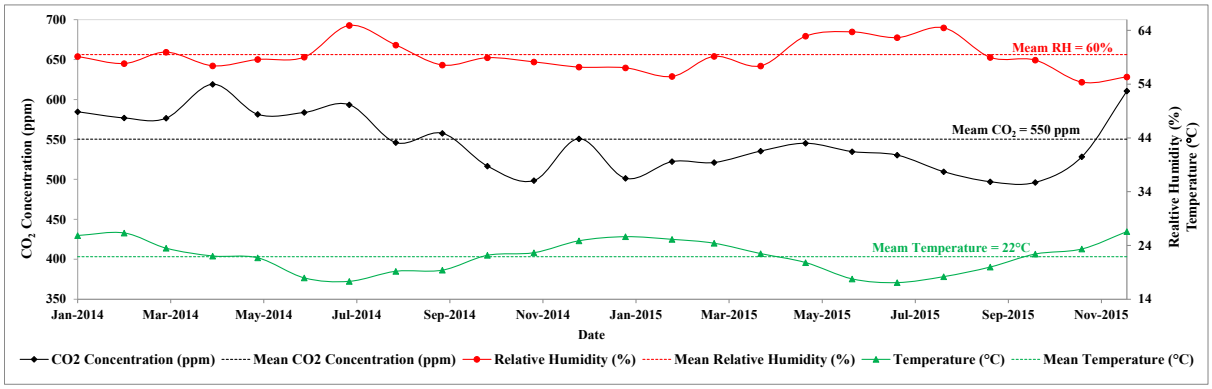

Figure 5.1 Average monthly values of temperature, CO_2 and RH at site CD

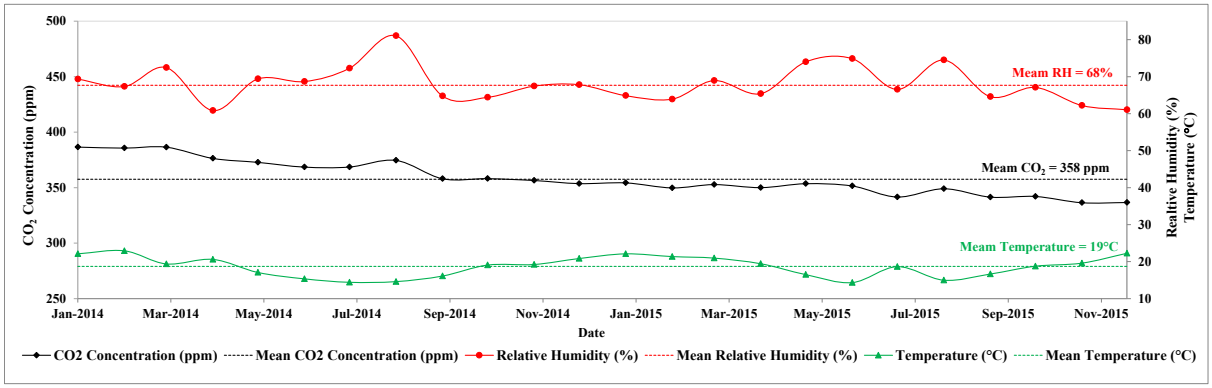

Figure 5.2 Average monthly values of temperature, CO_2 and RH at site ME and MS

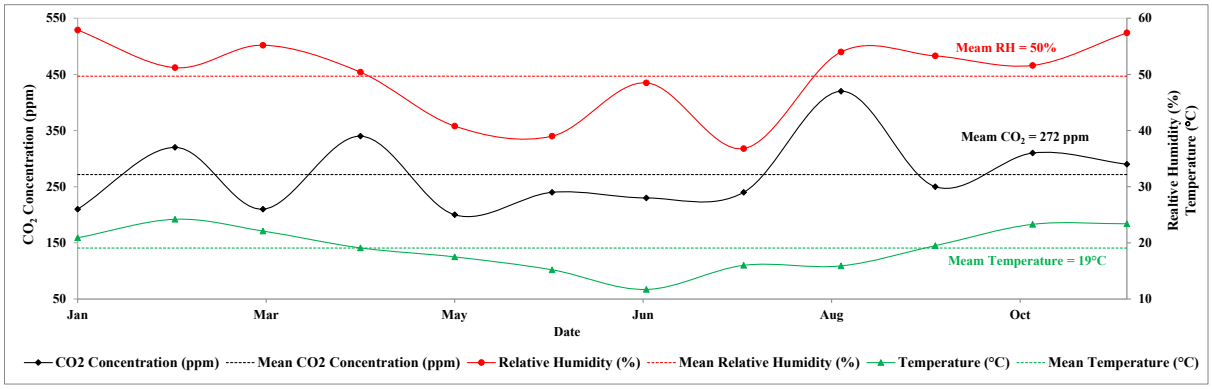

Figure 5.3 Average monthly values of temperature, CO_2 and RH at site WE and WS

The mean values of the environmental parameters (RH, temperature and CO_2) of the site as shown Figure 5.1 to Figure 5.3 were used for the purpose of modelling in this research, since they provide the true representation of the environmental parameter of that particular site.

5.3.2 Carbonatable Material

As mentioned, the amount of carbonatable material was assumed to be constant throughout the cement matrix in the derivation of Equation (5.4). Based on accelerated carbonation studies, Papadakis et al. (1989) showed that all the C-S-H and CH are potentially completely carbonatable. A similar conclusion was also made by Visser (2014), who stated that the carbonation front proceeds once all the buffering cement phases are carbonated. On the other hand, Castellote et al. (2009) showed that in natural conditions (i.e. non-accelerated conditions), not all the C-S-H is consumed (Castellote et al., 2009). Salvoldi et al. (2010) indicated that in natural conditions, the reaction layer of the CSH lags behind the reaction layer of CH, and the carbonation of CH is the critical factor associated with the pH drop. Hence, the initial CH content is usually adopted as the carbonatable material in modelling the carbonation of concrete by researchers (Salvoldi, 2010, Thiery et al., 2012), and this is also the case in the current research.

The total amount of carbonatable material therefore represent the number of moles of carbon dioxide required per cubic meter of concrete for carbonation of CH and is assumed to be constant throughout the cement matrix. The amount of CH produced during cement hydration at the end of the curing regime can be calculated by taking into account the chemical composition of the binder and the degree of cement hydration. Papadakis et al. (1991b) derived mass balance equations of CH based on cement hydration of PC. However the addition of cement extenders results in the consumption of CH and hence the reaction of the cement extenders needs to be taken into account for the calculation of CH. Therefore the total CH available in the hydrated cement paste will be the summation of CH produced by the hydration of C_3S and C_2S and the CH consumed by tricalcium aluminate (C_3A), tetracalcium aluminoferrite (C_4AF) and by the cement extenders. Based on Papadakis's approach and taking account of reactivity of the cement extenders, Salvoldi (2010) developed a generalised mass balance equation of CH for PC and any blended cements as shown in Equation (5.5). In this research the amount of carbonatable material will be calculated as per Equation (5.5) adopted from Salvoldi (2010), the details and the description of each variable being given below.

$$[CH]=1.5[C_3S]F_{C_3S}+1.5[C_2S]F_{C_2S}-4[C_4AF]F_{C_4AF}-[C_3A]F_{C_3A}+\left[C\hat{S}H_2\right]+[C]P_C - 1.5[S]\,P_S - [A]P_A \quad 5.5$$

Where,

[k] = molar concentration of compound 'k'

F_i = degree of hydration of compound 'i'

P_j = degree of reactivity of compound 'j'

C, S and A are Calcium oxide, Silica and Alumina respectively.

The degree of hydration F_i of the cement compounds was evaluated based on the hydration model adopted Papadakis et al. (1991-b) as shown below

$$F_i = 1 - \left(1 - k_i \times t_c(1 - n_i)\right)^{1/(1-n_i)} \quad 5.6$$

Where, t_c = duration of the curing regime in days. The values of k_i and n_i are empirical factors evaluated experimentally and are adopted from Papadakis et al. (1991b) as shown in Table 5.1

Table 5.1 Coefficients - Degree of hydration estimation (Papadakis (1991b)

Compound	**C_3S**	**C_2S**	**C_4AF**	**C_3A**
n_i	2.65	3.10	3.81	2.41
k_i (day^{-1})	1.17	0.16	1.00	2.46

However, Equation (5.6) adopted from Papadakis et al. (1991b) estimates the degree of hydration in the case where the concrete subjects to standard water curing. Equation (5.6) does not take into account the influence of partially cured or uncured concrete as well as the influence of the curing temperature. In order to accommodate the influence of curing regime and the curing temperature on the degree of hydration, Salvoldi (2010) adopted the coefficients C_{RH} and C_T developed by Parrott, et al. (1988) and Kada-Benameur, et al. (2000), respectively. C_{RH} and C_T account for no curing and the effect of temperature respectively on the degree of hydration. Therefore Equation (5.6) can be modified as follows (Salvoldi, 2010)

$$F_i = C_{RH}\left(1 - \left(1 - k_i \times C_T \times t(1-n_i)\right)^{1/(1-n_i)}\right) \quad 5.7$$

Where,

$$C_{RH} = \left(\frac{RH - 0.55}{0.45}\right)^4 \quad 5.8$$

and

$$C_T = e^{\left[\frac{E_a}{R}\left(\frac{1}{293} - \frac{1}{T}\right)\right]} \quad 5.9$$

Where, T = temperature in Kelvin, R = universal gas constant (R=8.314 J/mol.k), E_a = average activation energy (38.2kJ/mol (Kada-Benameur, et al. (2000)).

The degree of reactivity of cement extenders P_j can be estimated in a similar way to that of degree of hydration. However the maximum reactivity of the cement extender (C_b) is directly related to its glass phase content (Bahador and Cahyadi, 2009). Therefore, taking into account the influence of the glass content, the degree of reactivity of cement extenders P_j can be estimated as follows (adopted from Salvoldi (2010)).

$$P_j = C_b \times C_{RH} \left(1 - \left(1 - k_j \times C_T \times t\left(1 - n_j\right)\right)^{1/(1-n_j)}\right) \quad 5.10$$

Where, C_b=(1-crystalline phase content) 5.11

The empirical factors k_j and n_j of Equation (5.10) were adopted from Bahador and Cahyadi (2009), which are evaluated from the experimental measurements of CH from Papadakis (1999) and Saeki and Monteiro (2005) as shown in Table 5.2

Table 5.2 Coefficients – Estimation of degree of reactivity of cement extenders (Bahador and Cahyadi, 2009; Salvoldi et al., 2010)

Mineral admixture	Fly ash	GGBS
n_j	6.0	3.6
k_j (day^{-1})	$1/\sqrt{100 d_n}$	$1/\sqrt{50 d_n}$
d_n [average particle size] (μm)	20	45
Crystalline phase content (%)	11.9	1.7

The unreactive minerals represent the crystalline fraction of the cement extenders. The crystalline phase content of typical samples of fly ash and GGBS was evaluated experimentally by Salvoldi (2010) using X-ray diffraction studies, tabulated in Table 5.2. Since the fly ash and GGBS used for this research were from the same source as used in Salvoldi's research, the values of crystalline phase content in Table 5.2 were used. Salvoldi (2010) indicated that the crystalline phase contents were in good agreement with previous studies, where Hewlett (1998) pointed out variation of crystalline phase fly ash can range from 5% to 30% depending on the

region and composition of the material. Furthermore, Taylor (1997) indicates that the crystalline phase content of GGBS is usually less than 5%.

Therefore, the total amount of CH in the concrete mixture can be calculated using Equations (5.5), (5.7) and (5.10) based on the curing conditions, ambient temperature during curing, and the chemical composition of the binder. The chemical composition of the binders and the details of the curing regimes adopted in this research are given in Chapter 3, Table 3.1 and Table 3.5 respectively. Based on the above information, the total amount of CH evaluated for the current research is shown in Figure 5.4.

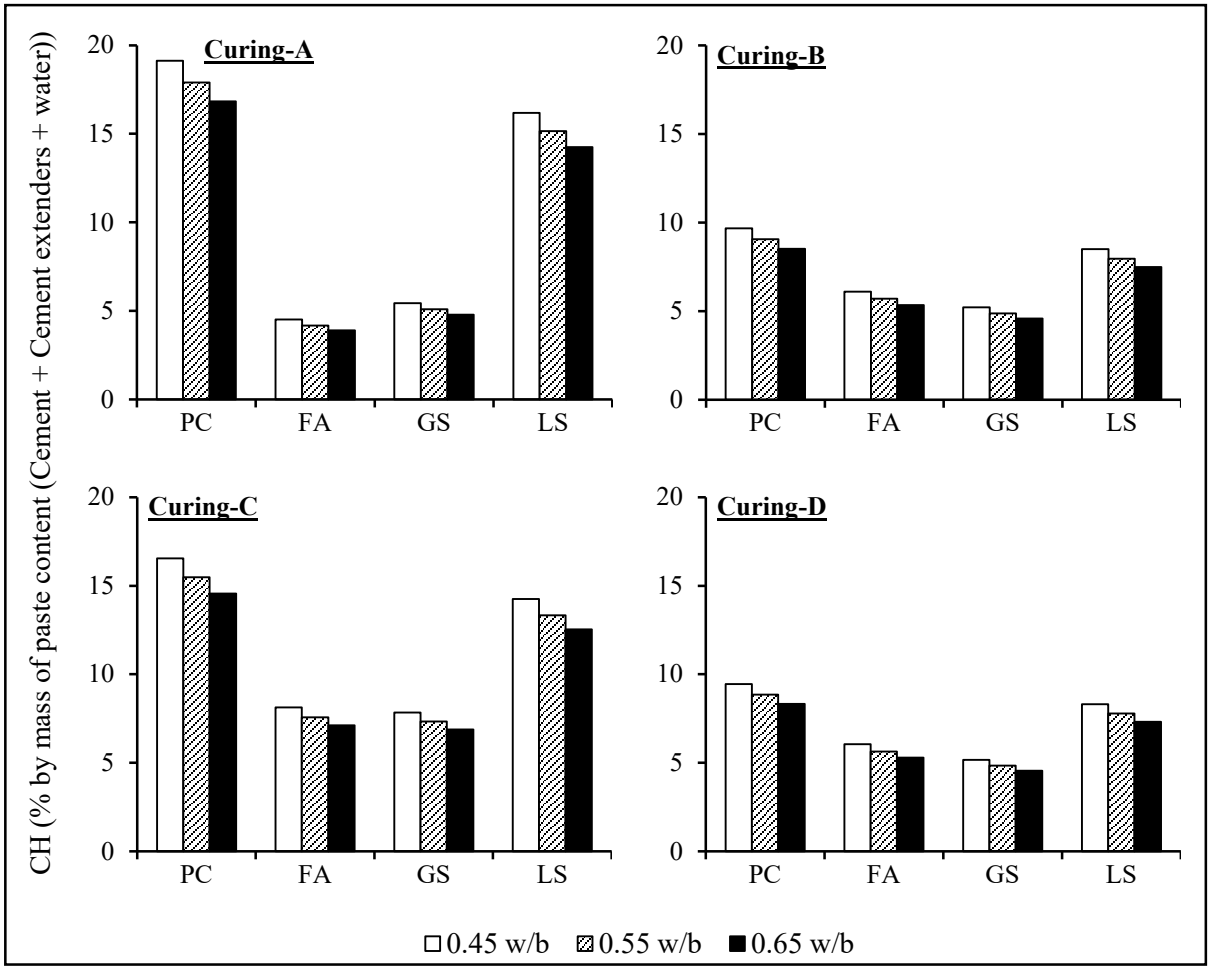

Figure 5.4 Estimated total amount of CH after 28 days of curing

It can be observed from Figure 5.4 that, with increase in the w/b or with reduction in the binder content, the CH content decreases irrespective of the type of concrete mix and the curing condition, which can be attributed to reduction in the cement content, and hence the CH content, as the water content is kept constant for all the mixes. Furthermore it can be seen that for PC concrete and LS concrete, the amount of CH increases with the increase in the number

of moist curing days in the order of Curing-B, Curing-C and Curing-A, which can be attributed to the increase in hydration because of the moist curing. On the other hand, with respect to Curing-A and Curing-C and for the concretes with cement extenders, an opposite behaviour was observed where the CH content was observed to decrease with increase in the number of moist curing days due to the increase in pozzolanic activity. Irrespective of w/b or curing conditions, the concrete mixes with cement extenders have a lower amount of CH than the PC concrete. Similar trends were observed by other researchers (Salvoldi, 2010; Alhassan, 2014)

5.3.3 Diffusion Coefficient

Diffusion of CO_2 through the concrete microstructure is the key mechanism with respect to the carbonation of concrete, and hence the diffusion coefficient is an integral variable of the carbonation model. Unlike the other variables of the carbonation model (Equation (5.4)), which can be estimated based on the quantity of materials used in the concrete and the environmental conditions, the diffusion coefficient is regarded as a material property. Therefore, it depends on the microstructure of the concrete, which along with RH of the pores, means that the diffusion coefficient needs to be established experimentally rather than simply defining a numerical value. Though measurement of the diffusion coefficient is not a simple process, attempts have been made by researchers (Papadakis et al., 1991a; Jung et al., 2011) to develop test methods to measure the CO_2 diffusion coefficient of concrete. However a simple, repeatable and reliable test method is yet to be developed.

Permeation is a transport mechanism based on the differential of pressure head, which can be determined relatively simply, and a number of standard test methods are established for the determination of the same. As discussed in Chapter 2, the South African Oxygen Permeability Index (OPI) test is a simple and repeatable gas permeability test, and can be used to address alteration or deterioration mechanisms such as carbonation. Even though diffusion and permeation are two different transport mechanisms, because they take place in the same pore structure of concrete and characterise the microstructure of concrete, a correlation between the two can be established in terms of their governing parameters. In this regard, a theoretical relationship between permeability and diffusion coefficient has been established by Nilsson and Luping (1995) as discussed in Chapter 2 (Equation (2.23)). Further, based on accelerated carbonation experiments, a relation between the diffusion coefficient and the permeability coefficient obtained from the OPI test was developed by Salvoldi (2010) (Equation (2.45)). The differences between accelerated carbonation tests and natural carbonation, and the

suitability of adopting the accelerated carbonation test results for carbonation model development, was discussed in detail in Chapter 2 (Section 2.6). Therefore a correlation between the permeability coefficient and the diffusion coefficient, using natural carbonation test results, needs to be established.

Even though the diffusion coefficient is regarded as a material property, the mechanism of diffusion is affected by the internal RH of the concrete pore structure. In the case of natural carbonation, it can be assumed that the internal RH of the concrete will be in equilibrium with the external RH on a time-averaged basis (Salvoldi et al., 2015). Based on the above assumption, it can be inferred that the variation in atmospheric RH influences the diffusion rate of CO_2 into the concrete. The process of carbonation can be idealised as a reaction-diffusion system (Papadakis et al., 1991a; Salvoldi, 2010), where the influence of RH is two-fold. At higher RH, the pores are filled with water, which restricts the diffusion of CO_2 further inside the concrete. On the other hand, the carbonation reaction will take place as soon as the CO_2 diffuses and dissolves in the pore water. At lower RH, the concrete pores dry out, which results in faster diffusion of CO_2. However, at lower RH, there is not enough water in the pores for the dissolution of all the diffused CO_2 and hence the carbonation reaction slows down or stops. Therefore at higher RH, the diffusion of CO_2 dictates the process of carbonation, and at lower RH, the reaction rate is the determining factor. The most favourable exposure conditions for carbonation to progress are observed to be in the range of 50 to 70 % RH (Verbeck, 1958; Saetta et al, 1995; Richardson, 2002; Neville, 2007).

The carbonation model developed in Equation (5.4) incorporates the diffusion coefficient, but Equation (5.4) does not account for the influence of RH on diffusion coefficient. Based on experimental data, Papadakis et al. (1991a) recommended a modification factor to account for the influence of RH on diffusion, using factor β as shown below.

$$\beta = \left(1 - \frac{RH}{100}\right)^2 \qquad 5.12$$

Salvoldi (2010) proposed a modification factor to accommodate the effect of RH on the reaction rate. Based on long-term carbonation data for varying RH presented by Wierig (1984), and taking into account the modification factor with respect to diffusion (Equation (5.12)), Salvoldi (2010) developed a comprehensive RH modification factor (H_S) addressing the influence of RH on both the diffusion and the reaction rate as shown below.

$$H_S = 23.32\left(1 - \frac{RH}{100}\right)^2 \left(\frac{RH}{100}\right)^{2.6} \quad 5.13$$

The variation of the RH modification factor with RH based on Equation (5.13) is shown in Figure 5.5. It can be observed that the RH modification factor is a maximum (closer to the value 1.0) in the range of RH from 50-70%, indicating less influence on the carbonation process. The influence of RH modification factor is in line with the common trend observed in literature with regard to the influence of RH on rate of carbonation. Furthermore, the RH modification factor proposed by Salvoldi (2010) was also adopted by other researchers (Ta et al., 2016) gives further confidence to adopt this factor for this research.

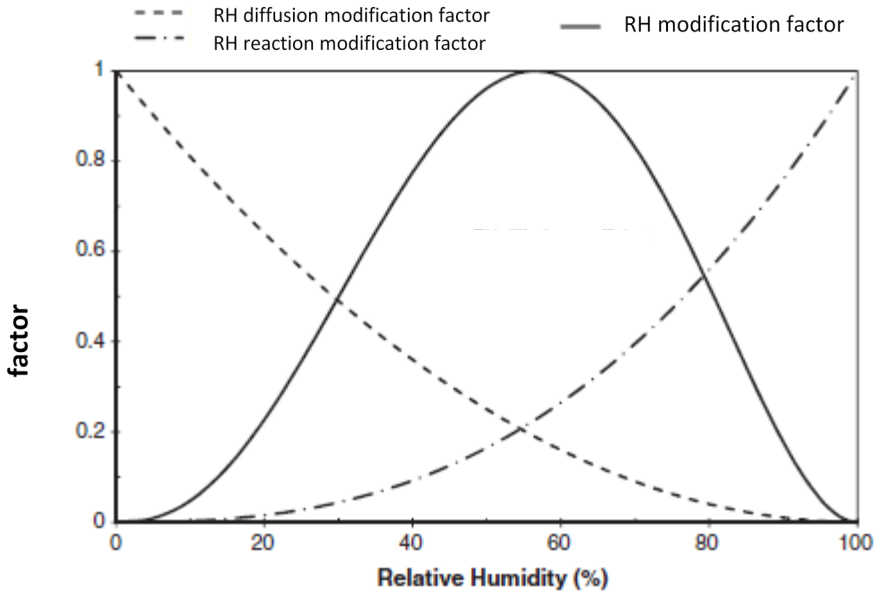

Figure 5.5 Variation of RH modification factor with relative humidity (Salvoldi (2010))

The carbonation model derived in Section 5.2 based on Fick's first law of diffusion is reproduced below ((Equation (5.4))

$$x = \sqrt{\frac{2Dc}{a}} \times \sqrt{t} \quad 5.4$$

Where, D is the diffusion coefficient. Taking into account the influence of RH on the process of carbonation as given in Equation (5.13), the diffusion coefficient can be defined as follows

$$D = D_{de} \times H_S \quad 5.14$$

Where, H_S = RH modification factor (from Equation (5.13)), which takes into account the influence of RH on the rate of diffusion and reaction rate of CO_2 in the pore solution;

D_{de} = effective dry diffusion coefficient of concrete.

As discussed in Section 5.2, the diffusion coefficient is regarded as a material property, and it can be affected by the RH and by the carbonation reaction itself. Therefore D_{de} represents the diffusion of CO_2 through the concrete pore structure without the influence of any RH and taking into account the variation in concrete microstructure due to the binding of diffusing CO_2 by the carbonatable materials in concrete. Substituting Equation (5.14) in Equation (5.4), the carbonation model taking into account the influence of RH on the reaction, and diffusion process of CO_2 through the concrete microstructure, can be presented as follows

$$x = \sqrt{\frac{2 \times D_{de} \times H_S \times c}{a}} \times \sqrt{t} \qquad 5.15$$

5.3.3.1 Relation between diffusion coefficient and permeability coefficient

As discussed above, the diffusion coefficient can be expressed in terms of a permeability coefficient, or a correlation between the two can be established. In order to develop the correlation between the diffusion and permeability coefficient, the effective dry diffusion coefficient 'D_{de}' was calculated using the carbonation model developed (Equation (5.15)) and natural carbonation data measured in this research. The natural carbonation data (between 150-850 days of natural carbonation) was obtained from concrete specimens exposed at site CD and MS. The natural carbonation data from site CD and MS was from a range of concrete mixes with different w/b and subjected to varying curing conditions (a total of 48 concrete samples made of 12 different concrete mixes as shown in Table 3.2, with each of the 12 concretes subjected to four different curing conditions as given in Table 3.5. The carbonation depth of individual samples at different ages exposed at different exposure sites is tabulated in Appendix D.1-D.5. Furthermore, taking into account the environmental parameters of sites (CD and MS) and by determining the amount of carbonatable material using Equation (5.5), the effective dry diffusion coefficient was calculated based on Equation (5.15). An example of the calculation of the effective dry diffusion coefficient based on natural carbonation data is given in Appendix G.1. The effective dry diffusion coefficient calculated was plotted against the permeability coefficient obtained based on the OPI test as shown in Figure 5.6.

Based on regression analysis, a power relationship between the effective dry diffusion coefficient based on natural carbonation data (measured in this research) and the permeability coefficient (from OPI test) was established with R-square value of 0.89 as shown in Equation (5.16).

$$D_{de} = (295 \times (k \times 10^{11})^{0.68}) \times 10^{-11} \qquad 5.16$$

Where, D_{de} and k are the effective dry diffusion coefficient and permeability coefficient in m^2/s and m/s respectively. Similar power relationships between the diffusion coefficient and the permeability coefficient were established previously in the literature (Nilsson and Luping, 1995).

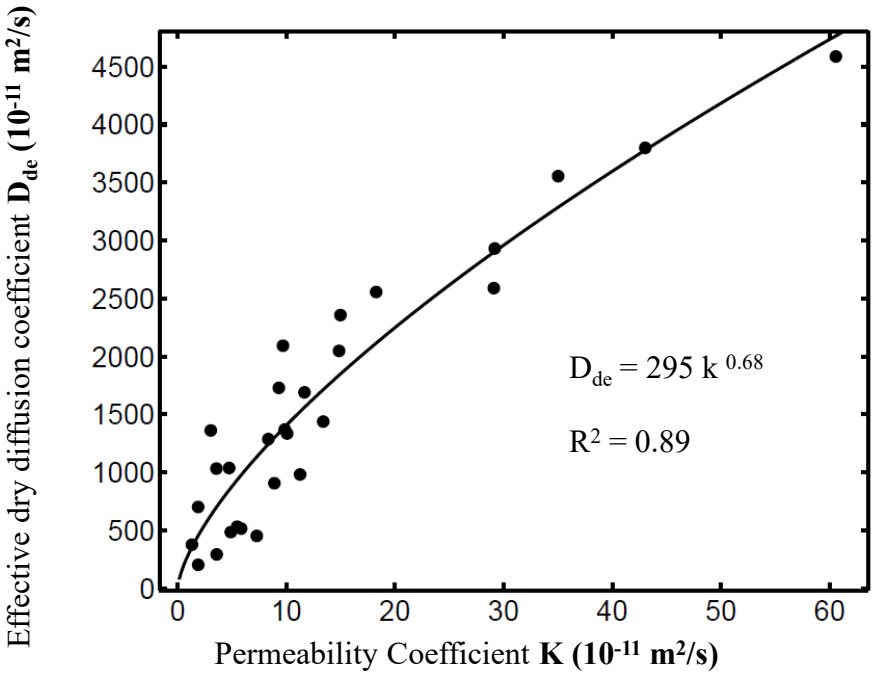

Figure 5.6 Correlation between effective dry diffusion coefficient and oxygen permeability coefficient (D_{de} vs k)

It is to be noted that in Figure 5.6, D_{de} is based on the concrete exposed to 150-850 days of natural carbonation data, taking into account of the carbonatable material based on their mix proportions and RH based on their exposure conditions. The permeability coefficient characterises the microstructure of the concrete after 28 days of curing without undergoing any carbonation. However, using Powers theory, Salvoldi (2010) calculated the change in concrete porosity due to carbonation, and indicated that the change in permeability due to such changes in porosity is insignificant from a practical point of view. Salvoldi (2010) also developed a similar correlation between diffusion coefficient and oxygen permeability coefficient (see Equation (2.45)). However, Salvoldi's correlation was based on accelerated carbonation data,

and did not cater for a wide range of permeability coefficients or curing regimes. Therefore Equation (5.16) is a major contribution of this research and provides a powerful correlation to establish the effective dry diffusion coefficient of concrete during natural carbonation. Also, the above correlation is based on the permeability coefficient from the OPI test (which is much faster than the actual diffusion measurements) after 28 days of curing and covers a range of concrete mixes with different cement extenders, w/b and curing conditions, used for normal reinforced concrete construction. This makes Equation (5.16) a practical tool in determining the dry diffusion coefficient of concrete using the OPI durability index test, towards predicting carbonation depth of concrete as per Equation (5.15) (i.e. the carbonation model).

5.4 CARBONATION MODEL VALIDATION

The carbonation model was derived based on the Fick's first law of diffusion, and is given in Equation (5.4). Equation (5.4) was further refined taking into account the factors that influence the variables of the model as discussed in Section 5.3.

The effective dry diffusion coefficient can be expressed in terms of a concrete permeability coefficient from Equation (5.16), and the influence of RH on the diffusion is taken into account by adopting the RH modification factor (H_S) given in Equation (5.13). The amount of carbonatable material buffering the progression of the carbonation front expressed in terms of CH can be calculated from Equation (5.5), which is based on the degree of hydration of cement compounds and degree of reactivity of cement extenders in the concrete mix, for the corresponding curing regimes.

In order to validate the carbonation model developed above, the carbonation depth at the age of 1000 days was predicted using Equation (5.15) based on the environmental conditions of the site, chemical composition of the binder, the curing regime tabulated in Chapter 3, and permeability coefficient at 28 days of curing tabulated in Appendix C. Some of the variables (e.g., D_{de}) of the carbonation model were defined using earlier age natural carbonation data (150-850 days). The carbonation depth predicted was compared with the carbonation depth measured on concrete samples exposed at different sites under natural carbonation. The carbonation depths measured and predicted using Equation (5.15) for different sites are tabulated in Appendix D.13, and the comparison is shown in Figure 5.7 to Figure 5.11.

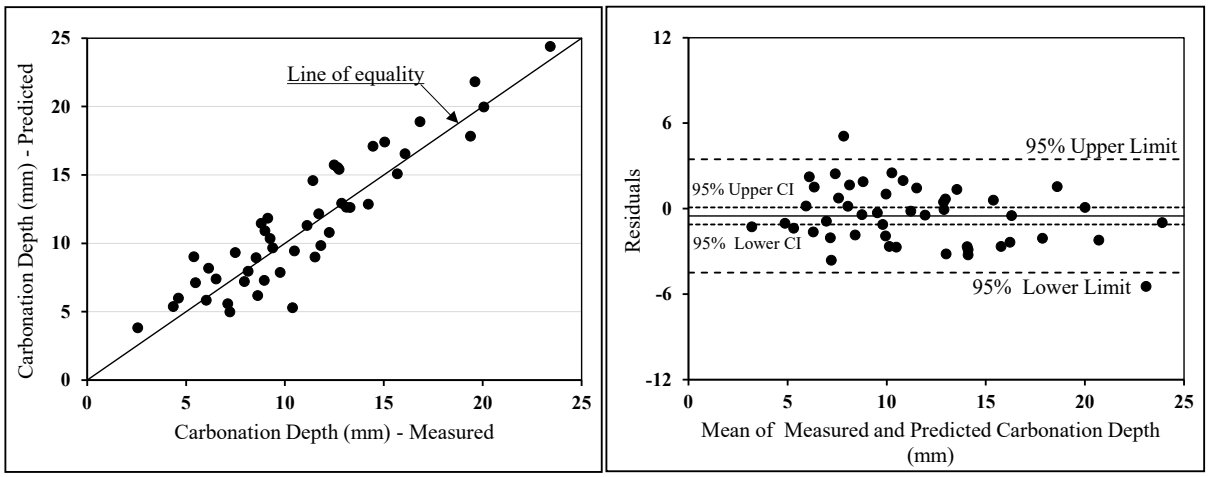

Figure 5.7 Exposure at site CD: (a) Predicted vs measured carbonation depth after 1000 days of exposure; (b) Residual plot displaying 95% limit of agreement

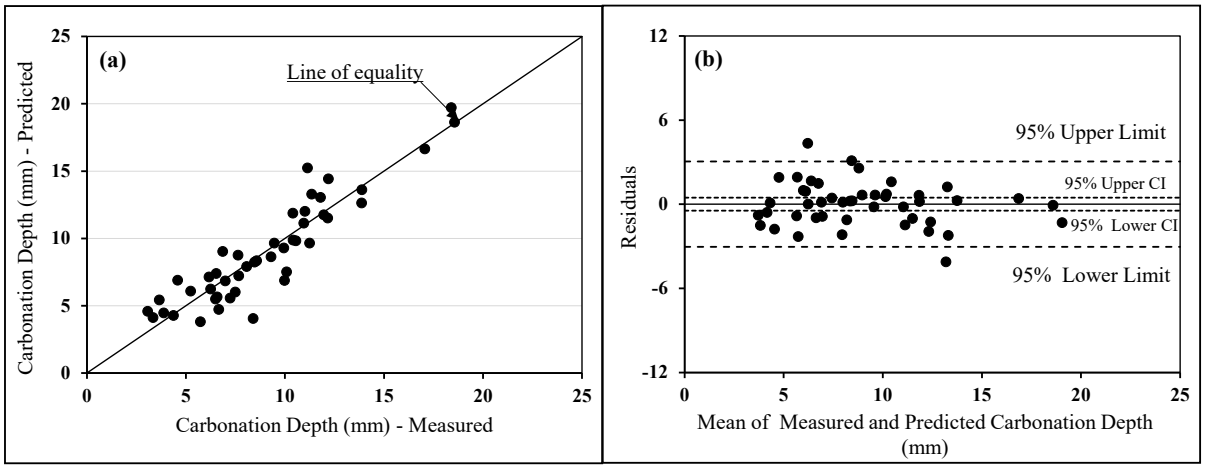

Figure 5.8 Exposure at site MS: (a) Predicted vs measured carbonation depth after 1000 days of exposure; (b) Residual plot displaying 95% limit of agreement

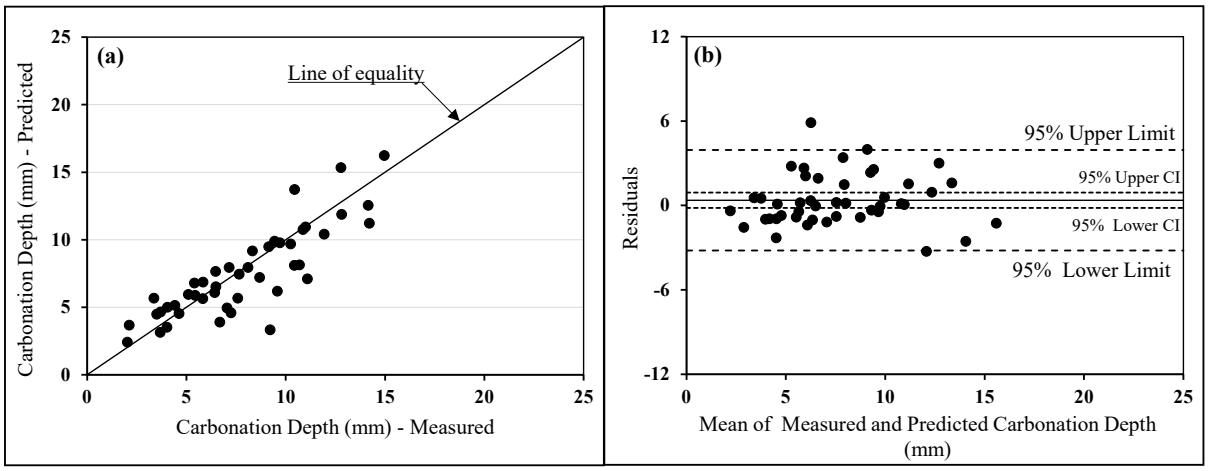

Figure 5.9 Exposure at site WS: (a) Predicted vs measured carbonation depth after 1000 days of exposure; (b) Residual plot displaying 95% limit of agreement

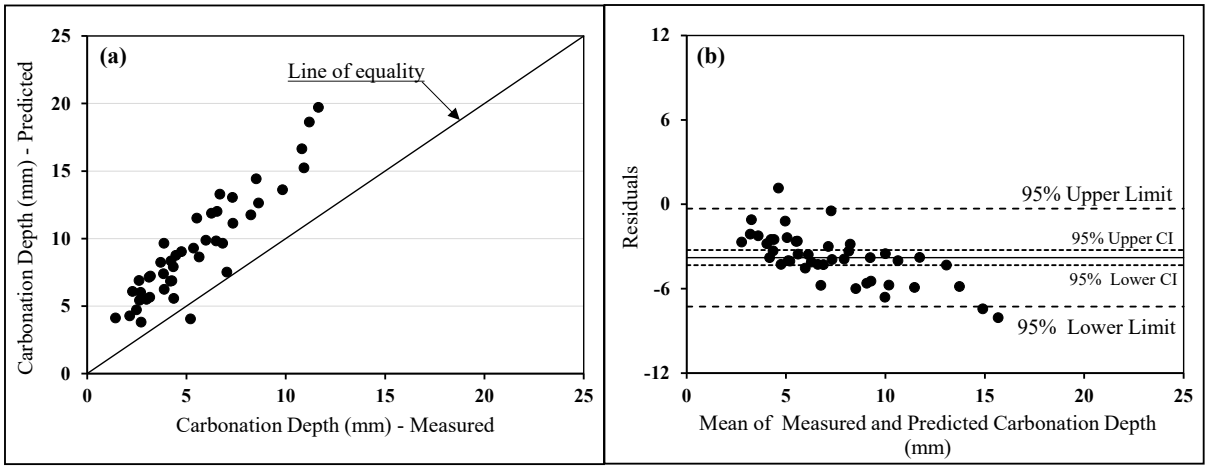

Figure 5.10 Exposure at site ME: (a) Predicted vs measured carbonation depth after 1000 days of exposure; (b) Residual plot displaying 95% limit of agreement

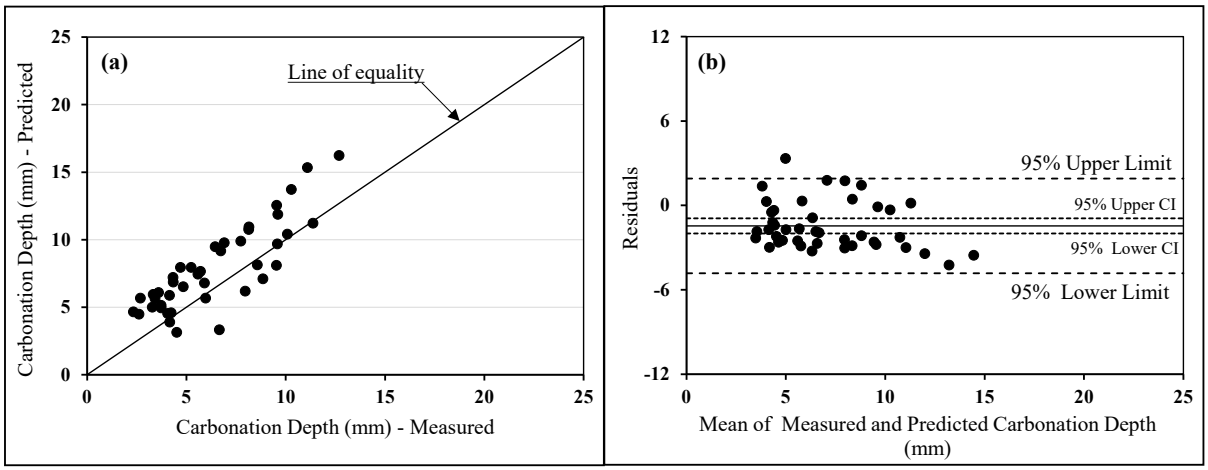

Figure 5.11 Exposure at site WE: (a) Predicted vs measured carbonation depth after 1000 days of exposure; (b) Residual plot displaying 95% limit of agreement

It can be observed from (a) of Figure 5.7 to Figure 5.9 that the predicted values of carbonation depth after 1000 days of exposure are generally in good agreement with the measured values. In order to assess the agreement between the predicted and measured carbonation depth values, a Bland and Altman (B&A) analysis (Altman and Bland, 1983; Giavarina, 2015) was conducted as shown in (b) of Figure 5.7 to Figure 5.9. A B&A analysis is based on studying the mean difference between two quantitative sets of values, and constructing limits of agreement between these two quantitative sets of values, rather than using a correlation coefficient and regression techniques as an indicator of agreement. Correlation coefficient and regression techniques indicate the relationship between two sets of data, and not the degree of agreement between them. The Y axis of (b) of Figure 5.7 to Figure 5.9 shows the difference between the measured and predicted values of carbonation depth after 1000 days of exposure (the so-called 'Residual'), and the X axis represents the mean value of measured and predicted

carbonation depth. The top-most and the bottom-most dotted lines indicated the limits of agreement or 95% reference range. The limits of agreement or 95% reference range is given by mean of differences ± 1.96 times the standard deviation of the differences. The limit of agreement therefore implies that 95% of the differences of the measured and predicted carbonation depth will fall in this range. The solid line on the graph indicates the mean of the difference between the measured and predicted values (called the 'bias') of the carbonation depth. A negative or positive value of the bias indicates whether the carbonation model overestimates or underestimates the carbonation depth respectively. The dotted lines in the middle indicated the upper and lower limits of the 95% confidence interval (CI) of the mean of differences. The bias is considered to be significant if the line of equality (which corresponds to the horizontal line parallel to x-axis intercepting y-axis of the residual plot at the origin) is not within the confidence interval of the mean difference, reflecting that the model significantly underestimates or overestimates the carbonation depth.

Therefore, based on the above analysis, it can be inferred that the carbonation model developed can predict the carbonation depth in the case of concrete sheltered from rain. The predictions are such that the differences between the measured and predicted values are within the agreement limits (see (b) of Figure 5.7 to Figure 5.9. Furthermore, since the line of equality is within the CI of the mean of the difference between the measured and predicted values, the carbonation model can reasonably predict the carbonation depth. Hence the carbonation model can be used as a tool both in the design phase of a new concrete structure, as well as to plan the repair strategies of an existing concrete structure.

However, in the case of concrete exposed to rain (see Figure 5.10 and Figure 5.11), the line of equality is not within the CI of the mean differences even though the differences between the measured and predicted values are within the agreement limits. The above observation indicates that the carbonation model significantly overestimates the carbonation depth in the case where the concrete was exposed to rain. Therefore, the developed model (Equation (5.15)) is not able to take into account the influence of rain, or more generally, moisture in the environment that affects the concrete pore structure. Even though the developed model is sensitive to the influence of RH on the diffusion coefficient, it does not take into account the effect of the drying/wetting cycles as proposed by Bakker (1988), whereby carbonation only takes place during the drying cycle. Hence the carbonation model predicts higher values for the depth of carbonation when compared to the experimental values for concrete exposed to

rain. The carbonation model needs to be modified so that the influence of drying/wetting cycles on carbonation can be incorporated, and this is discussed in the following section.

5.5 MODIFIED CARBONATION MODEL INCORPORATING THE EFFECT OF DRYING/WETTING CYCLES

5.5.1 Modification based on Time of Wetness (ToW) Concept

As discussed in the previous section, the carbonation model that was developed (Equation (5.15)) does not reflect the effect of drying/wetting cycles for concrete exposed to rain, and therefore overestimates the rate of carbonation for these conditions. In order to address the influence of rain, Salvoldi (2010) introduced the notion of effective exposure time (t_e), which is based on the time of wetness (ToW) concept described in the fib Model Code 2010 (2012). According to this, the effective exposure time is defined as the service life (exposure time) excluding ToW. ToW is defined in the fib Model Code 2010 (2012) as the total number of days with rainfall greater than or equal to 2.5 mm. Therefore a rainfall of 2.5 mm is assumed sufficiently to 'saturate' the concrete surface, thereby effectively stifling the carbonation progression due to the negligible diffusion of CO_2 through the saturated pores. The effective exposure time (t_e in days) from Salvoldi (2010) is as follows.

$$t_e = t - ToW \qquad 5.17$$

Therefore, the influence of rain can be incorporated in the carbonation model by adopting the effective time of exposure concept into Equation (5.15), and therefore the carbonation model (substituting Equation (5.17) in Equation (5.15)) can be written as shown below.

$$x = \sqrt{\frac{2 \times D_{de} \times H_S \times c}{a}} \times \sqrt{t_e} \qquad 5.18$$

Rainfall data can be obtained from the weather station closest to the exposure site. For example for the site ME, the daily rainfall data was obtained from the weather station (G2E005) located at Newlands, from The South African Weather Service (SAWS). The rainfall data during the exposure period of the sample is shown in Table 5.3. Depending on the date of first exposure of the sample, the ToW which corresponds to the total number of days with rainfall greater than 2.5 mm ranges from 199-214 days (details see Appendix D.13) for the exposure period of 1000 days. Based on the rainfall data, the carbonation depth of concrete samples exposed to rain at the site ME can be predicted using the modified carbonation model based on the ToW

concept using Equation (5.18). A comparison of the measured carbonation depth and predicted values using Equation (5.18) for the site ME is tabulated in Appendix D.13, and the comparison is graphically presented in Figure 5.12

Table 5.3 Daily rainfall data from Newlands weather station (G2E005), ca five kilometres from the site ME.

	Exposure Months																																				
Day	1	2	3	4	5	6	7	8	9	10	11	12	13	14	15	16	17	18	19	20	21	22	23	24	25	26	27	28	29	30	31	32	33	34	35	36	37
1						46.0	4.5	79.9										64.5		2.5	7.5																46.0
2						4.0	12.0	27.1			15.5						25.2	8.0		6.2	39.0										19.5				4.0	
3			9.3					13.5						1.5						55.7	6.9				4.3					19.8		19.5		9.5	
4								3.3				3.0						3.0	24.2	17.2	62.5	76.0			5.0		4.0				0.5		5.0			
5								0.2							2.0					6.0	7.5	10.5					26.0									
6									13.5	20.3			8.5		11.6						7.5	23.0	8.0											7.0		
7					6.5	7.0			5.0	9.5			1.0		7.7	5.5								0.3										18.0		
8					58.7	8.5	8.0	10.6		0.7	4.0		1.0		40.0				56.4	32.2				2.0												1.4
9			15.0	15.0		0.3									8.8				6.5	35.0														14.5	
10			1.5	14.5							1.8																						18.0		
11												1.9					0.7															17.4				
12								17.1		73.0		2.5										0.1			11.0							1.8	6.5			
13				7.5				16.2	3.0	17.0	45.5									1.5	1.0	28.5						8.0			8.0		24.0		2.5	
14				0.5				36.7	2.8	11.5	6.0									92.5		0.1			12.0				0.2		4.0			2.5	1.2	
15					2.0			2.0	2.5	60.0	19.5		82.0						36.5	28.5				1.3		32.0			3.5	15.0	52.0		49.6	9.0		
16	6.5		0.3			79.0			1.0	30.0	20.0		20.0								6.0			2.0				2.5			25.0	4.5	2.5			
17						79.6				7.0	16.0										77.0		15.5									127.0				
18				0.4	1.0			9.0	62.4								7.5			28.5	31.0	6.0	17.0					0.4								
19				5.0					29.5		48.0		7.5			4.2	8.0				2.0	8.5	2.5							2.3						18.0
20	10.0									6.0	21.0								1.5			36.5					0.3	0.5					1.0	4.5	
21							0.5	20.0		51.0	6.0											27.0													1.3	
22					3.0				20.7			0.3																			22.5					
23	16.0								6.0		1.0				4.6		13.5													2.0	56.0	32.0				
24	5.0	6.8	0.6					47.0	0.5								13.0				32.0										10.5	3.0	13.0			
25							26.0	10.5									50.0			42.0	28.0	19.4				42.0				13.5			1.5	2.5		1.0
26							80.0	8.0	34.5		40.5						27.0			12.0	21.0	4.0			15.0					31.5				6.0		
27				9.0			10.5		21.0	35.3	4.0								11.0			36.0			1.0						5.5			1.5		
28					3.5		8.0		6.5	95.5				10.0	0.1				28.5			19.8							4.0	2.0	16.5					
29							27.5			18.0		14.0							15.2					0.7					2.0	37.0	6.0	60.0		8.5		
30										21.0		12.0															14.0			1.0	15.2		17.0	7.5	7.5		
31					5.7					18.0		23.0					6.0		48.4												0.3			4.5		5.5	

The comparison between the predicted carbonation depth based on the modified carbonation model (adopting the ToW concept) and the measured values of concrete samples exposed at site ME (exposed to rain) reveals that the modified carbonation model is not able to adequately address the influence of rain. It can be seen from Figure 5.12 (b) that the modified model still overestimates the carbonation depth, as the CI of the mean differences is significantly below the line of equality (similar to Figure 5.10). Therefore, it can be deduced that modifying the current carbonation model (Equation (5.15)) using the ToW concept is not effective in predicting the carbonation depth of concrete exposed to rain, even though the ToW concept is purported to address the saturation of concrete microstructure due to rain. This clearly shows that there are other factors which hinder the progression of the carbonation front when exposed to rain or drying/wetting cycles.

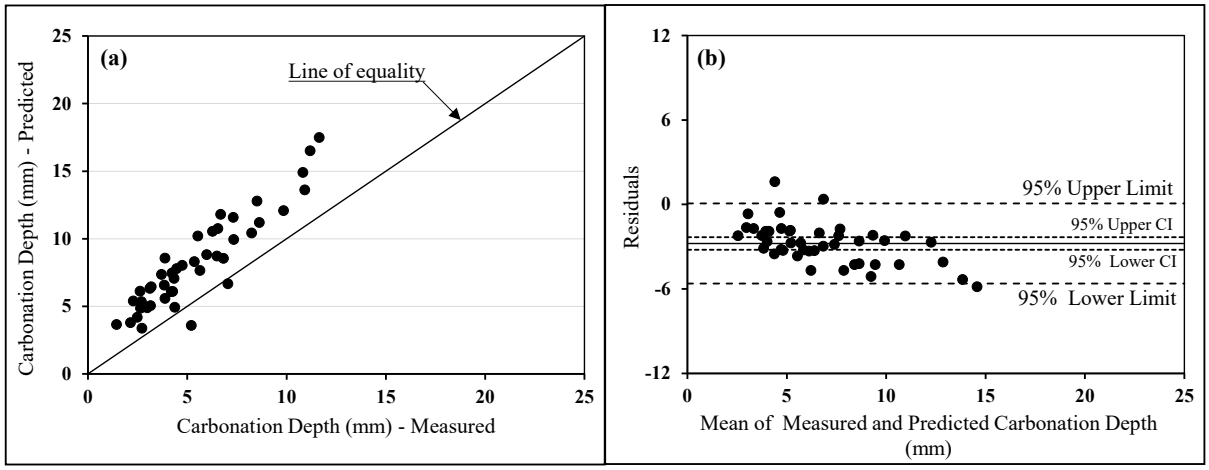

Figure 5.12 Exposure at site ME: (a) Predicted (using Equation (5.18), based on ToW concept) vs measured carbonation depth after 1000 days of exposure; (b) Residual plot displaying 95% limit of agreement

ToW concept is a simplistic approach based on the concept of pore saturation during rain (wetting period) and hence no carbonation during that period. However the time it takes for the concrete to start carbonate at a significant rate after the rain (during the drying period) is not taken into in ToW approach. Once the concrete is saturated during the rain, the further carbonation will depend on the rate of drying of concrete (since carbonation is effective only in a certain range of RH). The rate of drying depends on numerous factors including ambient RH. Ambient RH can increase or decrease the rate of drying. Lower the RH faster will be the rate of drying. Microstructure of concrete is another factor that influence the rate of drying. Concrete with coarse microstructure promotes faster drying when compared to concrete with fine pore structure (Parrott, 1988; Leemann et al., 2015). Duration of drying/wetting periods as well as the frequency of rain or drying/wetting cycles also influence on the rate of drying of concrete. For example, concrete exposed to frequent rain or drying/wetting cycles will have lower rate of drying. On the other hand, short drying period (number of days between subsequent rainfalls) also results in lower rate of drying. Therefore, taking into account of the above factors, the carbonation model (Equation (5.15)) needs to be further refined in order to be able to predict the carbonation depth of concrete when exposed to rain or drying/wetting cycles. However, since the duration of drying/wetting periods as well as the frequency of rain or drying/wetting cycles varies, modelling the exact environmental condition is difficult. Therefore a simplified approach by adopting a constant drying/wetting period was adopted in this research and this is discussed in Section 5.5.2 below.

5.5.2 Modification based on Drying/Wetting Cycles Concept

The influence of rain or drying/wetting cycles is complex. Deducing the number of days with rainfall more than 2.5 mm using the ToW concept as proposed by fib Model Code 2010 (2012) and Salvoldi (2010) does not represent explicitly the influence of rain or drying/wetting cycles, as shown in the previous section. The diffusion of CO_2 in the concrete pore structure depends on the saturation level of the pores, and the ideal condition for carbonation is observed when the RH of the pores is in the range of 50 to 70%. Therefore, rain or drying/wetting cycles have a major influence on the rate of carbonation, since they change the moisture condition of the concrete pores.

Bakker (1988) was the first to develop a carbonation model taking into account the influence of drying/wetting cycles. One of the assumptions of Bakker was that the carbonation is assumed to proceed as a sharp front, following a square root of time relationship, and that the carbonation only takes place if the concrete is sufficiently dry. Concrete can be considered as sufficiently 'dry' if the RH is in the range of 50 - 70%, corresponding to the ideal condition for carbonation as discusses earlier. However, in this research, the rate of carbonation is described using Equation (5.15). Another major assumption of Bakker's approach is that the wetting of concrete is considered to be instantaneous, when compared to carbonation and drying, and the carbonation is assumed to cease the moment the concrete gets wet. The carbonation is assumed to proceed once the drying front merges with the carbonation front. The influence of drying/wetting cycles on the rate of carbonation from Bakker is illustrated in Figure 5.13. A similar approach was also adopted by Thiery et al., (2012)

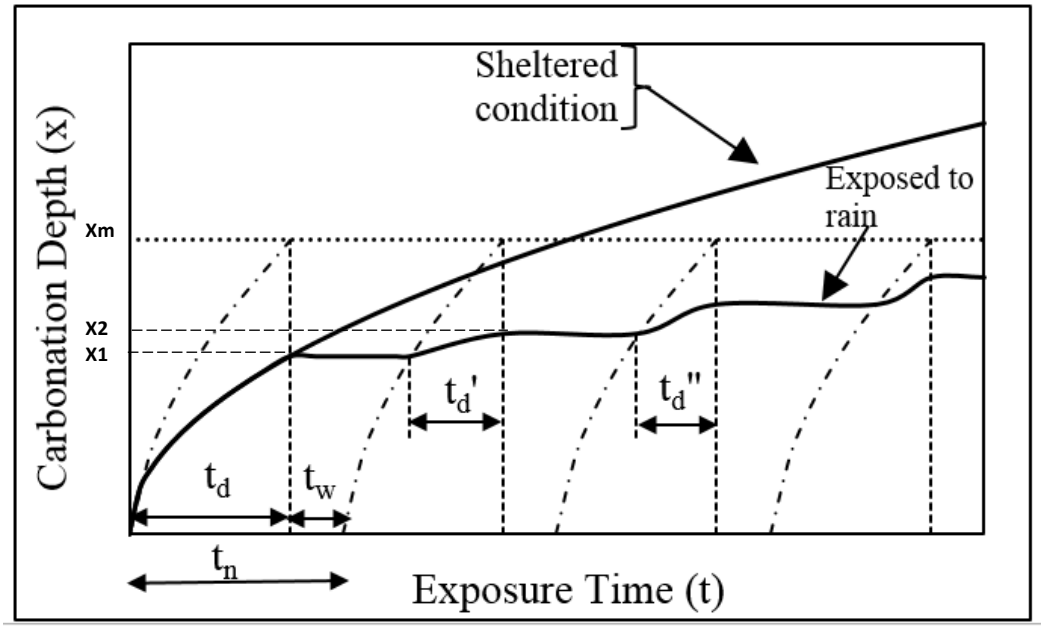

Figure 5.13 Illustration influence of drying/wetting cycles on rate of carbonation from Bakker's approach (Thiery et al., 2012)

Figure 5.13 illustrates Bakker's approach towards modelling carbonation, incorporating the influencing of drying/wetting cycles on the rate of carbonation. It can be seen from Figure 5.13 that when the concrete is sheltered from rain (i.e., the concrete is not saturated at any time and is in equilibrium with the ambient RH), the rate of carbonation is higher. However, in the case of concrete exposed to rain, the rate of carbonation is observed to be lower because of the drying/wetting cycles, and consequently the depth of carbonation at the end of the service life is lower when compared to the concrete sheltered from rain. From a practical point of view, assuming the wetting periods (t_w) and the time between the wetting periods (drying period, t_d) as constant for all drying/wetting cycles, one drying/wetting cycle $t_n = t_d + t_w$. During the drying period t_d of the first drying/wetting cycle, the concrete will carbonate to a depth X1, and during the wetting period t_w, the concrete is assumed to be saturated instantaneously and the carbonation ceases completely for the entire duration of t_w; hence at the end of the first cycle t_1, the carbonation front has reached the depth of X1. During the drying period of the second cycle, the carbonation will proceed once the drying depth of the concrete reaches the depth of carbonation (X1) at the end of the first cycle. Thereafter, the concrete will continue to carbonate for the rest of the drying period (t_d') to a depth of X2; again, the carbonation ceases during the wetting period and the process continues with the next cycle. However, the effective time of carbonation will continue to reduce with each cycle ($t_d > t_d' > t_d''$), and therefore the maximum depth of carbonation (Xm) will depend on the maximum drying depth, which in turn depends

on the material and the environmental conditions. The total effective time of carbonation at the end of 'n' drying/wetting cycles ($t_{e(n)}$) is therefore equal to the total drying period less the time taken for the concrete to dry during each cycle to the level of carbonation at the end of previous cycle, and can be presented as follows as per Bakker (1998) and Thiery (2005) (details see Appendix G.3)

$$t_{e(n)} = nt_d - m\sum_{i=1}^{n-1} t_{e(i)} \quad (n>1) \qquad 5.19$$

Where, $m = \left(\frac{A}{B}\right)^2$

A = rate of carbonation or carbonation co-efficient and B = rate of drying or drying coefficient.

It is to be noted that Equation (5.19) is valid in the case where the number of cycles exceed one (1). In the case where the number of drying/wetting cycle is restricted to one, or for the first drying/wetting cycle, or in the case of sheltered specimens:

$$t_{e(1)} = t_d \qquad 5.20$$

Idealising carbonation as a square root-time relationship as shown in Equation (5.21); the rate of carbonation (i.e. the carbonation co-efficient) can be deduced from Equation (5.15) as shown in Equation (5.22)

$$x = A \times \sqrt{t_e} \qquad 5.21$$

$$A = \sqrt{\frac{2 \times D_{de} \times H_S \times c}{a}} \qquad 5.22$$

Equation (5.19) is based on the assumption that the concrete is saturated instantaneously. During the drying period of the subsequent cycle, the concrete will be exposed to the ambient relative humidity which is lower than the saturation level. As a result, evaporation occurs at the gas-liquid interface within the pore structure of the concrete. The evaporation increases the local vapour concentration near the gas-liquid interface, resulting in a difference in vapour concentration between the interface and the concrete surface. The concentration gradient therefore induces the diffusion of vapour from the interface to the concrete surface. Idealising the drying of concrete as a one-dimensional evaporation-diffusion process, and assuming the evaporation rate to be infinitely large in comparison with the diffusion rate, the drying front position (x) can be written from Li et al. (2009) (details see Appendix G.2) as follows

$$x = 2 \times \lambda \times \sqrt{D_v} \times \sqrt{t} \qquad 5.23$$

where, D_v = vapour diffusion coefficient in concrete pore structure (m^2/s); λ = drying front coefficient which depends on the saturated vapour pressure (p_{vs}) and drying humidity gradient, which can be calculated from Li et al. (2009) as shown below

$$\lambda \, \mathrm{erf}(\lambda) \, \exp(\lambda^2) = \frac{1}{\sqrt{\pi}} \times \frac{p_{vs}}{\rho_l} \times \frac{M_v}{RT} \times (h_s - h_0) \qquad 5.24$$

where, h_s = relative humidity at gas–liquid interface; h_0 = relative humidity at the concrete surface (ambient relative humidity); R = gas constant (J/K/mol); T = temperature (K); M_V = molar mass of vapour (kg/mol); p_{vs} = saturated vapour pressure (Pa); ρ_l = water density (kg/m^3)

Similar to the square root-time relationship for concrete carbonation, Equation (5.23) can be deduced in the form of a square root-time relationship for concrete drying as shown in Equation (5.25).

$$x = B \times \sqrt{t} \qquad 5.25$$

where, B is the rate of drying (drying co-efficient; a function of vapour diffusion coefficient and drying front coefficient) can be deduced from Equation (5.23) as shown in Equation (5.26)

$$B = 2 \times \lambda \times \sqrt{D_v} \qquad 5.26$$

Therefore, the effective time of carbonation 't_e' can be calculated based on Equations (5.19 - 5.26), based on the number of drying/wetting cycles, and depending on the exposure site and the rate at which the concrete dries. The drying rate depends on the vapour diffusion coefficient in the concrete pore structure, which depends on the relative humidity, microstructure and transport properties of the concrete, and hence it can be related to the permeability coefficient obtained from the OPI test. The development of the correlation between the vapour diffusion coefficient and the permeability coefficient is given in the following section.

5.5.2.1 Vapour diffusion coefficient

The drying/wetting process has a major influence on the rate of carbonation as discussed previously. The rate of carbonation under conditions of wetting and drying directly depends on the rate of drying, as the carbonation will not proceed until the concrete RH at the level of the carbonation front is in the range of 50 - 70% as discussed above. Therefore, quantification of the drying rate is important to determine the rate of carbonation, as it is one of the key variables

of the carbonation model. Considering drying of concrete as a one-dimensional evaporation-diffusion process, and assuming the evaporation rate to be infinitely large in comparison with the diffusion rate, the progression of drying front can be expressed as shown in Equation (5.23). The progression of drying front (based on Equation (5.23)) therefore depends on the RH and the vapour diffusion coefficient (D_v) in the concrete pore structure. One approach towards determining the vapour diffusion coefficient in the concrete pore structure is to correlate the diffusion coefficient of vapour in dry air with the tortuosity of the concrete pore structure, which is a function of porosity (Li et al., 2009). However, this is not always the best approach as the porosity does not provide the true representation of the transport characteristics of the concrete microstructure. Therefore in the current study, a correlation between the vapour diffusion coefficient in the concrete pore structure and the gas permeability coefficient based on OPI has been established, since both transport mechanisms take place in the same concrete pore structure, and both relate to the movement of a gaseous phase. The advantage of this approach is that the permeability coefficient based on OPI is also used to model the effective dry diffusion coefficient (Equation (5.16)). Hence a single input parameter based on OPI test can be used in both carbonation as well as the moisture model, and this is one the major contribution of this research.

The development of the correlation between the vapour diffusion coefficient and the permeability coefficient was based on the current experimental investigation. A total of 48 concrete samples made of 12 different concrete mixes as shown in Table 3.2 were cast, and each of the 12 concretes subjected to four different curing conditions as given in Table 3.5. The concrete samples were then exposed to controlled environmental conditions in the laboratory, where the average temperature and humidity was maintained at 20°C and 50% respectively, and the RH profile of the concrete was measured at regular intervals. The experimental programme is detailed in Section 3.3.3 of Chapter 3. The permeability coefficients of all the 48 combinations were also determined using the OPI test as explained in Section 3.3.2. Based on the RH profile data, the vapour diffusion coefficient in the concrete pore structure (D_v) was calculated from the following equation proposed by Li et al. (2009) (details see Appendix G.2).

$$h - h_0 = \frac{h_s - h_0}{\mathrm{erf}(\lambda)} \times \mathrm{erf}\left(\frac{x}{2\times\sqrt{D_v \times t}}\right) \qquad 5.27$$

Where, 'h' is the relative humidity at depth 'x' from the surface at time 't'; h_s = relative humidity at gas–liquid interface; h_0 = relative humidity at the concrete surface (ambient relative humidity) The vapour diffusion coefficient (D_v) calculated based on Equation (5.27) using

experimental data and was plotted against the permeability coefficient (k) based on the OPI test, as shown in Figure 5.14.

Based on a regression analysis, a power relationship between vapour diffusion coefficient and permeability coefficient was established with a R-square value of 0.89 as shown in Equation (5.28).

$$D_v = (1.14 \times (k \times 10^{11})^{0.38}) \times 10^{-7} \qquad 5.28$$

Where, D_v and k are the vapour diffusion coefficient and permeability coefficient in m^2/s and m/s respectively.

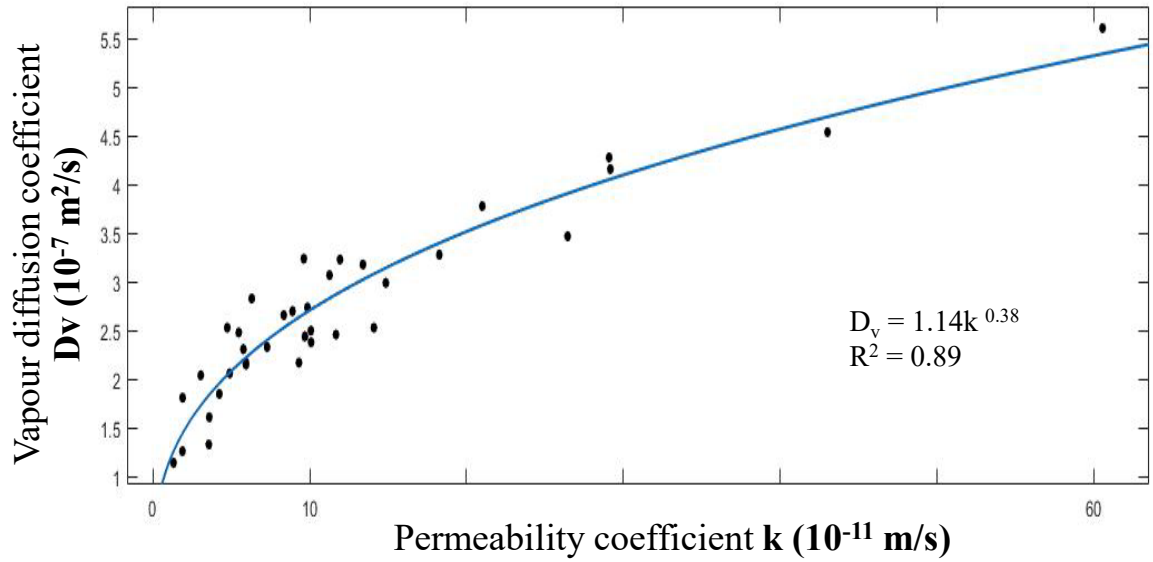

Figure 5.14 Correlation between vapour diffusion coefficient in concrete pore structure t and permeability coefficient (D_v vs k)

Therefore Equation (5.28) provides a useful correlation to establish the vapour diffusion coefficient in the concrete pore structure, based on a permeability coefficient from the OPI test after 28 days of curing for a range of concrete mixes and curing conditions. The vapour diffusion coefficient is in the range of (10^{-7} m^2/s), as proposed by Bakker (4 8 x 10^{-7} m^2/s) and as indicated in Thiery (2005), giving further confidence in its use.

5.5.3 Final Carbonation Model Summary and Validation

The carbonation model (Equation (5.15)) developed was able to predict the rate of carbonation of concretes sheltered from rain. However, the model overestimates the carbonation rate for concrete specimens exposed to rain or drying/wetting cycles. This drawback of the model was rectified by introducing the effective time of carbonation since the time of actual carbonation

is the not the total exposure time since the rain or drying/wetting cycles hinder the process of carbonation. Therefore the total effective time of carbonation at the end of 'n' drying/wetting cycles ($t_{e(n)}$) is therefore equal to the total drying period less the time taken for the concrete to dry during each cycle to the level of carbonation at the end of previous cycle, and can be determined using Equation (5.19 - 5.26). The effective dry diffusion coefficient (D_{de}) and the vapour diffusion coefficient in the concrete pore structure (D_v) can be expressed in terms of permeability coefficient (k) from Equation (5.16) and Equation (5.28) respectively. The variable 'm' in Equation (5.19) therefore can be expressed in terms of a permeability coefficient (k) as shown below.

$$\mathrm{m} = 0.3\left(\frac{\left(k\times 10^{11}\right)^{0.3}}{\lambda^2}\right)\left(\frac{c}{a}\right)\left(1-\frac{\mathrm{RH}}{100}\right)^2\left(\frac{\mathrm{RH}}{100}\right)^{2.6} \qquad 5.29$$

Where, k is the permeability coefficient in m/s and λ is the drying front coefficient calculated using Equation (5.24).

Therefore taking into account of the influence of rain or drying/wetting cycles, the carbonation model (Equation (5.15)) developed can be modified to its final form as shown below.

$$\mathrm{x} = \sqrt{\frac{2\times \mathrm{D_{de}}\times \mathrm{H_S}\times c}{a}}\times\sqrt{\mathrm{t_{e(n)}}} \qquad 5.30$$

Where, $t_{e(n)}$ = the total effective time of carbonation at the end of 'n' drying/wetting cycles and in the case there is only one drying/wetting cycle; the effective time will be equal to the total drying time.

However, it is to be noted that the accuracy of prediction of carbonation for concrete exposed to rain or drying/wetting cycles based on the model (as per Equation (5.30)) is therefore depended on the determination of the total effective time. Therefore the number of drying/wetting cycles and the duration of the drying and wetting period form essential input parameters of the model and are depended on the weather pattern of the site of exposure. Therefore, a framework needs to be developed which can predict the normalised frequency of drying/wetting cycles as well as the duration of drying and wetting periods of an area, based on the rainfall data. The above aspect is out of the scope of this research and remains an area which needs further research.

The summary of the carbonation model developed in this research which can predict the rate of carbonation of concrete sheltered as well as exposed to rain or drying/wetting cycles, with the permeability coefficient from the OPI test as the key prediction parameter is given below.

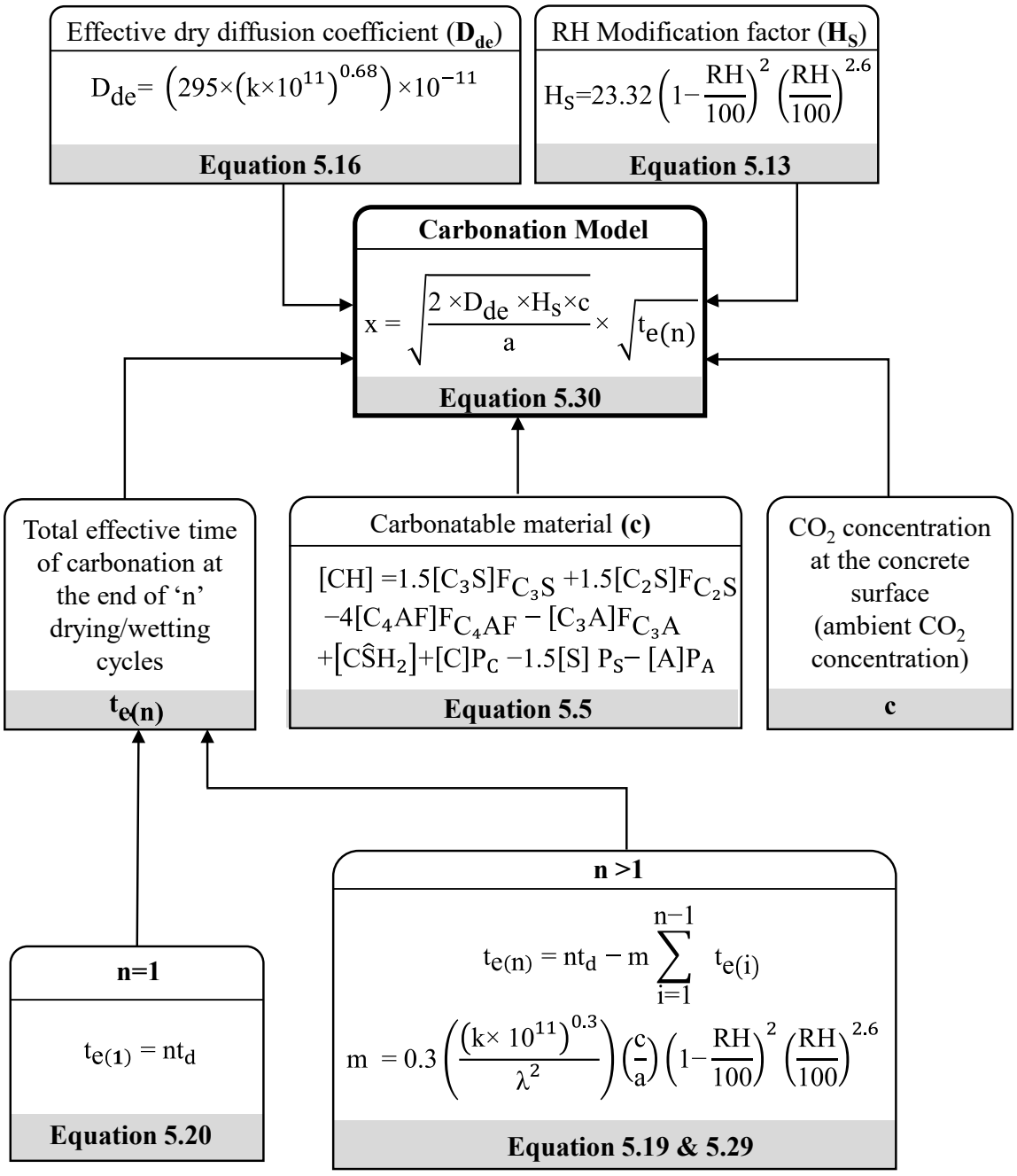

Figure 5.15 Summary of carbonation model developed.

5.5.3.1 Model validation – Concrete exposed to rain or drying/wetting cycles

For the validation of carbonation model, the carbonation depth of concrete specimens after 1000 days of exposure at the site ME and WE (exposed to rain or drying/wetting cycle) was calculated using Equation (5.30), and compared with the measured carbonation depth at the same age. However, for the purpose of validation; taking into account the rainfall data (see Appendix E) of the site ME and WE gathered from the nearest weather station, a normalised drying/wetting cycle with the wetting period (t_w) of 3.5 days per week ($t_d + t_w. = 7$ days) is adopted for the site ME, and a wetting period (t_w) of two days per week ($t_d + t_w. = 7$ days) is adopted for the site WE. Based on the above-mentioned frequency of the drying/wetting cycles, the depth of carbonation calculated using Equation (5.30) was compared with the measured carbonation depth at the age of 1000 days (tabulated in Appendix D.13) is as shown in Figure 5.16 and Figure 5.17

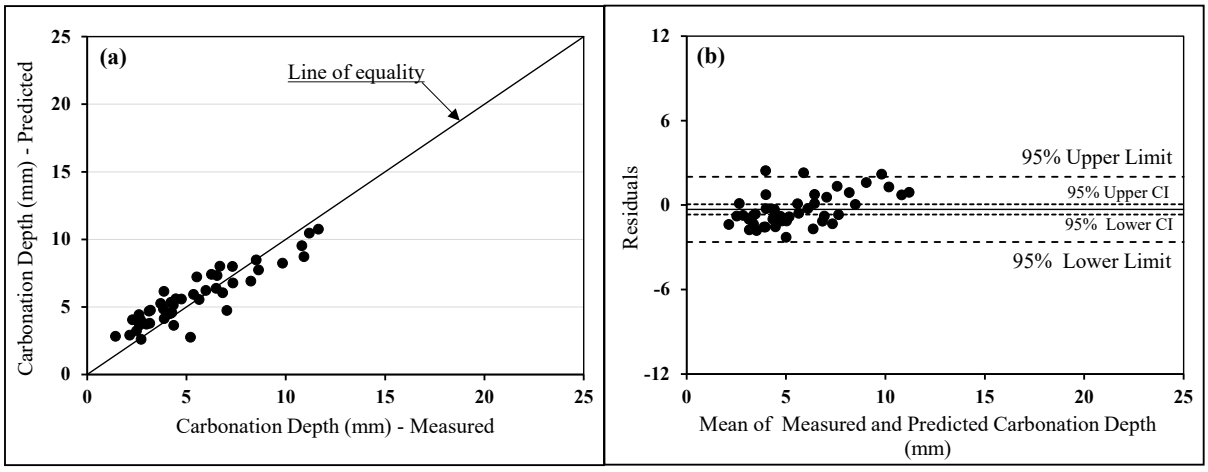

Figure 5.16 Exposure at site ME: (a) Predicted (using Equation(5.30), based on based on drying/wetting cycles concept concept) vs measured carbonation depth after 1000 days of exposure; (b) Residual plot displaying 95% limit of agreement

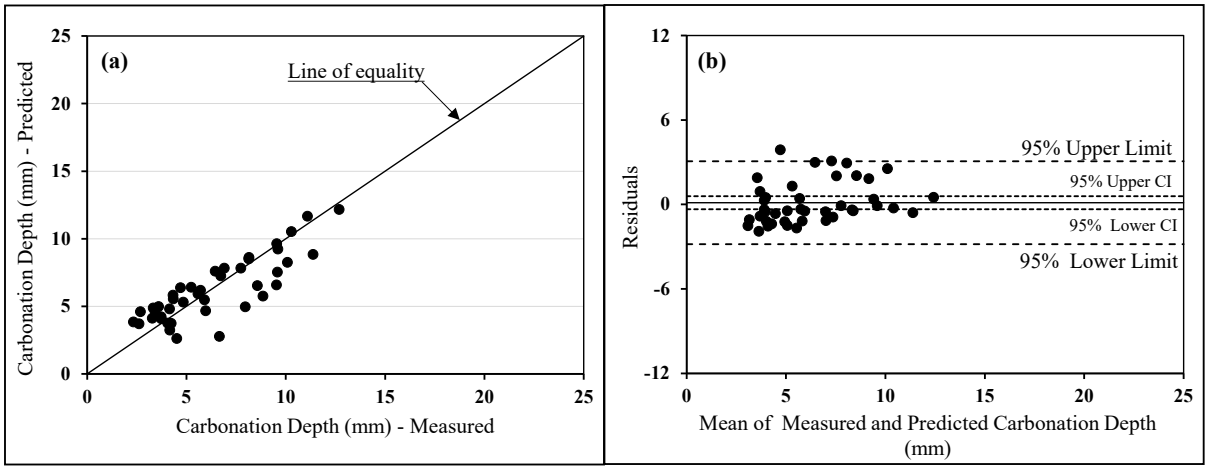

Figure 5.17 Exposure at site WE: (a) Predicted (using Equation(5.30), based on based on drying/wetting cycles concept concept) vs measured carbonation depth after 1000 days of exposure; (b) Residual plot displaying 95% limit of agreement

The predicted carbonation depth (using Equation (5.30), based on drying/wetting cycles concept) for 1000 days of exposure at site ME and WE is in good agreement with the measured values. The carbonation model developed takes into account the influence of rain or drying/wetting cycles on the carbonation rate. A comparison between Figure 5.10 & Figure 5.16 (for the site ME) and Figure 5.11 & Figure 5.17 (for the site WE) clearly indicates the sensitivity of the model towards the influence of rain or drying/wetting cycles. It can be observed that the differences between the measured and predicted values are within the agreement limits and the line of equality is within the CI of the mean of differences.

In order to check the validity of the normalised drying/wetting cycles adopted, another set of natural carbonation data of concrete exposed at site WE from a different project (Alhassan, 2014) was compared with the predicted values of carbonation depth using the carbonation model developed in this research (using Equation (5.30)). The natural carbonation data of different concrete specimens exposed at the site WE with a combination of w/b, cement extenders and curing conditions were obtained from Alhassan (2014) (both the authors shared the same site). The mix designs of the concrete, permeability coefficient (k) at 28 days, CH content measured using TGA and the carbonation data, are summarised in Appendix D.14. The carbonation depth calculated for 0.5, 1, 1.5 and 2 years of natural exposure based on the modified carbonation model adopting a wetting period (t_w) of two days per week ($t_d + t_w = 7$ days, as discussed earlier) is compared with the measured data from Alhassan (2014) for the same duration of exposure, and shown in Figure 5.18 to Figure 5.21.

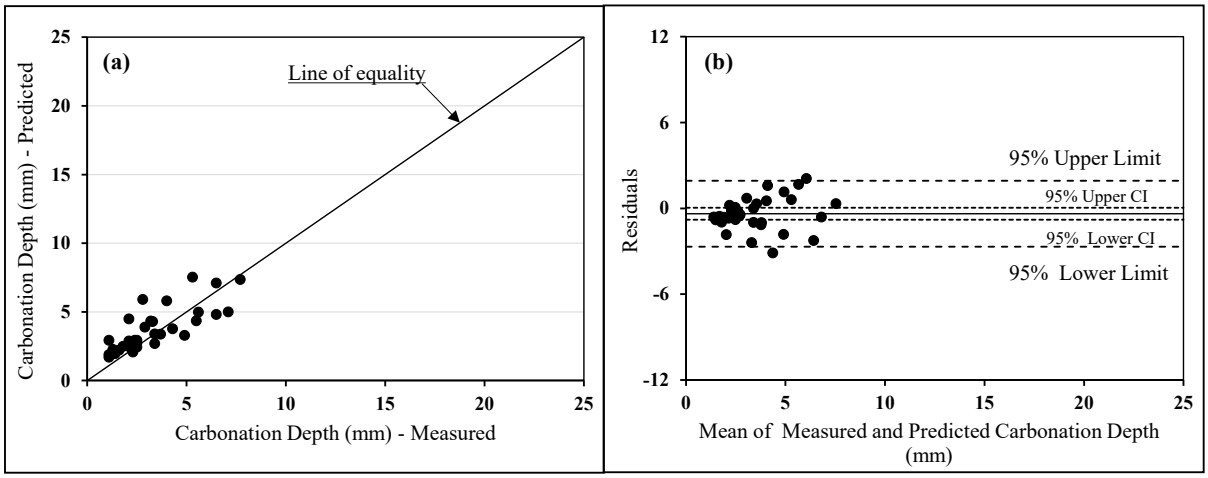

Figure 5.18 Exposure at site WE: (a) Predicted (using Equation(5.30), based on based on drying/wetting cycles concept concept) vs measured carbonation depth after 0.5 year of exposure (Alhassan (2014)); (b) Residual plot displaying 95% limit of agreement between predicted and measured carbonation depth

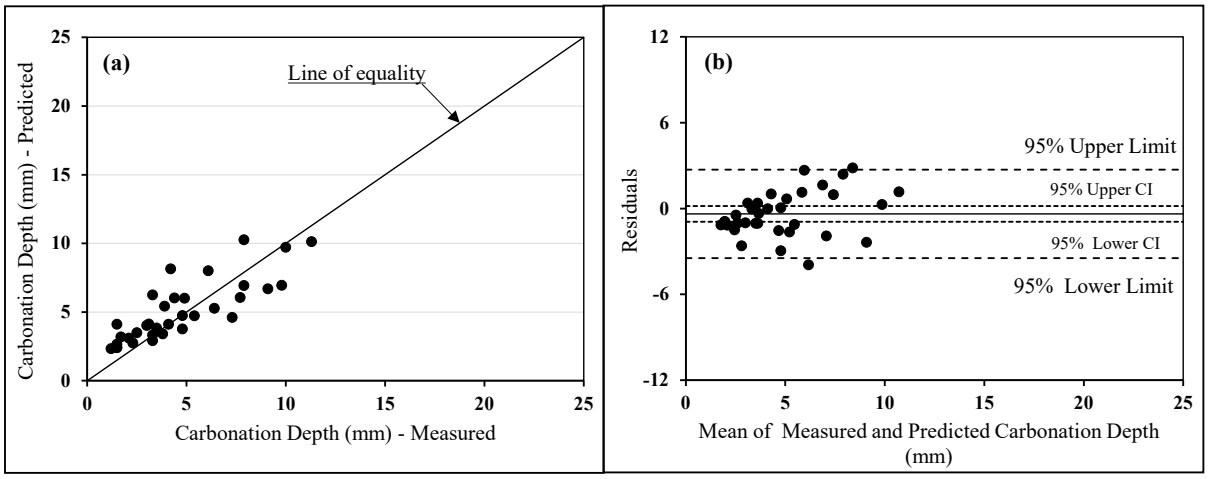

Figure 5.19 Exposure at site WE: (a) Predicted (using Equation(5.30), based on based on drying/wetting cycles concept concept) vs measured carbonation depth after 1.0 year of exposure (Alhassan (2014)); (b) Residual plot displaying 95% limit of agreement between predicted and measured carbonation depth

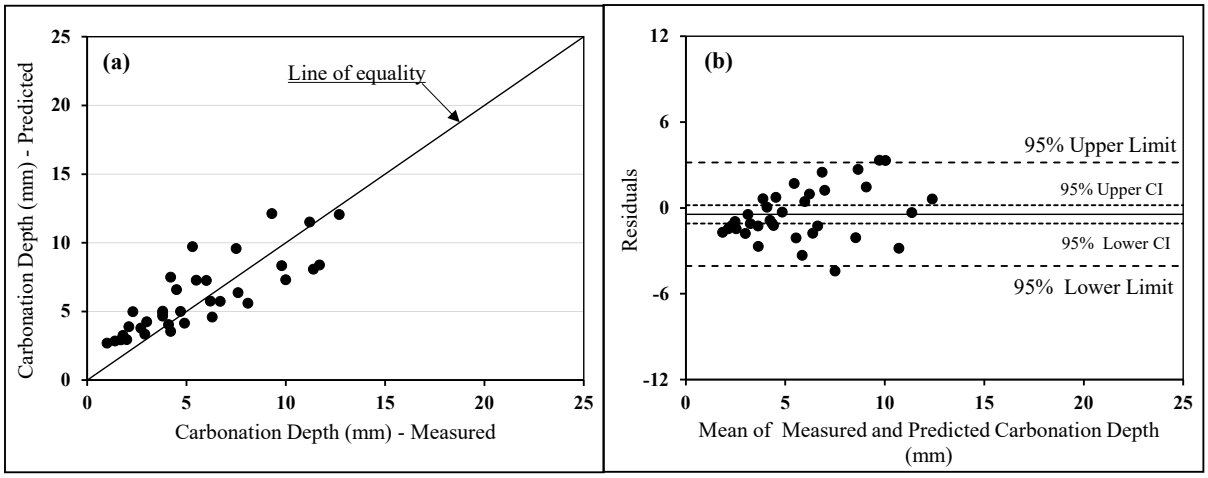

Figure 5.20 Exposure at site WE: (a) Predicted (using Equation(5.30), based on based on drying/wetting cycles concept concept) vs measured carbonation depth after 1.5 year of exposure (Alhassan (2014)); (b) Residual plot displaying 95% limit of agreement between predicted and measured carbonation depth

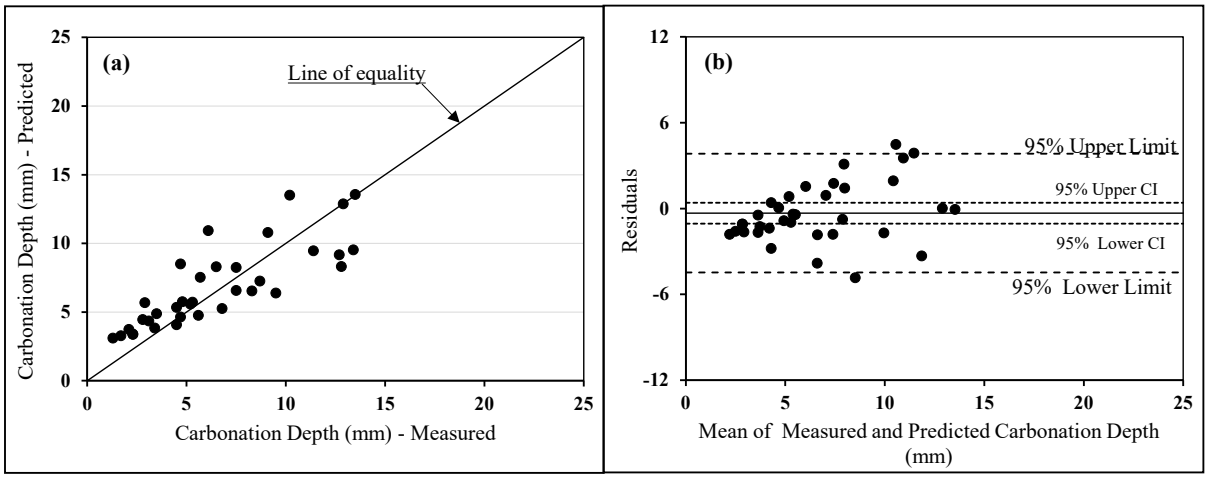

Figure 5.21 Exposure at site WE: (a) Predicted (using Equation(5.30), based on based on drying/wetting cycles concept) vs measured carbonation depth after 2.0 year of exposure (Alhassan (2014)); (b) Residual plot displaying 95% limit of agreement between predicted and measured carbonation depth

It can be observed from Figure 5.18 to Figure 5.21 that the modified carbonation models is able to predict the carbonation depth of concrete exposed to rain, with mix proportions different from the current research. Also the drying/wetting cycles with a frequency of two days of wetting period (t_w) per week is observed to be a practical approximation for the site WE and hence can be generalised for the area. Furthermore it is important to note that the amount of carbonatable component was determined experimentally (see Appendix D.14) in Alhassen (2014); and those values are used for the prediction of carbonation using Equation (5.30). This is an added advantage as the amount of carbonatable material can be determined experimentally and the model can still predict the rate of carbonation. Therefore the modified carbonation model is a key contribution of this research, enabling to predict the carbonation depth of

samples exposed to rain or drying/wetting cycles using the oxygen permeability coefficient as a key parameter, which can be easily determined based on a simple and practical durability index test.

5.6 SUMMARY

The development of the carbonation model has been detailed in this chapter. The basic principles of carbonation modelling and the derivation of the carbonation model have been detailed, and the assumptions made for the derivation have been emphasised. This was followed by refining the model by summarising or deriving each variable of the carbonation model. For example, the environmental parameters were summarised and a framework for calculating the amount of carbonatable material based on mix proportion, binder type, curing condition, and oxide composition of the binder was established. Thereafter, based on the experimental data, a correlation between the diffusion coefficient and the permeability coefficient was developed. Once all the variables were defined, the carbonation model developed was validated based on measured carbonation data after 1000 days of exposure, and the shortcoming of the model was evaluated. The model was able to predict the depth of carbonation with good precision for samples which are sheltered from rain, but was not able to address the influence of rain. Therefore, the carbonation model was further modified taking into account the influence of drying/wetting cycles by adopting Bakker's approach, but with the novel method of linking vapour diffusion coefficients to the OPI permeability coefficients, thus giving a unified approach to the model. Finally, the modified model was compared with the measured data and the validity of the model was analysed. Therefore a carbonation model which takes in to account the influence of rain or drying/wetting cycles with oxygen permeability coefficient as the key variable has been developed and validated.

CHAPTER 6: SUMMARY AND CONCLUSION

6.1 BACKGROUND

Durability of reinforced concrete structures is governed, inter alia, by the microstructure and transport characteristics of the concrete. The ‘‘Durability Index’’ (DI) approach has been developed in South Africa to improve the durability performance of reinforced concrete structures. One of the main causes of deterioration is related to reinforcement corrosion induced by penetration of carbon dioxide into the concrete cover. Protection of reinforcement against carbonation-induced corrosion can be achieved by selecting an appropriate cover depth and mix design (materials and mix proportions) for the cover concrete along with adequate construction quality The main aim of this research was to develop a carbonation model to predict carbonation rates for different environmental exposures and for concretes with different binder types and curing conditions. The above objectives were accomplished with the support of a comprehensive experimental programme. The details of the experimental program are presented in Chapter 3, followed by the test results and discussions in Chapter 4. Thereafter, based on the experimental data, a carbonation model was developed.

The current research relates to the use of the oxygen permeability coefficient (k) from the (South African) standard OPI test (durability index test) as the key prediction parameter for carbonation. The model development was based on natural carbonation data. The specific novelty of the current research is the incorporation of the influence of drying/wetting cycles towards developing the carbonation model by integrating with a moisture model. Furthermore, the moisture model was also developed with permeability coefficient from the OPI test as the major prediction parameter. The salient features of the outcome of the experimental programme, the summary of the carbonation model developed, and its key features are presented in the following sections. Finally, recommendations for further work based on various aspects arising from the current research are given at the end of this chapter.

6.2 EXPERIMENTAL RESULTS - SALIENT FEATURES

The main purpose of the experimental program was to collect data for carbonation modelling. An extensive experimental programme was set up in order to accomplish this objective. The concrete mixes were selected with a range of binders and w/b ratios commonly used in the South African concrete industry. Four different curing regimes were adopted so that concrete

with a wide range of permeability values could be obtained, since the mechanism of carbonation depends on the microstructure of the concrete. A total of 48 different concretes, each with a unique combination of w/b, binder type, and curing regime, was prepared for the current research. The concrete mixes reflect the wide range of w/b ratios, binder types, and curing regimes commonly used in industry, and as a result the microstructure of the concrete specimens varies from porous to denser microstructure. Test for compressive strength, oxygen permeability, carbonation and moisture (or RH) profiles were conducted. For carbonation and RH profile studies, all the concrete specimens were exposed to five different natural environmental conditions. The concrete specimens were also exposed to a controlled laboratory environment condition for RH profile studies. Based on the experimental results, some of the salient features of concrete carbonation which are in agreement with previous studies as presented in Chapter 2 and discussed in Chapter 4 are given below.

6.2.1 Effect of w/b on Rate of Carbonation

Three different w/b ratios (0.45, 0.55 and 0.65) were used in the research in order to assess the influence of w/b on carbonation rate. Keeping all other factors constant, it was observed that the carbonation resistance of concrete in general decreases with an increase in w/b, irrespective of the binder type or curing condition. This indicates a higher rate of carbonation with increase in w/b. The compressive strength results also showed similar trends, with a reduction is strength observed with increasing w/b ratio. The above trend can be attributed due to one or the combination of the following reasons.

- An increase in w/b results in the development of a more porous microstructure (less dense), and as a consequence, the permeability of the concert increases. The development of a permeable microstructure makes it easier for the CO_2 to enter and react with the carbonatable components in concrete, which results in a higher carbonation rate. This was confirmed based on the OPI test, which is a performance-based durability index test reflecting the concrete material properties relevant to gas ingress into concrete. Lower OPI values, indicating higher permeability, were observed with an increase in w/b ratio.

- Secondly, an increase in w/b enhances the drying process as the permeability increases. This was confirmed based on the RH profile measurements, where the concrete specimens were exposed to constant ambient RH and the internal RH was

measured at different depths from the exposed surface (see Section 3.3.3) RH profile measurements show a higher drying rate with an increase in w/b, creating a favourable (faster with increase in w/b) condition for the carbonation reaction to take place.

- The increase in carbonation rate with an increase in w/b ratio is also related to the amount of carbonatable material, which buffers the progression of the carbonation front. A higher w/b (for fixed water content) means a reduction in binder content in the concrete mix. A lower binder content in the concrete mix consequently reflects a reduction in the amount of carbonatable material in concrete, resulting in faster progression of carbonation.

Therefore, in general, it can be concluded that, from a practical and carbonation modelling point of view, the w/b is an important factor which influences the carbonation rate. The effect of w/b on rate of carbonation is the combined effect of different phenomena as discussed above. A number of carbonation models adopt compressive strength as an essential input parameter in order to reflect the influence of w/b. Even though the compressive strength results show similar trends to those of carbonation with respect to w/b, it is not a true representation of factors such as permeability, carbonatable material and RH, which influence carbonation with respect to the w/b. Therefore, it is based on this understanding that the carbonation model developed in this research (see Chapter 5) incorporates permeability, carbonatable material and RH as input parameters.

6.2.2 Influence of Curing on Rate of Carbonation

Curing is another major factor which has a direct impact on the rate of carbonation, since extended curing helps to develop a denser microstructure. Out of the four curing regimes (listed below), which were adopted in this research, the 28-day standard water curing (Curing-A) results in the highest resistance against carbonation, and the samples subjected to Curing-B showed the lowest resistance.

- Curing-A - Curing in water bath maintained at a temperature of 23 - 25°C (until 28 days after casting)
- Curing-B - 1 day in the moulds, then exposed to laboratory conditions (until 28 days after casting at 20-22°C and 60-70% RH)

- Curing-C - 1 day in the moulds, 6 days covered by plastic, followed by exposure to laboratory conditions (until 28 days after casting at 20-22°C and 60-70% RH)
- Curing-D - 1 day in the moulds, then kept in an outdoor sheltered environment (until 28 days after casting at 20-22°C and 50-55% RH).

The carbonation results are in agreement with the OPI test results with respect to different curing conditions. All the concrete mixes subjected to standard water curing (Curing-A) showed higher OPI values (lower permeability coefficient (k) values) when compared to the other curing regimes. This indicates the development of a denser microstructure when subjected to Curing-A. Therefore, permeability of concrete increases with respect to the curing regime in the order of Curing-A → (Curing-C or Curing-D) → Curing-B, with a corresponding reduction in carbonation resistance for the same w/b and binder type. However, the following conclusions can be made with respect to the influence of curing on carbonation of concrete with respect to different binder types.

- The effect of curing on the microstructure development is more pronounced in the case of concretes with cement extenders such as fly ash and GGBS. The difference in permeability and carbonation rate between concrete subjected to Curing-A and Curing-B is higher in the case of concrete with cement extenders when compared to PC and LS concrete. Therefore, it can be concluded that curing plays a major role towards the development of denser and less permeable microstructure and that a better curing practice is a requirement towards achieving carbonation resistance especially in the case of concrete with cement extenders.

Furthermore, specimens subjected to Curing-A retain moisture better, due to the development of a denser microstructure with finer pore structure, which was observed from the moisture profile measurements. This makes the transport of CO_2 into the concrete more constricted due to the presence of moisture; this further adds to the resistance related to the lower permeability, resulting in a lower rate of carbonation. In contrast, with Curing-B, the drying rate is higher resulting in favourable moisture conditions for carbonation. Therefore it is important to incorporate curing specifications at the design stage and implementation of strict quality control for curing practices during construction.

However, from a carbonation modelling point of view, curing is a critical factor which influences the rate of carbonation and the model must be able to reflect the influence of curing.

Since the carbonation test results correspond with the OPI test results with respect to the influence of curing and the OPI test can characterise the influence of curing and w/b; the permeability coefficient from the OPI test can be used as an essential input parameter of carbonation models. Such an approach towards carbonation modelling was adopted in this research.

6.2.3 Influence of Cement Extenders on Rate of Carbonation

Cement extenders are often used in construction in order to reduce the clinker content in concrete, thereby reducing the carbon footprint, to make use of industrial by-products, and to increase the durability of concrete structures. In the current study concrete mixes with fly ash and GGBS at cement replacement levels of 30 and 50% respectively were adopted. Concrete mixes with limestone-based (21-35%) blended cement (denoted as LS) was also used in the research. The use of cement extenders in concrete with Curing-A has the advantage of reduced permeability and rate of carbonation for the same w/b and binder type as discussed in the previous section. Based on the experimental results of the research, the following general conclusion can be drawn with regards to the influences of cement extenders on the rate of carbonation, permeability and drying of concrete for a given w/b.

- The performance of the concrete mixes with cement extenders differs with the curing condition and binder type. The concrete mixes with GGBS and fly ash (with 0.45 w/b) showed lower permeability in comparison with PC concrete for the same w/b, when subjected to Curing-A. For all other curing regimes, the permeability of concrete with GGBS and fly ash is higher than that of PC concrete. Similar trends were also observed in the case of LS concrete when subjected to Curing-A. In general it can be concluded that GS and LS concrete respond to better curing conditions in reducing permeability.

- The drying performance of concrete with cement extenders was similar to that of its permeability performance for the respective curing regime. The drying rate of concrete with cement extenders was lower than that of PC concrete, when subjected to Curing-A. Furthermore, the difference in the drying rate of concrete with Curing-A with respect to Curing-B is more prevalent in the case of concrete with cement extenders such as fly ash and GGBS. The internal RH profiles of LS concrete

showed similar trends to that of PC concrete, but with a slightly higher rate of drying.

- In general the carbonation resistance of concrete with cement extenders is lower when compared to PC concrete irrespective of the w/b and curing condition. Furthermore, with the beneficial effect of the reduction in permeability and rate of drying of concrete with cement extenders when subjected to Curing-A, the resistance to carbonation is expected to be higher than that of PC concrete. However, in contrast to the above, the carbonation resistance of concrete with cement extenders was observed to be lower irrespective of w/b or curing condition. This phenomenon is due to the reduction in the amount of carbonatable material in the case of concrete with cement extenders. LS Concrete shows slightly higher rates of carbonation when compared to PC concrete, even though the permeability performance when subjected to Curing-A is better than PC concrete. This can be attributed due to the lower clinker content in LS concrete in comparison with PC concrete.

Therefore it can be deduced that even though the permeability coefficient plays a key role in the rate of carbonation, the quantity of carbonatable material is also a governing factor affecting the rate of carbonation

6.2.4 Influence of Rain or Drying/Wetting Cycles on Rate of Carbonation

The environmental condition is another factor which has a major impact on the rate of carbonation. It is well established that the rate of carbonation depends on the internal RH, and the favourable conditions for carbonation are in the range of 50 - 70% RH. However, the internal RH is altered due to environmental factors such as rain or drying/wetting cycles. In order to study the influence of rain or drying/wetting cycles on the rate of carbonation, concrete specimens were exposed to natural carbonation at two different areas. In each area two different environmental conditions were created by sheltering one set of specimens from rain (site MS and WS) and the other set exposed to rain (site ME and WE). The carbonation test results provide the following observations:

- Based on the carbonation data measured after 1000 days of exposure, it can be concluded that drying/wetting cycles or rain hinder the rate of carbonation in concrete. Consequently, the concrete specimens exposed to rain showed lower depths of

carbonation when compared to the specimens sheltered from rain in the same area of exposure. In the case of specimens exposed to rain, the internal RH fluctuated due to the alternate drying and wetting periods, which results in the movement of water in and out of concrete. Therefore with an increase in RH or as a result of the saturation of pores, the carbonation reaction ceases, until such time that the internal RH of the pores drops to favourable conditions. However in the case of concrete sheltered from rain, the carbonation process is continuous (even though slight fluctuation in internal RH can be observed due to changes in environmental RH), resulting in a higher rate of carbonation, when compared to samples exposed to rain in the same location.

- The difference in rates of carbonation between concrete specimens sheltered and exposed to rain is observed to be different for different areas of exposure. For example, the difference between the rate of carbonation of concrete specimens exposed at site ME and MS (site in Cape Town with an average of 124 days of rainfall per annum) is higher than that of the specimens exposed to site WE and WS (site in Johannesburg with an average of 89 days of rainfall per annum). This can be attributed to the different weather pattern of the area and hence it can be inferred that, not only the exposure to rain but also the intensity and frequency of rain effects the rate of carbonation.

Therefore, in addition to the factors such as w/b, curing conditions, binder type, permeability, RH, etc., rain or drying/wetting cycles also influence the rate of carbonation and should be considered as an input parameter of carbonation models, as used in this research.

6.3 SUMMARY - CARBONATION MODEL DEVELOPMENT

One of the main objectives of the current research is to develop a carbonation model based on natural carbonation data, taking into account all the important parameters and relevant conditions; with the oxygen permeability coefficient (k) from OPI test as the key prediction parameter. Furthermore, this research also aimed at developing and integrating a moisture model into the carbonation model in order to take into account the influence of drying/wetting cycles (influence of rain).

At the initial phase of the modelling, the mechanism of carbonation was idealised using Fick's first law of diffusion and a square root-time relationship predicting the depth of carbonation and the variables of the model were then defined or derived individually. Thereafter, based on regression analysis, a power relationship between the effective dry diffusion coefficient (D_{de})

and the permeability coefficient (k) was established using natural carbonation depth data as shown in Equation (5.16).

$$D_{de} = (295 \times (k \times 10^{11})^{0.68}) \times 10^{-11} \qquad 5.16$$

Where, D_{de} and k are the effective dry diffusion coefficient and permeability coefficient in m^2/s and m/s respectively.

The concept of drying/wetting cycles was then introduced (especially in the case of concrete exposed to rain or drying/wetting cycles) according to which the total effective time of carbonation at the end of 'n' drying/wetting cycles ($t_{e(n)}$) was derived. The total effective time of carbonation is equal to the total drying period less the time taken for the concrete to dry during the drying period of each cycle to the level of carbonation at the end of the previous cycle, and can be presented as follows as per Bakker (1998) and Thiery (2005) (details see Appendix G.3)

$$t_{e(n)} = n\, t_d - m \sum_{i=1}^{n-1} t_{e(i)} \qquad (n > 1) \qquad 5.19$$

Where, $m = \left(\frac{A}{B}\right)^2$

t_d is the drying period, A is the rate of carbonation or the carbonation co-efficient and B is the rate of drying or the drying coefficient.

In the case where the number of drying/wetting cycles is restricted to one, or for the first drying/wetting cycle, or in the case of sheltered specimens:

$$t_{e(1)} = t_d \qquad 5.20$$

The drying coefficient (B) can be expressed as a function of the vapour diffusion coefficient (D_v) and the drying front coefficient. Based on the internal RH profile measurement data at controlled environmental temperature and RH, a power relationship between vapour diffusion coefficients and permeability coefficients was established with a R-square value of 0.89 as shown below.

$$D_v = \left(1.14 \times \left(k \times 10^{11}\right)^{0.38}\right) \times 10^{-7} \qquad 5.28$$

Therefore, the variable 'm' in Equation (5.19) can be expressed in terms of a permeability coefficient (k) as shown below.

$$m=0.3\left(\frac{(k\times 10^{11})^{0.3}}{\lambda^2}\right)\left(\frac{c}{a}\right)\left(1-\frac{RH}{100}\right)^2\left(\frac{RH}{100}\right)^{2.6} \quad 5.29$$

Where, a=Carbonatable material (mol/m^3); c = CO_2 concentration at the concrete surface (mol/m^3) and λ = drying front coefficient

Therefore, taking into account of all the major factors affecting the rate of carbonation, the final form and the summary of the carbonation model is given below.

$$x=\sqrt{\frac{2\times D_{de}\times H_S\times c}{a}}\times\sqrt{t_{e(n)}} \quad 5.30$$

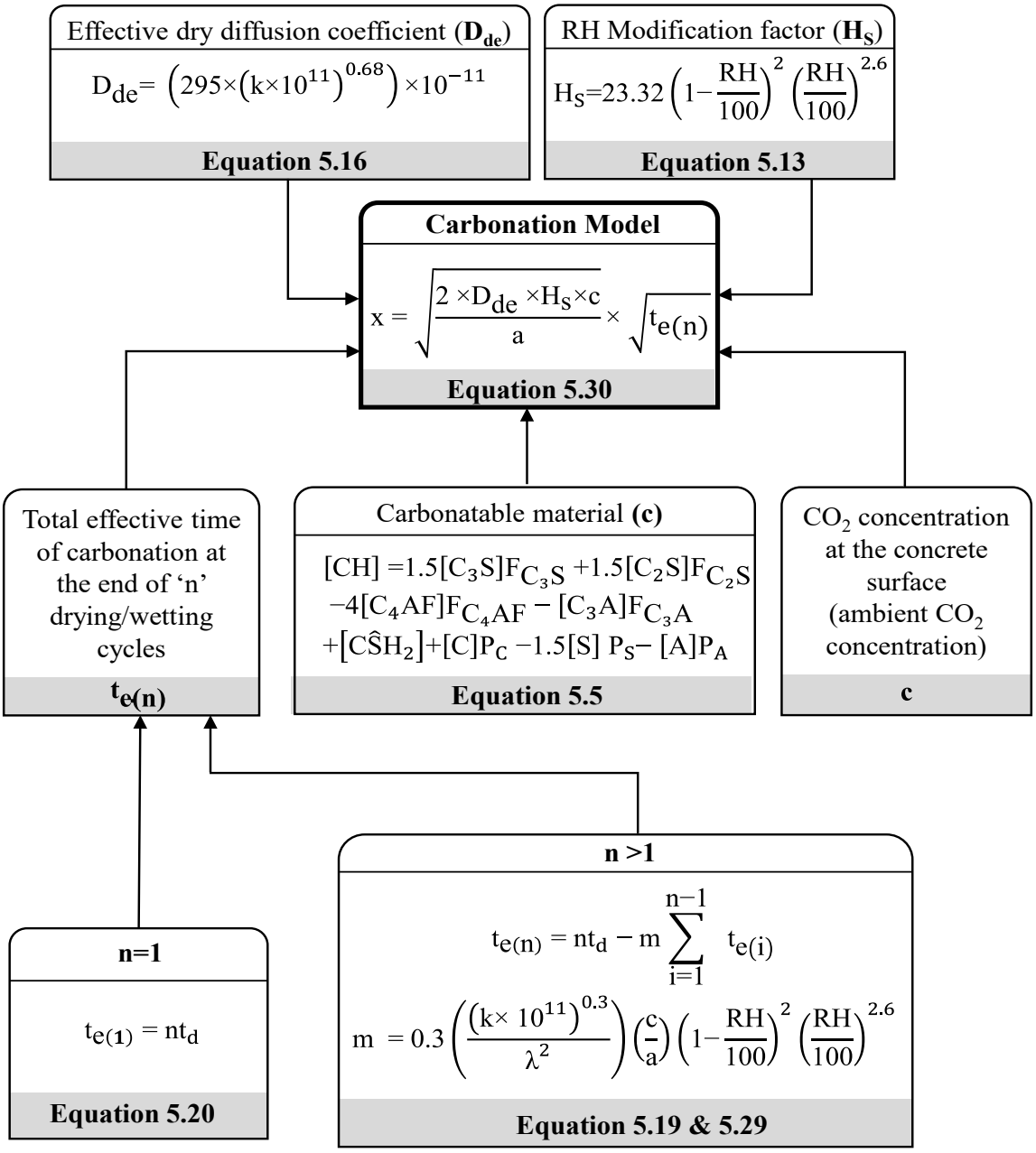

Figure 5.15 Summary of carbonation model developed.

Where,

x = Carbonation depth (m)

D_{de} = effective dry diffusion coefficient (m^2/s)

D_v = vapour diffusion coefficient (m^2/s)

c = CO_2 concentration at the concrete surface (mol/m^3)

k = permeability coefficient (m/s)

H_S = RH modification factor

a=Carbonatable material (mol/m^3)

t = Time (s)

6.3.2 General Discussion- Carbonation Model

The key features of the carbonation model developed in this research are given below.

- The carbonation model developed (see Equation (5.30)) is based on the oxygen permeability coefficient (k) from the OPI test as the key prediction parameter. The advantages of such an approach is that the OPI test and hence the permeability coefficient reflects the properties and proportions of the constituent materials of the concrete and account for concrete construction variables such as mixing, placing, compaction, finishing and curing. Therefore, any variation in the material properties or construction will be replicated in the prediction. Such an approach is more sensible and scientifically justifiable than predicting carbonation based on the compressive strength, which is not a good indicator of the transport mechanisms of concrete. For the development of the carbonation model in this research, a correlation between the permeability coefficient and diffusion coefficient was established. However, the correlation was based on the long-term natural carbonation data (unlike other models which are based on or use accelerated carbonation data), and hence this is one of the major contributions of this research.

- Even though diffusion is the driving mechanism which controls the rate of carbonation, the experimental measurement of diffusion is usually difficult and hence in most of the existing models, it is expressed in terms of porosity (Papadakis et al., 1991b; Thiery et al. (2007). However, this is not always the best approach as the same porosity can be associated with different carbonation rates. On the other hand, linking permeability with durability is a more practical approach, since permeability can be relatively easily measured both on site and in the laboratory.

- The carbonatable component of the cement paste is one of the input parameters of the carbonation model developed. The framework proposed by Salvoldi (2010) for the calculation of carbonatable components was adopted in this research. However, the carbonation model developed in this research (Equation (5.30)) is also able to predict the depth of carbonation based on the experimentally determined values of carbonatable material (see details in Section 5.5.3.1). This makes the model more user-friendly as the input parameters can be determined experimentally or can be calculated based on the composition of the binder.

- The carbonation model developed in this research (Equation (5.30)) is also able to account for the environmental CO_2 concentration. This was validated by comparing the natural carbonation data of concrete exposed to environments with different CO_2 concentration (site CD and MS, other environmental factors such are RH and temperature were similar), with the predicted values (see Figure 5.7 and Figure 5.8)

- A number of carbonation models are available, which can predict the rate of carbonation of concrete exposed to constant RH, or concrete that is exposed to environments sheltered from rain. The prediction of carbonation of concrete subjected to drying/wetting cycles or rain is challenging and appropriate models are sparse. Carbonation will not take place during the wetting period, and during the drying period the carbonation will start only when the depth of drying depth reaches the level of the carbonation front. Therefore the effective time of carbonation (for concrete exposed to rain) is the total time of exposure minus the time taken for the concrete to dry to the level of carbonation front achieved by the end of the drying period of the previous drying/wetting cycle. The carbonation model developed in this research takes this into account (Equation (5.19)) and makes provision for calculation of the effective time based on the environmental RH, drying/wetting cycles and the drying rate of concrete.

- One of the assumptions with respect to the carbonation modelling with drying/wetting cycles in this research, is that concrete is assumed to be saturated instantaneously during the wetting period. Taking into account the rate of natural carbonation as well as the cover depth of normal RC structure, the above justification is valid. However in reality the degree of saturation depends on the sorptivity of concrete and hence, the concrete may not be saturated up to the level of the carbonation front. The model developed in this research does not take this into account. Therefore the carbonation model

developed needs to be further refined taking into account the influence of the saturation capacity of concrete during the wetting period.

- In order to determine the rate of drying, a moisture model was integrated with the carbonation model. The moisture model was developed by establishing a correlation between the permeability and vapour diffusion coefficients, based on experimentally determined internal RH profile data with time. The influence of variation in concrete microstructure on the drying rate of concrete is therefore taken into account. The novel approach of linking effective dry diffusion coefficient as well as vapour diffusion coefficient with the permeability coefficient is the major contribution of this research. Therefore a single input parameter based on OPI test can be used to model relevant parameters like the effective dry diffusion coefficient as well as the vapour diffusion coefficient. This is one of the strongest features of the carbonation model developed in this research which make it a powerful practical carbonation model.

- The effective time of exposure also depends on the drying/wetting periods as well as on the frequency of the drying/wetting cycles. The actual duration of drying/wetting periods as well as the frequency of rain or drying/wetting cycles in a given loaclity is variable. Hence, a simplified approach of constant drying/wetting periods was adopted in this research. Therefore the accuracy of prediction of the carbonation depth in the case of concrete exposed to rain depends on the drying/wetting period adopted for that locality of exposure. This is one of the shortcomings of the carbonation model developed. Hence, the model needs to be further refined in terms of developing a framework towards determining the normalised drying and wetting period using the rainfall data of a given locality or region.

6.3.3 Recommendations for Further Research

The current research fulfils all the objectives highlighted in Chapter 1 and the research findings were summarised in the previous sections of this chapter. Based on the research findings and taking into account the limitations of the research, some of the areas that need further research are pointed out below.

- The amount of carbonatable material in concrete matrices is one of the critical input parameters of the carbonation model developed in this research. The framework for the calculation of the amount of carbonatable material was adopted from Salvoldi

(2010) and the calculations depend on the degree of hydration, chemical composition and quantity of the binders etc. Alternatively, the amount of carbonatable materials can be experimentally determined and can be used as the input parameter of the carbonation model. However the framework for the calculation of the amount of carbonatable material can be further refined or simplified in terms of the amount of calcium oxide in the mix.

- The correlation between the effective dry diffusion coefficient and permeability coefficient as well as vapour diffusion coefficient and permeability coefficient was developed based on a wide range of curing conditions, w/b and binder type, etc., but with limited replacement levels of cement extenders. However, the sensitivity of these correlations towards the prediction of natural carbonation for different replacement levels of the cement extenders therefore needs to be assessed further and the variations need to be incorporated in the model.

- The concrete is assumed to be saturated instantaneously during the wetting period, in this research. Since the degree of saturation of concrete depends on the sorptivity of concrete, the carbonation model developed needs to be further refined taking into account the influence of saturation capacity of concrete during the wetting period.

- The drying and wetting cycles affect the moisture transport in concrete and hence have an effect on the rate of carbonation. The carbonation model developed in this research takes in to account the influence of the drying and wetting cycles. However, the precision of the prediction depends on the input parameters of the model such as the frequency of drying/wetting cycles and the duration of the drying/wetting period. This area needs further research, specifically in terms of developing a framework towards predicting the frequency of drying/wetting cycles and the duration of drying/wetting periods based on rainfall data.

- The carbonation model developed in this research was validated using natural carbonation data after 1000 days of exposure. However the models needs to be verified with long term natural carbonation data (8-10 years), based on which further refinement of the model can be done if necessary.

- Other than the major parameters considered for the development of the carbonation model in this research, factors like cracks which can develop during the service life of the structure, can influence the rate of carbonation. Further research in this regard is necessary in order to incorporate the influence of these parameters in the model.

- The rate of carbonation and the factors affecting carbonation are susceptible to variations and uncertainties. Even though the random nature of these parameters was acknowledged, the variability of these parameters was not taken into account during the carbonation model development. Therefore the model developed provides a deterministic output, which is in contrast with the fact that concrete properties, moisture movement, etc. are inherently variable. Therefore, the current model needs to be further developed in to a probabilistic framework.

LIST OF REFERENCES

Alexander, M., Ballim, Y., &Mackechnie, J. 1999. *Concrete durability index testing manual.* 4. Cape Town: University of Cape Town.

Alexander, M.G., Ballim, Y. & Stanish, K. 2008. A framework for use of durability indexes in performance-based design and specifications for reinforced concrete structures. *Materials and Structures.* 41(5):921-936. DOI:10.1617/s11527-007-9295-0 Available: https://doi.org/10.1617/s11527-007-9295-0.

Alexander, M., Mackechnie, J., & Ballim, Y. 1999a. *Guide to the use of durability indexes for achieving durability in concrete structures.* 2. Cape Town: University of Cape Town.

Alexander, M.G., Bentur, A. & Mindess, S. 2017. *Durability of concrete: design and construction.* CRC Press (Taylor & Francis Group). 323 pp.

Alexander, M.G., Mackechnie, J.R. & Yam, W. 2007. *Carbonation of concrete bridge structures in three South African localities.* Available: http://www.sciencedirect.com/science/article/pii/S0958946507001084 .

Alexander, M. G. and Mindess, S. 2005. *Aggregate in concrete* . London: Taylor and Francis.

Alhassan, Y.A., 'The effect of materials and micro-climate variations on predictions of carbonation rate in reinforced concrete in the inland environment', (PhD. thesis, University of Witwatersrand, South Africa, 2014).

Altman, D.G. & Bland, J.M. 1983. Measurement in Medicine: The Analysis of Method Comparison Studies. *Journal of the Royal Statistical Society: Series D (the Statistician).* 32(3):307-317. DOI:10.2307/2987937 Available: https://doi.org/10.2307/2987937.

Audenaert, K., 2007. Degradation mechanisms: Carbonation. In De Schutter, G. & Audenaert, K. Durability of Self-Compacting Concrete; RILEM Report 38. RILEM. pp.61-74.

Bahador, S.D. & Cahyadi, J.H. 2009. Modelling of carbonation of PC and blended cement concrete. *The IES Journal Part A: Civil & Structural Engineering.* 2(1):59-67. DOI:10.1080/19373260802518091 Available: https://doi.org/10.1080/19373260802518091.

Bahador, S. & Jong, H.C. 2006. Effect of preconditioning of concrete under accelerated test. *Proceedings of the 31st Conference on our World in Concrete and Structures.* 127-134.

Bakker, R., 1988. Initiation period. In Scgiessl. P. Corrosion of steel in concrete : report of the Technical Committee 60 CSC, RILEM, Chapman and Hall.

Ballim, Y. 1994. *Curing and the durability of concrete.* Johannesburg: University of the Witwatersrand.

Ballim, Y., Alexander, M. & Beushausen, H. 2009. Durability of concrete. In *Fulton's concrete technology.* G. Owens, Ed. 155.

Ballim, Y., and Lampacher, B. (1996). *Long-term carbonation of concrete structures in the Johannesburg environment*. Journal-South African Institution of Civil Engineers, 38, 5-9.

Bary, B. & Sellier, A. 2004. Coupled moisture—carbon dioxide–calcium transfer model for carbonation of concrete. *Cement and Concrete Research.* 34(10):1859-1872. DOI://dx.doi.org/10.1016/j.cemconres.2004.01.025.

Bazant, Z.P. and Najjar, L.J. (1972) Non-linear water diffusion in non-saturated concrete. Materials and Structures, Vol. 5, pp. 1-20

Bernal, S.A., Provis, J.L., Brice, D.G., Kilcullen, A., Duxson, P. & van Deventer, Jannie S J. 2012. Accelerated carbonation testing of alkali-activated binders significantly underestimates service life: The role of pore solution chemistry. *Cement and Concrete Research.* 42(10):1317-1326. DOI://dx.doi.org/10.1016/j.cemconres.2012.07.002.

Beushausen, H. & Alexander, M. 2008. The South African durability index tests in an international comparison. *Journal of the South African Institution of Civil Engineering.* 50.

Beushausen, H. and Alexander, M., (2009), 'Application of durability indicators for quality control of concrete members - a practical example',*RILEM Conference on Concrete in Aggressive Aqueous Environments*, 3 - 5 June,Toulouse, France, pp. 548-556.

Borges, P.R., Milestone, N., Costa, J., Lynsdale, C., Panzera, T. & Christophoro, A. 2012. Carbonation durability of blended cement pastes used for waste encapsulation. *Materials and Structures.* 45(5):663-678. DOI:10.1617/s11527-011-9788-8.

Bouchaala, F., Payan, C., Garnier, V. & Balayssac, J.P. 2011. *Carbonation assessment in concrete by nonlinear ultrasound.* Available: http://www.sciencedirect.com/science/article/pii/S0008884611000639 .

CPC-18 Measurement of hardened concrete carbonation depth. 1988. *Materials and Structures.* 21(6):453-455. DOI:10.1007/BF02472327 Available: https://doi.org/10.1007/BF02472327.

Castellote, M. & Andrade, C. 2008. Modelling the carbonation of cementitious matrixes by means of the unreacted-core model, UR-CORE. *Cement and Concrete Research.* 38(12):1374-1384. DOI://dx.doi.org/10.1016/j.cemconres.2008.07.004.

Castellote, M., Fernandez, L., Andrade, C. & Alonso, C. 2009. Chemical changes and phase analysis of OPC pastes carbonated at different CO_2 concentrations. *Materials and Structures.* 42(4):515-525. DOI:10.1617/s11527-008-9399-1.

Chang, C. & Chen, J. 2006. *The experimental investigation of concrete carbonation depth.* Available: http://www.sciencedirect.com/science/article/pii/S0008884604003357 .

Chin, M.S.,‘ Carbonation of concrete’, (M. Eng. thesis, National University of Singapore, Singapore, 1991).

Chun, Q.L. 2004. Reliability Based Service Life Prediction of Corrosion Affected Concrete Structures. *Journal of Structural Engineering.* 130(10):1570-1577. DOI:10.1061/(ASCE)0733-9445(2004)130:10(1570) Available: https://doi.org/10.1061/(ASCE)0733-9445(2004)130:10(1570).

Dhir, R.K., Hewlett, P.C. & Chan, Y.N. 1991. Near-surface characteristics of concrete: abrasion resistance. *Materials and Structures.* 24(2):122. DOI:10.1007/BF02472473 Available: https://doi.org/10.1007/BF02472473.

Ekolu, S.O. 2018. *Model for practical prediction of natural carbonation in reinforced concrete: Part 1-formulation.* Available: http://www.sciencedirect.com/science/article/pii/S0958946516307570 .

fib, Model Code for Service-life Design, fib Bulletin 34, first ed., FederationInternational du Beton, Lausanne, 2006, 126pp., ISBN: 978-2-88394-074-1.

fib, Model Code 2010 Final Draft, vols. 1 & 2, 2010 fib bulletin N. 65 & 66, Lausanne, 2012.

Galan, I. and Andrade, C. 2009. Comparison of carbonation models . *3rd International PhD Workshop on Modelling the Durability of Reinforced Concrete.* 2009. R. M. Ferreira, J. Gulikers, C. Andrade, Ed. RILEM Publications SARL

Gebhart B., 1993, Heat conduction and mass diffusion. New York: McGraw-Hill.

Giavarina, D. 2015. Understanding Bland Altman analysis. *Biochemia Medica.* 25(2):141-151. DOI:10.11613/BM.2015.015 Available: https://www.ncbi.nlm.nih.gov/pubmed/26110027 https://www.ncbi.nlm.nih.gov/pmc/articles/PMC4470095/.

Githachuri, K, ‘Influence of the transport properties of a range of South African marine concrete’, (M. Eng. thesis, University of Cape Town, South Africa, 2010).

Githachuri, K. & Alexander, M.G. 2013. *Durability performance potential and strength of blended Portland limestone cement concrete.* Available: http://www.sciencedirect.com/science/article/pii/S0958946513000462 .

Gonen, T. & Yazicioglu, S. 2007. The influence of compaction pores on sorptivity and carbonation of concrete. *Construction and Building Materials.* 21(5):1040-1045. DOI://dx.doi.org/10.1016/j.conbuildmat.2006.02.010.

Gruyaert, E., Van den Heede, P. & De Belie, N. 2013. Carbonation of slag concrete: Effect of the cement replacement level and curing on the carbonation coefficient – Effect of carbonation on the pore structure. *Cement and Concrete Composites.* 35(1):39-48. DOI://dx.doi.org/10.1016/j.cemconcomp.2012.08.024.

Guiglia, M. & Taliano, M. 2013. *Comparison of carbonation depths measured on in-field exposed existing r.c. structures with predictions made using fib-Model Code 2010.* Available: http://www.sciencedirect.com/science/article/pii/S0958946513000334 .

Hewlett, P.C., 1998. Lea's Chemistry of Cement and Concrete. 4th ed. London: Arnold

Houst, Y.F. & Wittmann, F.H. 1994. *Influence of porosity and water content on the diffusivity of CO_2 and O_2 through hydrated cement paste.* Available: http://www.sciencedirect.com/science/article/pii/000888469490040X

Houst, Y.F. & Wittmann, F.H. 2002. *Depth profiles of carbonates formed during natural carbonation.* Available: http://www.sciencedirect.com/science/article/pii/S0008884602009080 .

Hui-sheng, S., Bi-wan, X. & Xiao-chen, Z. 2009. Influence of mineral admixtures on compressive strength, gas permeability and carbonation of high performance concrete. *Construction and Building Materials.* 23(5):1980-1985. DOI://dx.doi.org/10.1016/j.conbuildmat.2008.08.021.

Hyvert, N., Sellier, A., Duprat, F., Rougeau, P. & Francisco, P. 2010. *Dependency of C–S–H carbonation rate on CO_2 pressure to explain transition from accelerated tests to natural carbonation.* Available: http://www.sciencedirect.com/science/article/pii/S0008884610001456 .

Ihekwaba, N.M., Hope, B.B. & Hansson, C.M. 1996. Carbonation and electrochemical chloride extraction from concrete. *Cement and Concrete Research.* 26(7):1095-1107. DOI://dx.doi.org/10.1016/0008-8846(96)00076-2 Available: http://www.sciencedirect.com/science/article/pii/0008884696000762.

Ji, Y., Wu, M., Ding, B., Liu, F. & Gao, F. 2014. The experimental investigation of width of semi-carbonation zone in carbonated concrete. *Construction and Building Materials.* 65(0):67-75. DOI://dx.doi.org/10.1016/j.conbuildmat.2014.04.095.

Jung, S.H., Lee, M.K. & Hwan Oh, B. 2011. Measurement Device and Characteristics of Diffusion Coefficient of Carbon Dioxide in Concrete. *ACI Materials Journal.* 108(6) DOI:10.14359/51683461.

Jung, W., Yoon, Y. & Sohn, Y. 2003. *Predicting the remaining service life of land concrete by steel corrosion.* Available: http://www.sciencedirect.com/science/article/pii/S0008884602010347 .

Kada-Benameur, H., Wirquin, E. & Duthoit, B. 2000. *Determination of apparent activation energy of concrete by isothermal calorimetry.* Available: http://www.sciencedirect.com/science/article/pii/S0008884699002501 .

Khunthongkeaw, J., Tangtermsirikul, S. & Leelawat, T. 2006a. *A study on carbonation depth prediction for fly ash concrete.* Available: http://www.sciencedirect.com/science/article/pii/S0950061805000978 .

Khunthongkeaw, J., Tangtermsirikul, S. & Leelawat, T. 2006b. *A study on carbonation depth prediction for fly ash concrete.* Available: http://www.sciencedirect.com/science/article/pii/S0950061805000978 .

Kim, G., Kim, J., Kurtis, K.E., Jacobs, L.J., Le Pape, Y. & Guimaraes, M. 2016. Quantitative evaluation of carbonation in concrete using nonlinear ultrasound. *Materials and Structures.* 49(1):399-409. DOI:10.1617/s11527-014-0506-1 Available: https://doi.org/10.1617/s11527-014-0506-1.

Kollek, J.J. 1989. The determination of the permeability of concrete to oxygen by the Cembureau method—a recommendation. *Materials and Structures.* 22(3):225-230. DOI:10.1007/BF02472192 Available: https://doi.org/10.1007/BF02472192.

Kropp, J., 'Chapter 5 - Relations between different transport characteristics and durability'. Performance Criteria for Concrete Durability RILEM.1995

Leemann, A. & Moro, F. 2016. Carbonation of concrete: the role of CO_2 concentration, relative humidity and CO2 buffer capacity. *Materials and Structures.* 50(1):30. DOI:10.1617/s11527-016-0917-2 Available: https://doi.org/10.1617/s11527-016-0917-2.

Leemann, A., Nygaard, P., Kaufmann, J. & Loser, R. 2015. *Relation between carbonation resistance, mix design and exposure of mortar and concrete.* Available: http://www.sciencedirect.com/science/article/pii/S0958946515000967 .

Li, K., Li, C. & Chen, Z. 2009. Influential depth of moisture transport in concrete subject to drying–wetting cycles. *Cement and Concrete Composites.* 31(10):693-698. DOI://dx.doi.org/10.1016/j.cemconcomp.2009.08.006.

Mackechnie, J.R. & Alexander, M.G. 2002. Durability Predictions Using Early-Age Durability Index Testing. In *9th International Conference on Durability of Building Materials and Components.* Rotterdam (Netherlands): in house publishing. Available: http://www.irbnet.de/daten/iconda/CIB9338.pdf.

Martin, M, 'The influence of curing techniques and chemical admixtures on the properties of concrete', (M. Eng. thesis, University of Cape Town, South Africa, 2012).

Meier, S.A., Peter, M.A., Muntean, A. & Böhm, M. 2007. *Dynamics of the internal reaction layer arising during carbonation of concrete.* Available: http://www.sciencedirect.com/science/article/pii/S0009250906007196 .

Muigai, R.N., 'Probabilistic modelling for durability design of reinforced concrete structures', (M. Eng. thesis, University of Cape Town, South Africa, 2008).

Neville, A.M. 2007. *Properties of concrete.* Fourth Edition ed. Pearson Education Ltd.

Nilsson, L.O. and Luping, T., 'Chapter 3 - Relations between different transport parameters'. Performance Criteria for Concrete Durability RILEM.1995.

Nganga, G., Alexander, M. & Beushausen, H. 2013. *Practical implementation of the durability index performance-based design approach.* Available: http://www.sciencedirect.com/science/article/pii/S0950061813002791 .

Ohga, H. & Nagataki, S. 1988. Prediction and evaluation of the depth of carbonation of concrete by accelerated test. *Doboku Gakkai Ronbunshu.* 8:225-233. DOI:10.2208/jscej.1988.390_225.

Otieno, M.B., 'The development of emperical Chloride-induced corrosion rate prediction models for cracked and uncracked steel reinforced concrete structures in the marine tidalzone', (PhD. thesis, University of Cape Town, South Africa, 2014).

Otieno, M.B., Beushausen, H.D. & Alexander, M.G. 2011. *Modelling corrosion propagation in reinforced concrete structures – A critical review.* Available: http://www.sciencedirect.com/science/article/pii/S0958946510001873 .

Papadakis, V.G., Fardis, M.N. & Vayenas, C.G. 1992. Effect of composition, environmental factors and cement-lime mortar coating on concrete carbonation. *Materials and Structures.* 25(5):293-304. DOI:10.1007/BF02472670.

Papadakis, V.G., Vayenas, C.G. & Fardis, M.N. 1989. A reaction engineering approach to the problem of concrete carbonation. *AIChE Journal.* 35(10):1639-1650. DOI:10.1002/aic.690351008.

Papadakis, V.G. 2000. Effect of supplementary cementing materials on concrete resistance against carbonation and chloride ingress. *Cement and Concrete Research.* 30(2):291-299. DOI://dx.doi.org/10.1016/S0008-8846(99)00249-5.

Papadakis, V.G., Vayenas, C.G. & Fardis, M.N. 1991a. Fundamental modeling and experimental investigation of concrete carbonation. *Materials Journal.* 88(4):363-373.

Papadakis, V.G., Vayenas, C.G. & Fardis, M.N. 1991b. Physical and chemical characteristics affecting the durability of concrete. *Materials Journal.* 88(2):186-196.

Parrott, L.J. 1987. *A review of carbonation in reinforced concrete.* British Cement Association.

Parrott, L.J. 1994. Moisture conditioning and transport properties of concrete test specimens. *Materials and Structures.* 27(8):460-468. DOI:10.1007/BF02473450.

Parrott, L.J. 1996. Some effects of cement and curing upon carbonation and reinforcement corrosion in concrete. *Materials and Structures.* 29(3):164-173. DOI:10.1007/BF02486162.

Parrott, L.J. 1988a. Moisture profiles in drying concrete. *Advances in Cement Research.* 1(3):164-170. DOI:10.1680/1988.1.3.164.

Parrott, L.J. 1988b. Moisture profiles in drying concrete. *Advances in Cement Research.* 1(3):164-170. DOI:10.1680/1988.1.3.164 Available: https://doi.org/10.1680/1988.1.3.164.

Raupach, M. 2006. Models for the propagation phase of reinforcement corrosion – an overview. *Materials and Corrosion.* 57(8):605-613. DOI:10.1002/maco.200603991 Available: https://doi.org/10.1002/maco.200603991.

Richardson, M.G. 2002. *Fundamentals of Durable Reinforced Concrete.* 1st ed. London: CRC Press. Available: http://lib.myilibrary.com?ID=5667.

Rose, D.A. 1965 Water movement in unsaturated porous materials, RILEM. Bulletin, No. 29, pp. 119-23

Saeki, T., Ohga, H. & Nagataki, S. 1991. Mechanism of carbonation and prediction of carbonation process of concrete. *Concrete Library of JSCE.* 17(17):23-36. [21 December 2017].

Saeki, T. & Monteiro, P.J.M. 2005. *A model to predict the amount of calcium hydroxide in concrete containing mineral admixtures.* Available: http://www.sciencedirect.com/science/article/pii/S0008884605000682 .

Saetta, A.V., Schrefler, B.A. & Vitaliani, R.V. 1993. The carbonation of concrete and the mechanism of moisture, heat and carbon dioxide flow through porous materials. *Cement and Concrete Research.* 23(4):761-772. DOI://dx.doi.org/10.1016/0008-8846(93)90030-D.

Saetta, A.V., Schrefler, B.A. & Vitaliani, R.V. 1995. 2 — D model for carbonation and moisture/heat flow in porous materials. *Cement and Concrete Research.* 25(8):1703-1712. DOI://dx.doi.org/10.1016/0008-8846(95)00166-2 Available: http://www.sciencedirect.com/science/article/pii/0008884695001662.

SANS-3001-CO3-1, Civil Engineering Test Methods: Part CO3-1: Concrete Durability Index Testing - Preparation of test specimens, South African Bureau of Standards – Standards Division, Pretoria, South Africa, 2015. ISBN 978-0-626-32799-6.

SANS-3001-CO3-2, Civil Engineering Test Methods: Part CO3-2: Concrete Durability Index Testing – Oxygen permeability test, South African Bureau of Standards – Standards Division, Pretoria, South Africa, 2015. ISBN 978-0-626-32800-9.

SANS 5861-3:2006, Concrete tests: Part-3: Making and curing of test specimens, South African Bureau of Standards – Standards Division, Pretoria, South Africa, 2006.

SANS 5862-1:2006, Concrete tests — Consistence of freshly mixed concrete — Slump test, South African Bureau of Standards – Standards Division, Pretoria, South Africa.

SANS 5863:2006, Concrete tests — Compressive strength of hardened concrete, South African Bureau of Standards – Standards Division, Pretoria, South Africa, 2006.

Salvoldi, B.G., Beushausen, H. & Alexander, M.G. 2015. *Oxygen permeability of concrete and its relation to carbonation.* Available: http://www.sciencedirect.com/science/article/pii/S095006181500166X .

Salvoldi, B., 'Modelling the carbonation of concrete using early age oxygen permeability index tests', (M. Eng. thesis, University of Cape Town, South Africa, 2010).

Sanjuán, M.A., Andrade, C. & Cheyrezy, M. 2003. Concrete carbonation tests in natural and accelerated conditions. *Advances in Cement Research.* 15(4):171-180. DOI:10.1680/adcr.2003.15.4.171 Available: https://doi.org/10.1680/adcr.2003.15.4.171.

Sanjuán, M.Á, Estévez, E., Argiz, C. & Barrio, D.d. 2018. *Effect of curing time on granulated blast-furnace slag cement mortars carbonation.* Available: http://www.sciencedirect.com/science/article/pii/S0958946517308582 .

Sirivivantnanon, V., (2001), 'Effect of cracking on service life of concrete', *Concrete Institute of Australia conference proceedings*, 11-14 September, Perth, Western Australia, pp. 273-279.

Sisomphon, K. & Franke, L. 2007. *Carbonation rates of concretes containing high volume of pozzolanic materials.* Available: http://www.sciencedirect.com/science/article/pii/S0008884607001937 .

Steffens, A., Dinkler, D. & Ahrens, H. 2002. Modeling carbonation for corrosion risk prediction of concrete structures. *Cement and Concrete Research.* 32(6):935-941. DOI://dx.doi.org/10.1016/S0008-8846(02)00728-7.

Sulapha, P., Wong, S.F., Wee, T.H. & Swaddiwudhipong, S. 2003. Carbonation of Concrete Containing Mineral Admixtures. *Journal of Materials in Civil Engineering.* 15(2):134-143. DOI:10.1061/(ASCE)0899-1561(2003)15:2(134) Available: https://doi.org/10.1061/(ASCE)0899-1561(2003)15:2(134).

Ta, V., Bonnet, S., Senga Kiesse, T. & Ventura, A. 2016. *A new meta-model to calculate carbonation front depth within concrete structures.* Available: http://www.sciencedirect.com/science/article/pii/S0950061816317184 .

Taylor, H.W.F., 1997. Cement Chemistry. Thomas Telford.

Thiery, M., 'Modélisation de la carbonatation atmosphérique des matériaux cimentaires: prise en compte des effets cinétiques et des modifications microstructurales et hydriques', (PhD. thesis, Ecole Nationale des Ponts et Chaussées, 2005).

Thiery, M., Villain, G., Dangla, P. & Platret, G. 2007. *Investigation of the carbonation front shape on cementitious materials: Effects of the chemical kinetics.* Available: http://www.sciencedirect.com/science/article/pii/S0008884607000932 .

Thiery, M., Cremona, C. & Baroghel-Bouny, V. 2012. Application of the reliability theory to the assessment of carbonation-induced corrosion risk of rebars. *European Journal of Environmental and Civil Engineering.* 16(3-4):273-287. DOI:10.1080/19648189.2012.667987 Available: https://doi.org/10.1080/19648189.2012.667987.

Thomas, M.D.A. & Matthews, J.D. 1992. Carbonation of fly ash concrete. *Magazine of Concrete Research.* 44(160):217-228. DOI:10.1680/macr.1992.44.160.217.

Torrent, R.J. 1992. A two-chamber vacuum cell for measuring the coefficient of permeability to air of the concrete cover on site. *Materials and Structures.* 25(6):358-365. DOI:10.1007/BF02472595 Available: https://doi.org/10.1007/BF02472595.

Tuutti, K., (1982), 'Corrosion of steel in concrete', *Swedish Cement and Concrete Research Institute*, Stockholm, Report No. CBI Research 4:82, pp. 468.

UCT, 'Durability Index Testing Procedure Manual' (Ver 4.5.1) April (2018).https://docs.wixstatic.com/ugd/5586b6_07c436992a6d4768ba2ae42d86a0a88f.pdf

Van Balen, K. & Van Gemert, D. 1994. Modelling lime mortar carbonation. *Materials and Structures.* 27(7):393-398.

Verbeck, G.J. 1958. *Carbonation of Hydrated Portland Cement.* Research and Development Laboratories of the Portland Cement Assoc. Available: https://books.google.co.za/books?id=KiG8DAEACAAJ.

Villain, G. & Platret, G. 2006. Two experimental methods to determine carbonation profiles in concrete. *ACI Materials Journal.* 103(4):265-271.

Villain, G. & Thiery, M. 2006. *Gammadensimetry: A method to determine drying and carbonation profiles in concrete.* Available: http://www.sciencedirect.com/science/article/pii/S0963869505001507 .

Villain, G., Thiery, M. & Platret, G. 2007. Measurement methods of carbonation profiles in concrete: Thermogravimetry, chemical analysis and gammadensimetry. *Cement and Concrete Research.* 37(8):1182-1192. DOI://dx.doi.org/10.1016/j.cemconres.2007.04.015.

Visser, J.H.M. 2012. Accelerated carbonation testing of mortar with supplementary cement materials: limitation of the acceleration due to drying. *Heron.* 57(3):231-248.

Visser, J.H.M. 2014. Influence of the carbon dioxide concentration on the resistance to carbonation of concrete. *Construction and Building Materials.* 67, Part A(0):8-13. DOI://dx.doi.org/10.1016/j.conbuildmat.2013.11.005.

Wierig, H.-J., 1984. Longtime studies on the carbonation of concrete under normal outdoor exposure. In RILEM Seminar on Durability. Hannover University, 1984. RILEM.

Yam, W.,' Carbonation of bridges in three South Afican Localities', (M. Eng. thesis, University of Cape Town, South Africa, 2003).

Yoon, I., Copuroglu, O. & Park, K. 2007. Effect of global climatic change on carbonation progress of concrete. *Atmospheric Environment.* 41:7274-7285.

Younsi, A., Turcry, P., Rozière, E., Aït-Mokhtar, A. & Loukili, A. 2011. Performance-based design and carbonation of concrete with high fly ash content. *Cement and Concrete Composites.* 33(10):993-1000. DOI://dx.doi.org/10.1016/j.cemconcomp.2011.07.005.

Zhao, Q., He, X., Zhang, J. & Jiang, J. 2016. *Long-age wet curing effect on performance of carbonation resistance of fly ash concrete.* Available: http://www.sciencedirect.com/science/article/pii/S0950061816316786 .

APPENDIX A: DETAILS OF CHEMICAL ADMIXTURE USED

Table A.1 Physical and chemical properties of superplasticizer used

Admixture	Sika ViscoCrete -10
Type	Superplasticizer
Appearance	Light brown liquid
pH	4.25 ± 0.5
Specific gravity	1.06 (at +20°C)
Typical dosage for concrete indicated by supplier	0.4 – 1.5 % by mass of cement
Composition/information on ingredients	Modified Polycarboxylate in water
Other properties/ Effects given by the supplier	High range water reduction, resulting in increased workability, high density, strength and low permeability. Improved flow, placing and compaction characteristics.

APPENDIX B: DETAILED COMPRESSIVE STRENGTH TEST RESULTS

Table B.1 Compressive strength at 3-day

Mix Designation	Elements	w/b	3-day strength				
			1	2	3	**Mean**	**SD***
PC-45	Weight (gms)	0.45 w/b	2470	2435	2435	2446.7	20.2
	Load (kN)		557	548	522	542.3	18.2
	Stress (MPa)		**55.7**	**54.8**	**52.2**	**54.2**	**1.8**
FA-45	Weight (gms)		2410	2417	2463	2430.0	28.8
	Load (kN)		314	330	311	318.3	10.2
	Stress (MPa)		**31.4**	**33**	**31.1**	**31.8**	**1.0**
GS-45	Weight (gms)		2410	2417	2452	2426.3	22.5
	Load (kN)		293	324	292	303.0	18.2
	Stress (MPa)		**29.3**	**32.4**	**29.2**	**30.3**	**1.8**
PC-55	Weight (gms)	0.55 w/b	2420	2413	2352	2395.0	37.4
	Load (kN)		423	388	403	404.7	17.6
	Stress (MPa)		**42.3**	**38.8**	**40.3**	**40.5**	**1.8**
FA-55	Weight (gms)		2350	2343	2394	2362.3	27.6
	Load (kN)		240	254	262	252.0	11.1
	Stress (MPa)		**24**	**25.4**	**26.2**	**25.2**	**1.1**
GS-55	Weight (gms)		2392	2334	2386	2370.7	31.9
	Load (kN)		211	206	202	206.3	4.5
	Stress (MPa)		**21.1**	**20.6**	**20.2**	**20.6**	**0.5**
PC-65	Weight (gms)	0.66 w/b	2421	2410	2370	2400.3	26.8
	Load (kN)		284	263	260	269.0	13.1
	Stress (MPa)		**28.4**	**26.3**	**26**	**26.9**	**1.3**
FA-65	Weight (gms)		2417	2426	2379	2407.3	24.9
	Load (kN)		170	183	186	179.7	8.5
	Stress (MPa)		**17**	**18.3**	**18.6**	**18.0**	**0.9**
GS-65	Weight (gms)		2375	2310	2354	2346.3	33.2
	Load (kN)		149	135	148	144.0	7.8
	Stress (MPa)		**14.9**	**13.5**	**14.8**	**14.4**	**0.8**

*Standard deviation

Table B.2 Compressive strength at 28-day

Mix Designation	Elements	w/b	28-day strength				
			1	2	3	**Mean**	**SD***
PC-45	Weight (gms)	0.45 w/b	2504	2454	2421	2459.7	41.8
	Load (kN)		722	702	760	728.0	29.5
	Stress (MPa)		**72.2**	**70.2**	**76**	**72.8**	**2.9**
FA-45	Weight (gms)		2398	2413	2344	2385.0	36.3
	Load (kN)		628	610	634	624.0	12.5
	Stress (MPa)		**62.8**	**61**	**63.4**	**62.4**	**1.2**
GS-45	Weight (gms)		2326	2330	2343	2333.0	8.9
	Load (kN)		638	648	690	658.7	27.6
	Stress (MPa)		**63.8**	**64.8**	**69**	**65.9**	**2.8**
PC-55	Weight (gms)	0.55 w/b	2459	2437	2475	2457.0	19.1
	Load (kN)		580	576	592	582.7	8.3
	Stress (MPa)		**58**	**57.6**	**59.2**	**58.3**	**0.8**
FA-55	Weight (gms)		2415	2369	2390	2391.3	23.0
	Load (kN)		444	452	456	450.7	6.1
	Stress (MPa)		**44.4**	**45.2**	**45.6**	**45.1**	**0.6**
GS-55	Weight (gms)		2330	2423	2306	2353.0	61.8
	Load (kN)		550	536	548	544.7	7.6
	Stress (MPa)		**55**	**53.6**	**54.8**	**54.5**	**0.8**
PC-65	Weight (gms)	0.66 w/b	2367	2396	2359	2374.0	19.5
	Load (kN)		424	430	426	426.7	3.1
	Stress (MPa)		**42.4**	**43**	**42.6**	**42.7**	**0.3**
FA-65	Weight (gms)		2432	2404	2402	2412.7	16.8
	Load (kN)		302	310	316	309.3	7.0
	Stress (MPa)		**30.2**	**31**	**31.6**	**30.9**	**0.7**
GS-65	Weight (gms)		2347	2366	2354	2355.7	9.6
	Load (kN)		396	412	398	402.0	8.7
	Stress (MPa)		**39.6**	**41.2**	**39.8**	**40.2**	**0.9**

*Standard deviation

Table B.3 Compressive strength at 90-day

Mix Designation	Elements	w/b	90-day strength				
			1	2	3	**Mean**	**SD***
PC-45	Weight (gms)	0.45 w/b	2434	2453	2389	2425.3	32.9
	Load (kN)		808	776	854	812.7	39.2
	Stress (MPa)		**80.8**	**77.6**	**85.4**	**81.3**	**3.9**
FA-45	Weight (gms)		2404	2450	2452	2435.3	27.2
	Load (kN)		736	708	742	728.7	18.1
	Stress (MPa)		**73.6**	**70.8**	**74.2**	**72.9**	**1.8**
GS-45	Weight (gms)		2356	2392	2355	2367.7	21.1
	Load (kN)		740	760	712	737.3	24.1
	Stress (MPa)		**74**	**76**	**71.2**	**73.7**	**2.4**
PC-55	Weight (gms)	0.55 w/b	2372	2476	2443	2430.3	53.1
	Load (kN)		646	624	632	634.0	11.1
	Stress (MPa)		**64.6**	**62.4**	**63.2**	**63.4**	**1.1**
FA-55	Weight (gms)		2429	2429	2406	2421.3	13.3
	Load (kN)		596	590	576	587.3	10.3
	Stress (MPa)		**59.6**	**59**	**57.6**	**58.7**	**1.0**
GS-55	Weight (gms)		2340	2401	2350	2363.7	32.7
	Load (kN)		668	626	632	642.0	22.7
	Stress (MPa)		**66.8**	**62.6**	**63.2**	**64.2**	**2.3**
PC-65	Weight (gms)	0.66 w/b	2383	2424	2419	2408.7	22.4
	Load (kN)		510	520	522	517.3	6.4
	Stress (MPa)		**51**	**52**	**52.2**	**51.7**	**0.6**
FA-65	Weight (gms)		2318	2403	2295	2338.7	56.9
	Load (kN)		452	434	414	433.3	19.0
	Stress (MPa)		**45.2**	**43.4**	**41.4**	**43.3**	**1.9**
GS-65	Weight (gms)		2364	2387	2416	2389.0	26.1
	Load (kN)		464	444	484	464.0	20.0
	Stress (MPa)		**46.4**	**44.4**	**48.4**	**46.4**	**2.0**

*Standard deviation

APPENDIX C: OXYGEN PERMEABILITY INDEX TEST RESULTS

Table C.1 Oxygen permeability index test results – (Curing-A)

Mix Designation	Elements	w/b	Curing-A						
			Specimen-1	Specimen-2	Specimen-3	Specimen-4	**Mean**	**SD***	**COV#**
PC-45	k (m/s):	0.45 w/b	2.91E-11	3.75E-11	4.63E-11	5.62E-11	4.23E-11	1.16E-11	2.75E+01
	OPI:		10.54	10.43	10.33	10.25	**10.37**	0.12	1.18
FA-45	k (m/s):		1.49E-11	2.48E-11	3.12E-11	7.24E-11	3.59E-11	2.53E-11	7.05E+01
	OPI:		10.83	10.60	10.51	10.14	**10.45**	0.29	2.74
GS-45	k (m/s):		9.86E-12	1.37E-11	1.75E-11	1.13E-11	1.31E-11	3.36E-12	2.56E+01
	OPI:		11.01	10.86	10.76	10.95	**10.88**	0.11	1.00
LS-45	k (m/s):		2.48E-11	1.75E-11	1.26E-11	2.05E-11	1.89E-11	5.12E-12	2.72E+01
	OPI:		10.61	10.76	10.90	10.69	**10.72**	0.12	1.16
PC-55	k (m/s):	0.55 w/b	6.40E-11	4.87E-11	3.29E-11	4.98E-11	4.89E-11	1.27E-11	2.60E+01
	OPI:		10.19	10.31	10.48	10.30	**10.31**	0.12	1.16
FA-55	k (m/s):		6.45E-11	5.30E-11	4.29E-11	7.32E-11	5.84E-11	1.32E-11	2.27E+01
	OPI:		10.19	10.28	10.37	10.14	**10.23**	0.10	0.99
GS-55	k (m/s):		2.86E-11	2.80E-11	8.93E-12	9.64E-12	1.88E-11	1.10E-11	5.84E+01
	OPI:		10.54	10.55	11.05	11.02	**10.73**	0.28	2.61
LS-55	k (m/s):		4.60E-11	2.07E-11	2.11E-11	3.43E-11	3.05E-11	1.21E-11	3.96E+01
	OPI:		10.34	10.68	10.68	10.47	**10.52**	0.17	1.61
PC-65	k (m/s):	0.65 w/b	6.01E-11	9.27E-11	3.91E-11	3.89E-11	5.77E-11	2.53E-11	4.39E+01
	OPI:		10.22	10.03	10.41	10.41	**10.24**	0.18	1.76
FA-65	k (m/s):		1.35E-10	1.58E-10	4.57E-11	5.64E-11	9.86E-11	5.58E-11	5.66E+01
	OPI:		9.87	9.80	10.34	10.25	**10.01**	0.27	2.68
GS-65	k (m/s):		4.69E-11	3.53E-11	2.57E-11	3.44E-11	3.56E-11	8.68E-12	2.44E+01
	OPI:		10.33	10.45	10.59	10.46	**10.45**	0.11	1.02
LS-65	k (m/s):		3.14E-11	2.50E-11	2.83E-11	2.97E-11	2.86E-11	2.70E-12	9.44E+00
	OPI:		10.50	10.60	10.55	10.53	**10.54**	0.04	0.40

*Standard deviation

#coefficient of variation

k- oxygen permeability coefficient

Table C.2 Oxygen permeability index test results – (Curing-B)

Mix Designation	Elements	w/b	Curing-B						
			Specimen-1	Specimen-2	Specimen-3	Specimen-4	**Mean**	**SD***	**COV#**
PC-45	k (m/s):	0.45 w/b	5.41E-11	3.97E-11	6.78E-11	5.70E-11	5.47E-11	1.16E-11	2.11E+01
	OPI:		10.27	10.40	10.17	10.24	**10.26**	0.10	0.94
FA-45	k (m/s):		1.39E-10	1.16E-10	1.09E-10	8.62E-11	1.13E-10	2.18E-11	1.94E+01
	OPI:		9.86	9.93	9.96	10.06	**9.95**	0.09	0.86
GS-45	k (m/s):		1.30E-10	1.09E-10	1.22E-10	1.17E-10	1.19E-10	8.77E-12	7.35E+00
	OPI:		9.89	9.96	9.92	9.93	**9.92**	0.03	0.32
LS-45	k (m/s):		7.05E-11	6.18E-11	6.13E-11	5.82E-11	6.30E-11	5.26E-12	8.36E+00
	OPI:		10.15	10.21	10.21	10.23	**10.20**	0.04	0.35
PC-55	k (m/s):	0.55 w/b	9.34E-11	8.62E-11	1.16E-10	1.07E-10	1.01E-10	1.34E-11	1.33E+01
	OPI:		10.03	10.06	9.93	9.97	**10.00**	0.06	0.58
FA-55	k (m/s):		2.72E-10	2.86E-10	2.95E-10	2.93E-10	2.87E-10	1.03E-11	3.59E+00
	OPI:		9.56	9.54	9.53	9.53	**9.54**	0.02	0.17
GS-55	k (m/s):		4.49E-10	3.08E-10	2.03E-10	2.03E-10	2.91E-10	1.17E-10	4.01E+01
	OPI:		9.35	9.51	9.69	9.69	**9.54**	0.17	1.74
LS-55	k (m/s):		1.52E-10	1.72E-10	1.96E-10	2.11E-10	1.83E-10	2.57E-11	1.41E+01
	OPI:		9.82	9.77	9.71	9.68	**9.74**	0.06	0.64
PC-65	k (m/s):	0.65 w/b	2.79E-10	2.70E-10	3.09E-10	3.09E-10	2.92E-10	2.01E-11	6.88E+00
	OPI:		9.55	9.57	9.51	9.51	**9.54**	0.03	0.31
FA-65	k (m/s):		7.60E-10	6.89E-10	4.26E-10	5.47E-10	6.06E-10	1.49E-10	2.46E+01
	OPI:		9.12	9.16	9.37	9.26	**9.22**	0.11	1.22
GS-65	k (m/s):		5.76E-10	4.08E-10	5.28E-10	7.73E-10	5.71E-10	1.52E-10	2.66E+01
	OPI:		9.24	9.39	9.28	9.11	**9.24**	0.11	1.24
LS-65	k (m/s):		2.86E-10	2.93E-10	4.52E-10	3.65E-10	3.49E-10	7.77E-11	2.23E+01
	OPI:		9.54	9.53	9.34	9.44	**9.46**	0.09	0.99

*Standard deviation

#coefficient of variation

k- oxygen permeability coefficient

Table C.3 Oxygen permeability index test results – (Curing-C)

Mix Designation	Elements	w/b	Curing-C						
			Specimen-1	Specimen-2	Specimen-3	Specimen-4	Mean	SD*	COV#
PC-45	k (m/s):	0.45 w/b	4.41E-11	5.36E-11	6.60E-11	1.27E-10	7.28E-11	3.75E-11	51.50167048
	OPI:		10.36	10.27	10.18	9.89	10.14	0.20	1.97
FA-45	k (m/s):		1.23E-10	1.06E-10	3.96E-11	6.47E-11	8.34E-11	3.81E-11	45.68659527
	OPI:		9.91	9.97	10.40	10.19	10.08	0.22	2.22
GS-45	k (m/s):		8.38E-11	5.27E-11	5.96E-11	1.60E-10	8.90E-11	4.91E-11	55.18023646
	OPI:		10.08	10.28	10.22	9.80	10.05	0.22	2.15
LS-45	k (m/s):		5.13E-11	5.60E-11	3.74E-11	4.48E-11	4.74E-11	8.06E-12	17.02265439
	OPI:		10.29	10.25	10.43	10.35	10.32	0.08	0.74
PC-55	k (m/s):	0.55 w/b	6.74E-11	9.40E-11	1.05E-10	1.06E-10	9.31E-11	1.80E-11	19.29488811
	OPI:		10.17	10.03	9.98	9.97	10.03	0.09	0.92
FA-55	k (m/s):		3.29E-10	3.87E-10	2.88E-10	2.48E-10	3.13E-10	5.93E-11	18.96643617
	OPI:		9.48	9.41	9.54	9.61	9.50	0.08	0.87
GS-55	k (m/s):		1.51E-10	9.51E-11	1.53E-10	6.70E-11	1.17E-10	4.27E-11	36.58515978
	OPI:		9.82	10.02	9.82	10.17	9.93	0.17	1.75
LS-55	k (m/s):		9.63E-11	9.67E-11	1.00E-10	9.45E-11	9.69E-11	2.33E-12	2.39963602
	OPI:		10.02	10.01	10.00	10.02	10.01	0.01	0.10
PC-65	k (m/s):	0.65 w/b	1.67E-10	1.63E-10	9.51E-11	1.39E-10	1.41E-10	3.29E-11	23.37230187
	OPI:		9.78	9.79	10.02	9.86	9.85	0.11	1.14
FA-65	k (m/s):		3.82E-10	3.16E-10	3.03E-10	1.76E-10	2.94E-10	8.62E-11	29.29606353
	OPI:		9.42	9.50	9.52	9.75	9.53	0.14	1.52
GS-65	k (m/s):		3.08E-10	4.50E-10	2.60E-10	3.82E-10	3.50E-10	8.39E-11	23.9678461
	OPI:		9.51	9.35	9.59	9.42	9.46	0.11	1.11
LS-65	k (m/s):		2.95E-10	3.56E-10	3.29E-10	3.13E-10	3.23E-10	2.59E-11	8.011138922
	OPI:		9.53	9.45	9.48	9.50	9.49	0.03	0.36

*Standard deviation

#coefficient of variation

k- oxygen permeability coefficient

Table C.4 Oxygen permeability index test results – (Curing-D)

Mix Designation	Elements	w/b	Curing-D						
			Specimen-1	Specimen-2	Specimen-3	Specimen-4	**Mean**	**SD***	**COV#**
PC-45	k (m/s):	0.45 w/b	4.08E-11	6.07E-11	8.88E-11	4.67E-11	5.93E-11	2.14E-11	3.61E+01
	OPI:		10.39	10.22	10.05	10.33	**10.23**	0.15	1.45
FA-45	k (m/s):		8.67E-11	8.60E-11	Invalid	1.16E-10	9.62E-11	1.71E-11	1.77E+01
	OPI:		10.06	10.07	Invalid	9.94	**10.02**	0.07	0.74
GS-45	k (m/s):		5.56E-11	7.02E-11	8.92E-11	8.10E-11	7.40E-11	1.45E-11	1.96E+01
	OPI:		10.25	10.15	10.05	10.09	**10.13**	0.09	0.88
LS-45	k (m/s):		9.18E-11	1.09E-10	1.16E-10	8.73E-11	1.01E-10	1.35E-11	1.34E+01
	OPI:		10.04	9.96	9.94	10.06	**10.00**	0.06	0.58
PC-55	k (m/s):	0.55 w/b	6.04E-11	4.57E-11	5.63E-11	7.50E-11	5.93E-11	1.21E-11	2.04E+01
	OPI:		10.22	10.34	10.25	10.12	**10.23**	0.09	0.87
FA-55	k (m/s):		1.27E-10	4.17E-10	1.68E-10	1.28E-10	2.10E-10	1.39E-10	6.62E+01
	OPI:		9.90	9.38	9.78	9.89	**9.68**	0.24	2.52
GS-55	k (m/s):		1.13E-10	8.93E-11	1.52E-10	1.82E-10	1.34E-10	4.10E-11	3.06E+01
	OPI:		9.95	10.05	9.82	9.74	**9.87**	0.14	1.39
LS-55	k (m/s):		1.00E-10	8.80E-11	9.17E-11	1.14E-10	9.85E-11	1.16E-11	1.18E+01
	OPI:		10.00	10.06	10.04	9.94	**10.01**	0.05	0.50
PC-65	k (m/s):	0.65 w/b	1.52E-10	1.36E-10	1.82E-10	1.29E-10	1.50E-10	2.35E-11	1.57E+01
	OPI:		9.82	9.87	9.74	9.89	**9.82**	0.07	0.67
FA-65	k (m/s):		2.53E-10	3.18E-10	4.24E-10	7.25E-10	4.30E-10	2.09E-10	4.85E+01
	OPI:		9.60	9.50	9.37	9.14	**9.37**	0.20	2.10
GS-65	k (m/s):		2.79E-10	2.91E-10	2.56E-10	2.30E-10	2.64E-10	2.69E-11	1.02E+01
	OPI:		9.55	9.54	9.59	9.64	**9.58**	0.05	0.47
LS-65	k (m/s):		1.13E-10	1.61E-10	1.38E-10	1.83E-10	1.48E-10	3.02E-11	2.04E+01
	OPI:		9.95	9.79	9.86	9.74	**9.83**	0.09	0.92

*Standard deviation

#coefficient of variation

k- oxygen permeability coefficient

APPENDIX D: CARBONATION TEST RESULTS

D.1 CARBONATION DEPTH OF SPECIMENS EXPOSED AT SITE CD

Table D.1 Carbonation depth of specimens exposed at site CD (w/b = 0.45)

Curing Regime	Mix Designation	Time (days)	Carbonation Depth (mm)		Time (days)	Carbonation Depth (mm)		Time (days)	Carbonation Depth (mm)		Time (days)	Carbonation Depth (mm)	
			Mean	SD		Mean	SD		Mean	SD		Mean	SD
Curing-A	PC-45	148	0.0	0.0	266	0.0	0.0	570	0.0	0.0	1000	0.0	0.0
	FA-45	148	1.6	0.1	266	2.5	0.4	570	4.4	0.4	1000	5.4	0.5
	GS-45	212	2.8	0.4	508	4.4	0.5	889	5.7	0.8	1000	6.0	0.7
	LS-45	212	0.0	0.0	508	0.0	0.0	889	2.4	0.3	1000	2.6	0.5
Curing-B	PC-45	148	0.5	0.0	266	3.0	0.4	570	5.5	0.7	1000	5.5	0.4
	FA-45	148	3.3	0.4	266	4.7	0.5	570	7.5	0.6	1000	8.8	0.6
	GS-45	212	6.7	1.9	508	12.8	1.3	889	11.0	1.5	1000	13.1	1.5
	LS-45	212	3.8	0.8	508	5.1	0.7	889	7.5	1.3	1000	8.1	0.8
Curing-C	PC-45	148	0.0	0.0	266	2.6	0.2	570	3.4	0.4	1000	4.6	0.5
	FA-45	148	2.2	0.3	266	4.8	0.5	570	6.8	0.7	1000	8.5	1.2
	GS-45	212	4.4	0.6	508	6.2	0.6	889	6.9	0.6	1000	7.5	0.9
	LS-45	212	2.6	0.4	508	3.6	0.5	889	5.8	0.6	1000	7.1	0.4
Curing-D	PC-45	103	0.0	0.0	315	3.4	0.6	611	6.9	0.6	1000	6.5	0.4
	FA-45	103	0.7	0.3	315	6.2	0.8	611	6.3	0.9	1000	9.0	1.5
	GS-45	159	3.9	1.0	277	7.8	1.0	581	7.2	1.4	1000	12.2	1.4
	LS-45	159	3.4	0.7	277	2.3	0.4	581	9.4	0.6	1000	10.5	1.0

Table D.2 Carbonation depth of specimens exposed at site CD (w/b = 0.55)

Curing Regime	Mix Designation	Time (days)	Carbonation Depth (mm)		Time (days)	Carbonation Depth (mm)		Time (days)	Carbonation Depth (mm)		Time (days)	Carbonation Depth (mm)	
			Mean	SD		Mean	SD		Mean	SD		Mean	SD
Curing-A	PC-55	148	0.0	0.0	266	2.2	0.5	570	3.2	0.3	1000	4.4	0.5
	FA-55	148	2.4	0.2	266	4.3	0.5	570	6.6	0.7	1000	9.1	0.7
	GS-55	212	4.7	0.6	508	6.7	0.5	889	8.9	0.9	1000	9.0	0.8
	LS-55	212	3.0	0.6	508	4.4	0.5	889	6.9	0.9	1000	7.2	1.2
Curing-B	PC-55	148	2.2	0.6	266	5.2	0.8	570	7.3	0.7	1000	9.4	0.7
	FA-55	148	4.8	0.5	266	8.9	0.4	570	11.4	0.8	1000	15.0	0.7
	GS-55	212	9.9	1.1	508	14.0	0.6	889	16.2	0.7	1000	16.8	0.9
	LS-55	212	5.6	0.6	508	9.6	0.8	889	11.0	1.2	1000	13.3	1.1
Curing-C	PC-55	148	0.0	0.0	266	4.3	0.7	570	6.3	0.5	1000	7.9	0.4
	FA-55	148	4.2	0.6	266	7.7	0.8	570	9.7	0.6	1000	12.7	0.8
	GS-55	212	5.6	0.4	508	10.0	0.7	889	10.3	0.8	1000	11.1	1.0
	LS-55	212	4.4	0.5	508	6.9	0.5	889	8.5	0.8	1000	9.8	0.5
Curing-D	PC-55	103	0.0	0.0	315	4.3	1.5	611	4.9	0.6	1000	6.1	1.4
	FA-55	103	1.0	0.3	315	8.2	0.9	611	9.8	0.5	1000	12.5	1.0
	GS-55	159	5.3	0.5	277	6.7	0.5	581	8.9	0.8	1000	11.4	0.8
	LS-55	159	3.2	0.6	277	5.3	0.8	581	7.8	0.8	1000	9.3	0.8

Table D.3 Carbonation depth of specimens exposed at site CD (w/b = 0.65)

Curing Regime	Mix Designation	Time (days)	Carbonation Depth (mm)		Time (days)	Carbonation Depth (mm)		Time (days)	Carbonation Depth (mm)		Time (days)	Carbonation Depth (mm)	
			Mean	SD		Mean	SD		Mean	SD		Mean	SD
Curing-A	PC-65	212	4.1	0.4	508	6.0	0.5	889	8.1	0.4	1000	8.6	0.6
	FA-65	212	6.3	0.4	508	9.7	0.9	889	11.8	0.8	1000	12.7	0.7
	GS-65	212	4.7	0.7	508	7.9	0.4	889	10.7	1.0	1000	11.8	0.6
	LS-65	212	4.1	0.8	508	7.3	0.7	889	9.1	0.6	1000	10.4	0.6
Curing-B	PC-65	212	7.4	0.6	508	14.9	0.9	889	13.5	0.9	1000	15.7	1.0
	FA-65	212	10.7	0.6	508	19.2	0.7	889	18.7	1.3	1000	23.4	0.7
	GS-65	212	12.0	2.0	508	15.6	1.1	889	19.1	1.7	1000	20.4	1.3
	LS-65	212	7.5	1.0	508	12.2	1.2	889	12.6	0.5	1000	14.4	1.1
Curing-C	PC-65	212	5.8	0.7	508	8.8	0.6	889	10.7	0.9	1000	11.5	1.2
	FA-65	212	7.6	0.6	508	11.3	1.0	889	14.9	0.9	1000	16.1	1.4
	GS-65	212	9.7	0.6	508	15.7	1.2	889	18.3	1.4	1000	19.4	0.6
	LS-65	212	7.9	0.3	508	10.6	0.5	889	13.8	0.7	1000	14.2	0.9
Curing-D	PC-65	103	1.2	0.3	315	8.3	0.6	611	10.1	0.8	1000	11.7	0.3
	FA-65	103	2.7	0.5	315	12.9	1.1	611	16.4	1.0	1000	19.6	1.1
	GS-65	159	8.9	0.9	277	10.6	1.1	581	13.0	1.0	1000	20.1	1.2
	LS-65	159	4.7	0.4	277	8.6	0.9	581	9.8	0.6	1000	12.9	1.3

D.2 CARBONATION DEPTH OF SPECIMENS EXPOSED AT SITE ME

Table D.4 Carbonation depth of specimens exposed at site ME (w/b = 0.45)

Curing Regime	Mix Designation	Time (days)	Carbonation Depth (mm)		Time (days)	Carbonation Depth (mm)		Time (days)	Carbonation Depth (mm)		Time (days)	Carbonation Depth (mm)	
			Mean	SD		Mean	SD		Mean	SD		Mean	SD
Curing-A	PC-45	125	0.0	0.0	321	0.0	0.0	507	0.0	0.0	1000	0.0	0.0
	FA-45	101	0.5	0.0	297	1.8	0.3	483	2.1	0.4	1000	2.6	0.5
	GS-45	154	0.0	0.0	448	0.5	0.0	885	0.5	0.0	1000	0.5	0.0
	LS-45	137	0.0	0.0	431	0.0	0.0	875	0.5	0.0	1000	0.5	0.0
Curing-B	PC-45	125	1.0	0.1	321	1.8	0.2	507	2.0	0.2	1000	2.6	0.5
	FA-45	101	2.5	0.5	297	3.3	0.3	483	3.8	0.4	1000	4.5	0.5
	GS-45	154	6.4	0.6	448	5.7	0.7	885	7.5	0.6	1000	6.8	0.6
	LS-45	137	1.3	0.2	431	2.2	0.3	875	2.7	0.6	1000	2.3	0.3
Curing-C	PC-45	125	0.5	0.0	321	0.5	0.0	507	0.5	0.0	1000	0.5	0.0
	FA-45	101	3.0	0.5	297	2.7	0.3	483	3.4	0.3	1000	4.2	1.2
	GS-45	154	2.6	0.7	448	2.7	0.6	885	3.0	0.5	1000	3.1	0.4
	LS-45	137	0.9	0.2	431	1.8	0.3	875	2.4	0.5	1000	2.1	0.3
Curing-D	PC-45	158	2.3	0.3	354	2.7	0.4	540	3.0	0.4	1000	3.1	0.5
	FA-45	158	4.3	0.5	354	3.8	0.4	540	4.7	0.7	1000	4.2	0.5
	GS-45	125	2.7	0.6	321	3.2	0.5	507	3.0	0.6	1000	3.7	0.6
	LS-45	125	3.1	0.5	321	2.9	0.7	507	3.6	0.6	1000	3.2	0.7

Table D.5 Carbonation depth of specimens exposed at site ME (w/b = 0.55)

Curing Regime	Mix Designation	Time (days)	Carbonation Depth (mm)		Time (days)	Carbonation Depth (mm)		Time (days)	Carbonation Depth (mm)		Time (days)	Carbonation Depth (mm)	
			Mean	SD		Mean	SD		Mean	SD		Mean	SD
Curing-A	PC-55	101	0.0	0.0	297	0.5	0.0	483	0.5	0.0	1000	1.4	0.4
	FA-55	90	1.6	0.3	290	2.9	0.3	472	3.8	0.4	1000	4.7	0.8
	GS-55	154	1.6	0.4	448	2.3	0.6	885	3.8	0.5	1000	4.4	0.7
	LS-55	137	1.1	0.2	431	1.5	0.3	875	2.6	0.5	1000	2.7	0.7
Curing-B	PC-55	101	2.4	0.3	297	2.8	0.5	483	3.4	0.5	1000	3.8	0.4
	FA-55	90	3.9	0.4	290	5.9	0.4	472	6.0	0.7	1000	6.7	0.8
	GS-55	154	6.9	0.6	448	7.0	0.6	885	9.8	1.0	1000	8.5	0.8
	LS-55	137	4.3	0.6	431	3.5	0.5	875	5.2	0.6	1000	3.9	0.6
Curing-C	PC-55	101	1.8	0.5	297	2.1	0.2	483	2.6	0.3	1000	3.0	0.4
	FA-55	90	3.5	0.4	290	4.6	0.4	472	4.9	0.4	1000	6.3	0.5
	GS-55	154	3.0	0.2	448	4.8	0.8	885	5.2	0.4	1000	5.6	1.0
	LS-55	137	2.2	0.3	431	2.3	0.5	875	3.1	0.4	1000	2.7	0.3
Curing-D	PC-55	158	1.9	0.2	354	3.2	0.3	540	2.4	1.0	1000	3.9	0.5
	FA-55	158	3.9	0.3	354	5.5	0.5	540	5.6	0.5	1000	6.5	1.1
	GS-55	125	4.3	0.5	321	5.2	0.6	507	5.2	0.5	1000	7.3	0.7
	LS-55	125	3.4	0.8	321	3.4	0.7	507	4.0	0.6	1000	4.3	0.8

Table D.6 Carbonation depth of specimens exposed at site ME (w/b = 0.65)

Curing Regime	Mix Designation	Time (days)	Carbonation Depth (mm)		Time (days)	Carbonation Depth (mm)		Time (days)	Carbonation Depth (mm)		Time (days)	Carbonation Depth (mm)	
			Mean	SD		Mean	SD		Mean	SD		Mean	SD
Curing-A	PC-65	154	1.5	0.3	448	1.8	0.3	885	3.1	0.6	1000	2.5	0.7
	FA-65	154	2.9	0.9	448	4.6	0.8	885	7.9	0.8	1000	8.2	0.9
	GS-65	137	3.0	0.4	431	4.3	1.1	875	6.3	0.7	1000	7.0	0.7
	LS-65	137	2.0	0.3	431	2.6	0.7	875	5.6	0.9	1000	5.2	0.9
Curing-B	PC-65	154	5.0	0.7	448	4.3	0.5	885	5.5	0.6	1000	5.5	0.7
	FA-65	154	6.4	0.7	448	7.8	0.9	885	9.8	0.9	1000	11.2	1.2
	GS-65	137	8.0	1.1	431	9.1	0.5	875	11.2	0.7	1000	11.6	0.9
	LS-65	137	3.6	0.5	431	5.5	0.5	875	6.1	1.9	1000	7.3	0.6
Curing-C	PC-65	154	2.3	0.4	448	2.7	0.4	885	3.8	0.5	1000	4.3	0.7
	FA-65	154	5.1	0.6	448	6.4	0.7	885	8.3	1.3	1000	8.6	0.8
	GS-65	137	6.0	0.6	431	7.4	0.7	875	10.2	1.3	1000	9.8	0.6
	LS-65	137	3.6	0.7	431	5.0	0.7	875	4.7	1.0	1000	6.5	1.0
Curing-D	PC-65	158	4.3	0.3	354	4.4	0.3	540	4.8	0.3	1000	5.3	0.7
	FA-65	158	7.0	1.0	354	7.6	0.7	540	8.4	1.0	1000	10.8	0.7
	GS-65	125	5.9	0.5	321	8.1	1.2	507	8.1	0.9	1000	10.9	0.9
	LS-65	125	3.7	0.6	321	4.3	0.5	507	5.1	0.4	1000	6.0	0.7

D.3 CARBONATION DEPTH OF SPECIMENS EXPOSED AT SITE MS

Table D.7 Carbonation depth of specimens exposed at site MS (w/b = 0.45)

Curing Regime	Mix Designation	Time (days)	Carbonation Depth (mm)		Time (days)	Carbonation Depth (mm)		Time (days)	Carbonation Depth (mm)		Time (days)	Carbonation Depth (mm)	
			Mean	SD		Mean	SD		Mean	SD		Mean	SD
Curing-A	PC-45	139	0.0	0.0	321	0.0	0.0	517	0.0	0.0	1000	0.0	0.0
	FA-45	115	1.5	0.4	297	2.3	0.4	493	3.2	0.3	1000	4.6	0.7
	GS-45	172	2.0	0.5	343	2.1	0.2	458	2.3	0.4	1000	3.9	0.6
	LS-45	155	0.0	0.0	326	0.0	0.0	441	0.5	0.0	1000	0.5	0.0
Curing-B	PC-45	139	1.2	0.2	321	2.6	0.3	517	2.6	0.4	1000	3.6	0.3
	FA-45	115	3.8	0.5	297	4.5	0.6	493	5.3	0.7	1000	7.6	1.4
	GS-45	172	5.3	1.2	343	5.9	1.4	458	6.9	1.7	1000	9.5	1.6
	LS-45	155	2.8	0.7	326	3.5	0.7	441	3.7	0.7	1000	5.2	1.0
Curing-C	PC-45	139	1.2	0.3	321	1.6	0.3	517	1.7	0.2	1000	3.1	0.4
	FA-45	115	2.3	0.2	297	4.0	0.5	493	4.7	0.5	1000	7.0	0.6
	GS-45	172	3.1	0.6	343	3.6	0.5	458	4.1	0.7	1000	6.2	0.8
	LS-45	155	2.5	0.5	326	2.9	0.4	441	2.9	0.4	1000	4.4	0.8
Curing-D	PC-45	172	2.2	0.8	354	3.9	0.6	550	3.2	0.9	1000	6.2	0.7
	FA-45	172	3.5	0.4	354	5.0	0.7	550	5.9	0.4	1000	8.6	0.9
	GS-45	139	5.3	1.2	321	4.9	1.7	517	7.9	1.4	1000	8.5	1.1
	LS-45	139	2.9	0.7	321	6.1	0.7	517	5.2	0.6	1000	7.7	1.0

Table D.8 Carbonation depth of specimens exposed at site MS (w/b = 0.55)

Curing Regime	Mix Designation	Time (days)	Carbonation Depth (mm)		Time (days)	Carbonation Depth (mm)		Time (days)	Carbonation Depth (mm)		Time (days)	Carbonation Depth (mm)	
			Mean	SD		Mean	SD		Mean	SD		Mean	SD
Curing-A	PC-55	115	0.5	0.0	297	1.5	0.2	493	2.0	0.2	1000	3.3	0.5
	FA-55	104	1.8	0.2	286	3.0	0.2	482	4.5	0.5	1000	6.9	0.7
	GS-55	172	2.9	0.4	343	3.4	0.4	458	4.6	0.7	1000	7.2	0.7
	LS-55	155	2.5	0.4	326	3.3	0.4	441	3.5	0.7	1000	5.7	0.6
Curing-B	PC-55	115	2.8	0.3	297	4.3	0.8	493	4.9	0.5	1000	6.5	0.6
	FA-55	104	5.3	0.5	286	7.1	1.1	482	8.1	0.7	1000	11.4	0.4
	GS-55	172	6.9	0.6	343	8.7	0.9	458	9.5	0.9	1000	12.2	1.4
	LS-55	155	6.7	0.5	326	7.1	0.5	441	8.5	0.7	1000	11.2	0.7
Curing-C	PC-55	115	2.1	0.3	297	3.3	0.5	493	3.4	0.3	1000	6.5	0.6
	FA-55	104	4.2	0.7	286	6.2	0.8	482	7.6	0.8	1000	10.4	1.1
	GS-55	172	4.6	0.5	343	5.5	0.5	458	6.2	0.6	1000	9.3	0.6
	LS-55	155	3.1	0.5	326	4.2	0.4	441	4.5	0.5	1000	7.5	0.7
Curing-D	PC-55	172	4.1	0.6	354	4.7	0.5	550	5.8	0.5	1000	6.6	0.8
	FA-55	172	6.4	0.3	354	7.6	1.1	550	9.3	0.6	1000	11.0	0.4
	GS-55	139	5.1	0.6	321	6.9	0.7	517	8.1	1.0	1000	11.0	1.2
	LS-55	139	3.5	1.0	321	4.5	1.2	517	5.7	1.1	1000	8.1	1.8

Table D.9 Carbonation depth of specimens exposed at site MS (w/b = 0.65)

Curing Regime	Mix Designation	Time (days)	Carbonation Depth (mm)		Time (days)	Carbonation Depth (mm)		Time (days)	Carbonation Depth (mm)		Time (days)	Carbonation Depth (mm)	
			Mean	SD		Mean	SD		Mean	SD		Mean	SD
Curing-A	PC-65	172	2.6	0.4	343	2.8	0.5	458	4.3	0.5	1000	6.7	0.6
	FA-65	172	5.4	0.5	343	6.3	0.6	458	7.8	0.3	1000	12.0	0.8
	GS-65	155	4.1	0.6	326	5.1	0.6	441	6.3	0.6	1000	10.1	0.7
	LS-65	155	3.8	0.5	326	4.5	1.1	441	5.6	0.6	1000	8.4	1.0
Curing-B	PC-65	172	6.5	0.7	343	7.0	0.7	458	7.4	0.9	1000	12.2	1.0
	FA-65	172	9.6	0.4	343	11.1	0.6	458	12.7	0.5	1000	18.6	1.2
	GS-65	155	9.5	1.2	326	13.4	0.6	441	12.7	0.6	1000	18.4	1.3
	LS-65	155	6.6	0.4	326	7.4	0.4	441	8.7	0.5	1000	11.8	0.9
Curing-C	PC-65	172	4.5	0.8	343	5.6	0.4	458	6.6	0.6	1000	10.0	0.7
	FA-65	172	6.6	0.8	343	9.4	0.7	458	9.9	0.6	1000	13.9	0.7
	GS-65	155	7.5	1.0	326	9.1	0.6	441	10.8	0.9	1000	13.9	1.1
	LS-65	155	5.8	0.5	326	6.7	0.6	441	7.3	0.6	1000	10.5	0.7
Curing-D	PC-65	172	4.8	0.5	354	6.5	0.4	550	7.8	0.9	1000	9.9	0.6
	FA-65	172	7.9	0.7	354	10.9	0.7	550	12.8	0.9	1000	17.1	0.8
	GS-65	139	5.9	1.0	321	7.6	0.9	517	8.4	0.9	1000	11.1	0.9
	LS-65	139	4.2	0.6	321	6.0	1.4	517	7.7	0.6	1000	10.4	1.3

D.4 CARBONATION DEPTH OF SPECIMENS EXPOSED AT SITE WE

Table D.10 Carbonation depth of specimens exposed at site WE (w/b = 0.45)

Curing Regime	Mix Designation	Time (days)	Carbonation Depth (mm)		Time (days)	Carbonation Depth (mm)		Time (days)	Carbonation Depth (mm)		Time (days)	Carbonation Depth (mm)	
			Mean	SD		Mean	SD		Mean	SD		Mean	SD
Curing-A	PC-45	91	0.0	0.0	232	0.0	0.0	637	0.0	0.0	1000	0.0	0.0
	FA-45	91	0.0	0.0	232	1.4	0.3	637	1.5	0.0	1000	2.7	0.5
	GS-45	76	0.0	0.0	217	0.0	0.0	622	0.5	0.0	1000	0.0	0.0
	LS-45	76	0.0	0.0	217	0.0	0.0	622	0.0	0.0	1000	0.5	0.0
Curing-B	PC-45	91	0.5	0.0	232	0.5	0.0	637	1.0	0.0	1000	2.6	0.4
	FA-45	91	2.2	0.5	232	2.9	0.4	637	4.0	0.5	1000	4.3	0.4
	GS-45	76	2.9	0.5	217	2.9	0.6	622	3.6	0.4	1000	4.7	0.5
	LS-45	76	1.1	0.3	217	1.8	0.3	622	2.9	0.5	1000	3.3	0.4
Curing-C	PC-45	91	0.0	0.0	232	0.5	0.0	637	0.5	0.0	1000	0.0	0.0
	FA-45	91	0.9	0.1	232	2.5	0.4	637	2.9	0.5	1000	3.4	0.4
	GS-45	76	1.6	0.4	217	2.1	0.3	622	2.6	0.5	1000	4.1	0.4
	LS-45												
Curing-D	PC-45	92	0.0	0.0	283	0.5	0.0	688	1.5	0.0	1000	2.3	0.4
	FA-45	92	1.2	0.3	283	3.1	0.4	688	3.7	0.4	1000	4.3	0.6
	GS-45	112	4.0	0.5	253	4.6	0.4	658	5.2	0.4	1000	5.9	0.7
	LS-45	112	2.1	0.5	253	2.7	0.5	658	2.9	0.4	1000	3.3	0.3

Table D.11 Carbonation depth of specimens exposed at site WE (w/b = 0.55)

Curing Regime	Mix Designation	Time (days)	Carbonation Depth (mm)		Time (days)	Carbonation Depth (mm)		Time (days)	Carbonation Depth (mm)		Time (days)	Carbonation Depth (mm)	
			Mean	SD		Mean	SD		Mean	SD		Mean	SD
Curing-A	PC-55	91	0.0	0.0	232	0.5	0.0	637	1.8	0.5	1000	0.0	0.0
	FA-55	91	1.7	0.3	232	2.6	0.4	637	4.1	0.4	1000	5.6	0.7
	GS-55	76	1.4	0.4	217	2.2	0.4	622	3.8	0.4	1000	4.2	0.5
	LS-55	76	0.0	0.0	217	1.4	0.2	622	2.2	0.3	1000	4.5	0.4
Curing-B	PC-55	91	1.4	0.3	232	1.7	0.3	637	3.4	0.3	1000	3.6	0.6
	FA-55	91	4.2	0.5	232	5.0	0.2	637	7.4	0.5	1000	8.1	0.7
	GS-55	76	4.6	0.6	217	6.4	0.6	622	7.7	0.7	1000	9.6	0.4
	LS-55	76	2.3	0.6	217	2.8	0.8	622	5.1	0.5	1000	5.2	0.5
Curing-C	PC-55	91	0.9	0.1	232	1.3	0.2	637	2.4	0.4	1000	4.0	0.4
	FA-55	91	2.6	0.3	232	3.3	0.6	637	5.1	0.7	1000	6.9	0.9
	GS-55	76	2.2	0.4	217	5.2	0.7	622	7.0	0.5	1000	8.8	0.6
	LS-55	76	1.4	0.3	217	2.0	0.2	622	2.8	0.2	1000	3.7	0.6
Curing-D	PC-55	92	0.9	0.1	283	2.0	0.5	688	2.3	0.4	1000	3.7	0.5
	FA-55	92	2.5	0.3	283	4.7	0.5	688	5.3	0.5	1000	7.7	0.8
	GS-55	112	3.7	0.6	253	3.5	0.5	658	6.2	0.6	1000	6.7	0.9
	LS-55	112	2.6	0.6	253	2.7	0.5	658	4.8	0.6	1000	4.8	0.8

Table D.12 Carbonation depth of specimens exposed at site WE (w/b = 0.65)

Curing Regime	Mix Designation	Time (days)	Carbonation Depth (mm)		Time (days)	Carbonation Depth (mm)		Time (days)	Carbonation Depth (mm)		Time (days)	Carbonation Depth (mm)	
			Mean	SD		Mean	SD		Mean	SD		Mean	SD
Curing-A	PC-65	91	1.0	0.3	232	1.6	0.4	637	3.2	0.4	1000	4.2	0.6
	FA-65	91	2.2	0.3	232	3.7	0.6	637	6.2	1.1	1000	9.6	1.0
	GS-65	76	2.1	0.4	217	3.5	0.4	622	6.0	0.6	1000	8.0	0.9
	LS-65	76	1.6	0.4	217	3.5	0.4	622	5.7	0.7	1000	6.7	0.7
Curing-B	PC-65	91	2.6	0.2	232	3.3	0.3	637	5.4	0.5	1000	6.4	0.7
	FA-65	91	4.6	0.3	232	8.2	1.0	637	8.9	0.7	1000	11.1	0.9
	GS-65	76	4.3	1.1	217	7.5	0.8	622	9.4	0.8	1000	12.7	0.7
	LS-65	76	3.1	0.4	217	4.1	0.7	622	6.4	0.7	1000	8.1	0.7
Curing-C	PC-65	91	2.0	0.5	232	3.2	0.4	637	5.2	0.7	1000	6.0	0.8
	FA-65	91	4.3	0.6	232	5.5	0.5	637	8.1	0.5	1000	10.1	0.6
	GS-65	76	4.1	0.7	217	6.1	0.7	622	9.6	0.6	1000	11.4	0.6
	LS-65	76	3.3	0.3	217	4.5	0.4	622	6.9	0.5	1000	9.5	0.5
Curing-D	PC-65	92	2.1	0.4	283	4.1	0.6	688	4.9	0.4	1000	5.7	0.5
	FA-65	92	3.6	0.5	283	7.2	0.6	688	9.4	0.6	1000	10.3	0.9
	GS-65	112	5.4	0.9	253	5.7	0.6	658	8.8	1.1	1000	9.5	0.8
	LS-65	112	3.8	0.4	253	4.7	0.6	658	6.6	0.6	1000	8.6	0.6

D.5 CARBONATION DEPTH OF SPECIMENS EXPOSED AT SITE WS

Table D.13 Carbonation depth of specimens exposed at site WS (w/b = 0.45)

Curing Regime	Mix Designation	Time (days)	Carbonation Depth (mm)		Time (days)	Carbonation Depth (mm)		Time (days)	Carbonation Depth (mm)		Time (days)	Carbonation Depth (mm)	
			Mean	SD		Mean	SD		Mean	SD		Mean	SD
Curing-A	PC-45	91	0.0	0.0	232	0.0	0.0	637	0.0	0.0	1000	0.0	0.0
	FA-45	91	0.0	0.0	232	1.5	0.3	637	2.9	0.3	1000	3.4	0.5
	GS-45	76	0.0	0.0	217	0.0	0.0	622	1.0	0.0	1000	2.1	0.5
	LS-45	76	0.0	0.0	217	0.0	0.0	622	0.0	0.0	1000	2.0	0.2
Curing-B	PC-45	91	1.0	0.2	232	1.8	0.5	637	3.1	0.4	1000	3.5	0.5
	FA-45	91	2.3	0.4	232	3.8	0.5	637	5.7	0.7	1000	8.7	0.8
	GS-45	76	2.6	0.4	217	4.8	0.4	622	6.3	0.7	1000	8.1	1.2
	LS-45	76	2.2	0.4	217	2.0	0.4	622	3.7	0.5	1000	4.0	0.5
Curing-C	PC-45	91	0.0	0.0	232	0.0	0.0	637	0.5	0.0	1000	0.5	0.0
	FA-45	91	1.8	0.4	232	2.8	0.4	637	4.3	0.4	1000	5.8	1.3
	GS-45	76	1.3	0.3	217	3.5	2.4	622	4.2	0.3	1000	5.4	0.9
	LS-45	76	0.0	0.0	217	1.7	0.6	622	2.6	0.5	1000	4.0	0.5
Curing-D	PC-45	92	0.8	0.2	283	2.5	0.8	688	2.8	0.5	1000	3.7	0.5
	FA-45	92	1.8	0.4	283	4.0	0.4	688	5.4	0.5	1000	5.8	0.6
	GS-45	112	2.6	0.6	253	2.8	0.4	658	5.0	0.6	1000	5.4	0.8
	LS-45	112	2.1	0.5	253	2.6	0.5	658	4.0	0.7	1000	5.1	0.5

Table D.14 Carbonation depth of specimens exposed at site WS (w/b = 0.55)

Curing Regime	Mix Designation	Time (days)	Carbonation Depth (mm)		Time (days)	Carbonation Depth (mm)		Time (days)	Carbonation Depth (mm)		Time (days)	Carbonation Depth (mm)	
			Mean	SD		Mean	SD		Mean	SD		Mean	SD
Curing-A	PC-55	91	0.0	0.0	232	0.0	0.0	637	0.5	0.0	1000	0.0	0.0
	FA-55	91	1.8	0.4	232	2.6	0.3	637	5.2	0.7	1000	7.6	0.5
	GS-55	76	1.4	0.3	217	2.7	0.4	622	5.5	0.6	1000	7.2	0.7
	LS-55	76	0.0	0.0	217	1.5	0.2	622	2.9	0.4	1000	3.7	0.5
Curing-B	PC-55	91	2.2	0.5	232	3.1	0.3	637	5.0	0.8	1000	6.4	0.8
	FA-55	91	3.6	0.5	232	6.6	0.6	637	7.6	0.8	1000	11.0	1.4
	GS-55	76	4.7	1.0	217	7.0	0.9	622	9.1	1.5	1000	12.8	1.1
	LS-55	76	2.3	0.7	217	3.7	1.0	622	5.8	1.1	1000	7.1	1.0
Curing-C	PC-55	91	0.9	0.4	232	2.6	0.5	637	3.2	0.4	1000	4.6	0.8
	FA-55	91	3.0	0.5	232	4.5	0.4	637	7.2	0.8	1000	9.7	0.8
	GS-55	76	3.2	0.6	217	4.8	0.7	622	7.9	0.6	1000	11.1	0.7
	LS-55	76	1.4	0.3	217	2.6	0.3	622	4.6	0.5	1000	7.0	0.6
Curing-D	PC-55	92	1.0	0.2	283	2.8	0.5	688	3.3	0.5	1000	4.4	0.7
	FA-55	92	2.8	0.3	283	7.3	0.9	688	7.6	1.2	1000	9.4	1.1
	GS-55	112	2.8	0.5	253	4.5	0.5	658	6.3	0.8	1000	8.3	0.9
	LS-55	112	1.7	0.5	253	2.7	0.6	658	4.7	0.4	1000	6.5	0.8

Table D.15 Carbonation depth of specimens exposed at site WS (w/b = 0.65)

Curing Regime	Mix Designation	Time (days)	Carbonation Depth (mm)		Time (days)	Carbonation Depth (mm)		Time (days)	Carbonation Depth (mm)		Time (days)	Carbonation Depth (mm)	
			Mean	SD		Mean	SD		Mean	SD		Mean	SD
Curing-A	PC-65	91	0.0	0.0	232	2.1	0.4	637	4.7	0.8	1000	6.7	0.7
	FA-65	91	2.8	0.3	232	4.1	0.8	637	8.1	0.8	1000	10.2	0.5
	GS-65	76	2.3	0.5	217	4.5	0.7	622	7.1	0.9	1000	9.6	0.9
	LS-65	76	1.9	0.4	217	3.7	0.5	622	6.9	0.7	1000	9.2	1.0
Curing-B	PC-65	91	4.4	1.4	232	4.8	0.5	637	7.3	1.1	1000	9.1	1.0
	FA-65	91	4.9	0.5	232	6.4	0.6	637	10.7	1.0	1000	12.8	0.8
	GS-65	76	4.7	0.9	217	7.0	0.6	622	9.3	1.0	1000	15.0	1.1
	LS-65	76	3.9	0.5	217	3.1	0.5	622	8.0	0.8	1000	10.9	1.1
Curing-C	PC-65	91	3.0	0.4	232	3.7	0.4	637	6.4	0.8	1000	7.6	0.7
	FA-65	91	4.2	0.6	232	5.6	0.5	637	9.4	0.5	1000	11.9	0.5
	GS-65	76	4.2	0.6	217	6.4	0.3	622	11.3	0.5	1000	14.2	0.7
	LS-65	76	2.2	0.4	217	3.9	0.4	622	6.7	0.5	1000	10.4	0.9
Curing-D	PC-65	92	2.2	0.4	283	4.3	0.6	688	6.0	0.8	1000	6.5	0.5
	FA-65	92	3.4	0.7	283	6.9	0.7	688	8.6	0.9	1000	10.4	1.0
	GS-65	112	7.6	1.1	253	7.7	0.5	658	12.3	1.0	1000	14.2	0.9
	LS-65	112	2.3	0.6	253	4.7	0.6	658	7.4	0.8	1000	10.7	1.0

D.6 PROGRESSION OF CARBONATION DEPTH WITH TIME AT SITE CD

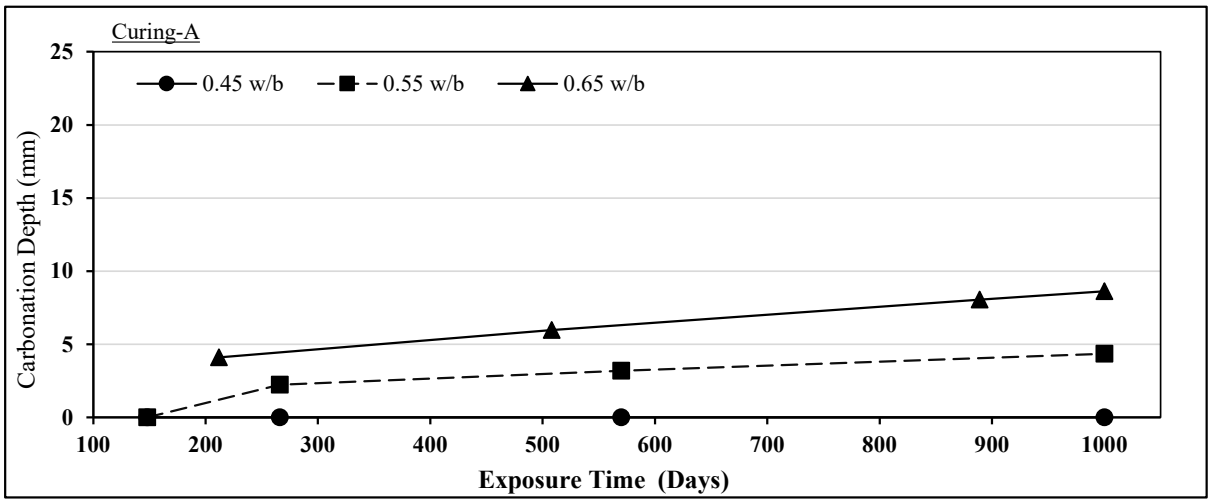

Figure D.1 Carbonation depth of PC concrete specimens exposed at site CD (Curing-A)

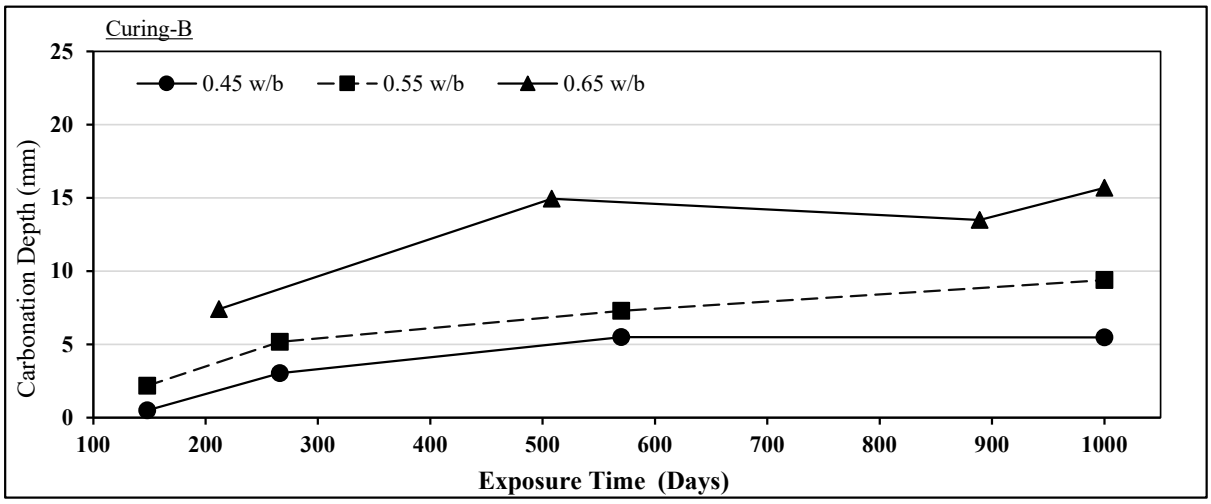

Figure D.2 Carbonation depth of PC concrete specimens exposed at site CD (Curing-B)

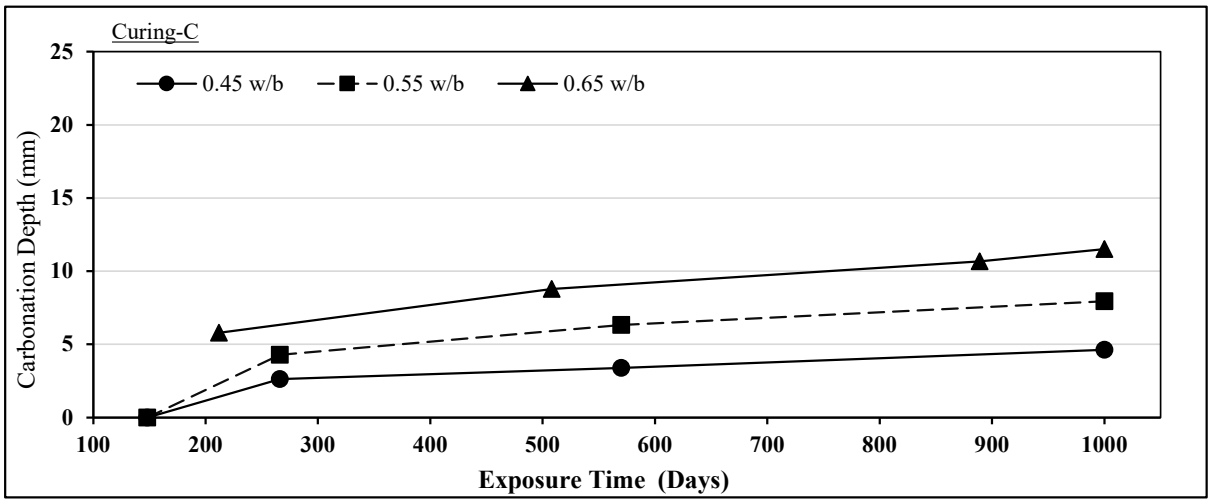

Figure D.3 Carbonation depth of PC concrete specimens exposed at site CD (Curing-C)

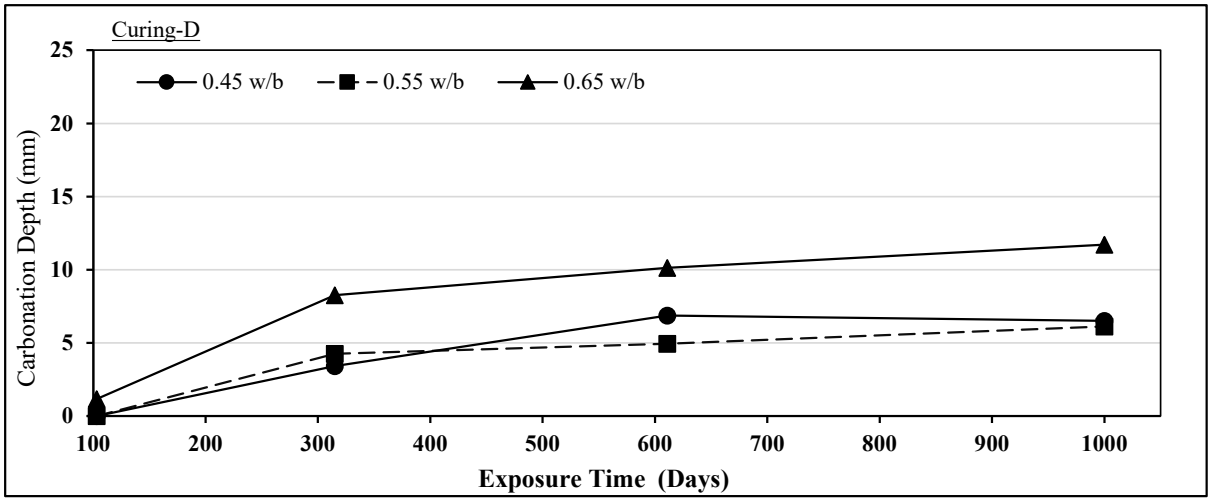

Figure D.4 Carbonation depth of PC concrete specimens exposed at site CD (Curing-D)

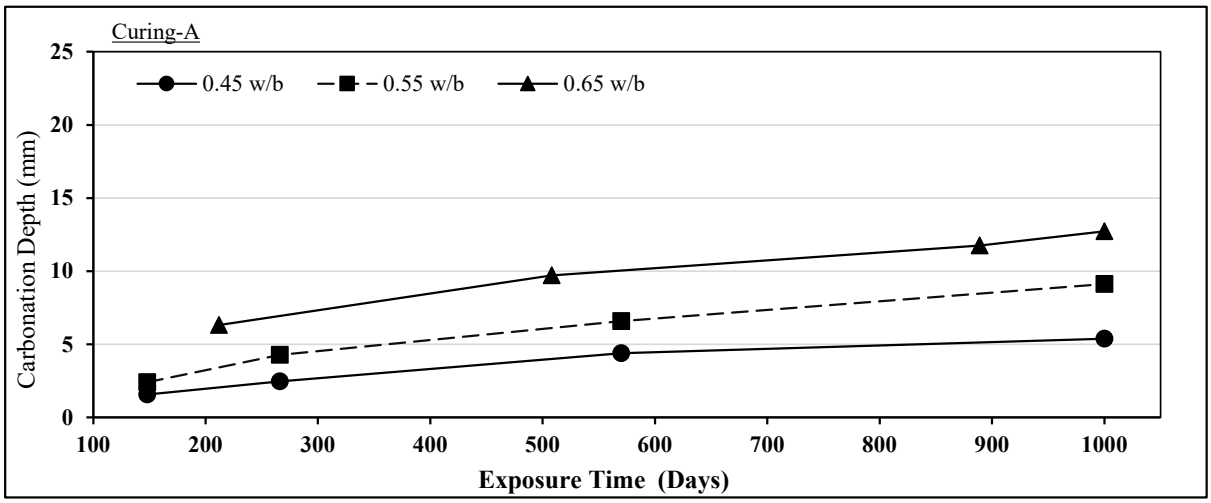

Figure D.5 Carbonation depth of FA concrete specimens exposed at site CD (Curing-A)

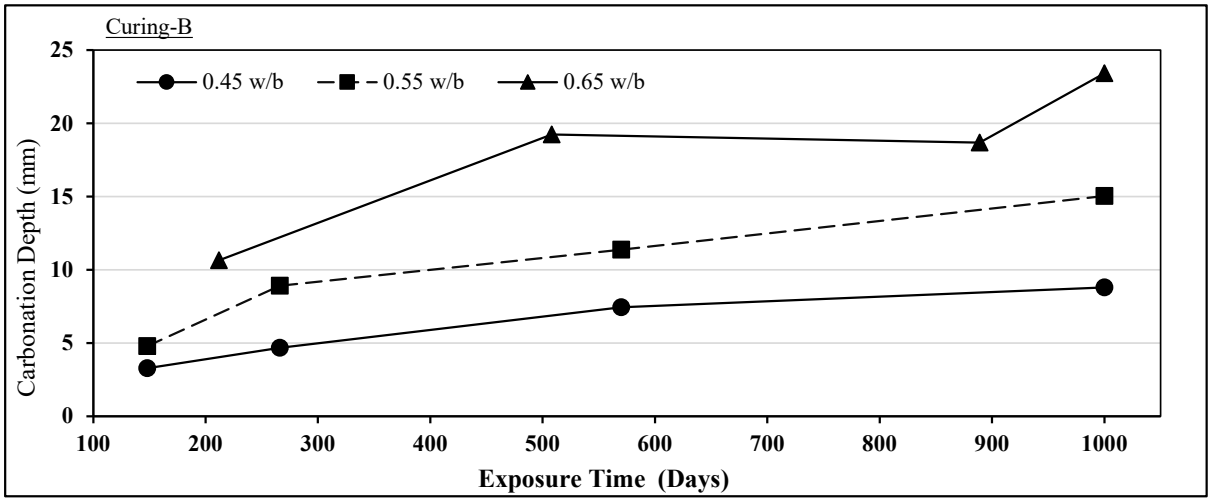

Figure D.6 Carbonation depth of FA concrete specimens exposed at site CD (Curing-B)

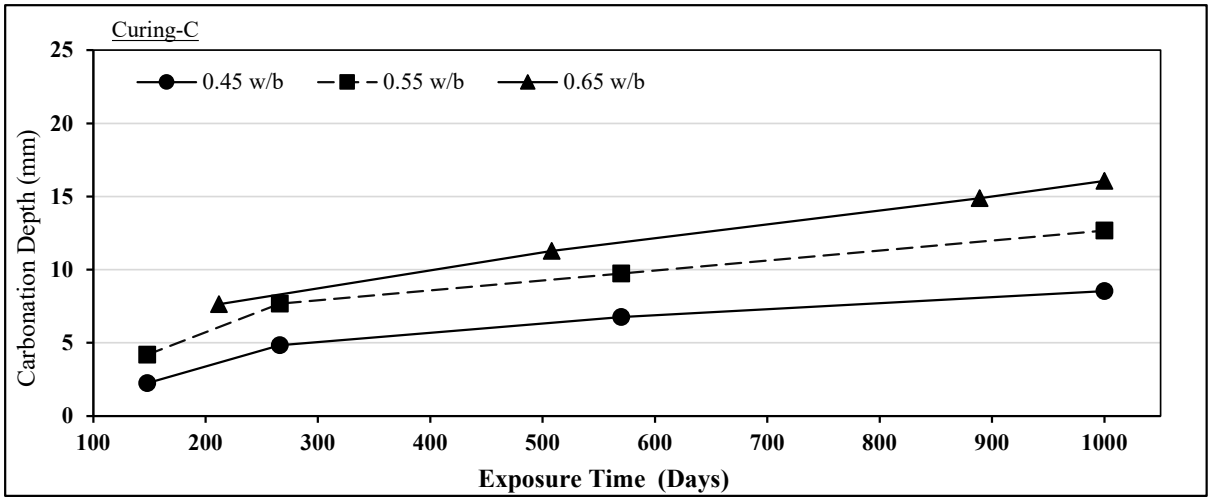

Figure D.7 Carbonation depth of FA concrete specimens exposed at site CD (Curing-C)

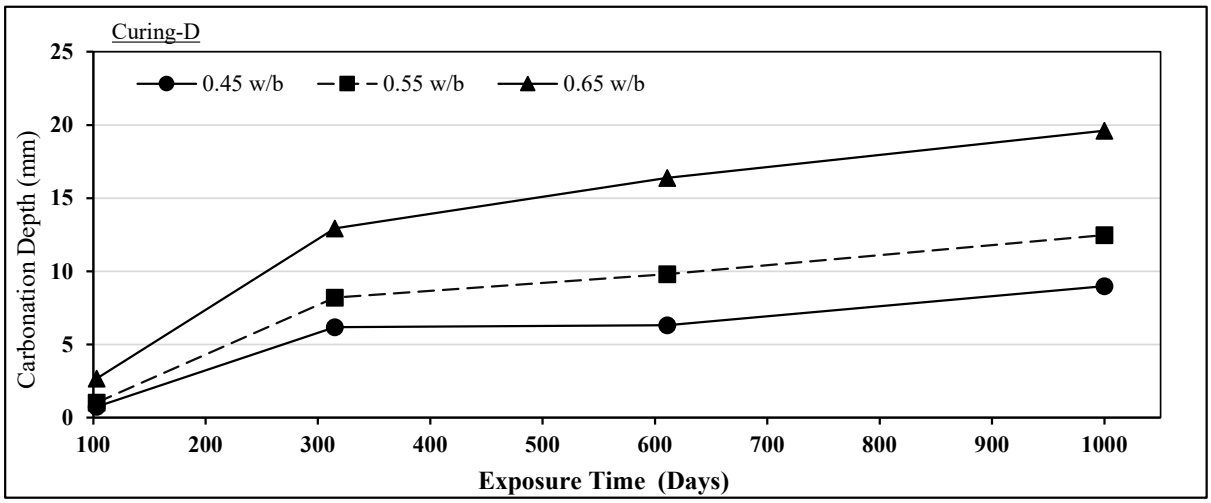

Figure D.8 Carbonation depth of FA concrete specimens exposed at site CD (Curing-D)

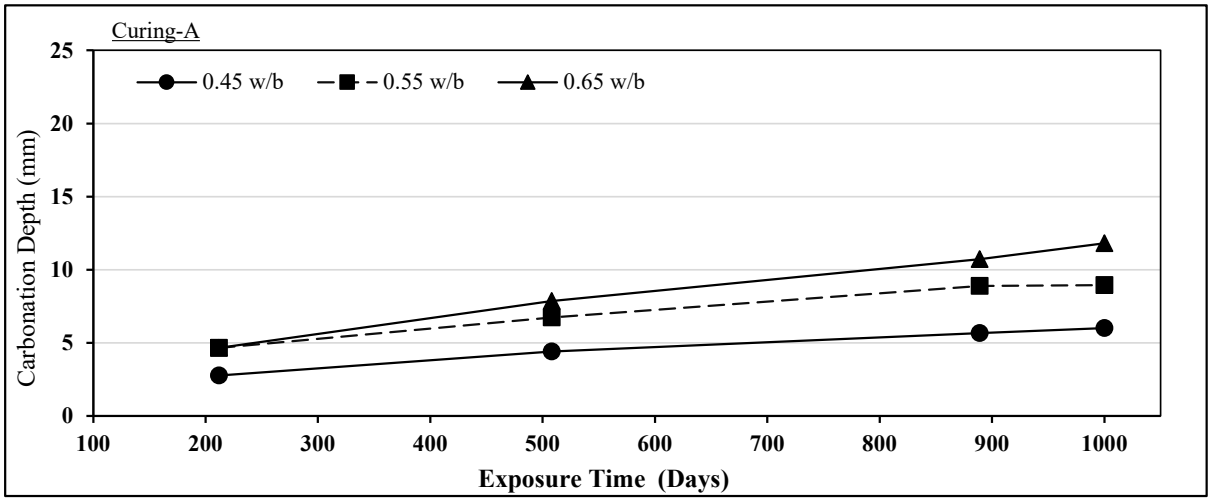

Figure D.9 Carbonation depth of GS concrete specimens exposed at site CD (Curing-A)

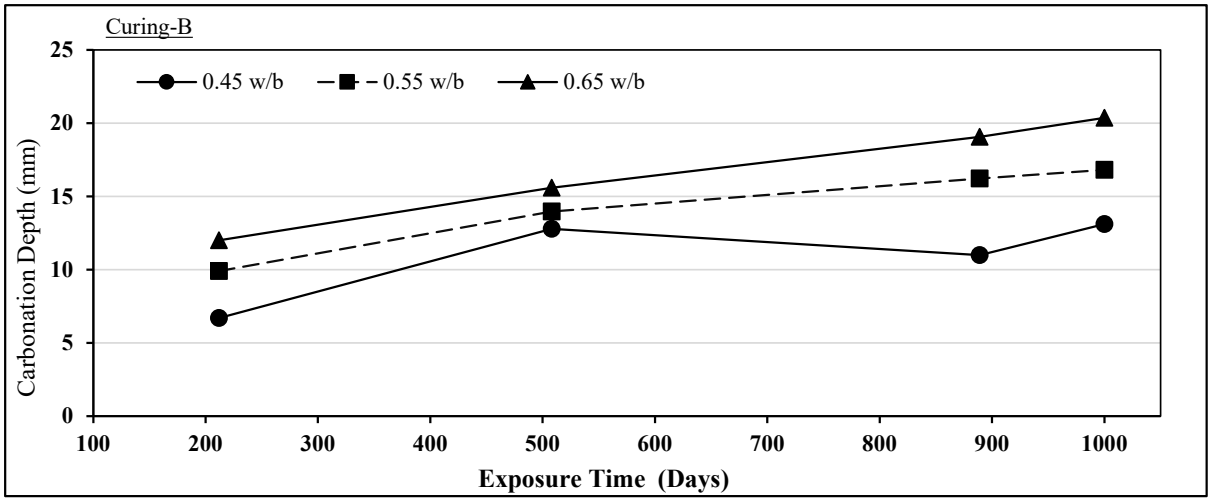

Figure D.10 Carbonation depth of GS concrete specimens exposed at site CD (Curing-B)

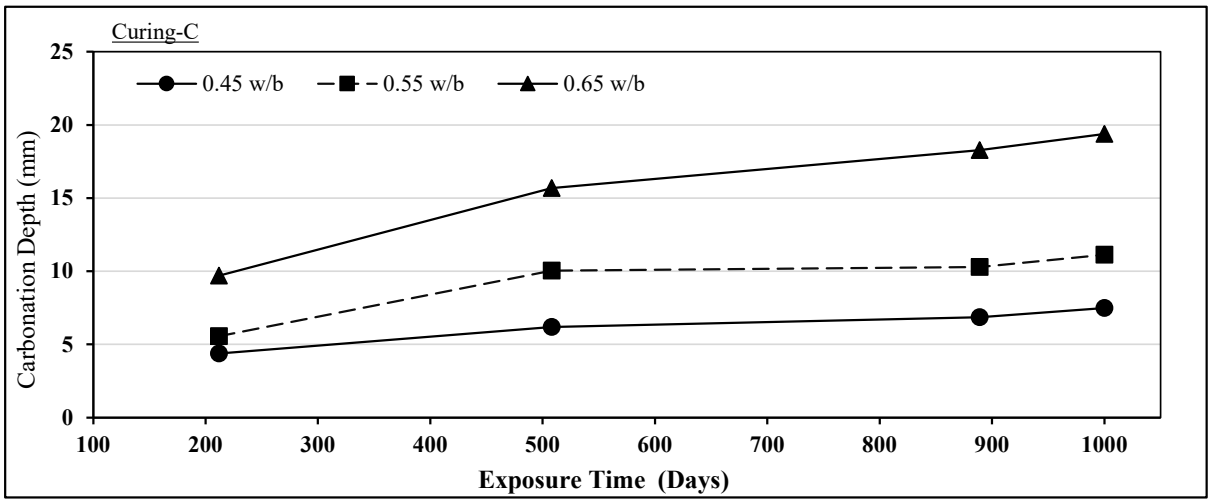

Figure D.11 Carbonation depth of GS concrete specimens exposed at site CD (Curing-C)

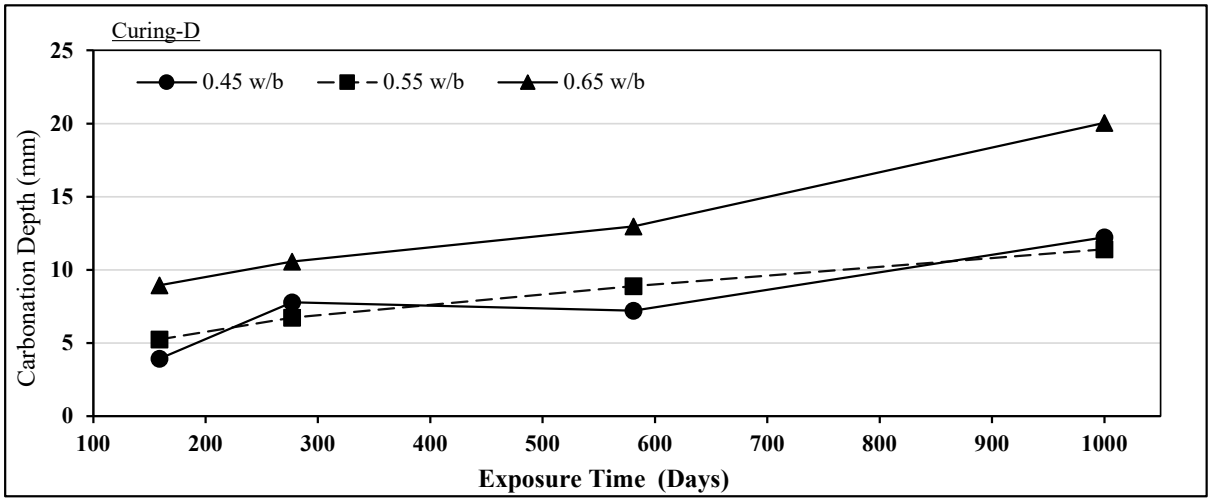

Figure D.12 Carbonation depth of GS concrete specimens exposed at site CD (Curing-D)

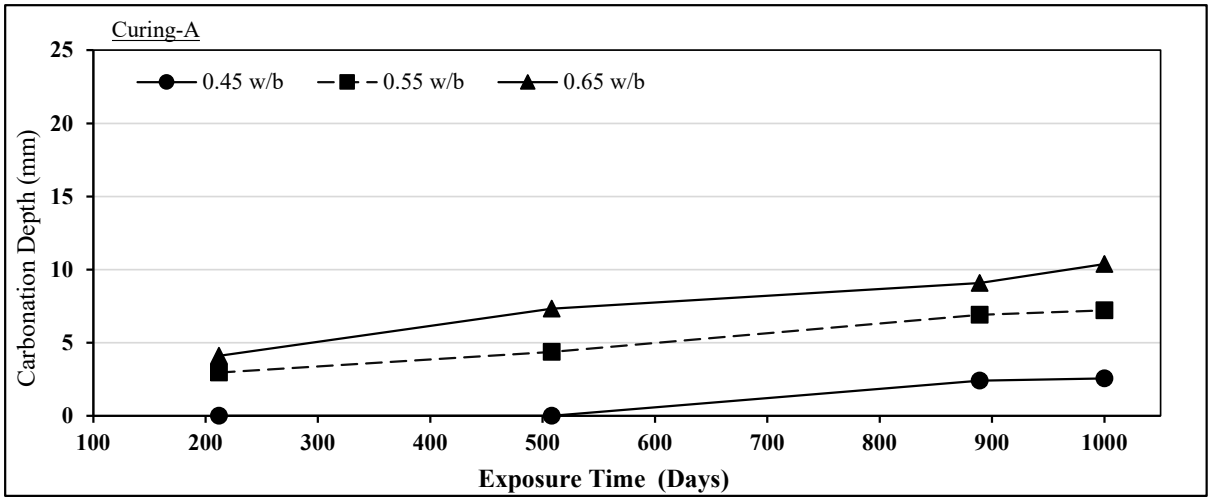

Figure D.13 Carbonation depth of LS concrete specimens exposed at site CD (Curing-A)

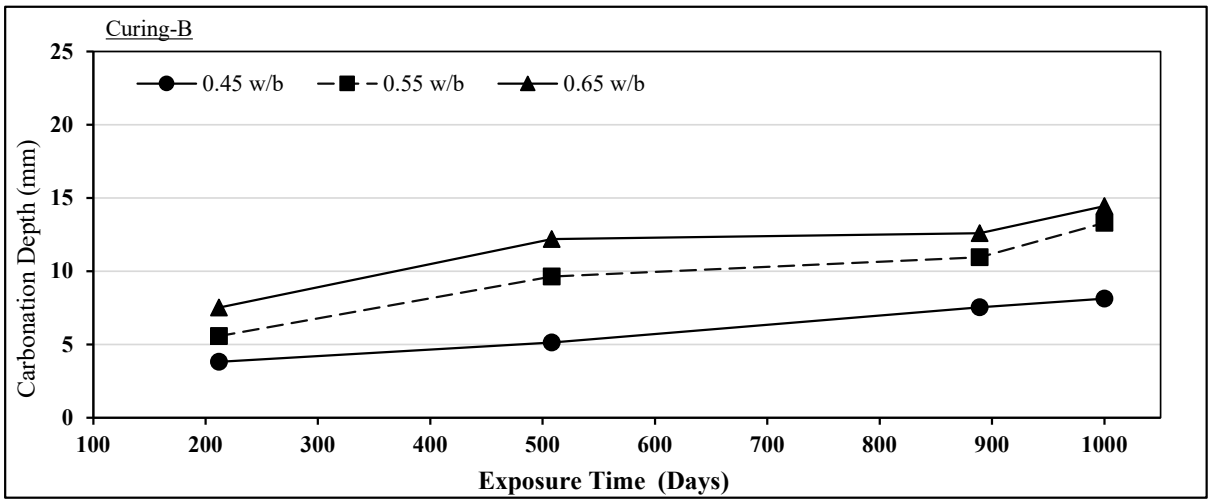

Figure D.14 Carbonation depth of LS concrete specimens exposed at site CD (Curing-B)

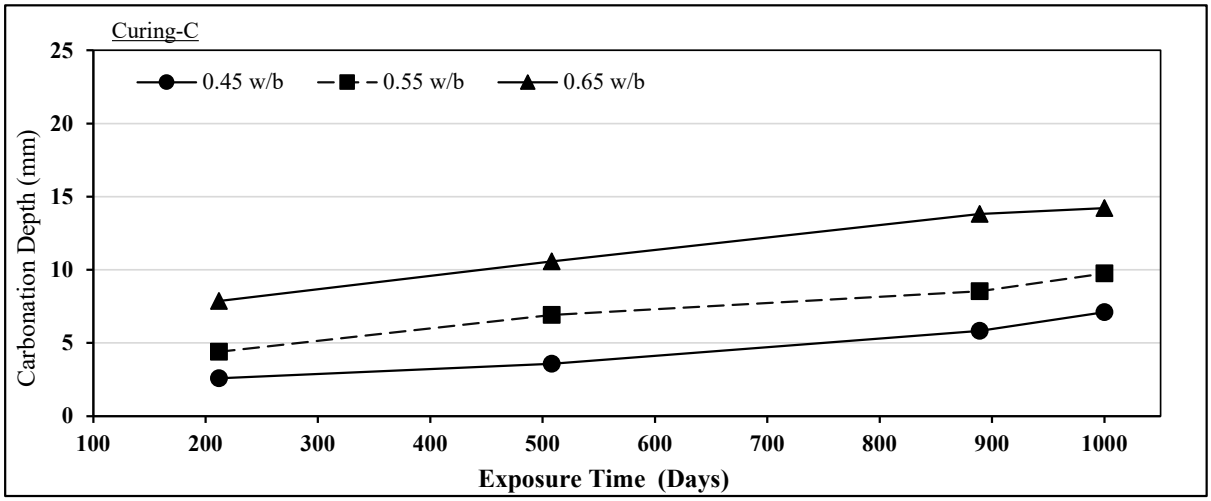

Figure D.15 Carbonation depth of LS concrete specimens exposed at site CD (Curing-C)

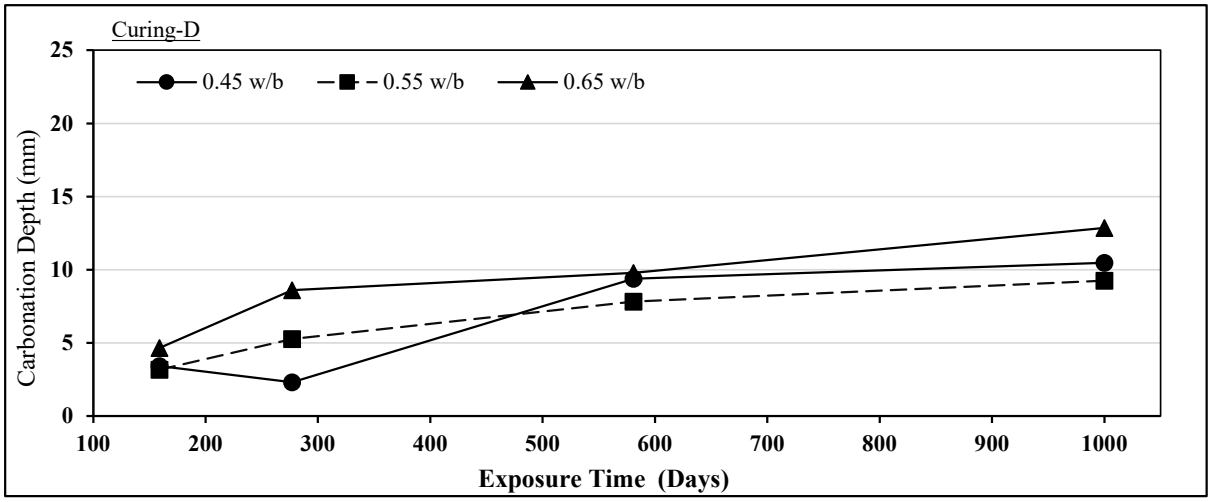

Figure D.16 Carbonation depth of LS concrete specimens exposed at site CD (Curing-D)

D.7 PROGRESSION OF CARBONATION DEPTH WITH TIME AT SITE ME

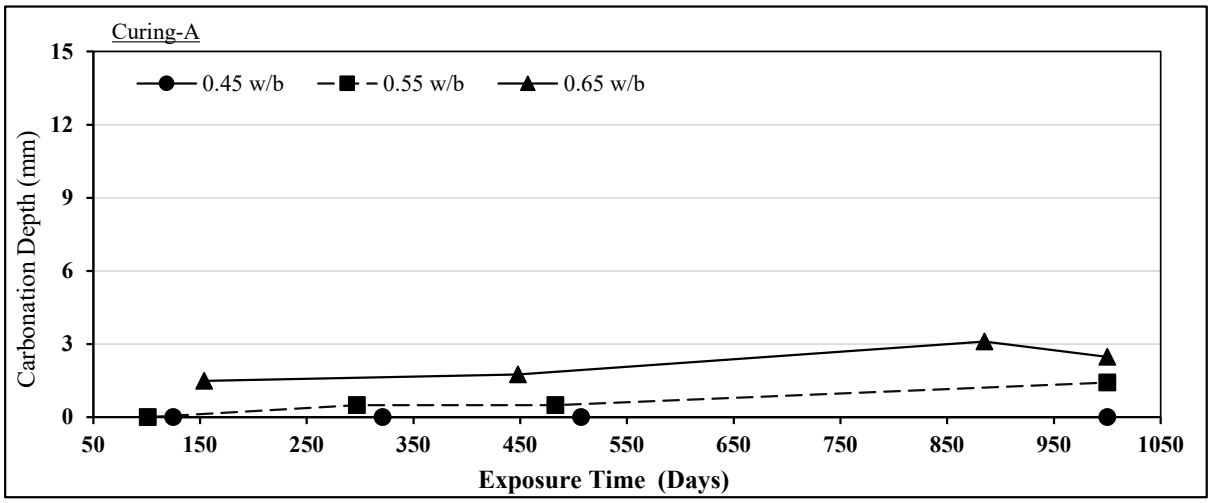

Figure D.17 Carbonation depth of PC concrete specimens exposed at site ME (Curing-A)

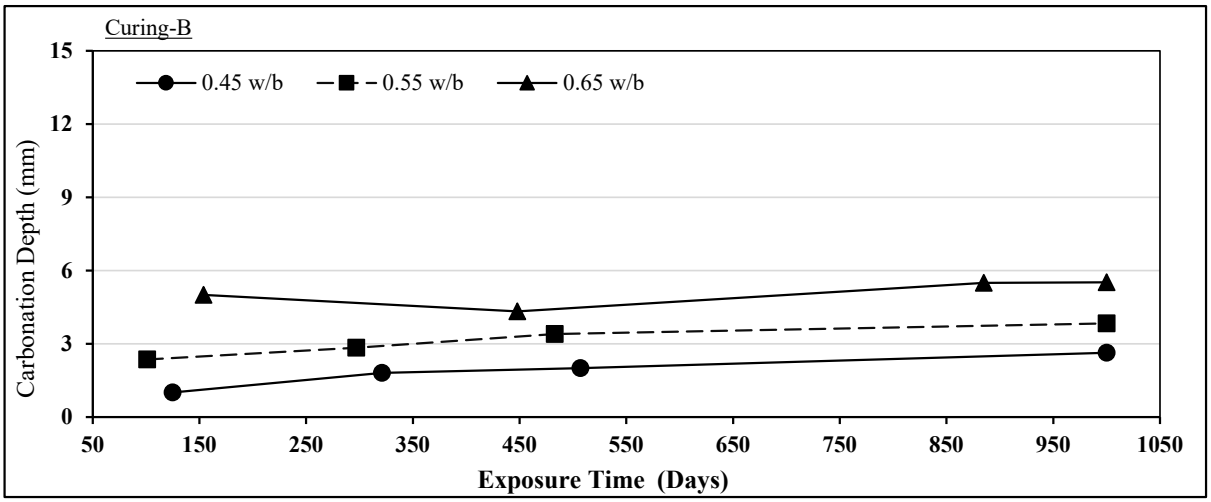

Figure D.18 Carbonation depth of PC concrete specimens exposed at site ME (Curing-B)

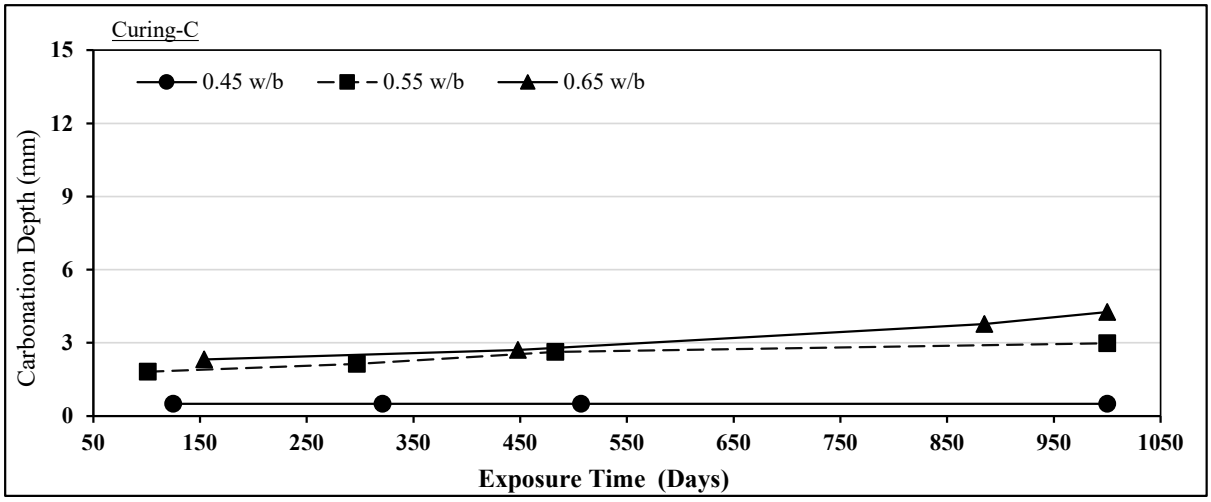

Figure D.19 Carbonation depth of PC concrete specimens exposed at site ME (Curing-C)

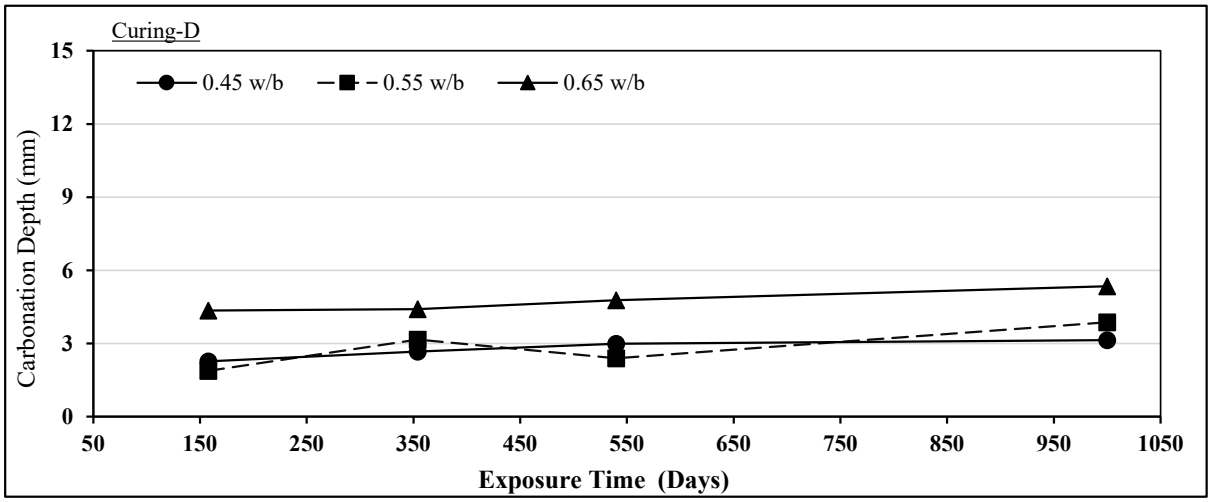

Figure D.20 Carbonation depth of PC concrete specimens exposed at site ME (Curing-D)

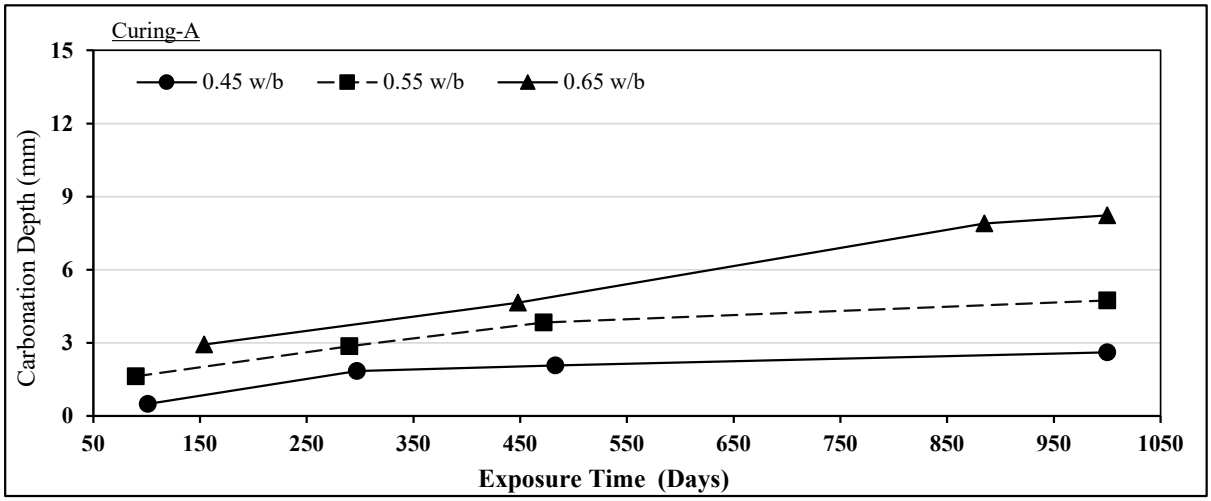

Figure D.21 Carbonation depth of FA concrete specimens exposed at site ME (Curing-A)

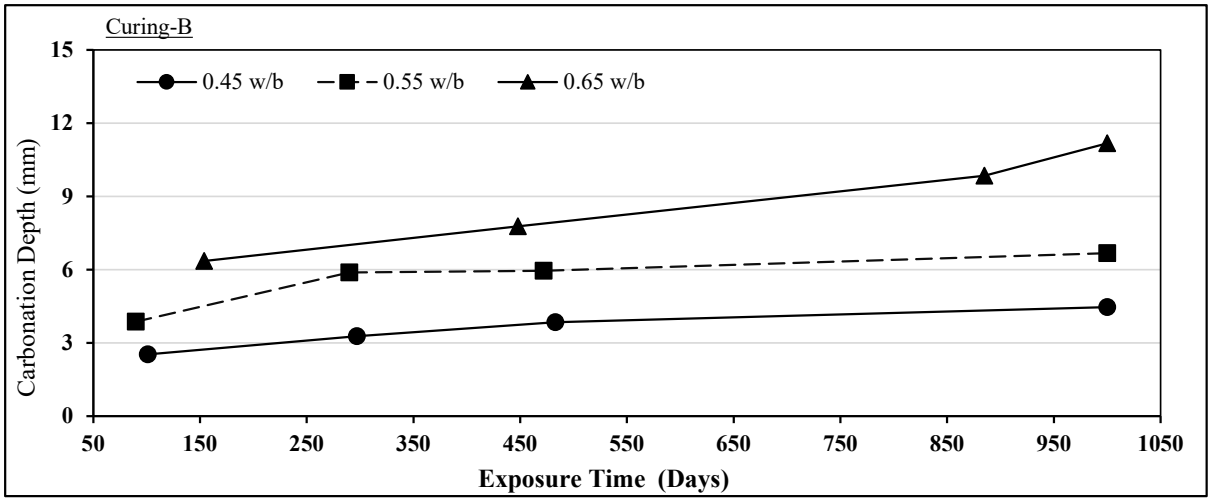

Figure D.22 Carbonation depth of FA concrete specimens exposed at site ME (Curing-B)

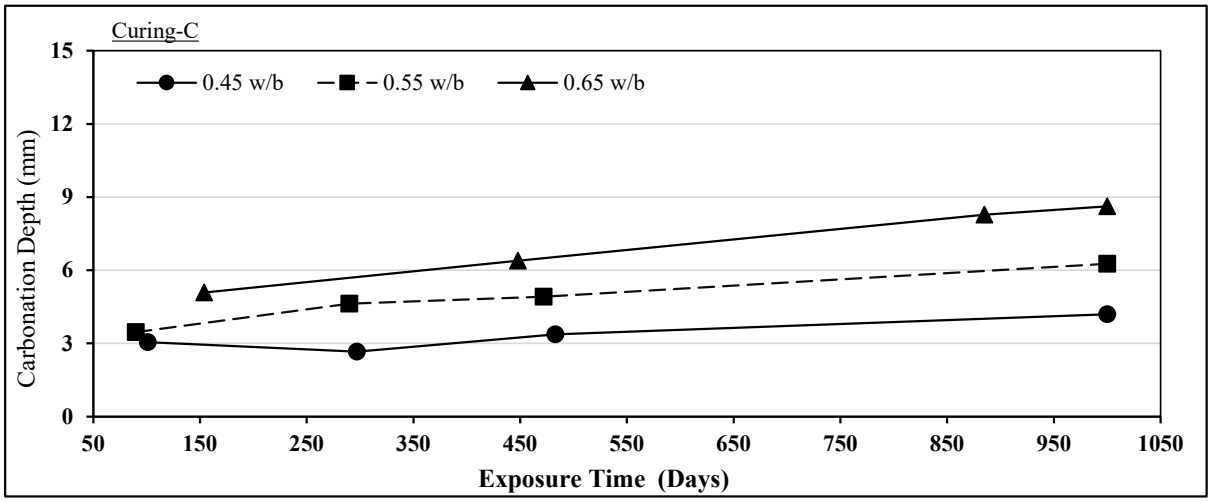

Figure D.23 Carbonation depth of FA concrete specimens exposed at site ME (Curing-C)

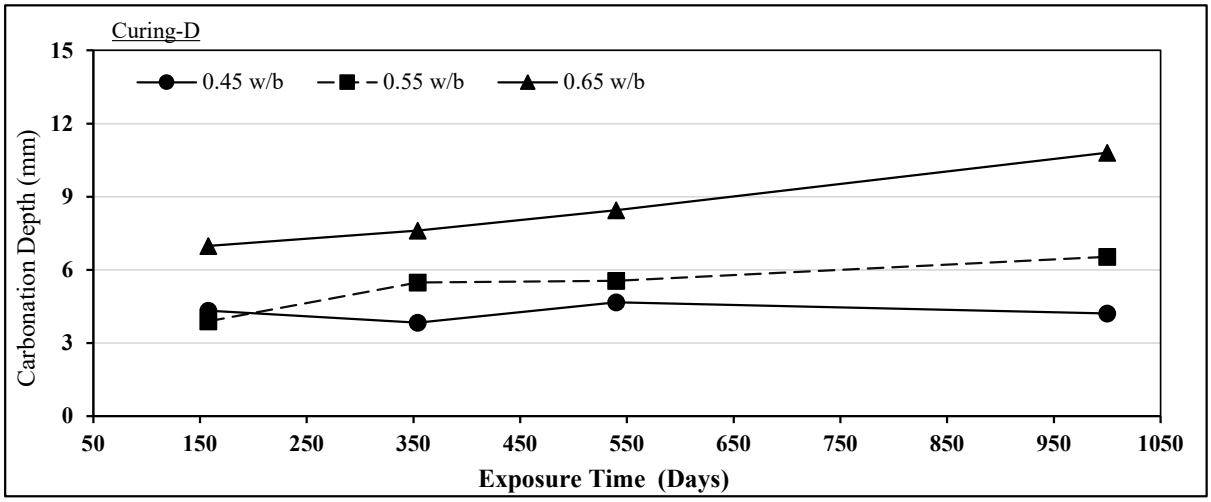

Figure D.24 Carbonation depth of FA concrete specimens exposed at site ME (Curing-D)

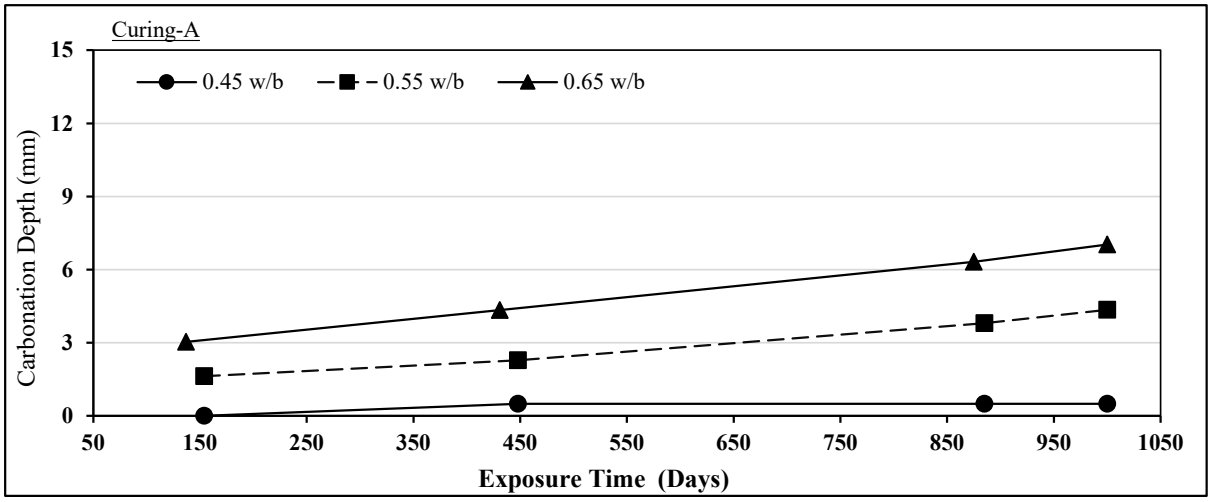

Figure D.25 Carbonation depth of GS concrete specimens exposed at site ME (Curing-A)

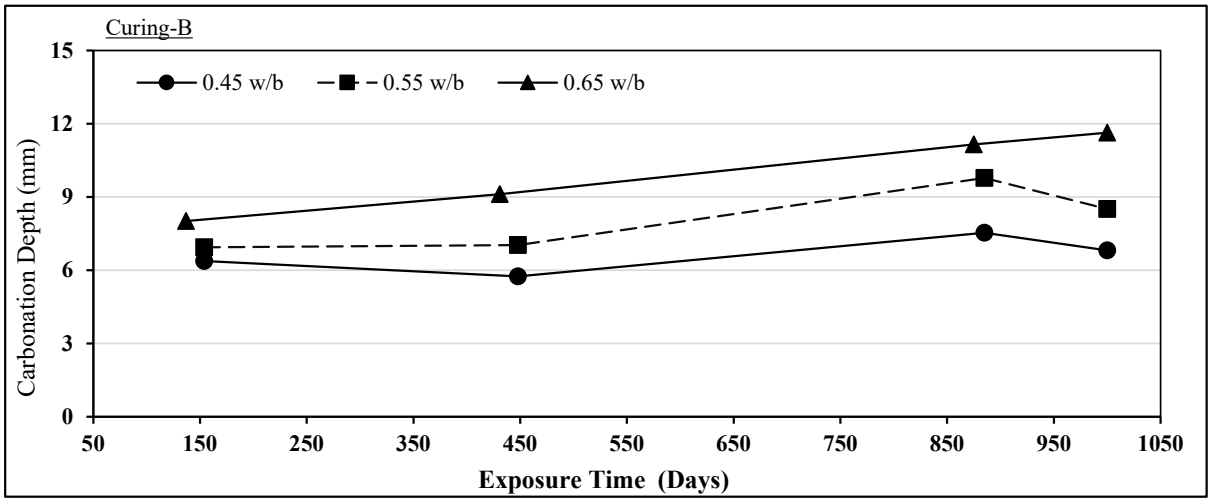

Figure D.26 Carbonation depth of GS concrete specimens exposed at site ME (Curing-B)

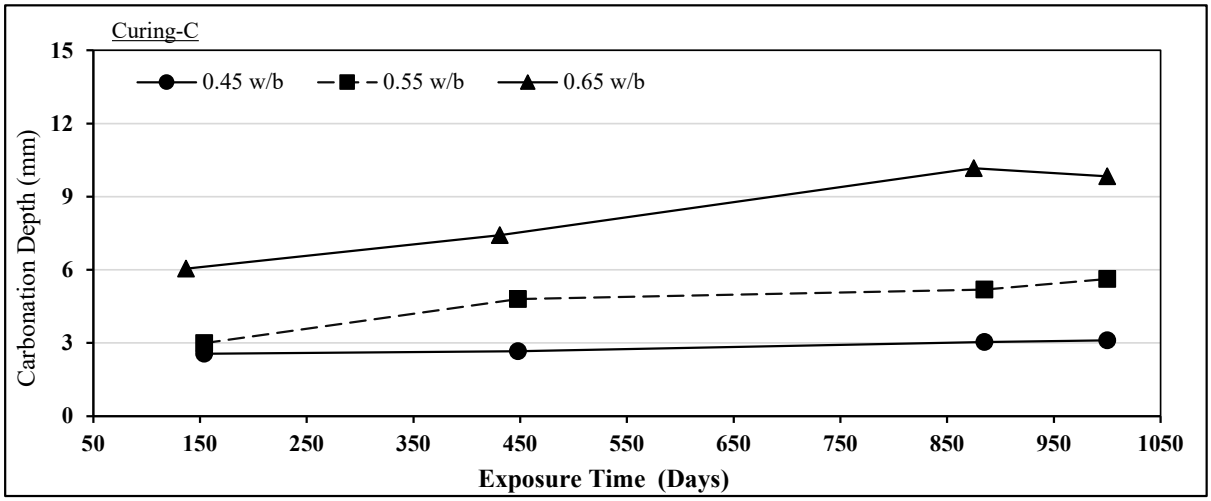

Figure D.27 Carbonation depth of GS concrete specimens exposed at site ME (Curing-C)

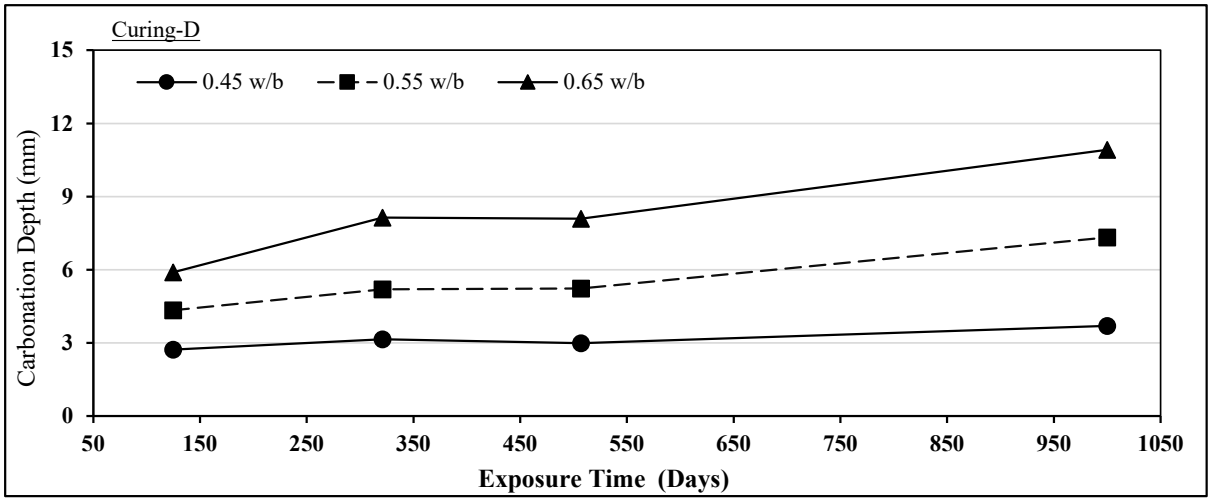

Figure D.28 Carbonation depth of GS concrete specimens exposed at site ME (Curing-D)

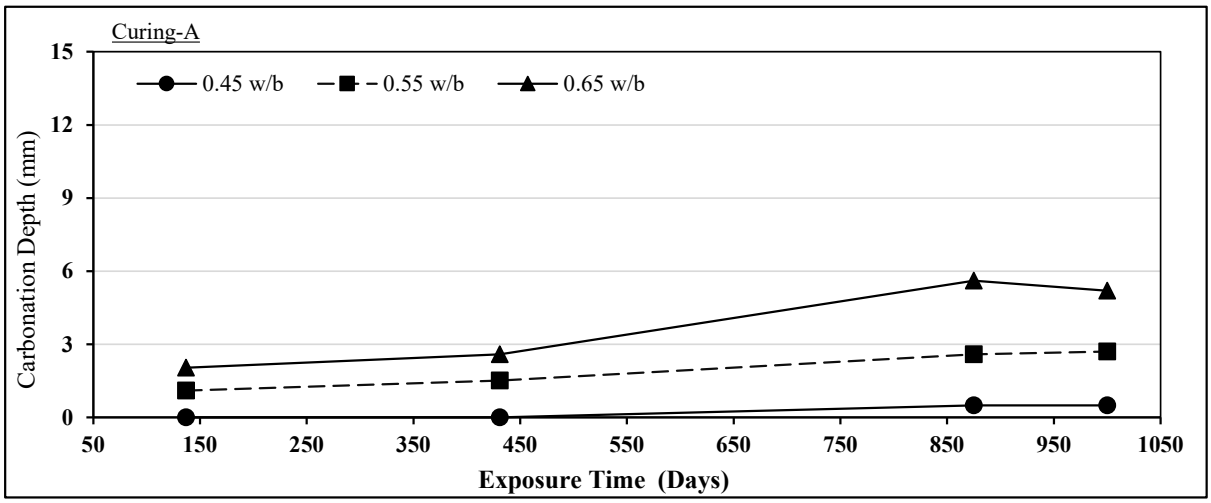

Figure D.29 Carbonation depth of LS concrete specimens exposed at site ME (Curing-A)

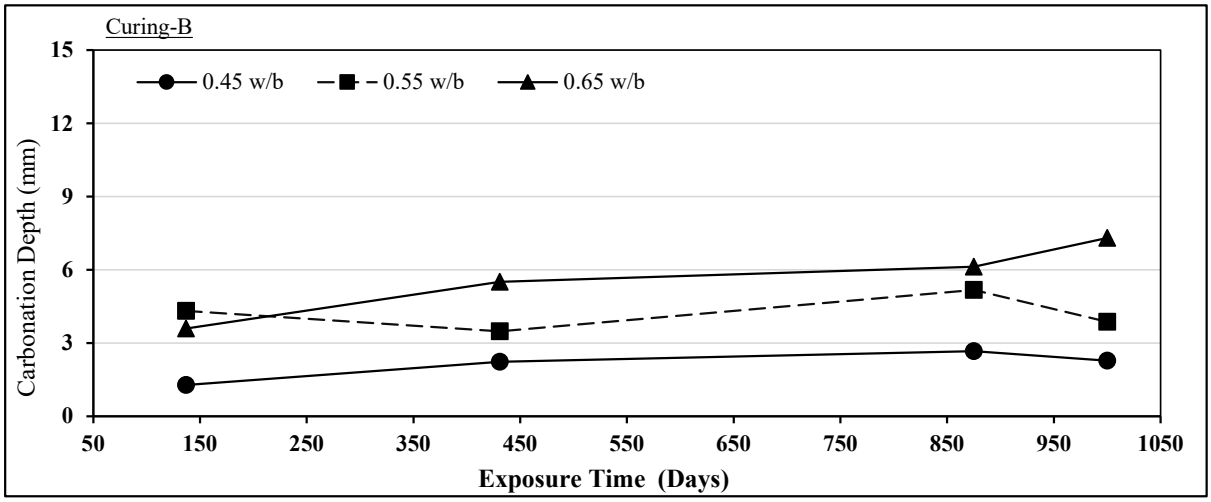

Figure D.30 Carbonation depth of LS concrete specimens exposed at site ME (Curing-B)

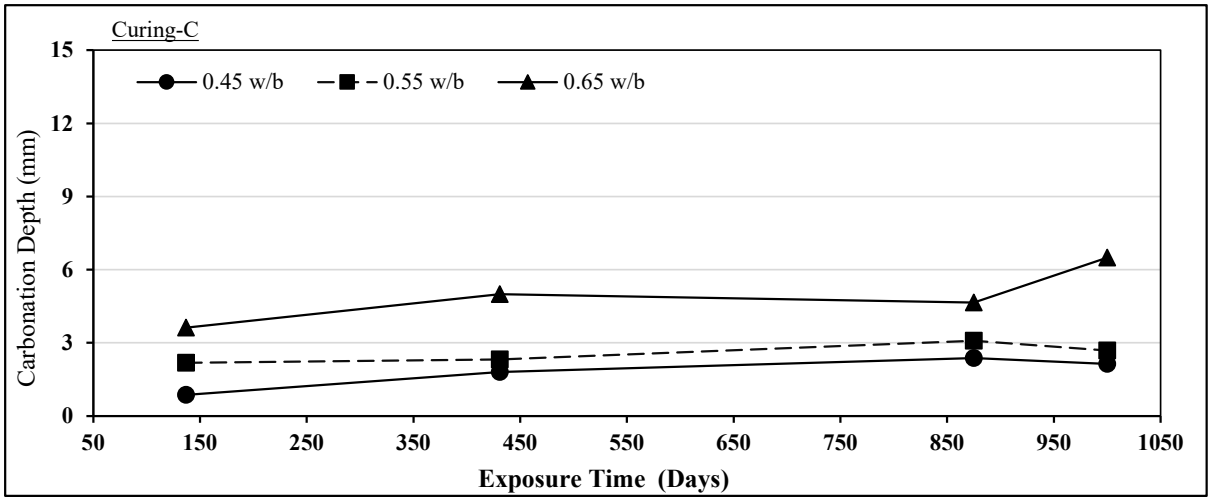

Figure D.31 Carbonation depth of LS concrete specimens exposed at site ME (Curing-C)

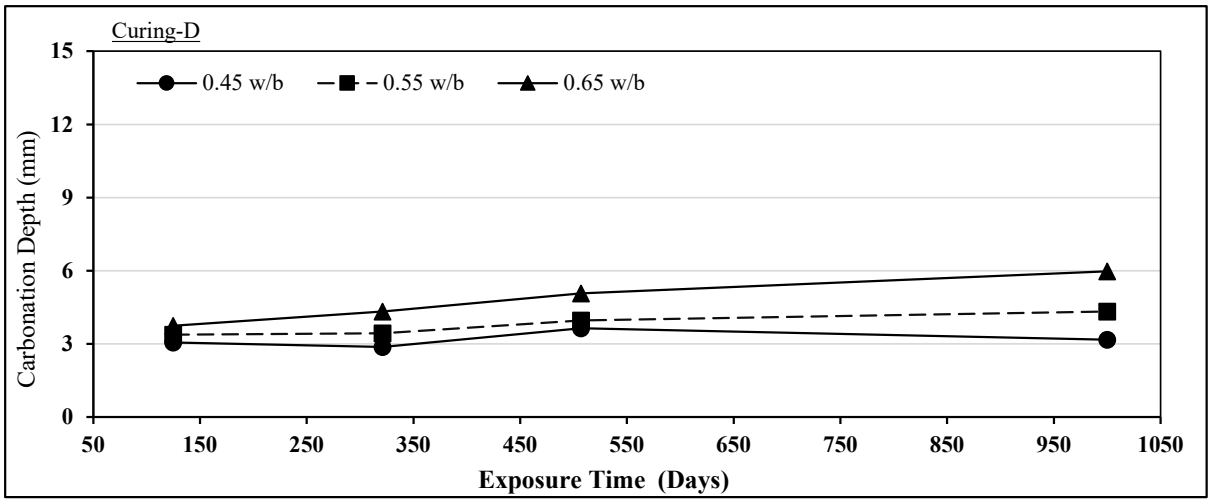

Figure D.32 Carbonation depth of LS concrete specimens exposed at site ME (Curing-D)

D.8 PROGRESSION OF CARBONATION DEPTH WITH TIME AT SITE MS

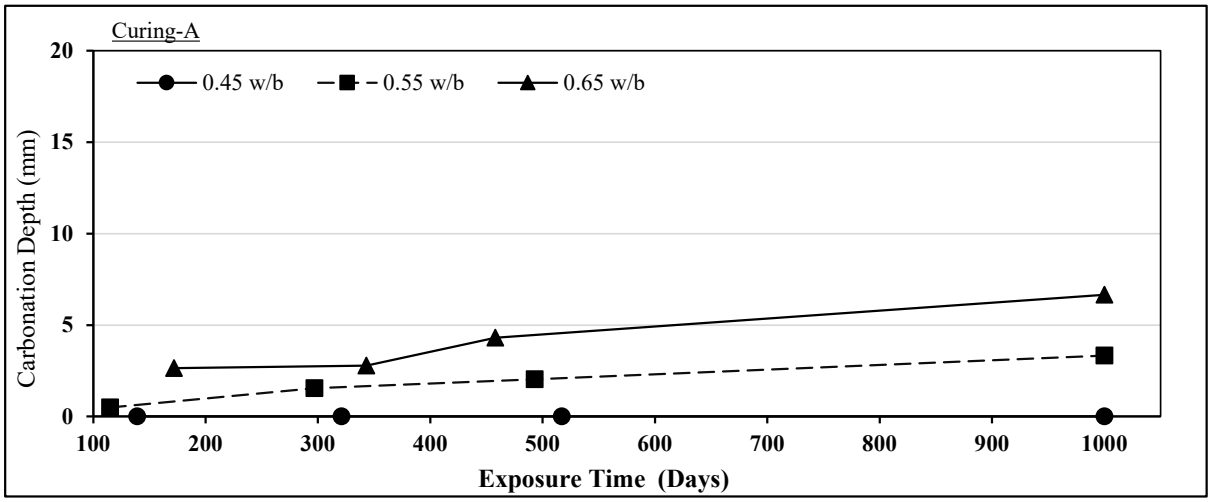

Figure D.33 Carbonation depth of PC concrete specimens exposed at site MS (Curing-A)

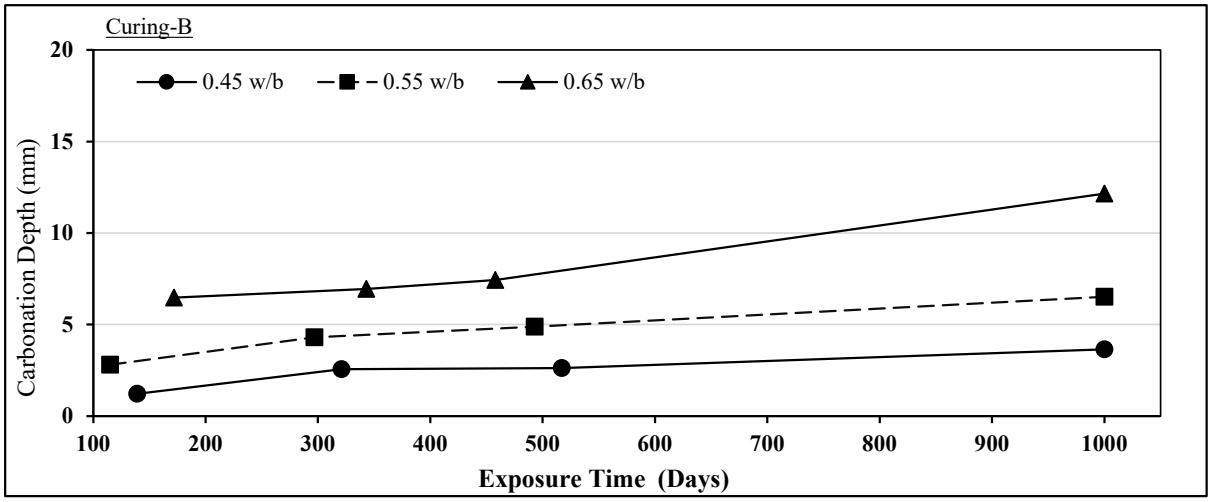

Figure D.34 Carbonation depth of PC concrete specimens exposed at site MS (Curing-B)

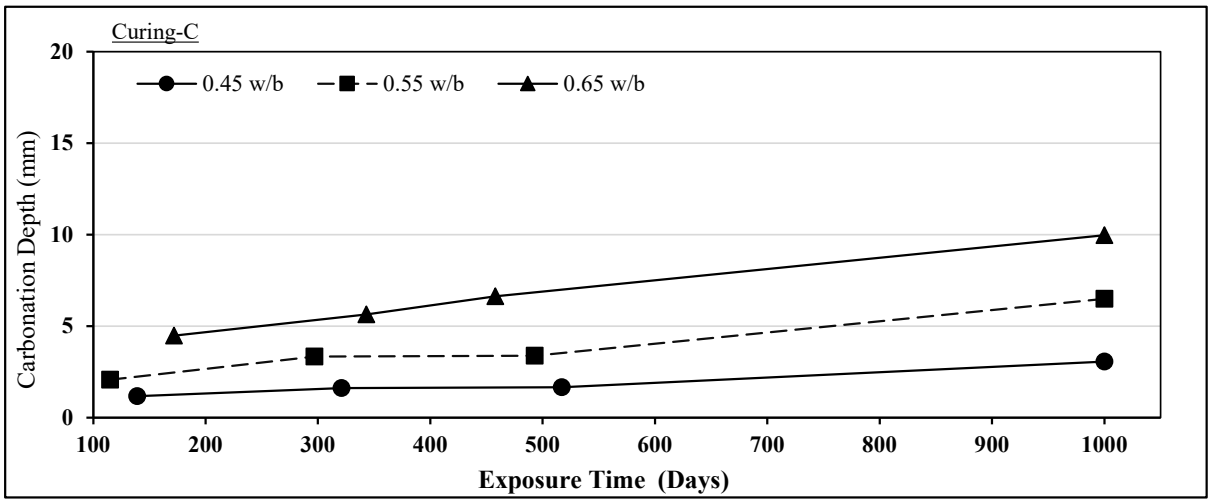

Figure D.35 Carbonation depth of PC concrete specimens exposed at site MS (Curing-C)

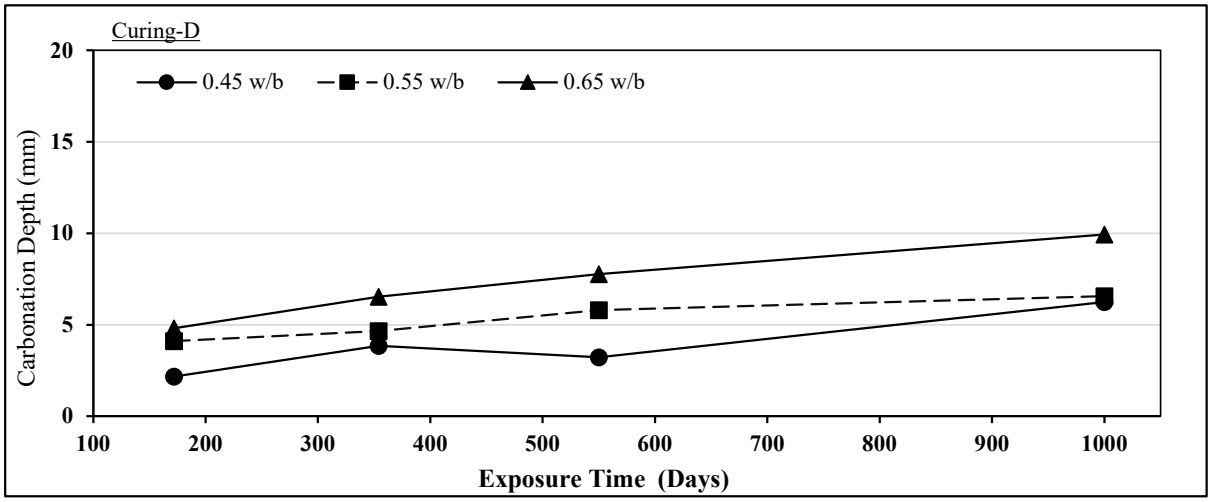

Figure D.36 Carbonation depth of PC concrete specimens exposed at site MS (Curing-D)

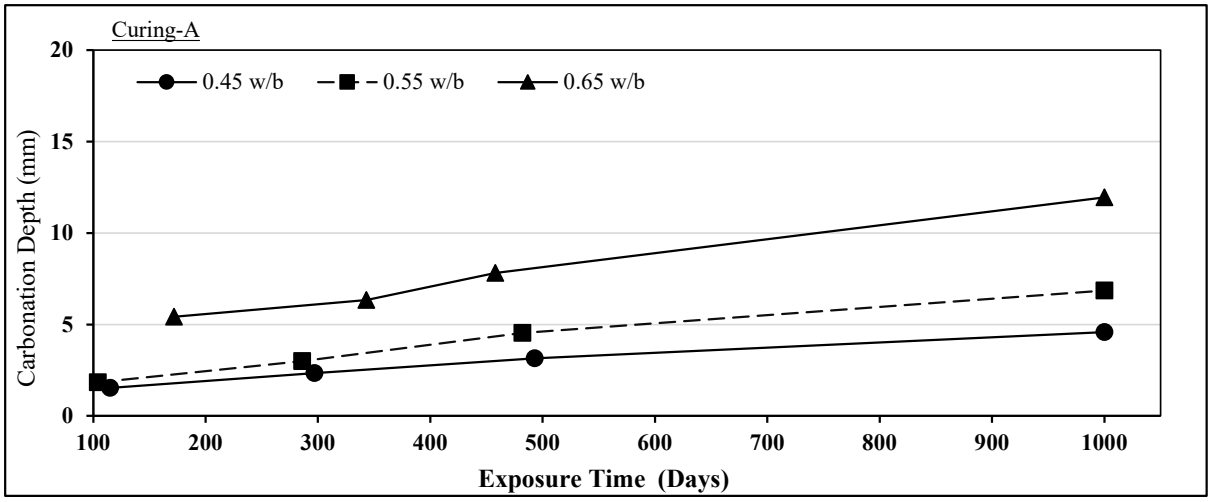

Figure D.37 Carbonation depth of FA concrete specimens exposed at site MS (Curing-A)

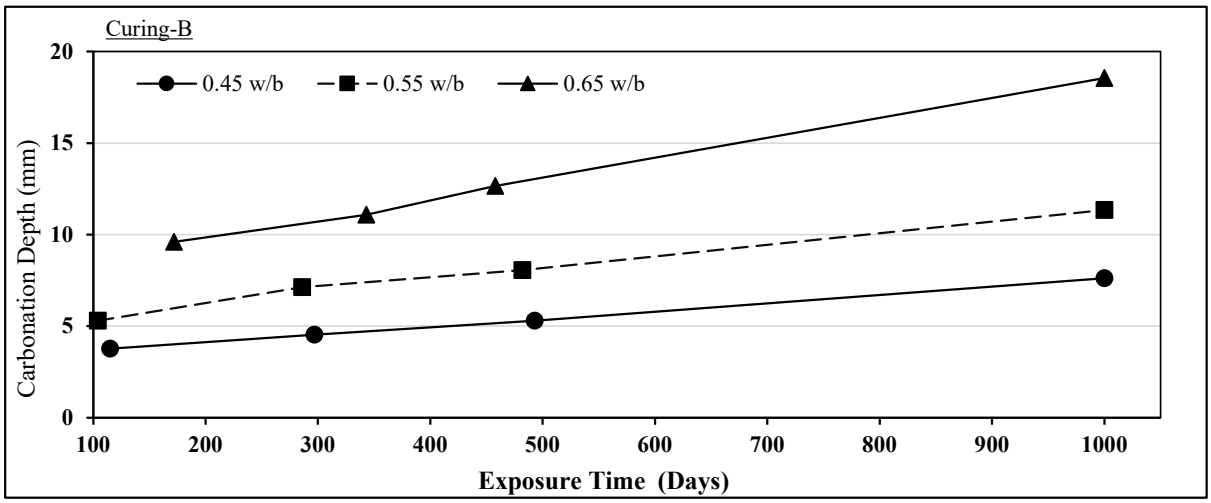

Figure D.38 Carbonation depth of FA concrete specimens exposed at site MS (Curing-B)

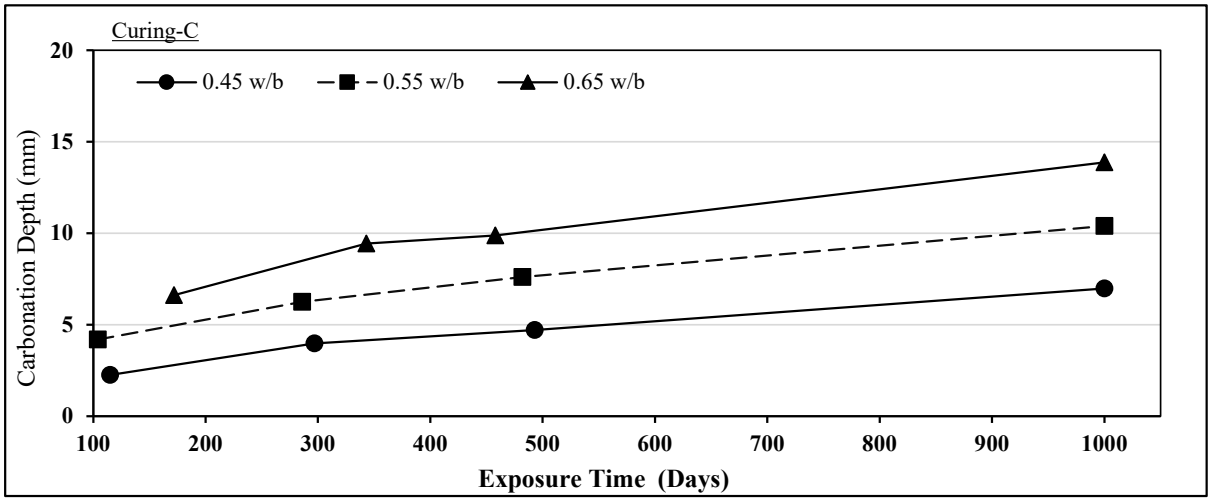

Figure D.39 Carbonation depth of FA concrete specimens exposed at site MS (Curing-C)

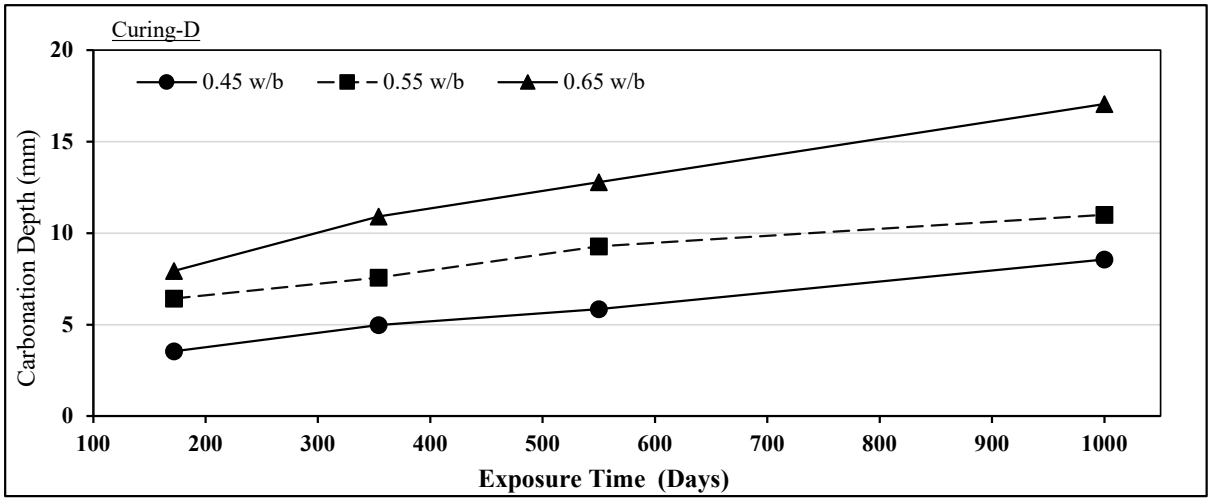

Figure D.40 Carbonation depth of FA concrete specimens exposed at site MS (Curing-D)

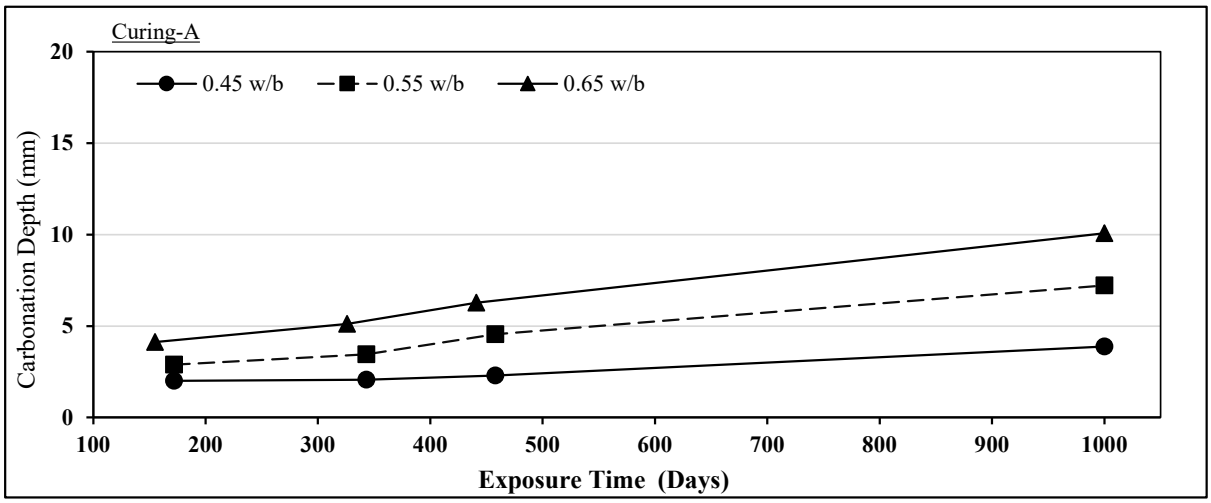

Figure D.41 Carbonation depth of GS concrete specimens exposed at site MS (Curing-A)

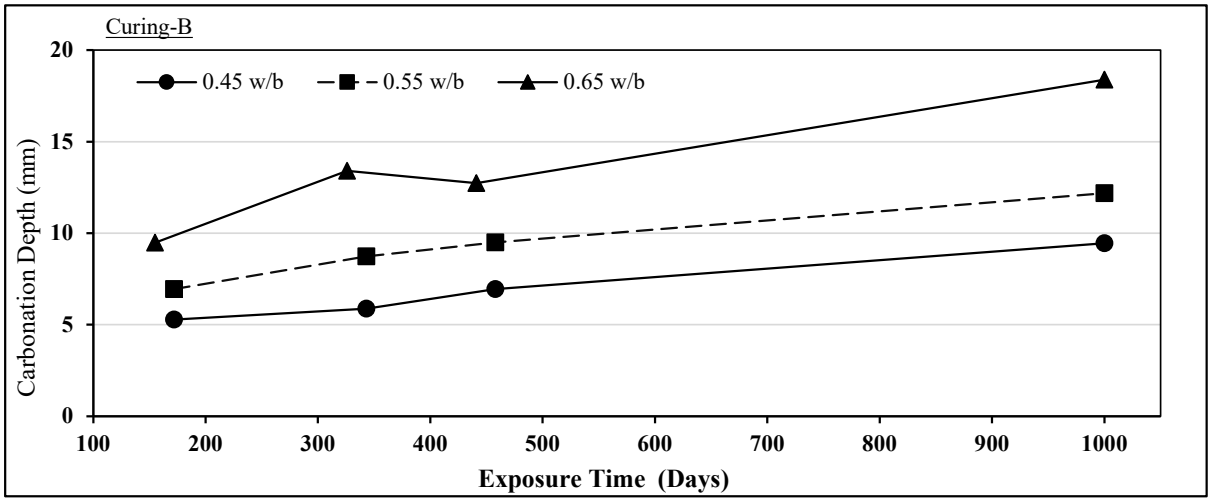

Figure D.42 Carbonation depth of GS concrete specimens exposed at site MS (Curing-B)

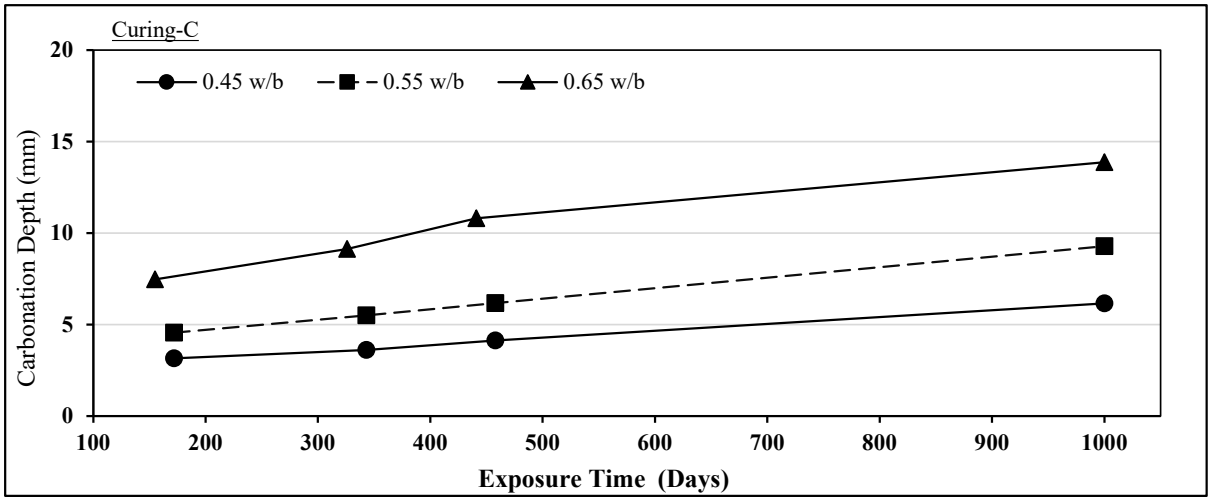

Figure D.43 Carbonation depth of GS concrete specimens exposed at site MS (Curing-C)

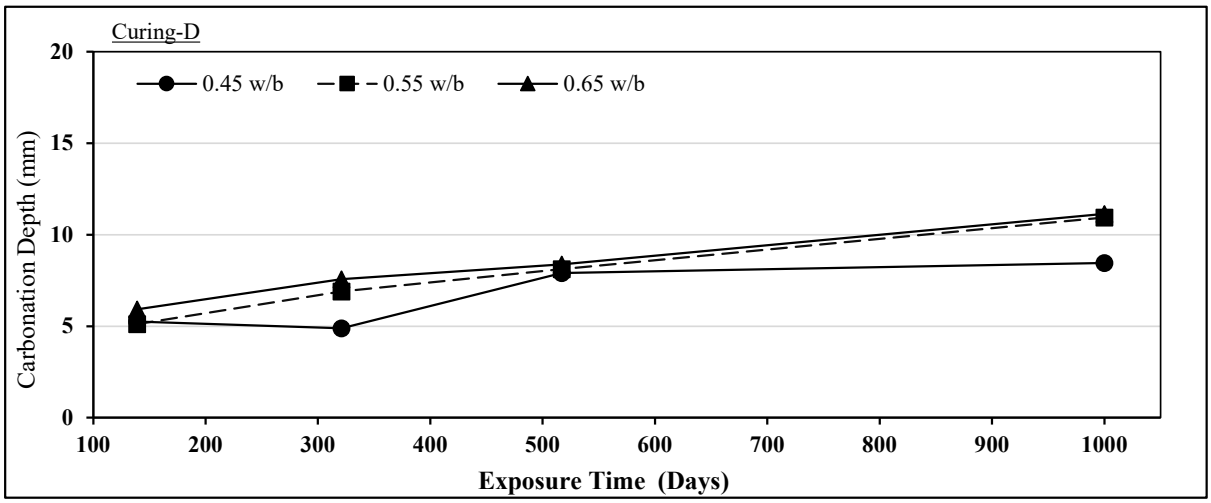

Figure D.44 Carbonation depth of GS concrete specimens exposed at site MS (Curing-D)

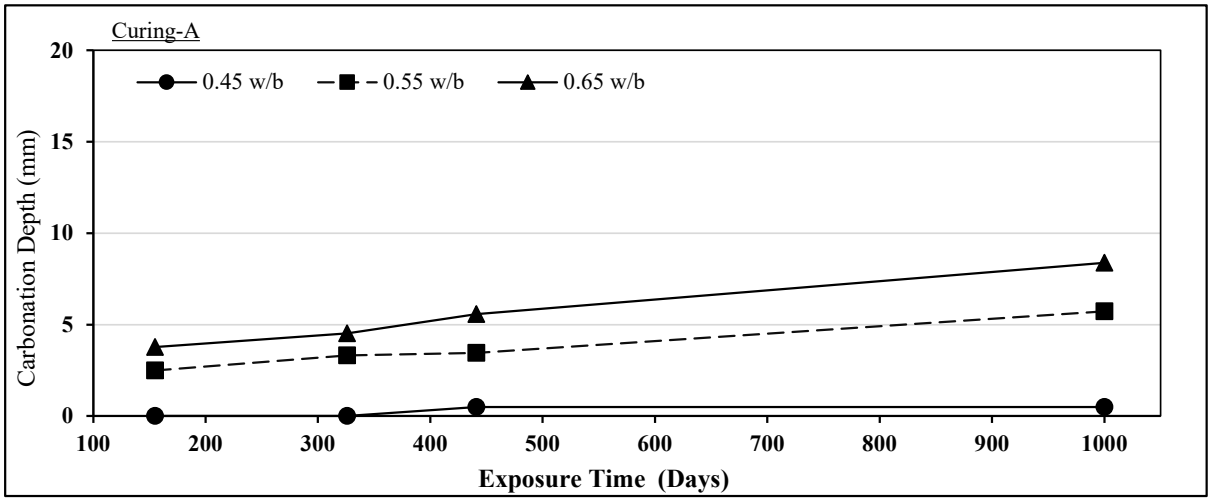

Figure D.45 Carbonation depth of LS concrete specimens exposed at site MS (Curing-A)

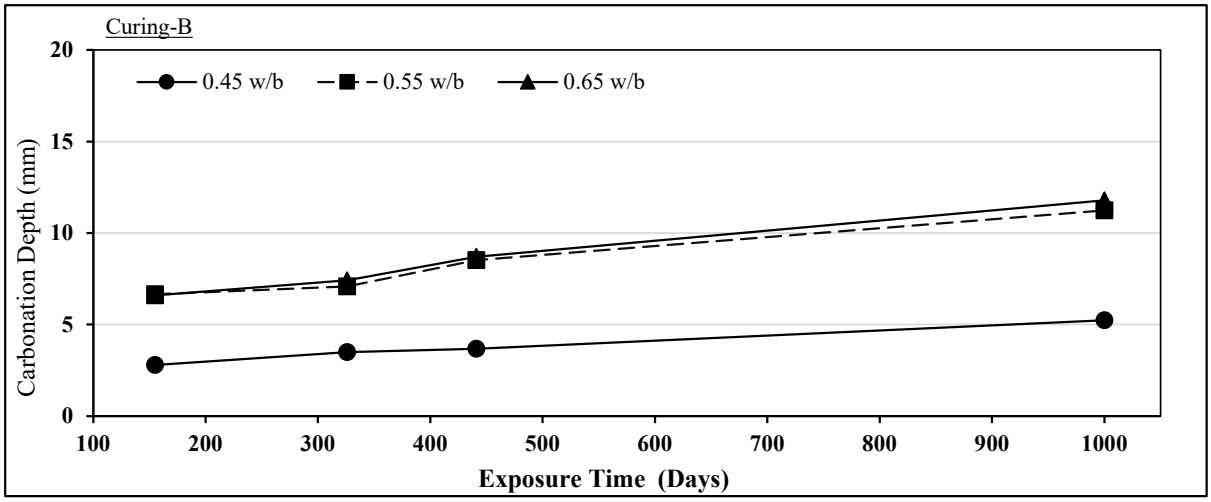

Figure D.46 Carbonation depth of LS concrete specimens exposed at site MS (Curing-B)

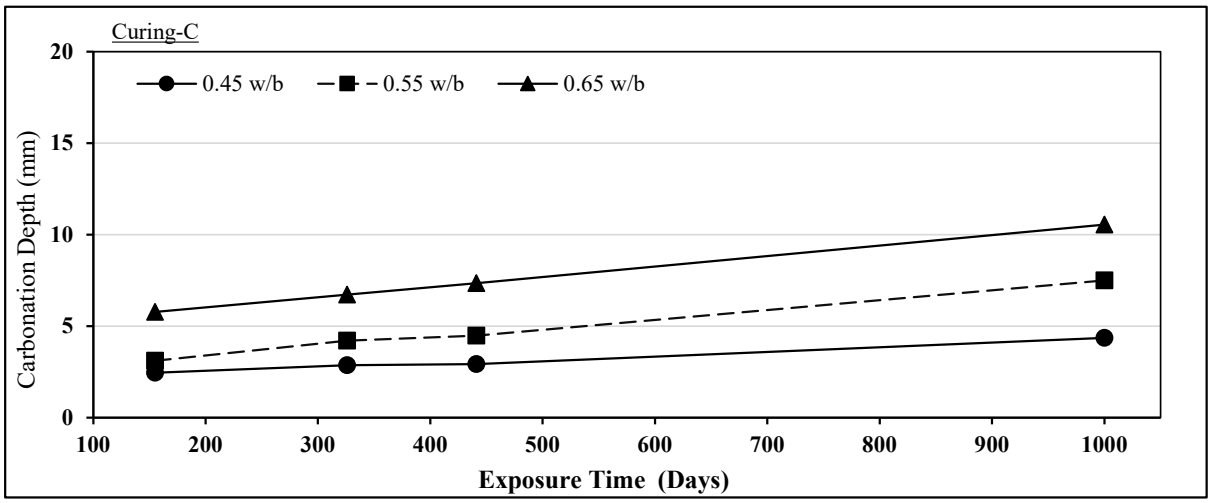

Figure D.47 Carbonation depth of LS concrete specimens exposed at site MS (Curing-C)

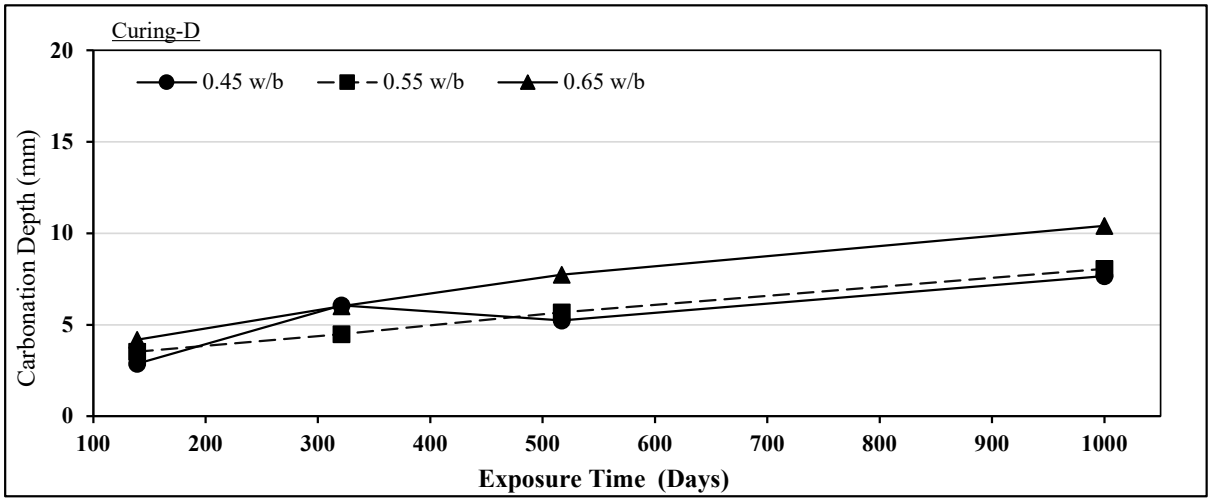

Figure D.48 Carbonation depth of LS concrete specimens exposed at site MS (Curing-D)

D.9 PROGRESSION OF CARBONATION DEPTH WITH TIME AT SITE WE

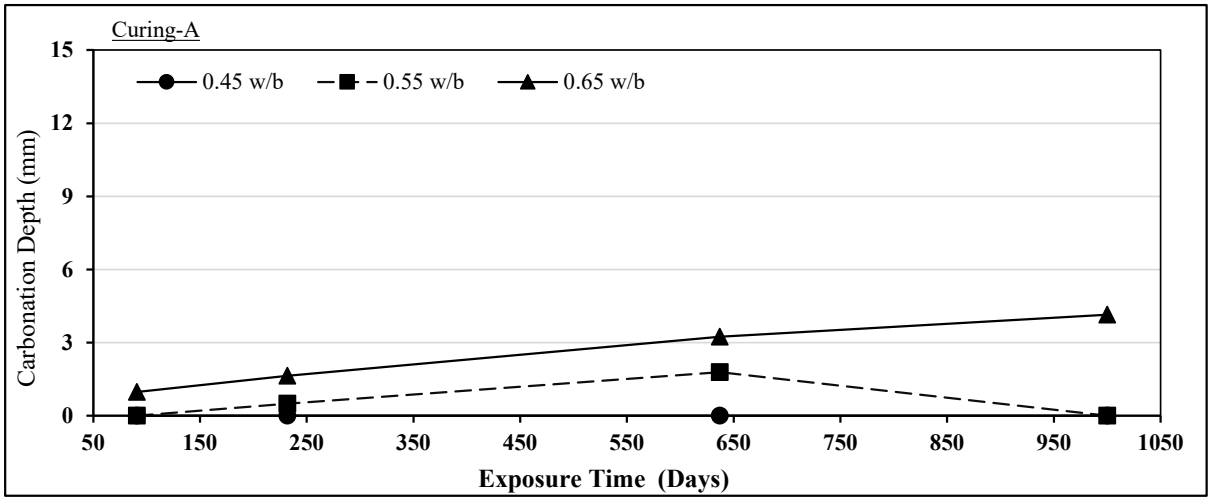

Figure D.49 Carbonation depth of PC concrete specimens exposed at site WE (Curing-A)

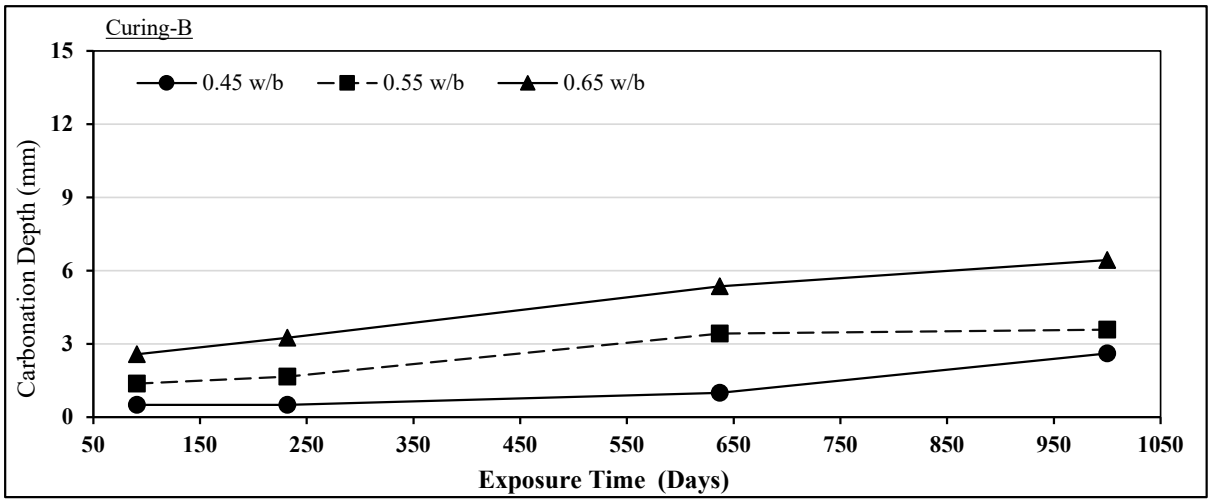

Figure D.50 Carbonation depth of PC concrete specimens exposed at site WE (Curing-B)

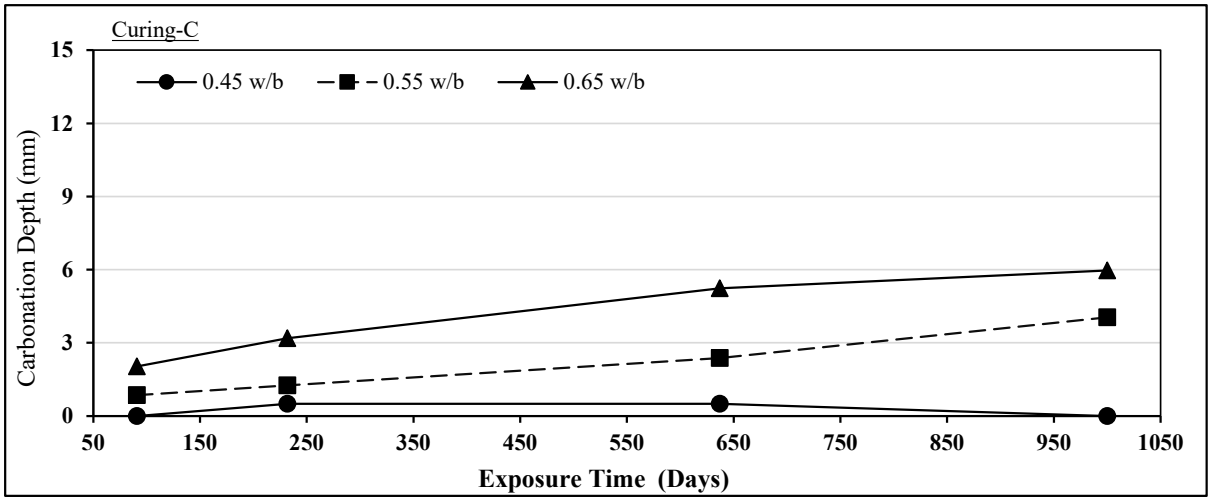

Figure D.51 Carbonation depth of PC concrete specimens exposed at site WE (Curing-C)

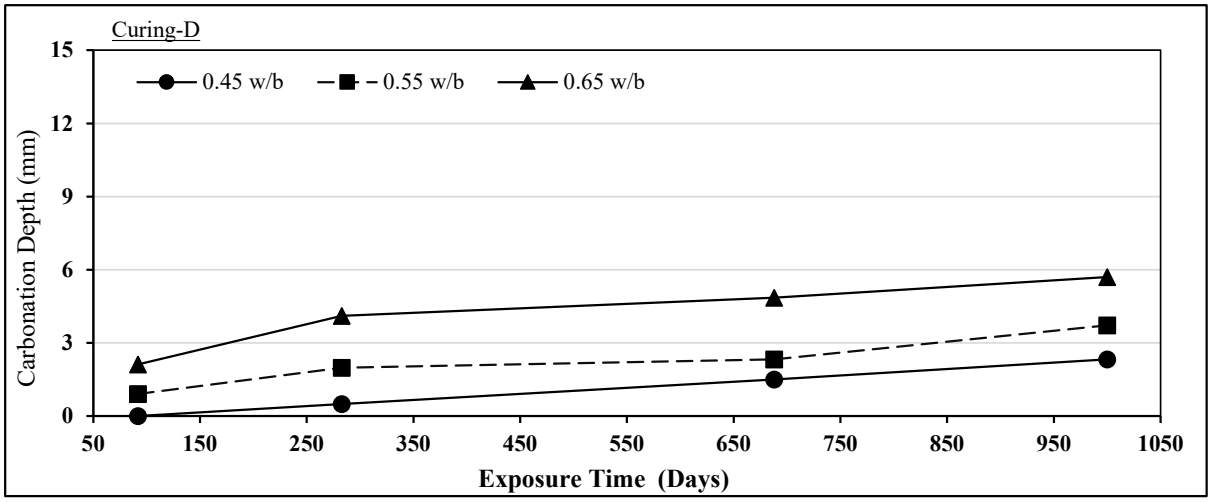

Figure D.52 Carbonation depth of PC concrete specimens exposed at site WE (Curing-D)

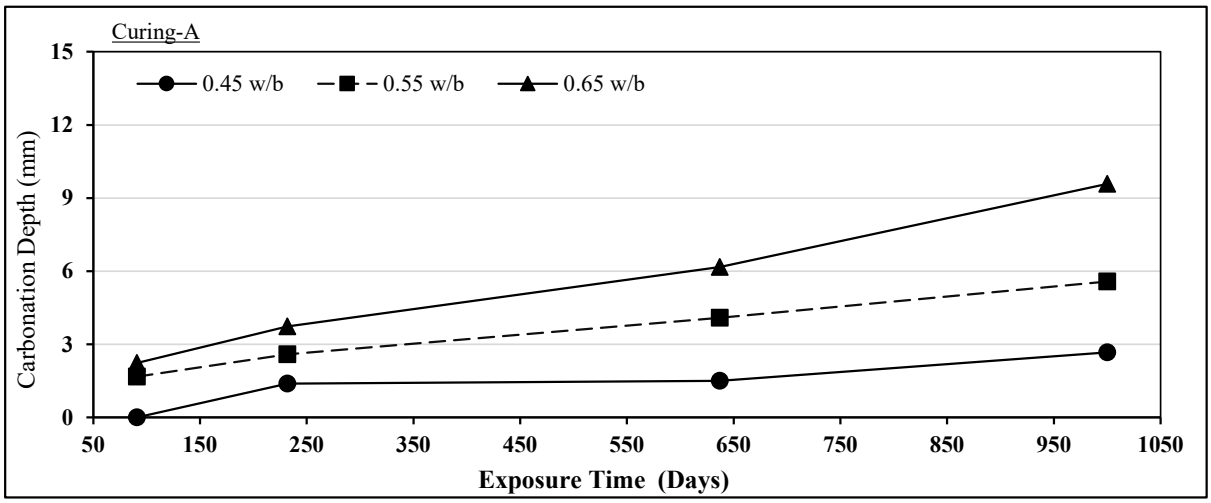

Figure D.53 Carbonation depth of FA concrete specimens exposed at site WE (Curing-A)

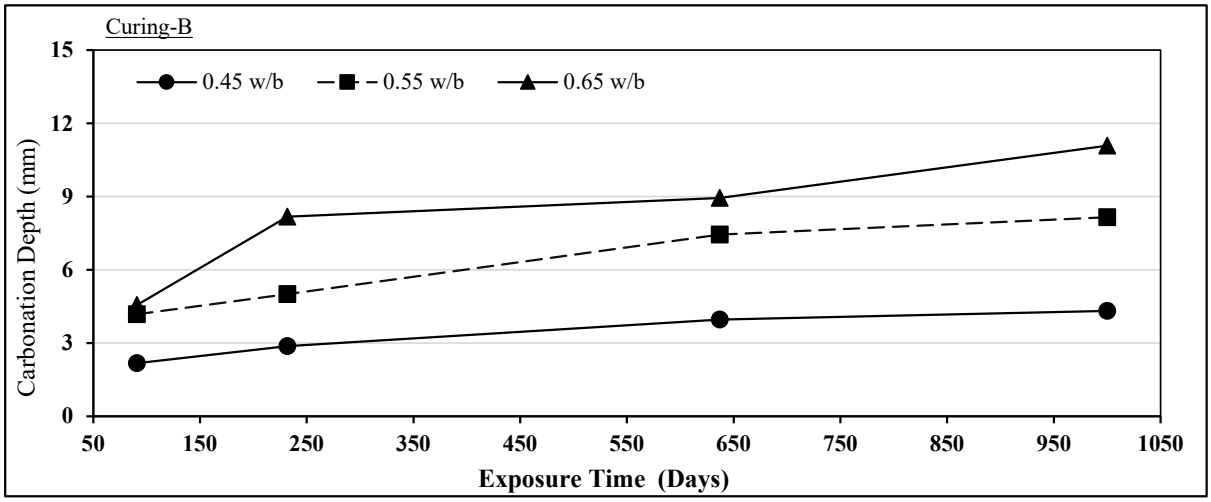

Figure D.54 Carbonation depth of FA concrete specimens exposed at site WE (Curing-B)

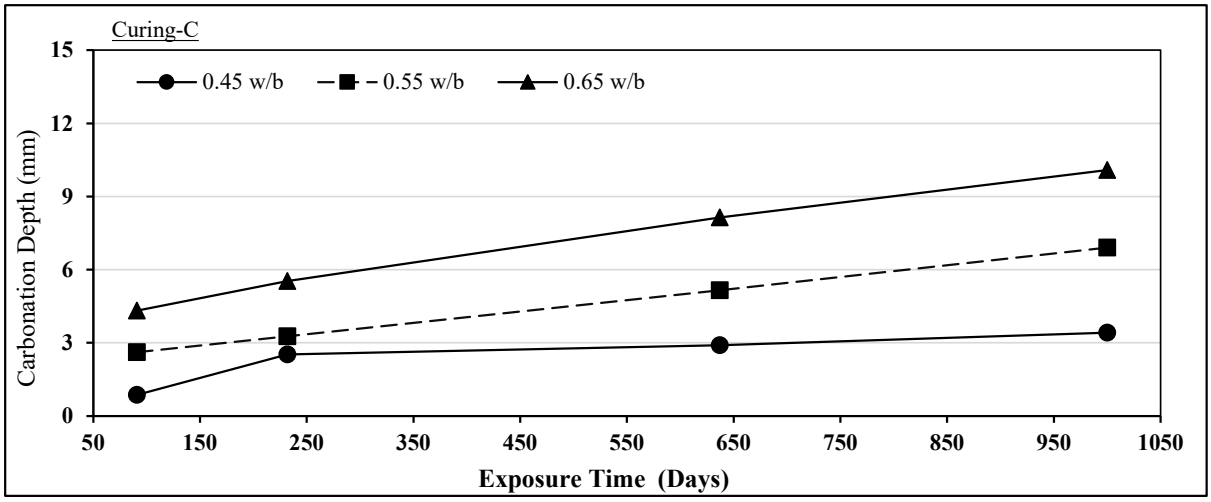

Figure D.55 Carbonation depth of FA concrete specimens exposed at site WE (Curing-C)

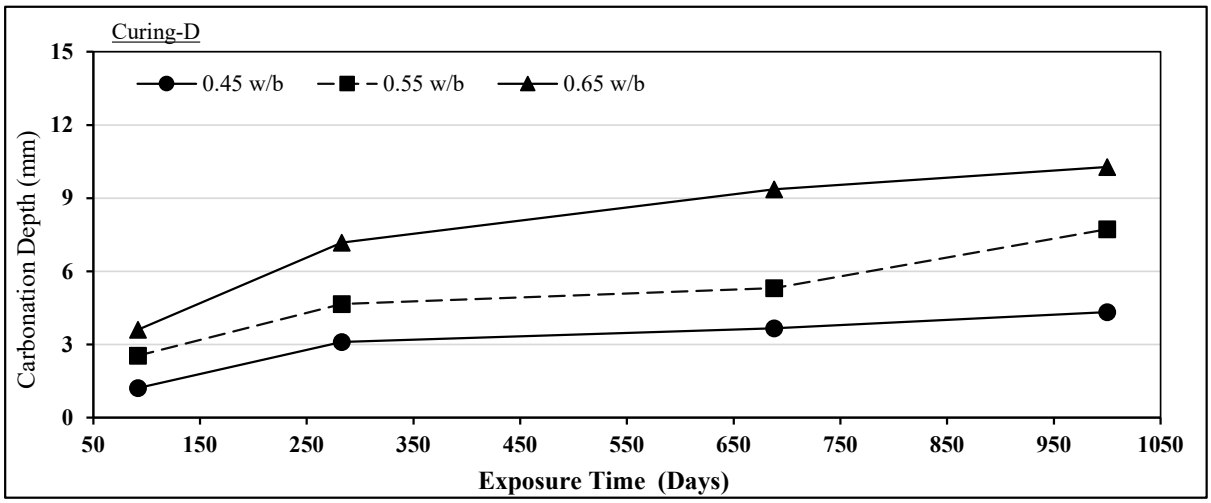

Figure D.56 Carbonation depth of FA concrete specimens exposed at site WE (Curing-D)

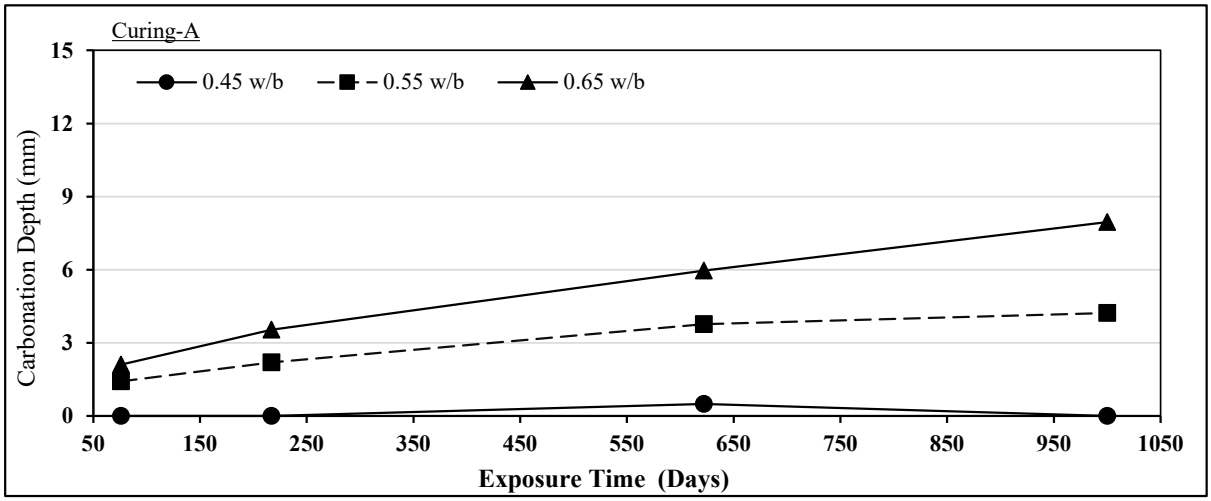

Figure D.57 Carbonation depth of GS concrete specimens exposed at site WE (Curing-A)

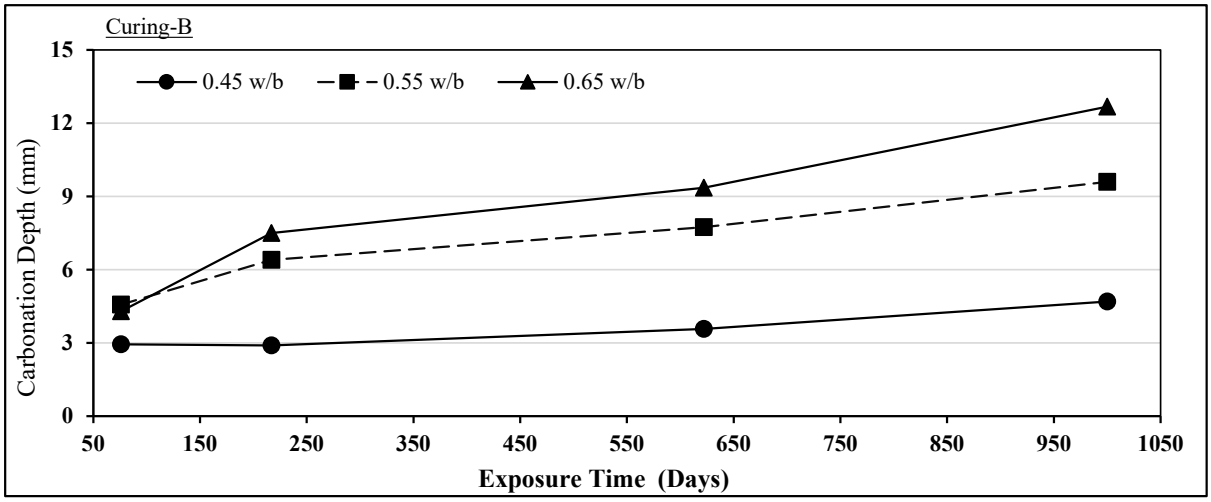

Figure D.58 Carbonation depth of GS concrete specimens exposed at site WE (Curing-B)

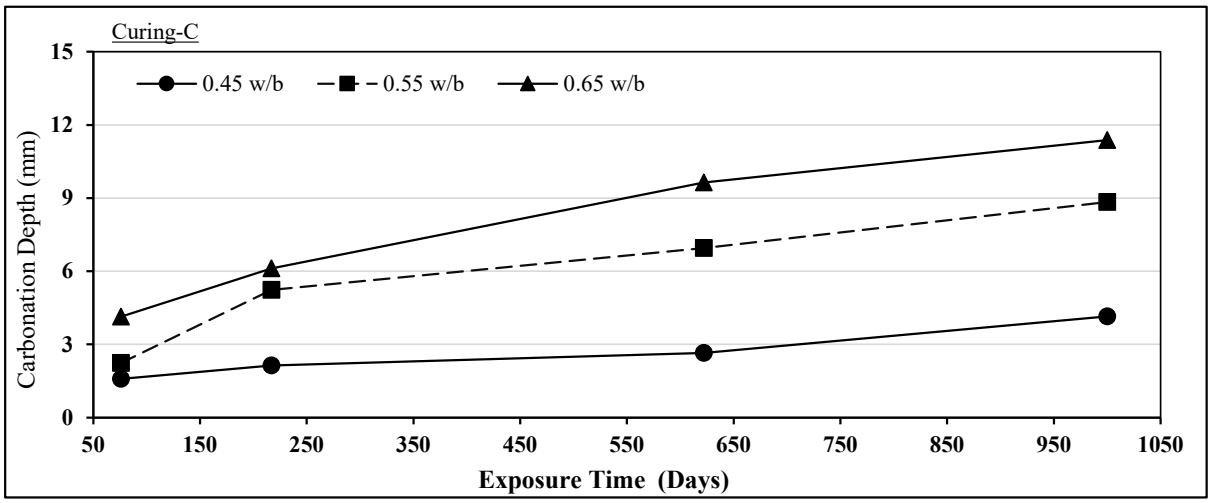

Figure D.59 Carbonation depth of GS concrete specimens exposed at site WE (Curing-C)

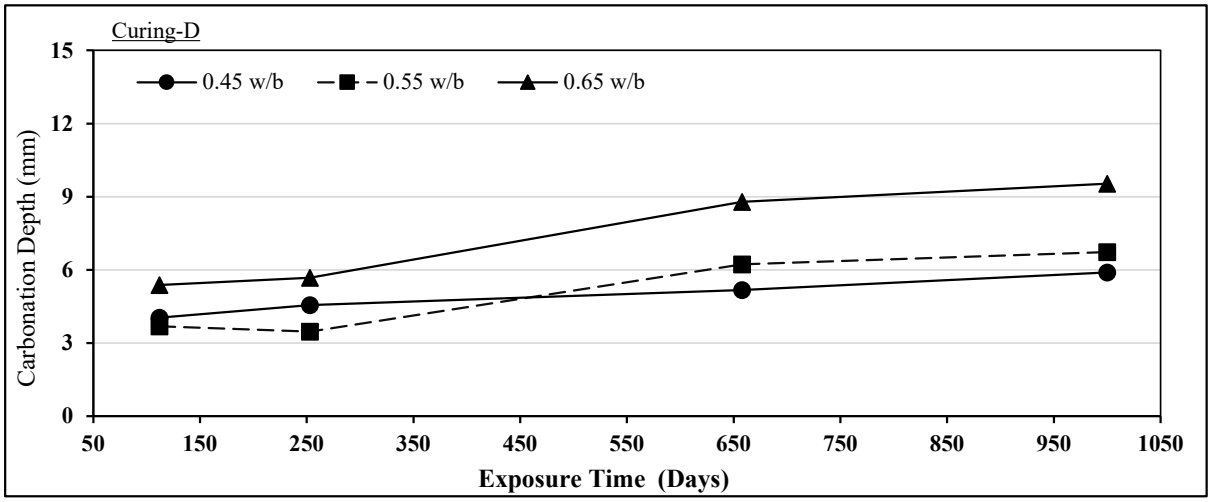

Figure D.60 Carbonation depth of GS concrete specimens exposed at site WE (Curing-D)

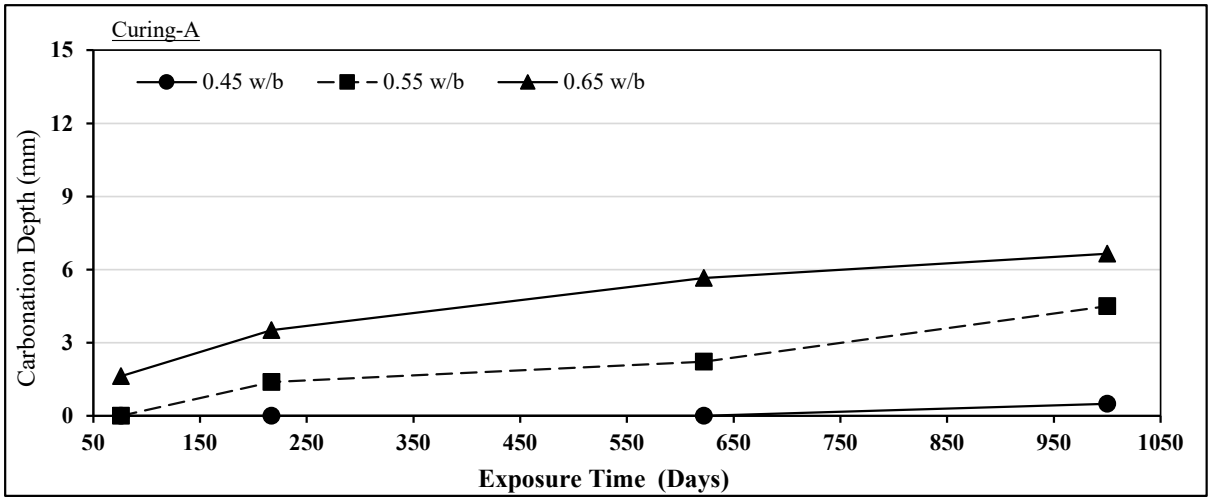

Figure D.61 Carbonation depth of LS concrete specimens exposed at site WE (Curing-A)

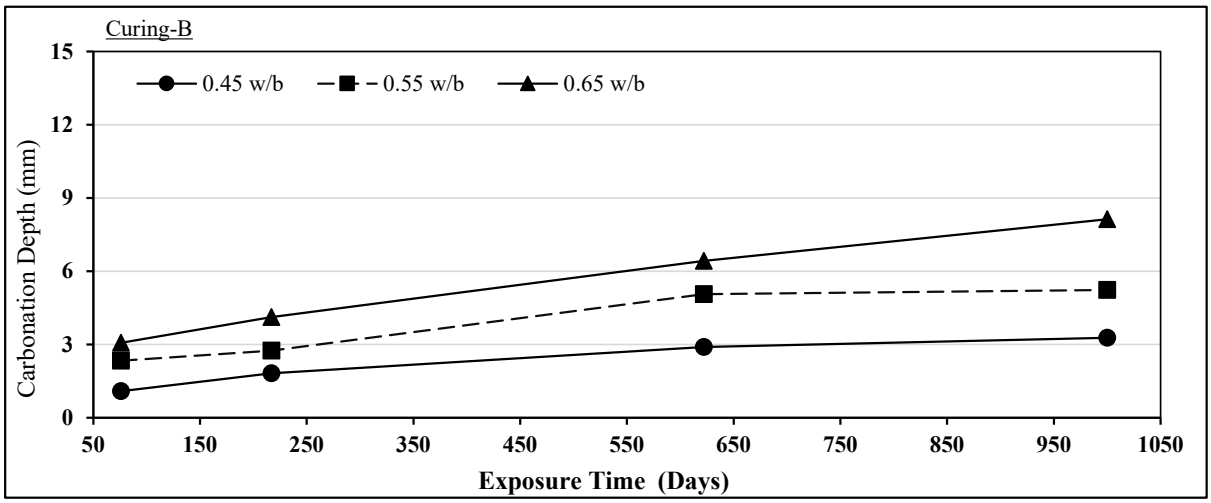

Figure D.62 Carbonation depth of LS concrete specimens exposed at site WE (Curing-B)

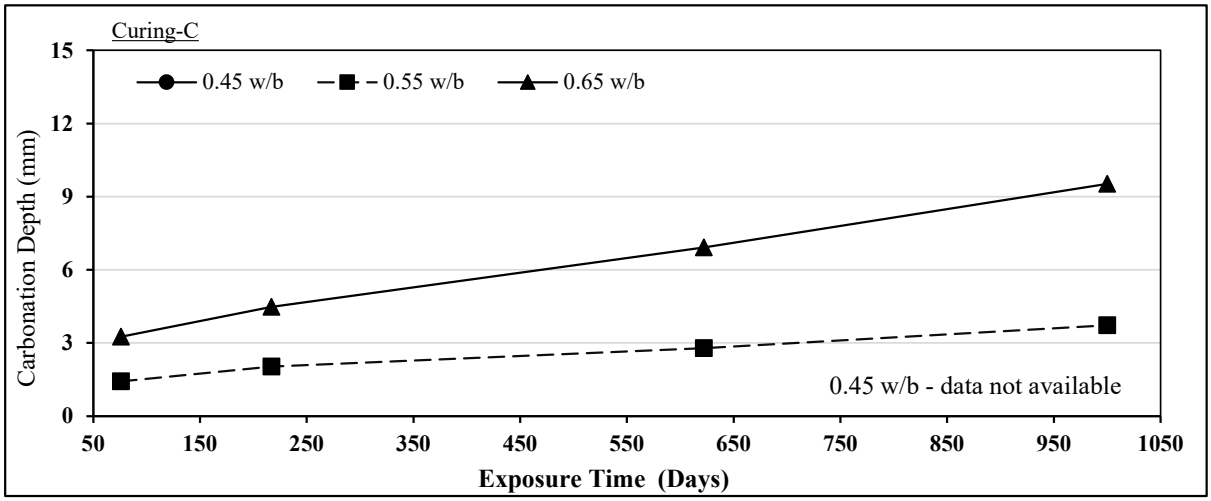

Figure D.63 Carbonation depth of LS concrete specimens exposed at site WE (Curing-C)

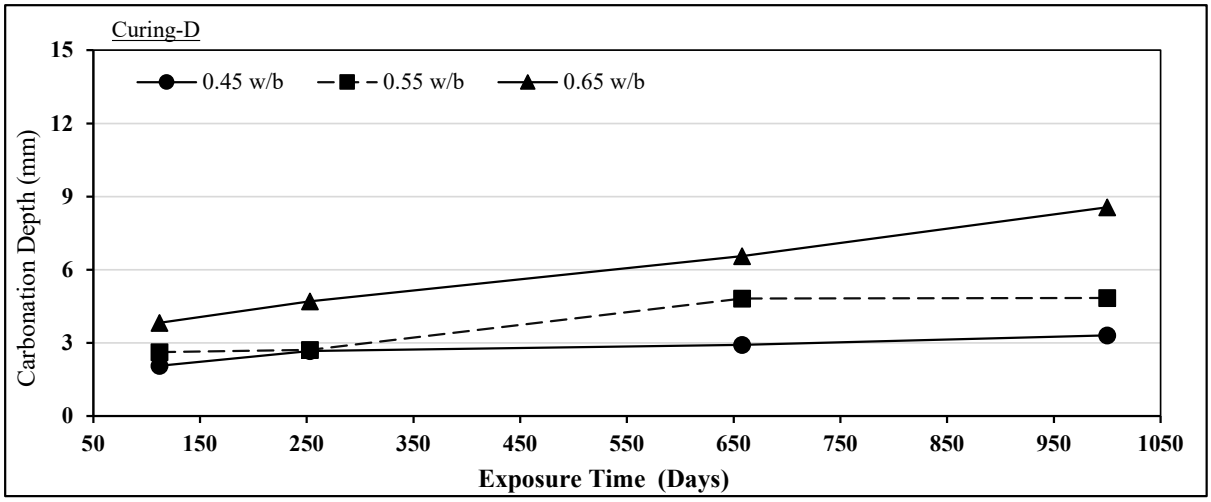

Figure D.64 Carbonation depth of LS concrete specimens exposed at site WE (Curing-D)

D.10 PROGRESSION OF CARBONATION DEPTH WITH TIME AT SITE WS

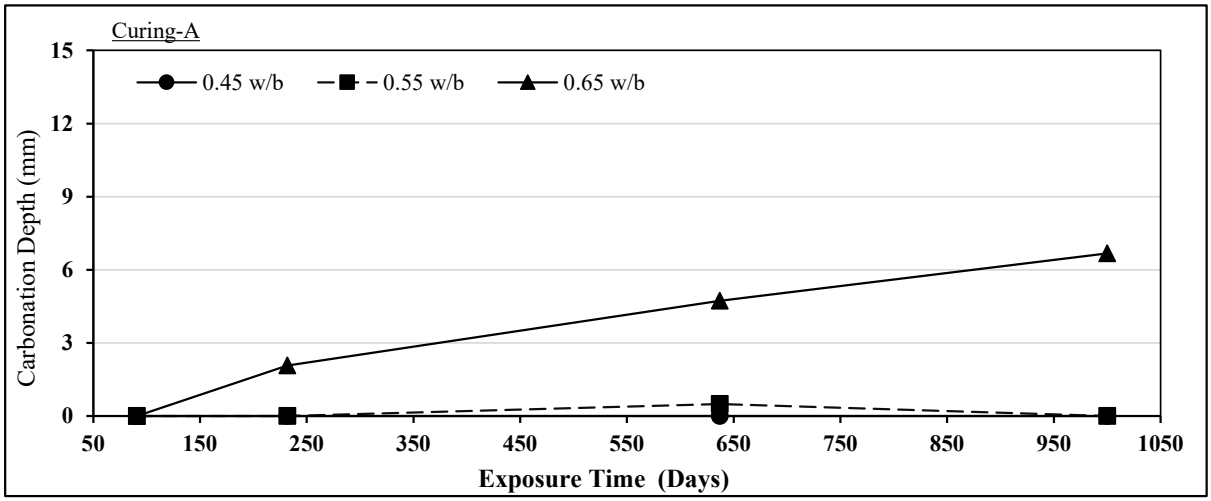

Figure D.65 Carbonation depth of PC concrete specimens exposed at site WS (Curing-A)

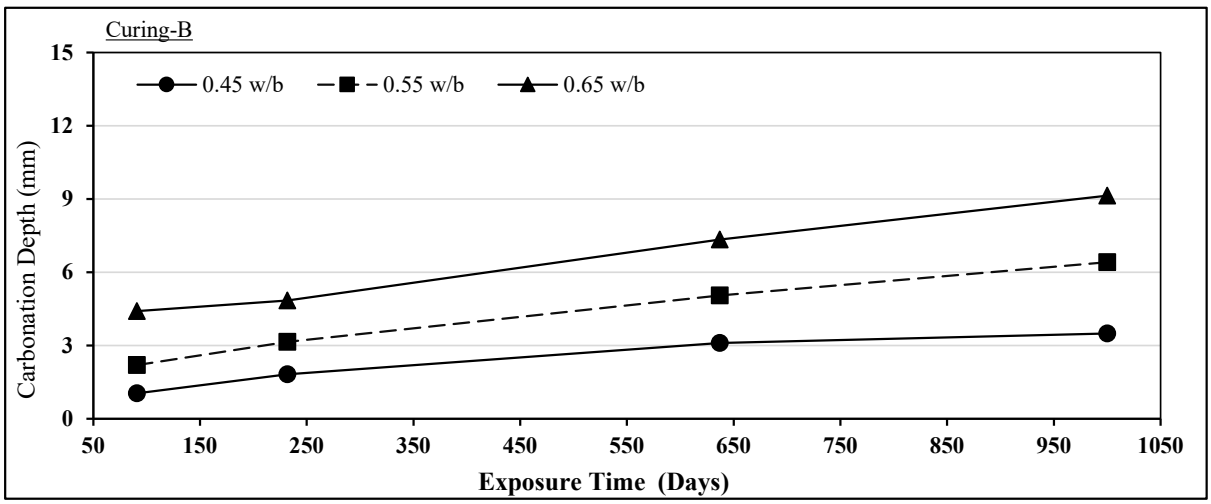

Figure D.66 Carbonation depth of PC concrete specimens exposed at site WS (Curing-B)

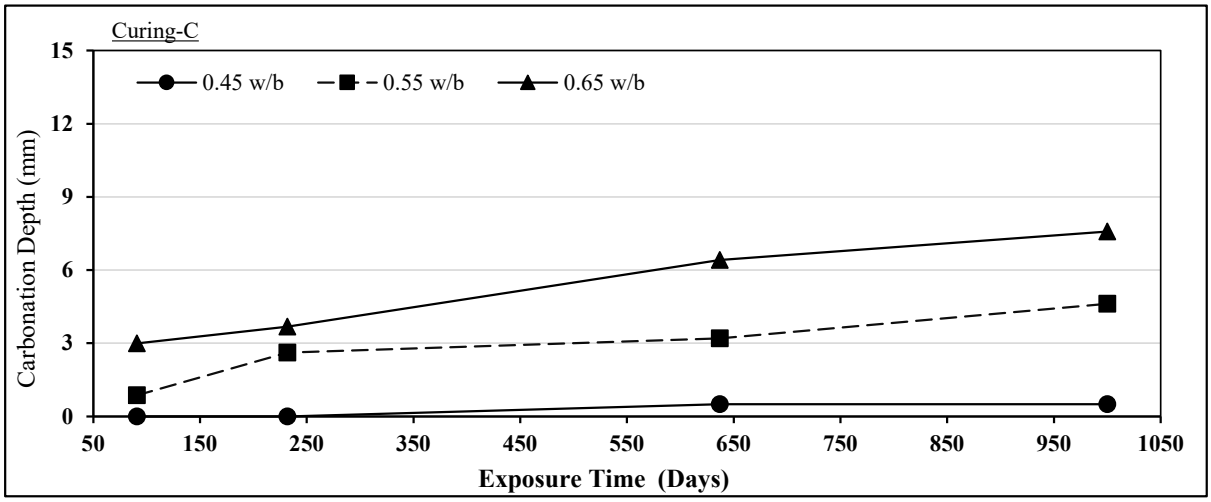

Figure D.67 Carbonation depth of PC concrete specimens exposed at site WS (Curing-C)

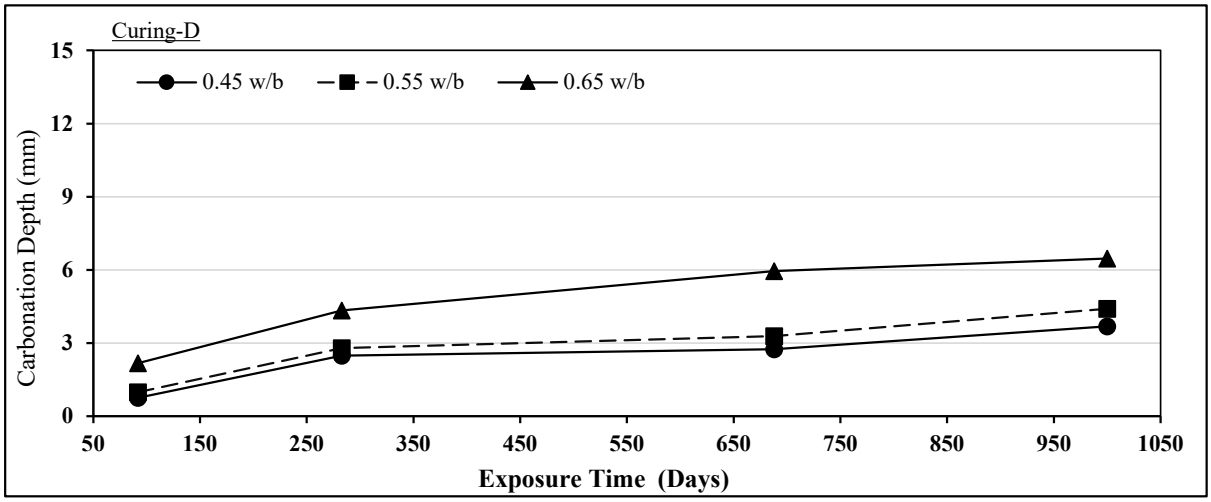

Figure D.68 Carbonation depth of PC concrete specimens exposed at site WS (Curing-D)

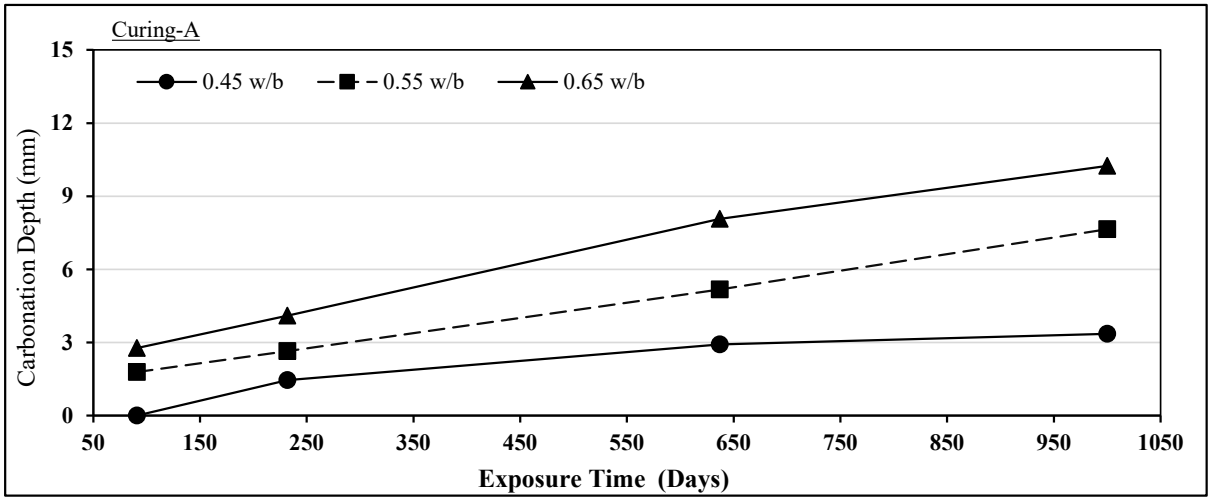

Figure D.69 Carbonation depth of FA concrete specimens exposed at site WS (Curing-A)

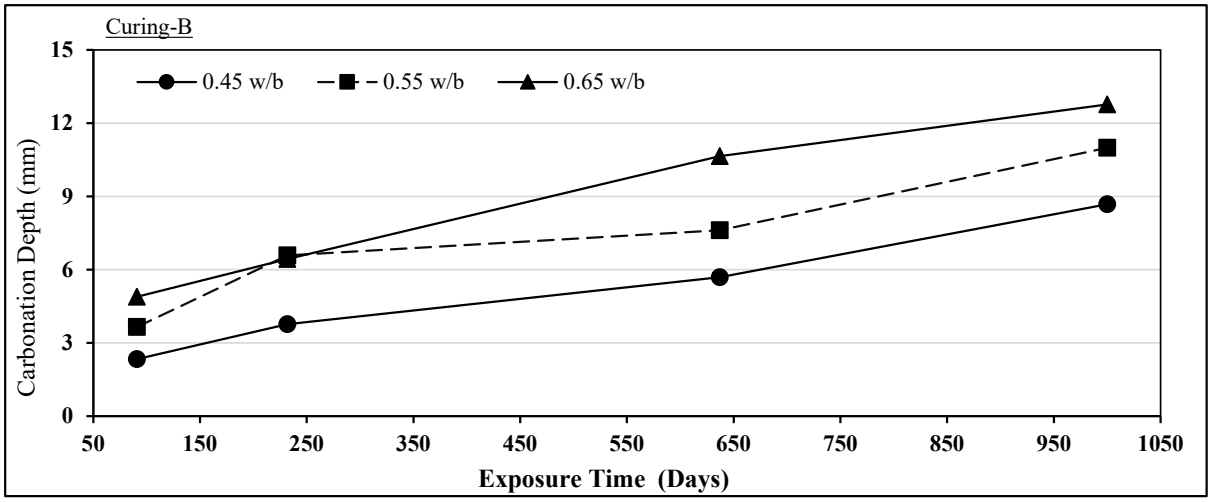

Figure D.70 Carbonation depth of FA concrete specimens exposed at site WS (Curing-B)

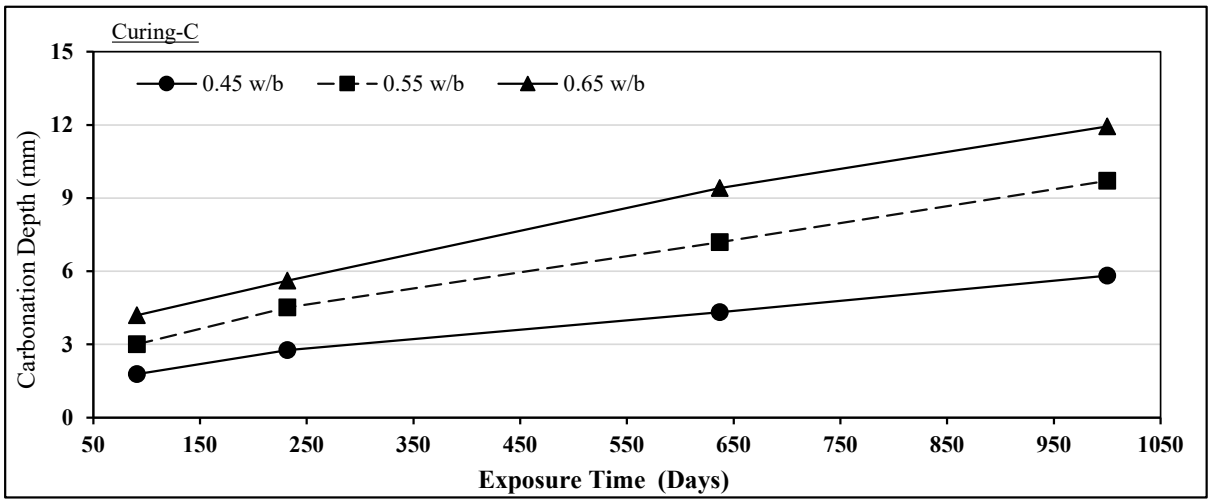

Figure D.71 Carbonation depth of FA concrete specimens exposed at site WS (Curing-C)

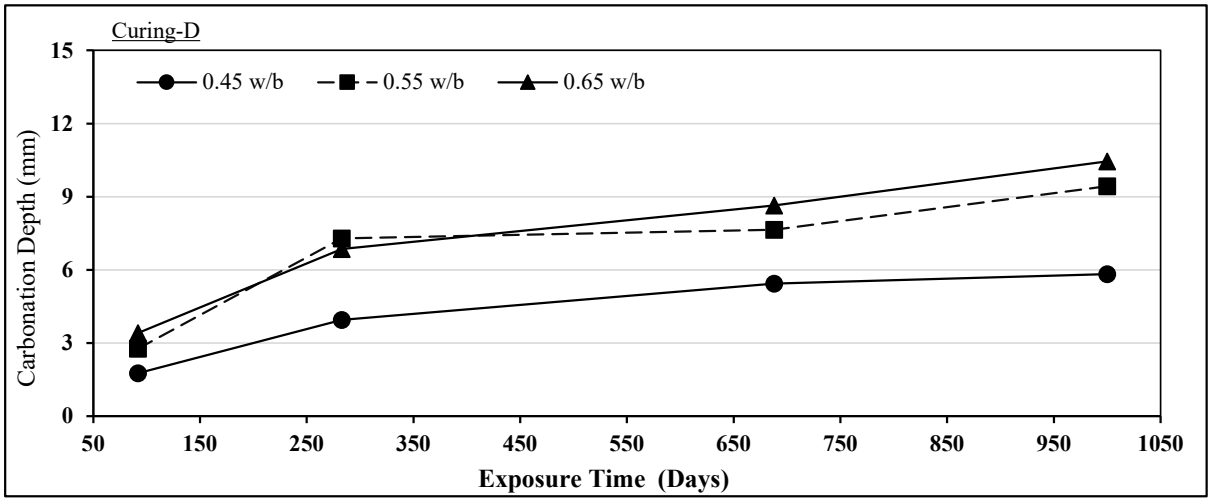

Figure D.72 Carbonation depth of FA concrete specimens exposed at site WS (Curing-D)

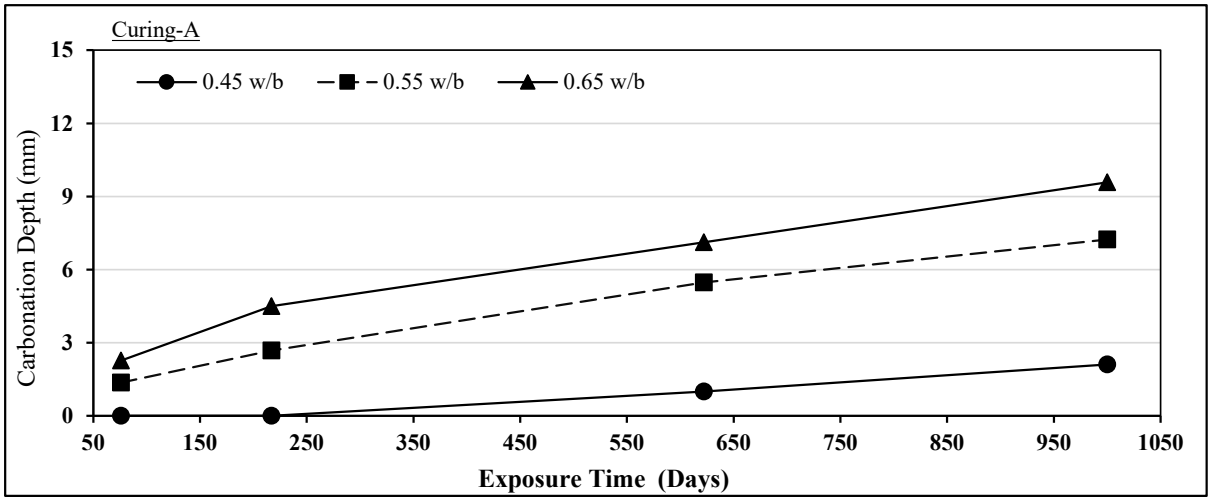

Figure D.73 Carbonation depth of GS concrete specimens exposed at site WS (Curing-A)

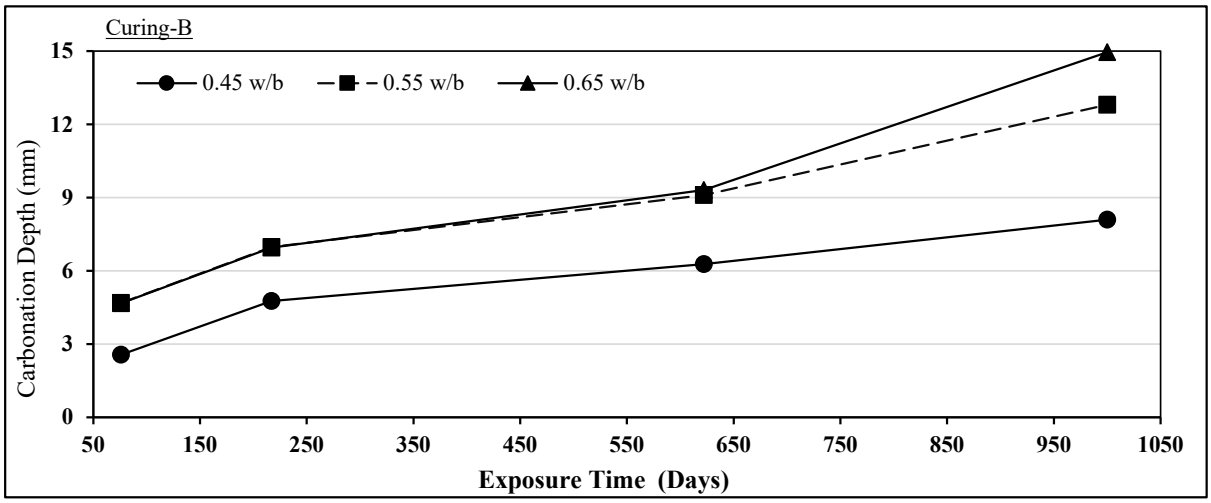

Figure D.74 Carbonation depth of GS concrete specimens exposed at site WS (Curing-B)

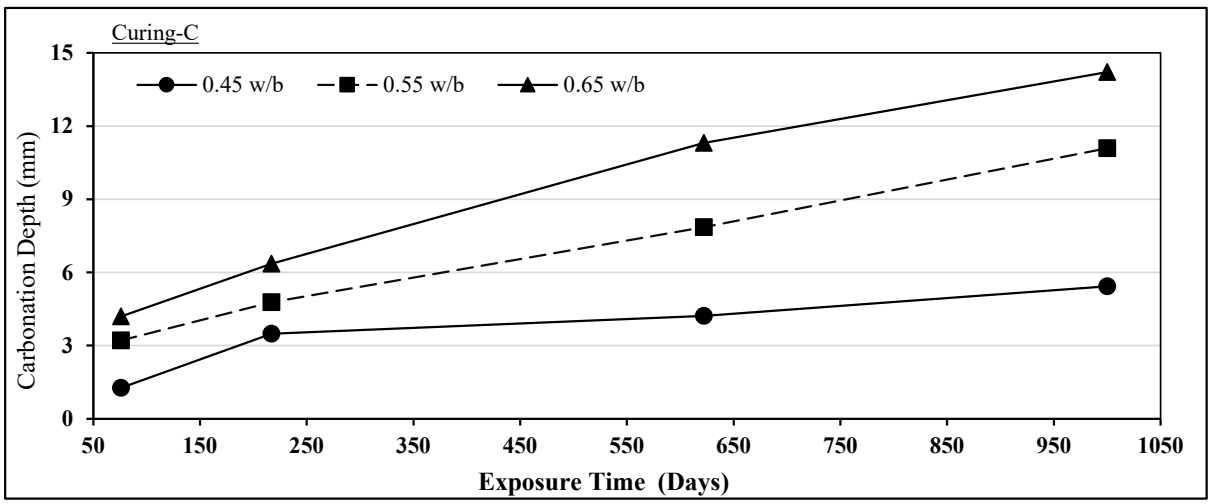

Figure D.75 Carbonation depth of GS concrete specimens exposed at site WS (Curing-C)

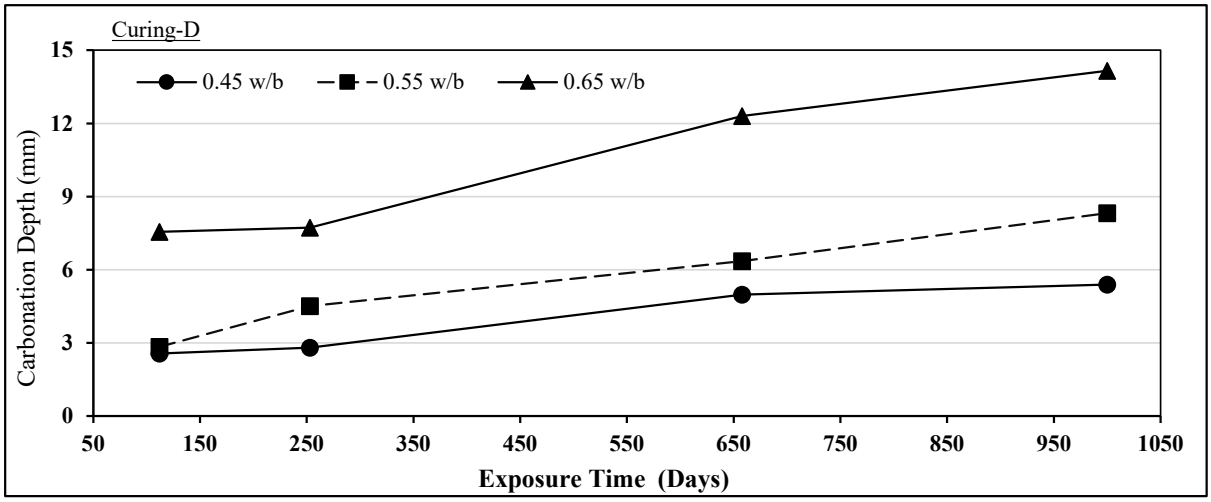

Figure D.76 Carbonation depth of GS concrete specimens exposed at site WS (Curing-D)

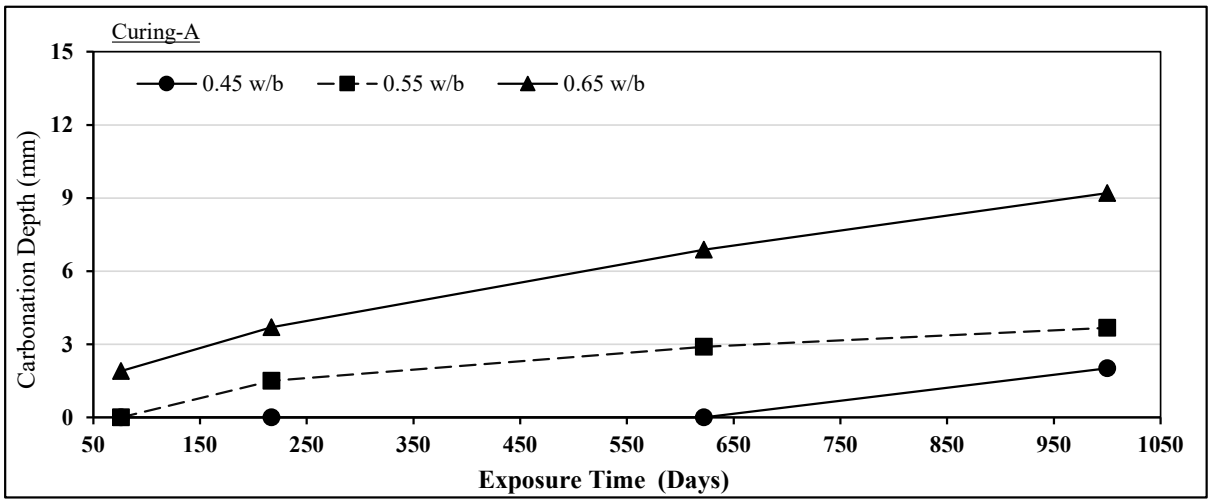

Figure D.77 Carbonation depth of LS concrete specimens exposed at site WS (Curing-A)

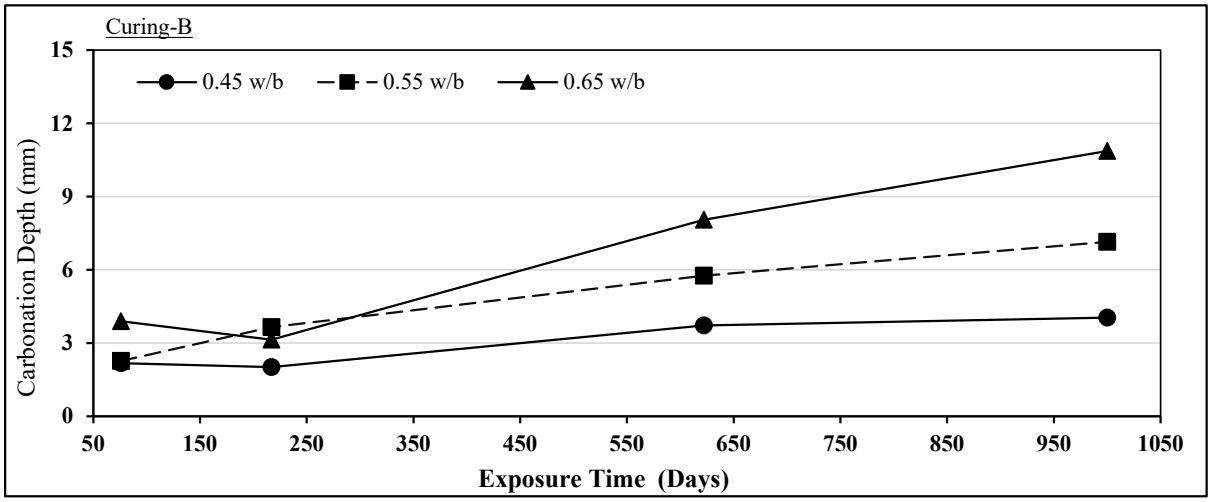

Figure D.78 Carbonation depth of LS concrete specimens exposed at site WS (Curing-B)

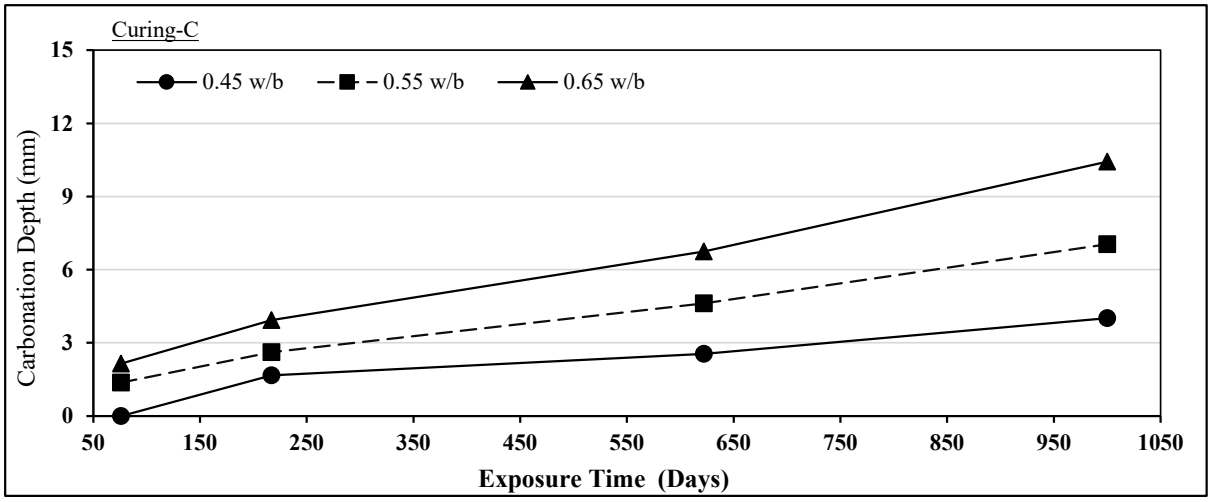

Figure D.79 Carbonation depth of LS concrete specimens exposed at site WS (Curing-C)

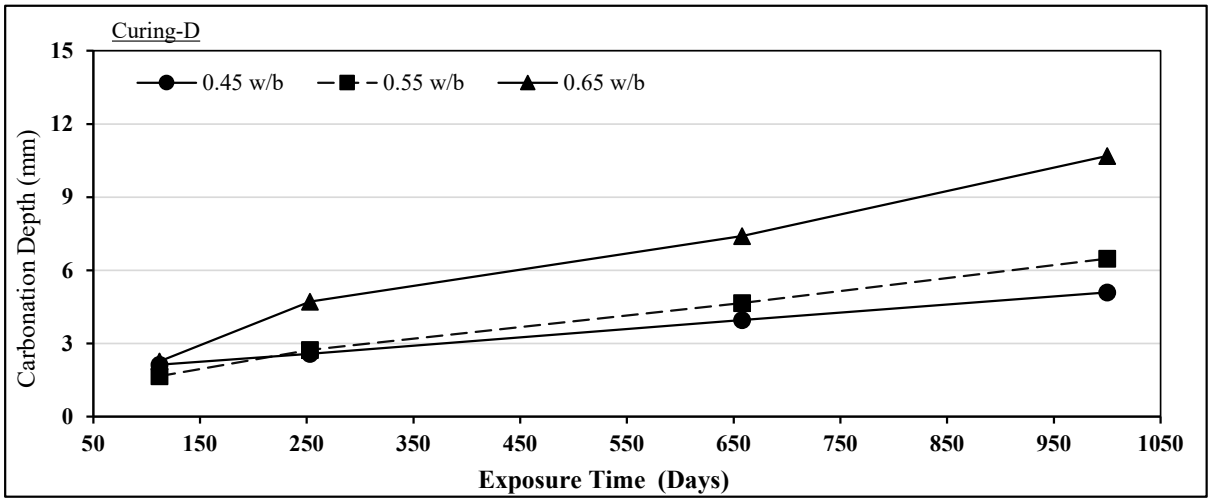

Figure D.80 Carbonation depth of LS concrete specimens exposed at site WS (Curing-D)

D.11 CARBONATION DEPTH OF CONCRETE AFTER 1000 DAYS OF EXPOSURE: (CURING-B, CURING-C AND CURING-D) VS CURING-A

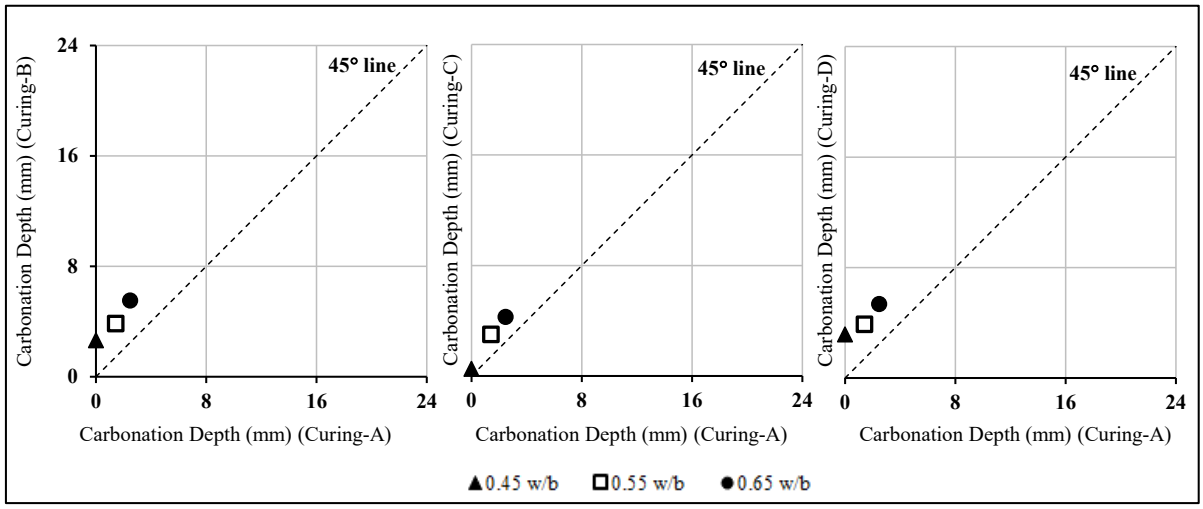

Figure D.81 Carbonation depth of PC concrete after 1000 days of exposure at ME: (Curing-B, Curing-C and Curing-D) vs Curing-A

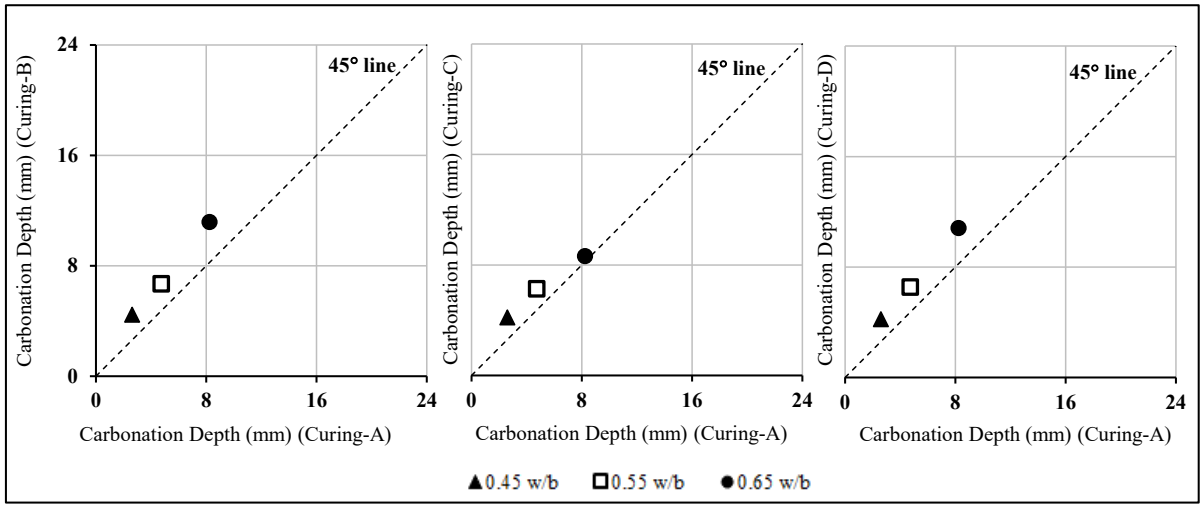

Figure D.82 Carbonation depth of FA concrete after 1000 days of exposure at ME: (Curing-B, Curing-C and Curing-D) vs Curing-A

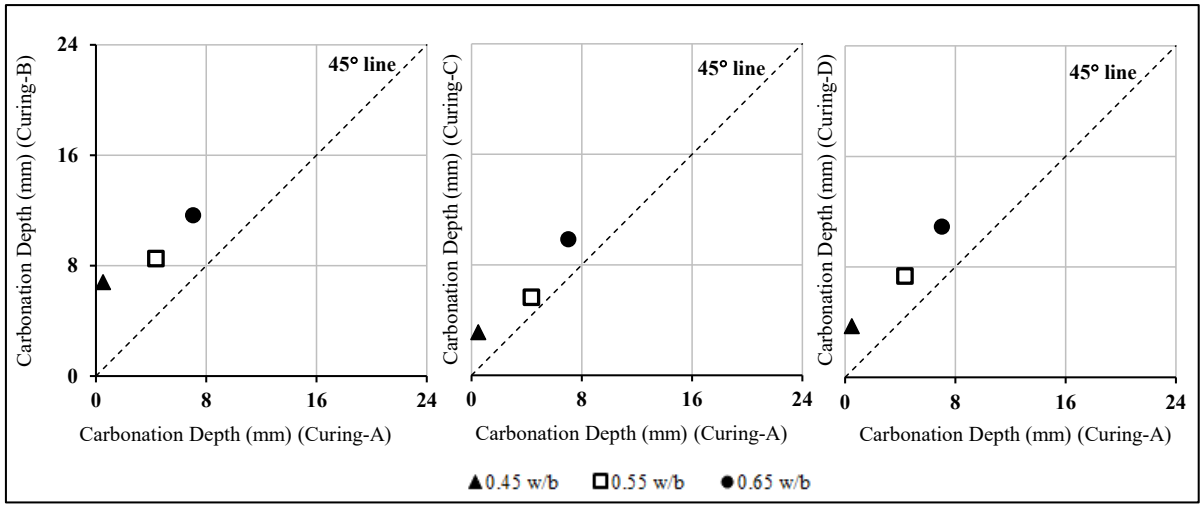

Figure D.83 Carbonation depth of GS concrete after 1000 days of exposure at ME: (Curing-B, Curing-C and Curing-D) vs Curing-A

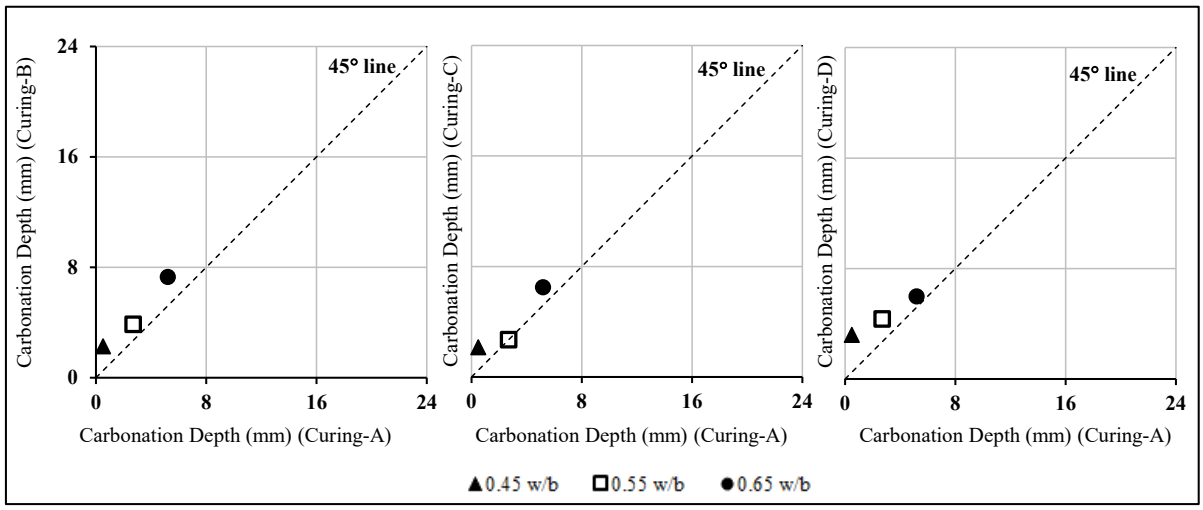

Figure D.84 Carbonation depth of LS concrete after 1000 days of exposure at ME: (Curing-B, Curing-C and Curing-D) vs Curing-A

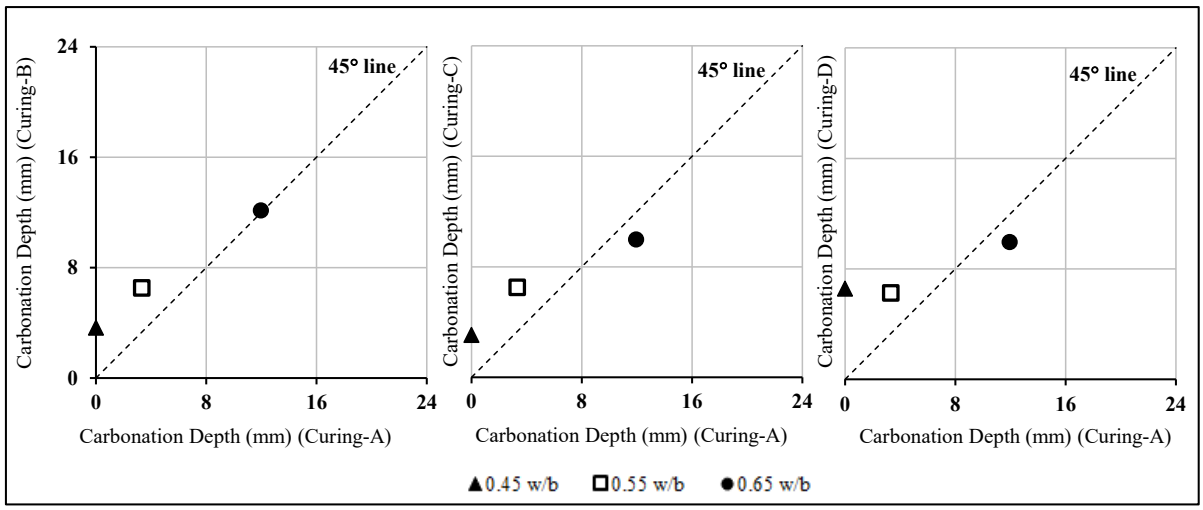

Figure D.85 Carbonation depth of PC concrete after 1000 days of exposure at MS: (Curing-B, Curing-C and Curing-D) vs Curing-A

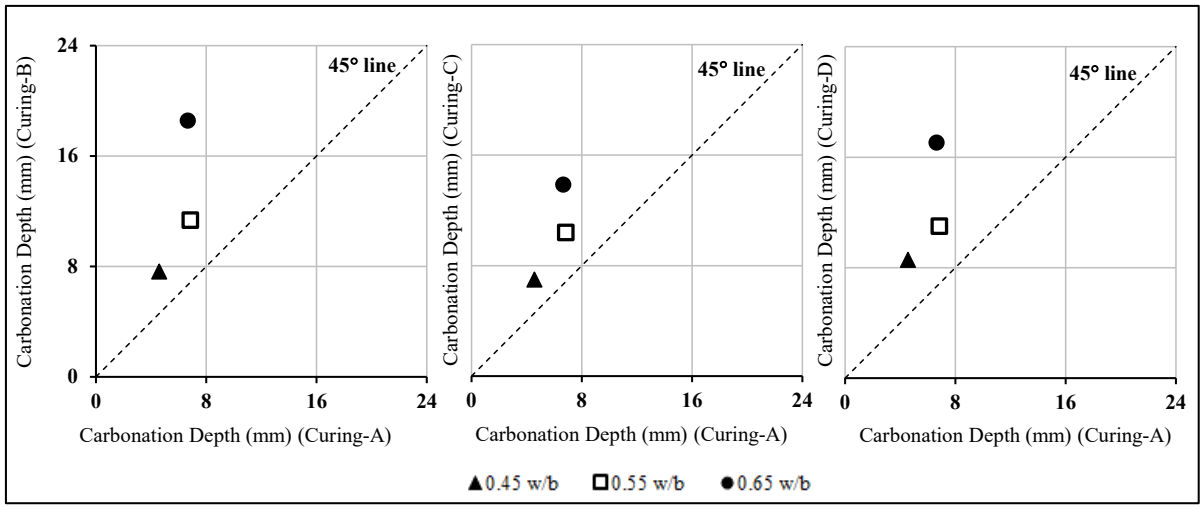

Figure D.86 Carbonation depth of FA concrete after 1000 days of exposure at MS: (Curing-B, Curing-C and Curing-D) vs Curing-A

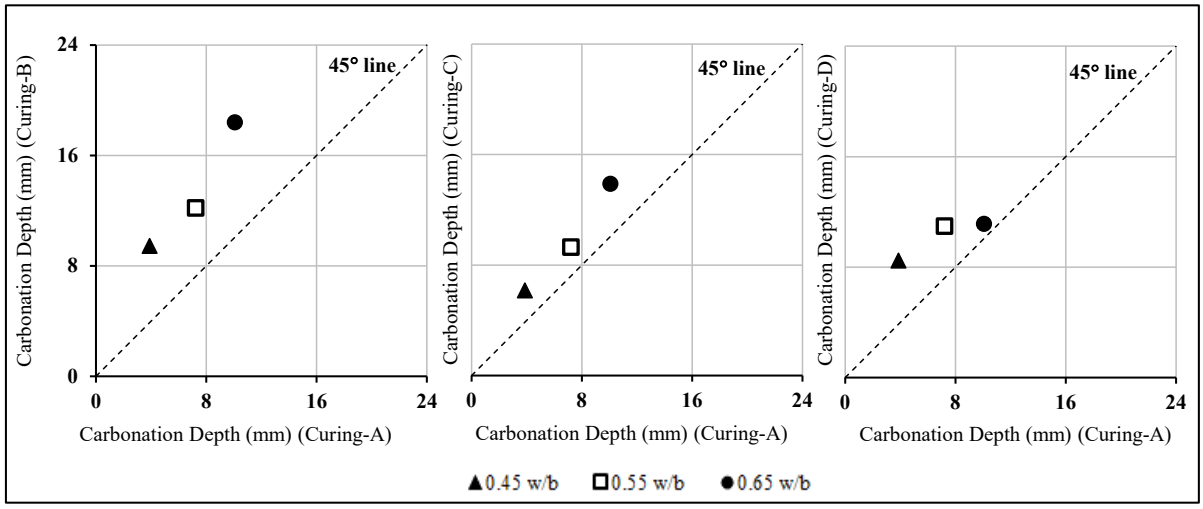

Figure D.87 Carbonation depth of GS concrete after 1000 days of exposure at MS: (Curing-B, Curing-C and Curing-D) vs Curing-A

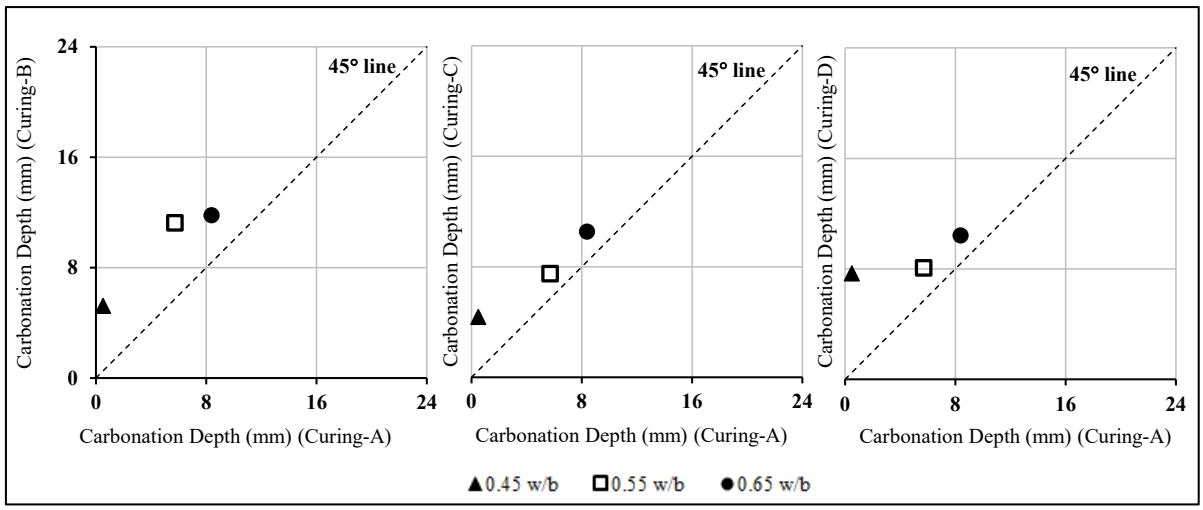

Figure D.88 Carbonation depth of LS concrete after 1000 days of exposure at MS: (Curing-B, Curing-C and Curing-D) vs Curing-A

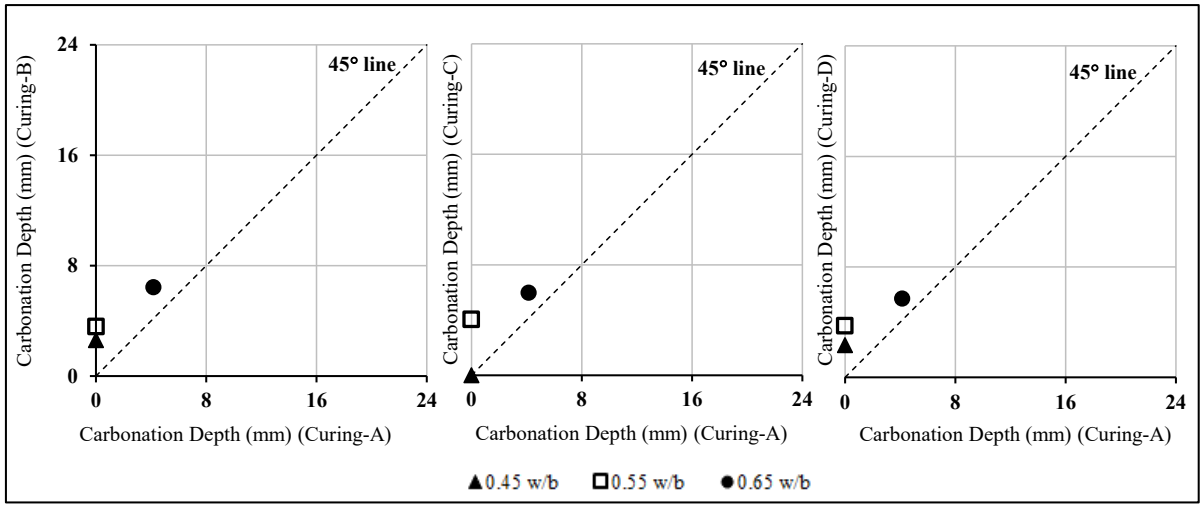

Figure D.89 Carbonation depth of PC concrete after 1000 days of exposure at WE: (Curing-B, Curing-C and Curing-D) vs Curing-A

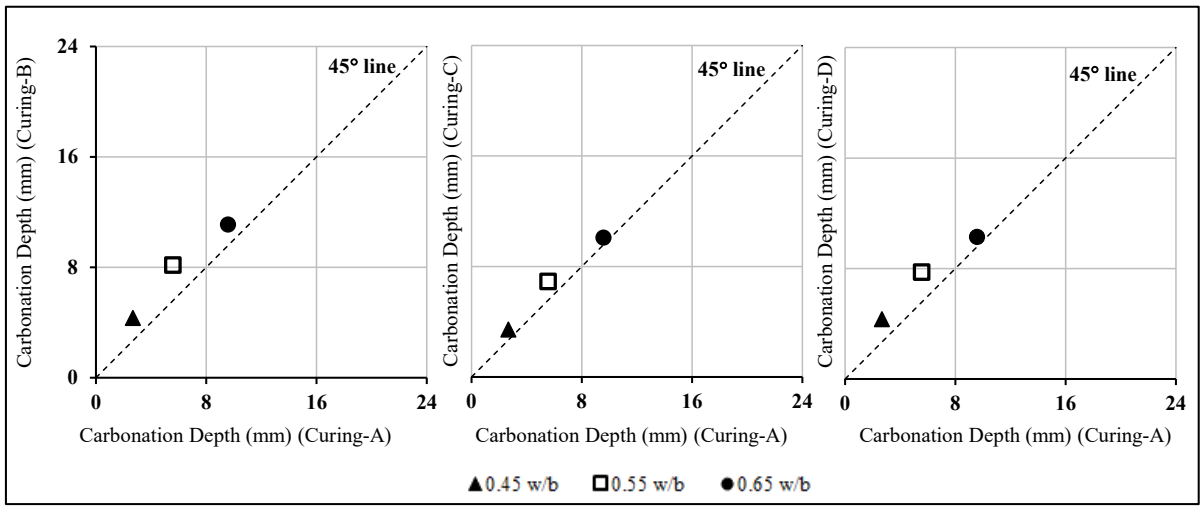

Figure D.90 Carbonation depth of FA concrete after 1000 days of exposure at WE: (Curing-B, Curing-C and Curing-D) vs Curing-A

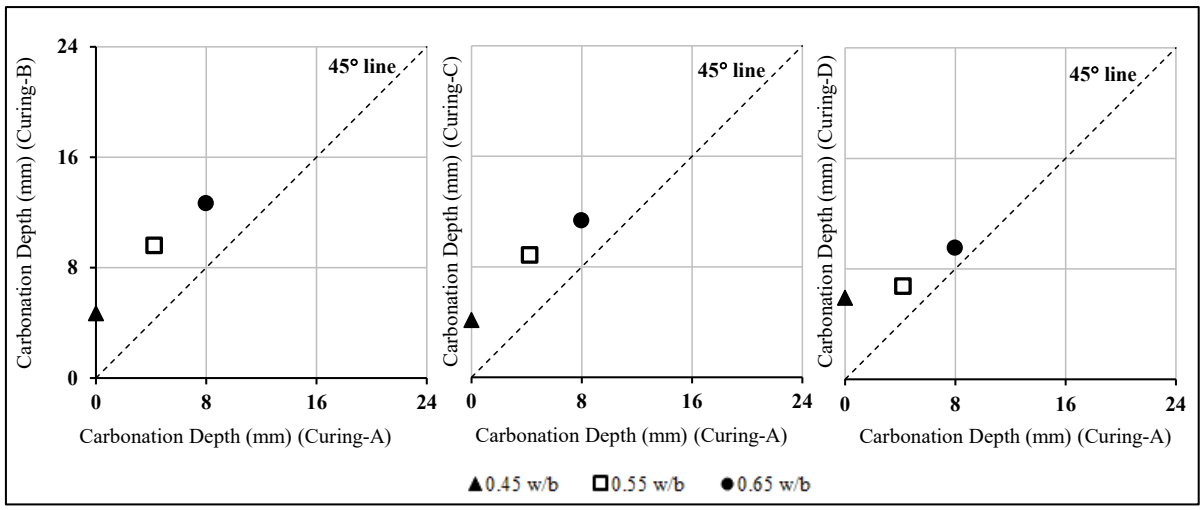

Figure D.91 Carbonation depth of GS concrete after 1000 days of exposure at WE: (Curing-B, Curing-C and Curing-D) vs Curing-A

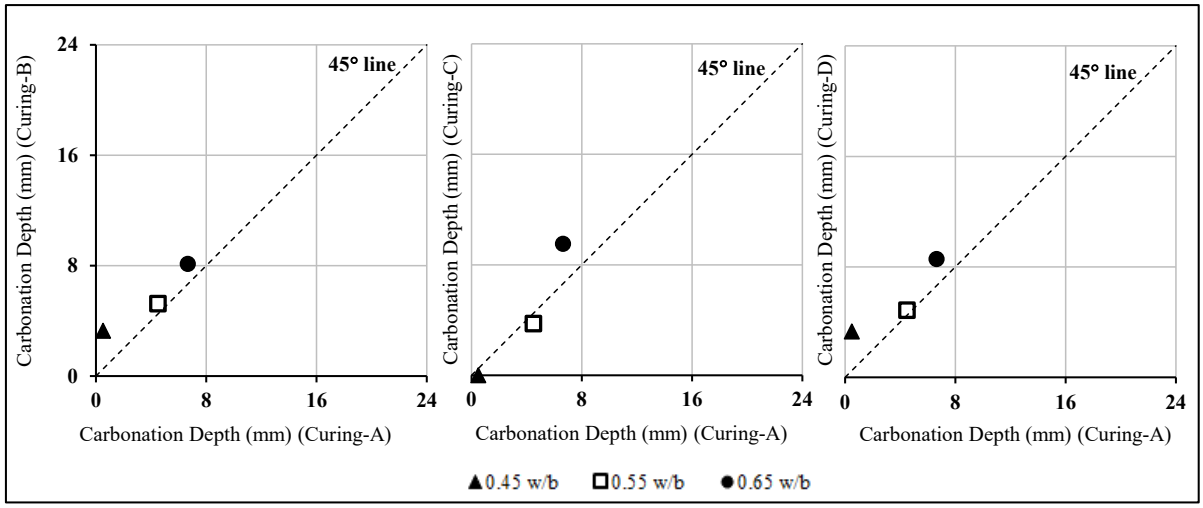

Figure D.92 Carbonation depth of LS concrete after 1000 days of exposure at WE: (Curing-B, Curing-C and Curing-D) vs Curing-A

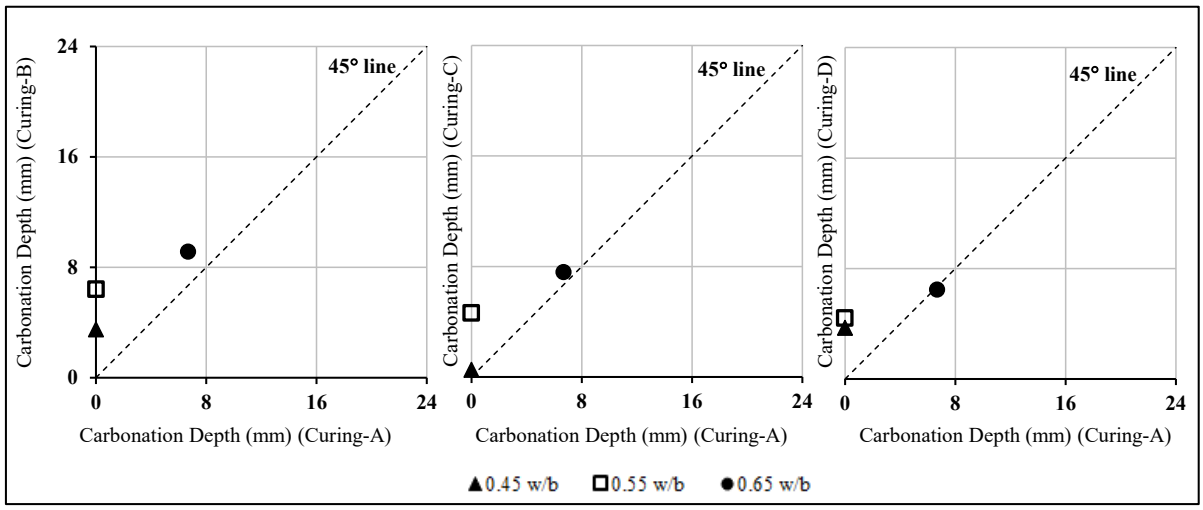

Figure D.93 Carbonation depth of PC concrete after 1000 days of exposure at WS: (Curing-B, Curing-C and Curing-D) vs Curing-A

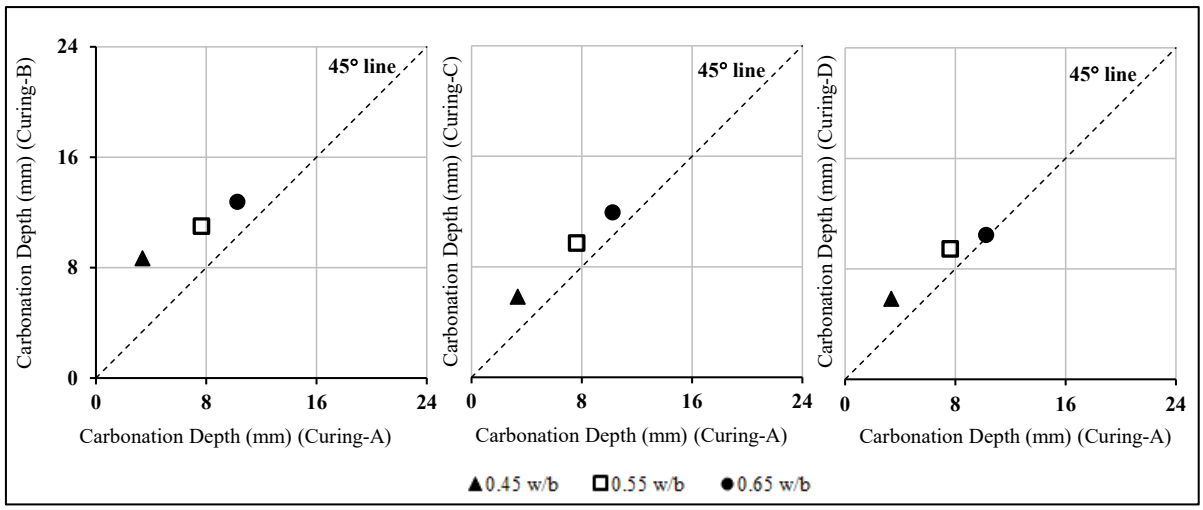

Figure D.94 Carbonation depth of FA concrete after 1000 days of exposure at WS: (Curing-B, Curing-C and Curing-D) vs Curing-A

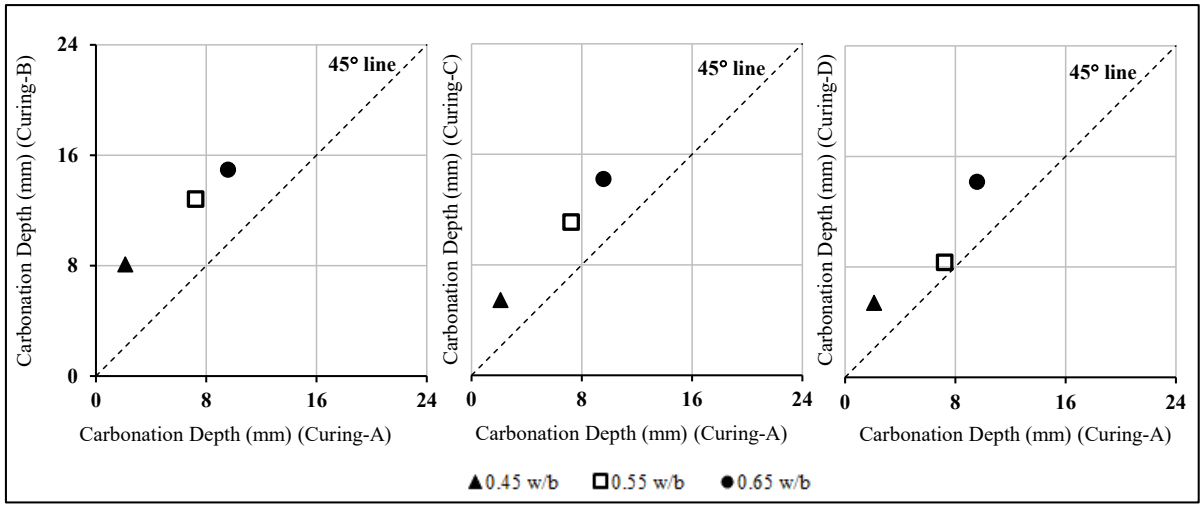

Figure D.95 Carbonation depth of GS concrete after 1000 days of exposure at WS: (Curing-B, Curing-C and Curing-D) vs Curing-A

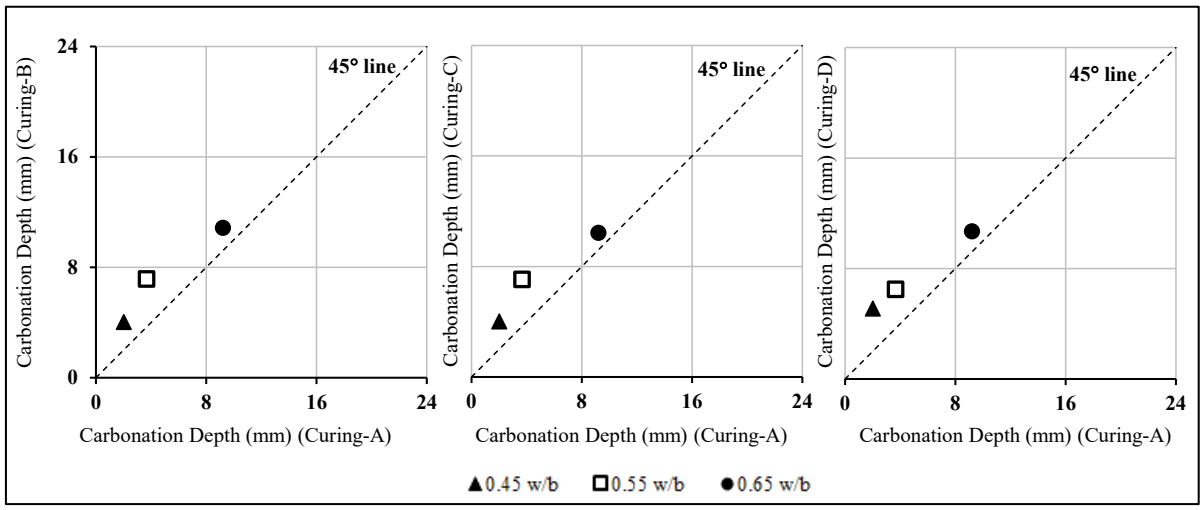

Figure D.96 Carbonation depth of LS concrete after 1000 days of exposure at WS: (Curing-B, Curing-C and Curing-D) vs Curing-A

D.12 CARBONATION DEPTH OF CONCRETE AFTER 1000 DAYS OF EXPOSURE: (FA, GS AND LS) VS PC CONCRETE

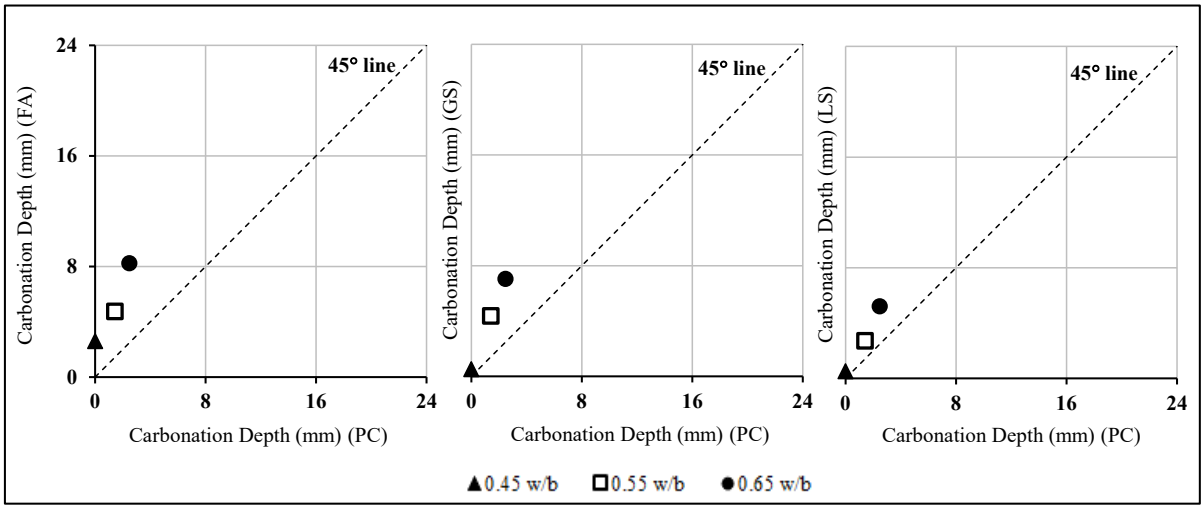

Figure D.97 Carbonation depth of specimens with Curing-A, after 1000 days of exposure at site ME: (FA, GS and LS) vs PC concrete

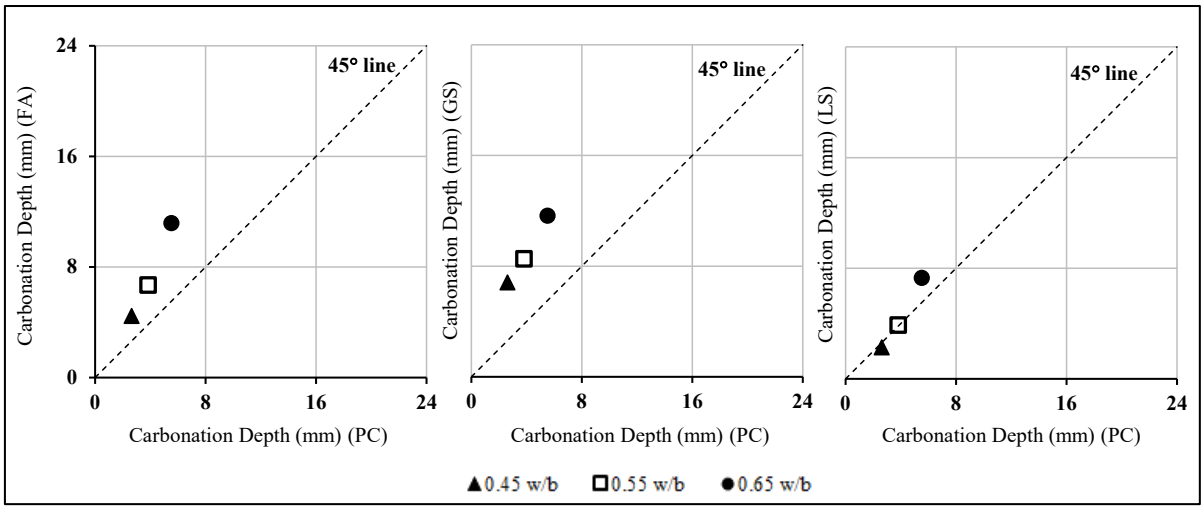

Figure D.98 Carbonation depth of specimens with Curing-B, after 1000 days of exposure at site ME: (FA, GS and LS) vs PC concrete

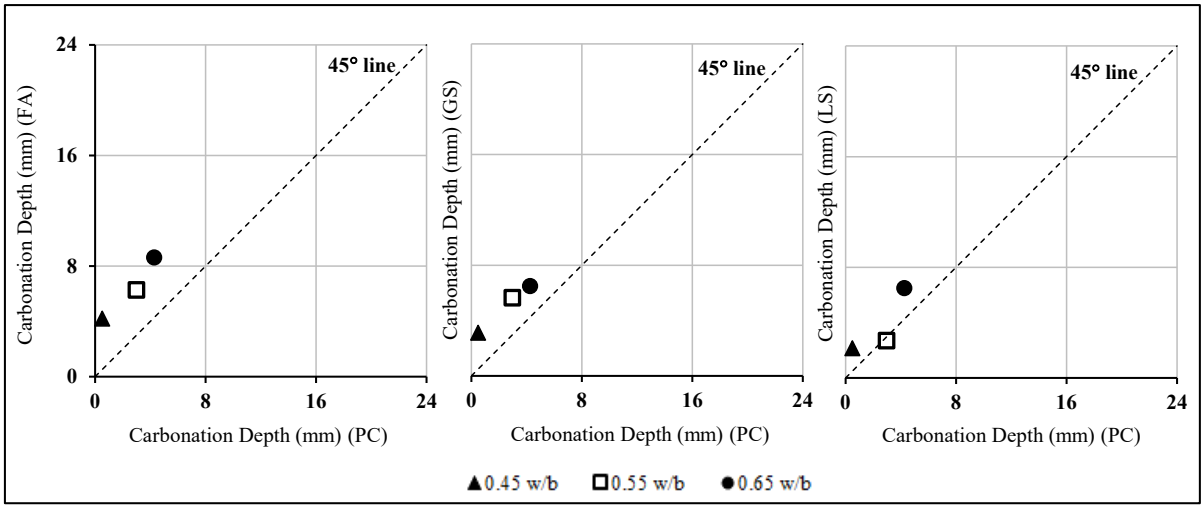

Figure D.99 Carbonation depth of specimens with Curing-C, after 1000 days of exposure at site ME: (FA, GS and LS) vs PC concrete

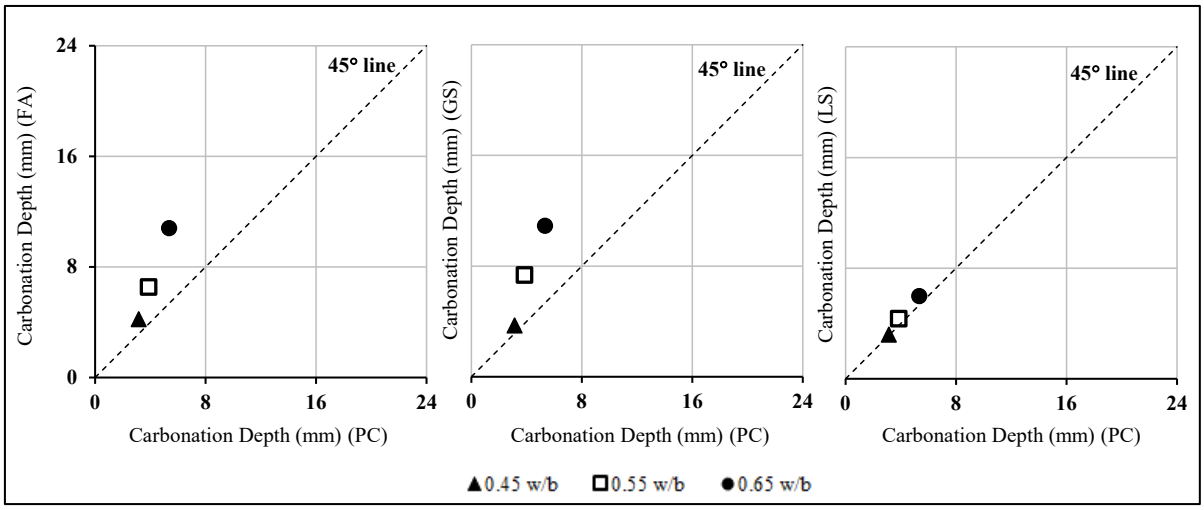

Figure D.100 Carbonation depth of specimens with Curing-D, after 1000 days of exposure at site ME: (FA, GS and LS) vs PC concrete

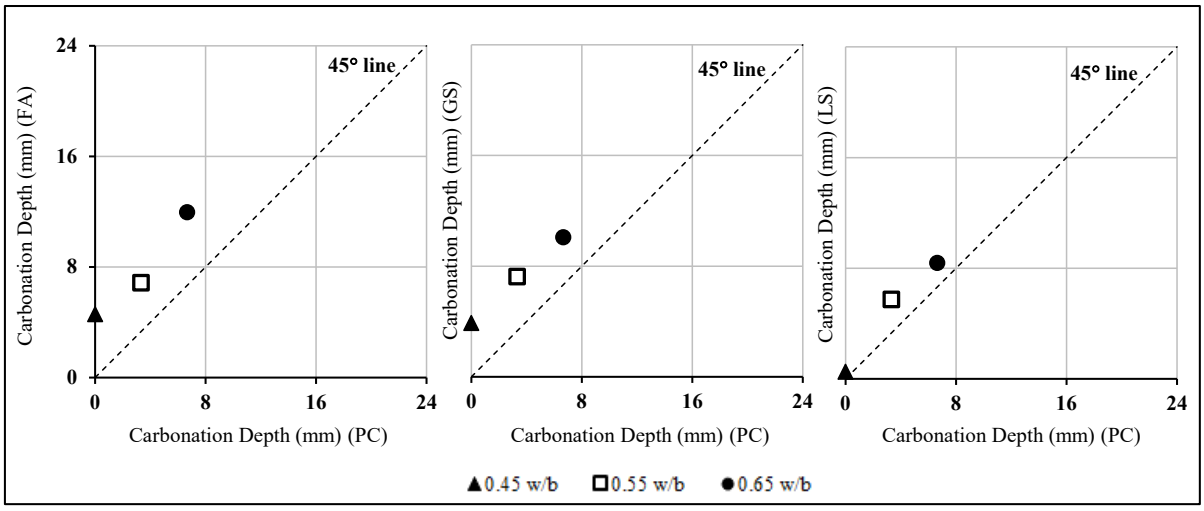

Figure D.101 Carbonation depth of specimens with Curing-A, after 1000 days of exposure at site MS: (FA, GS and LS) vs PC concrete

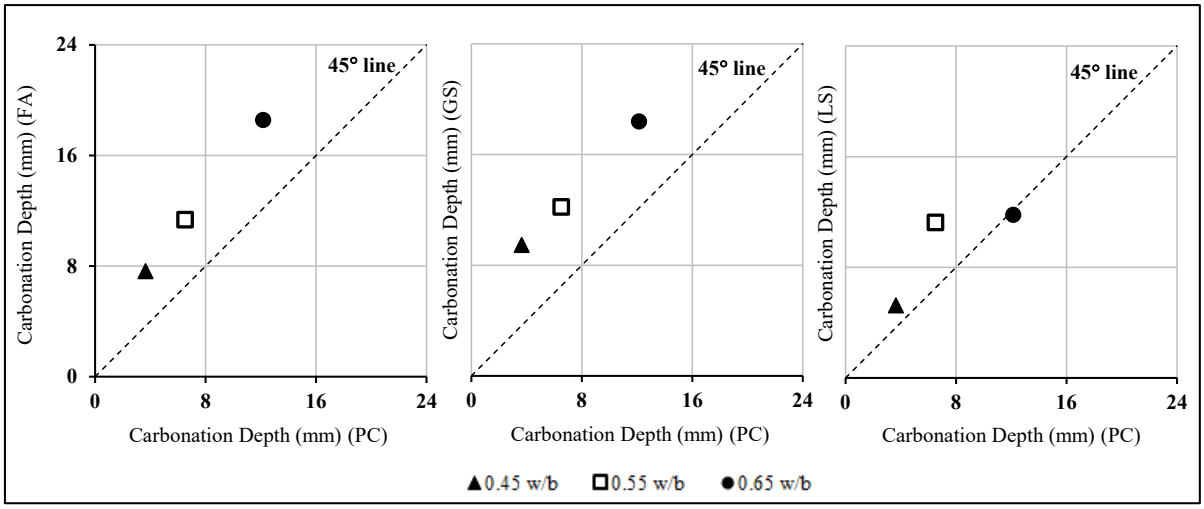

Figure D.102 Carbonation depth of specimens with Curing-B, after 1000 days of exposure at site MS: (FA, GS and LS) vs PC concrete

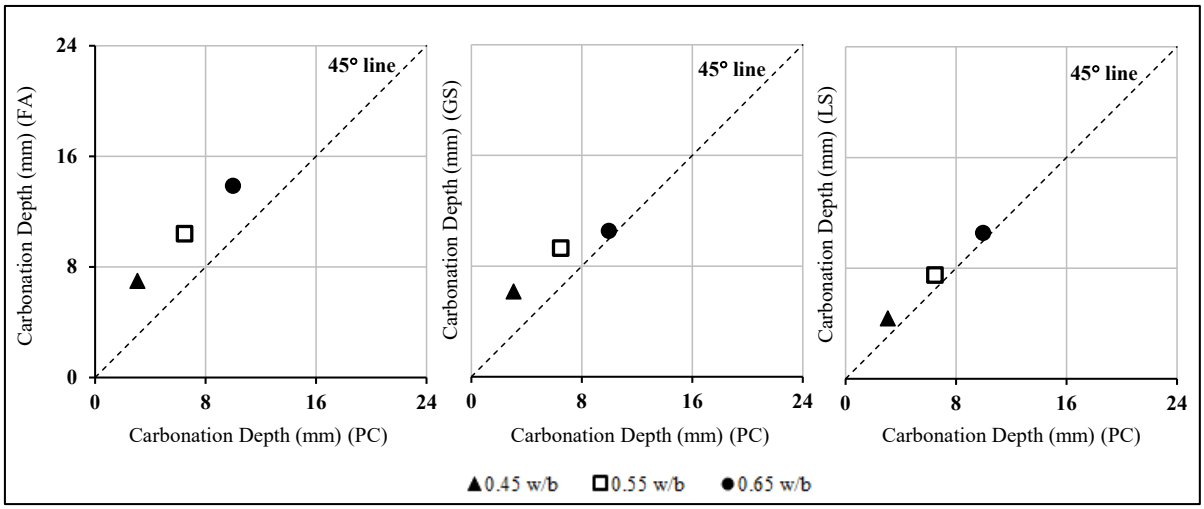

Figure D.103 Carbonation depth of specimens with Curing-C, after 1000 days of exposure at site MS: (FA, GS and LS) vs PC concrete

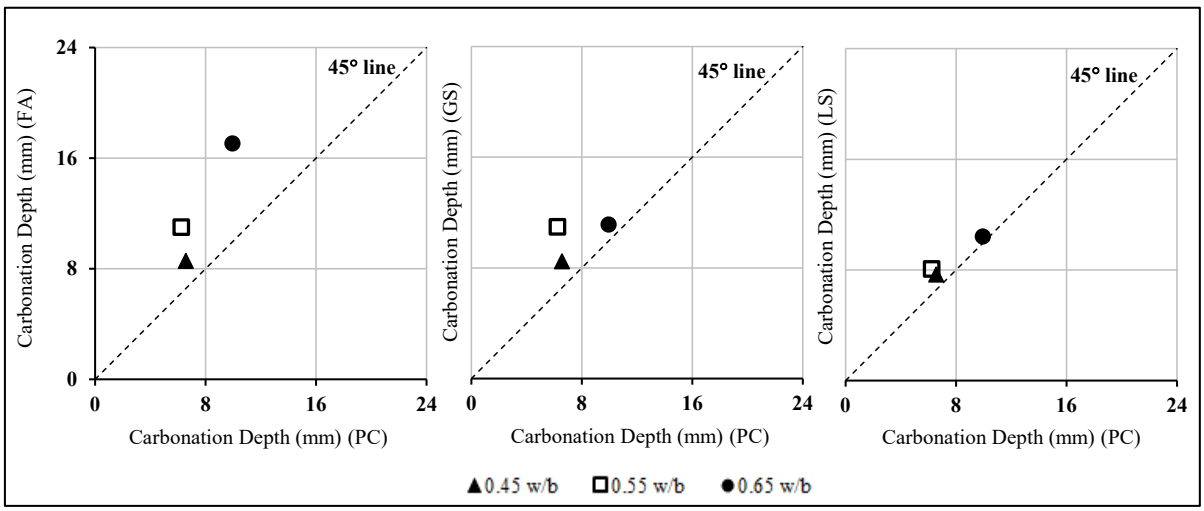

Figure D.104 Carbonation depth of specimens with Curing-D, after 1000 days of exposure at site MS: (FA, GS and LS) vs PC concrete

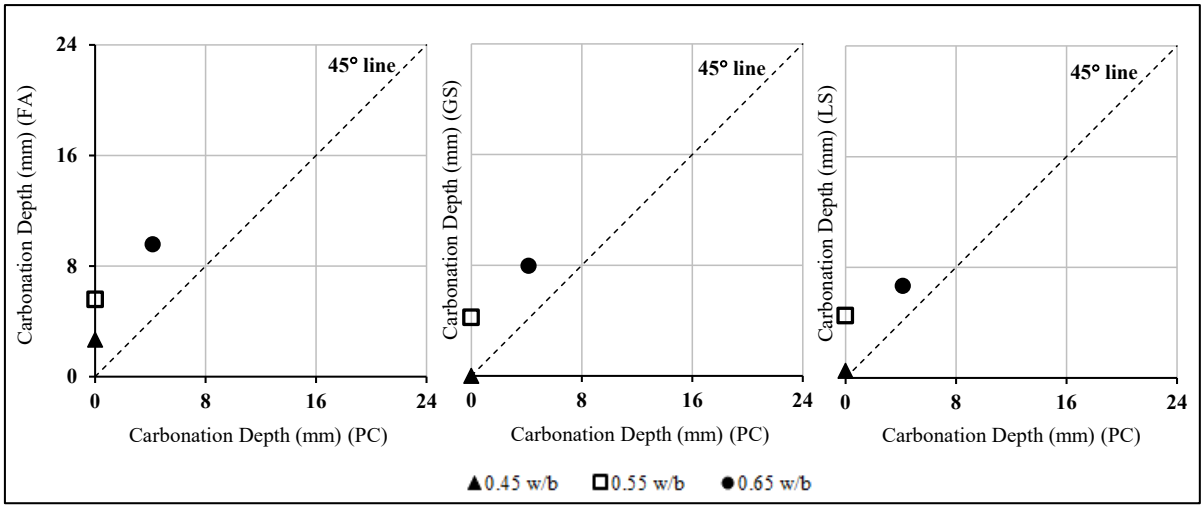

Figure D.105 Carbonation depth of specimens with Curing-A, after 1000 days of exposure at site WE: (FA, GS and LS) vs PC concrete

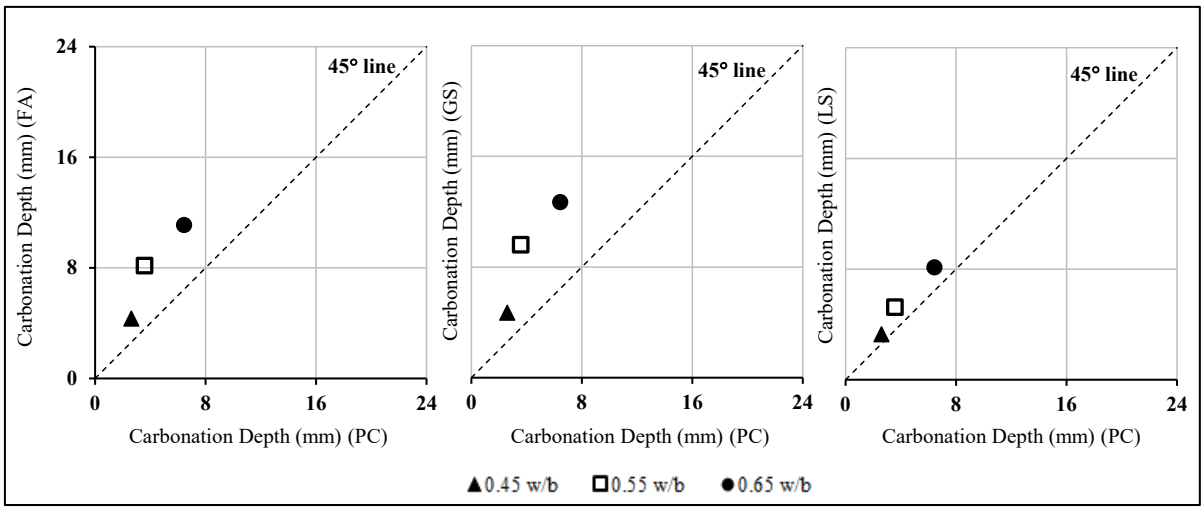

Figure D.106 Carbonation depth of specimens with Curing-B, after 1000 days of exposure at site WE: (FA, GS and LS) vs PC concrete

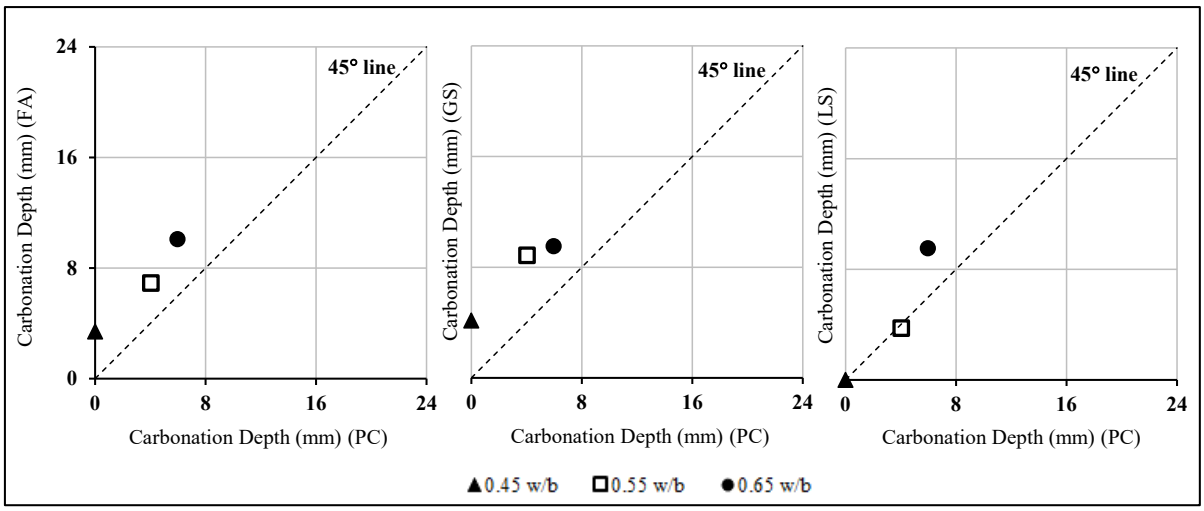

Figure D.107 Carbonation depth of specimens with Curing-C, after 1000 days of exposure at site WE: (FA, GS and LS) vs PC concrete

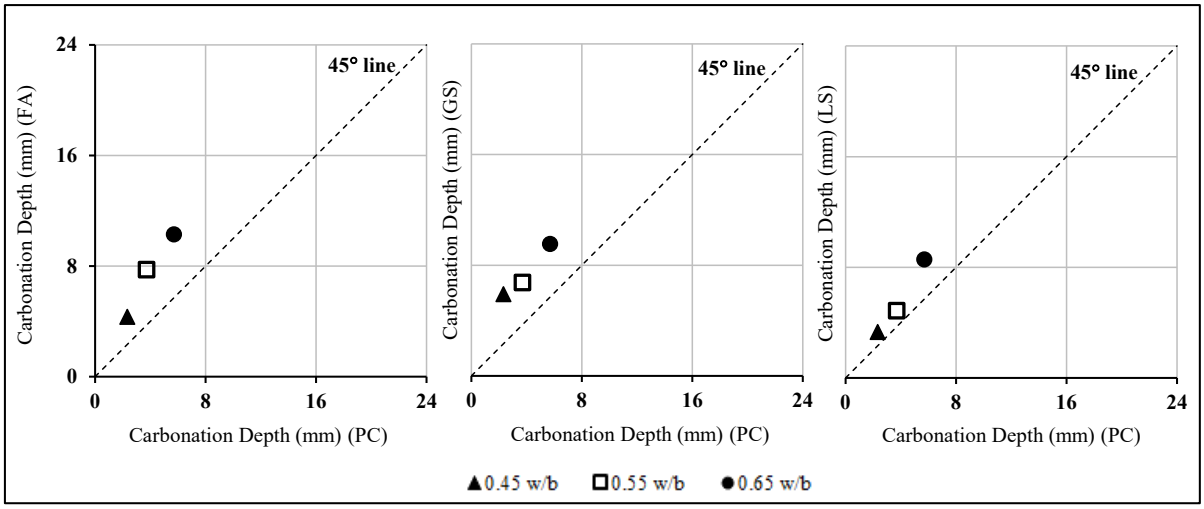

Figure D.108 Carbonation depth of specimens with Curing-D, after 1000 days of exposure at site WE: (FA, GS and LS) vs PC concrete

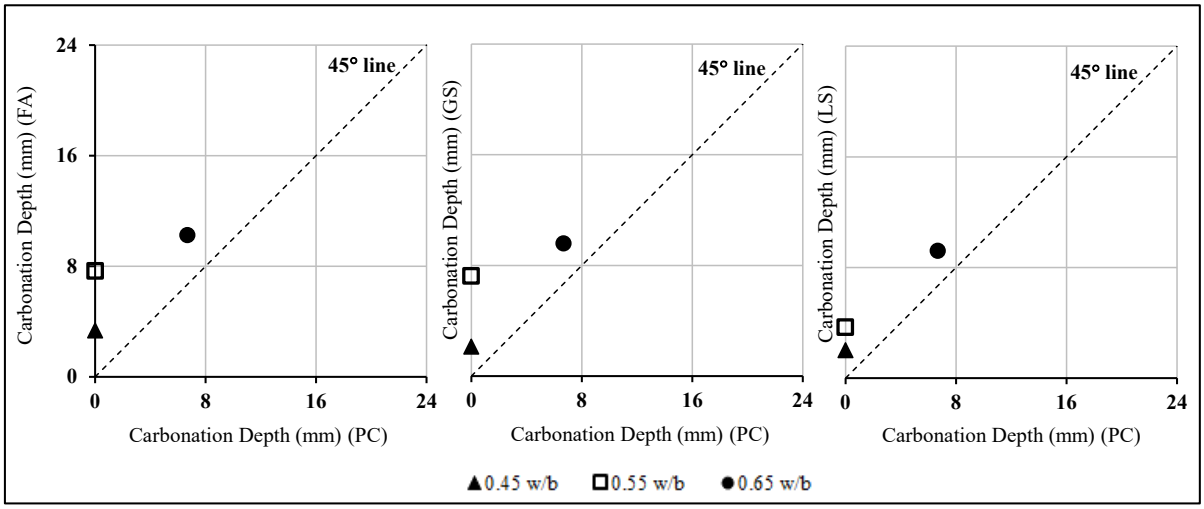

Figure D.109 Carbonation depth of specimens with Curing-A, after 1000 days of exposure at site WS: (FA, GS and LS) vs PC concrete

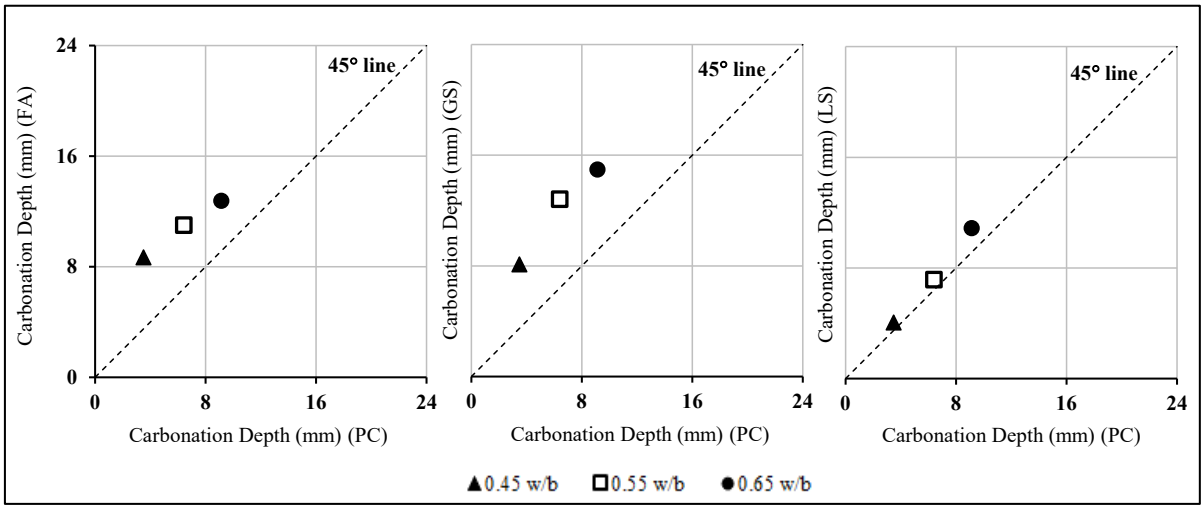

Figure D.110 Carbonation depth of specimens with Curing-B, after 1000 days of exposure at site WS: (FA, GS and LS) vs PC concrete

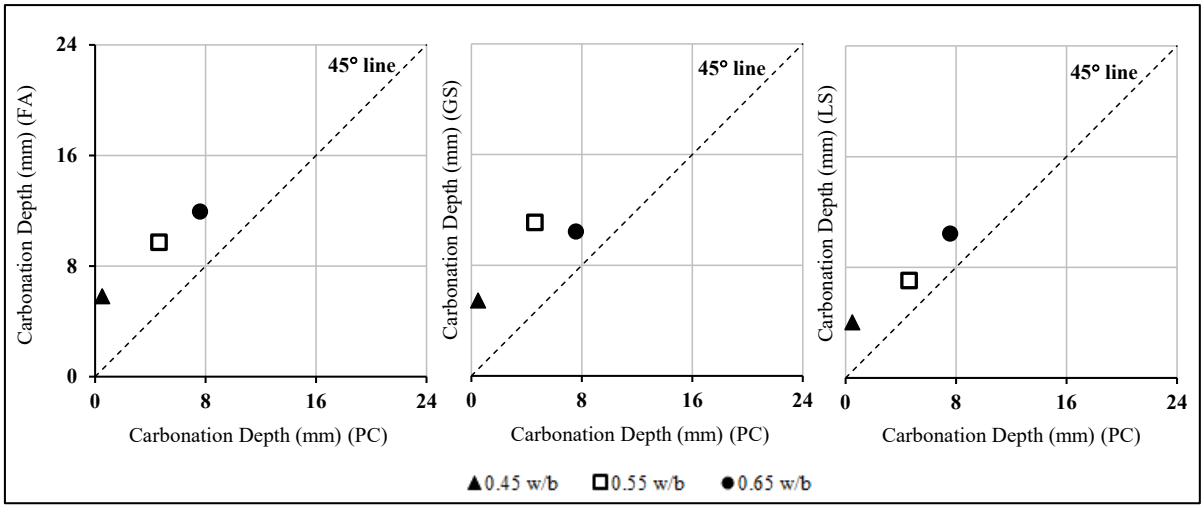

Figure D.111 Carbonation depth of specimens with Curing-C, after 1000 days of exposure at site WS: (FA, GS and LS) vs PC concrete

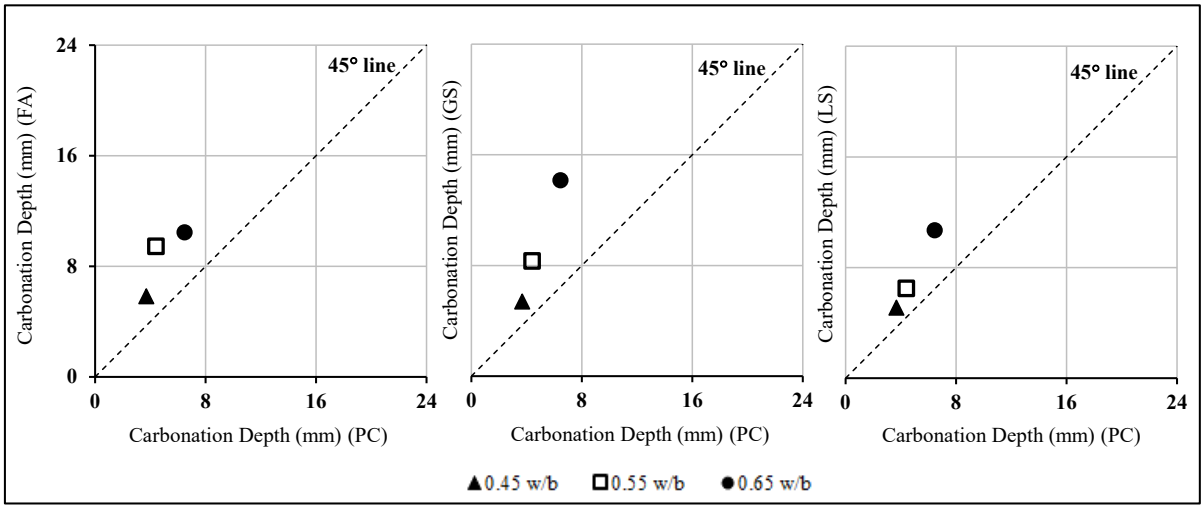

Figure D.112 Carbonation depth of specimens with Curing-D, after 1000 days of exposure at site WS: (FA, GS and LS) vs PC concrete

D.13 PREDICTED VS MEASURED CARBONATION DEPTH

Table D.16 Carbonation depth (mm) after 1000 days of exposure - Measured and Model Prediction (using Equation (5.15))

Mix Designation	Carbonation depth (mm) after 1000 days of exposure - Measured and Model Prediction									
	CD		MS		ME		WS		WE	
	Measured	Predicted	Measured	Predicted	Measured	Predicted	Measured	Predicted	Measured	Predicted
PC-A4		0.0		0.0	0.0	0.0	0.0	2.9	0.0	2.9
FA-A4	5.4	9.0	4.6	6.9	2.6	6.9	3.4	5.7	2.7	5.7
GS-A4	6.0	5.8	3.9	4.5	0.5	4.5	2.1	3.7	0.0	3.7
LS-A4	2.6	3.8		0.0	0.5	0.0	2.0	2.4	0.5	2.4
PC-B4	5.5	7.1	3.6	5.4	2.6	5.4	3.5	4.5	2.6	4.5
FA-B4	8.8	11.5	7.6	8.7	4.5	8.7	8.7	7.2	4.3	7.2
GS-B4	13.1	12.6	9.5	9.6	6.8	9.6	8.1	7.9	4.7	7.9
LS-B4	8.1	8.0	5.2	6.1	2.3	6.1	4.0	5.0	3.3	5.0
PC-C4	4.6	6.0	3.1	4.6	0.5	4.6	0.5	3.8	0.0	3.8
FA-C4	8.5	9.0	7.0	6.8	4.2	6.8	5.8	5.6	3.4	5.6
GS-C4	7.5	9.3	6.2	7.1	3.1	7.1	5.4	5.9	4.1	5.9
LS-C4	7.1	5.6	4.4	4.3	2.1	4.3	4.0	3.5		3.5
PC-D4	6.5	7.4	6.6	5.6	3.1	5.6	3.7	4.6	2.3	4.6
FA-D4	9.0	10.9	8.6	8.3	4.2	8.3	5.8	6.9	4.3	6.9
GS-D4	12.2	10.8	8.5	8.2	3.7	8.2	5.4	6.8	5.9	6.8
LS-D4	10.5	9.5	7.7	7.2	3.2	7.2	5.1	5.9	3.3	5.9
PC-A5	4.4	5.4	3.3	4.1	1.4	4.1	0.0	3.4	0.0	3.4
FA-A5	9.1	11.8	6.9	9.0	4.7	9.0	7.6	7.4	5.6	7.4
GS-A5	9.0	7.3	7.2	5.6	4.4	5.6	7.2	4.6	4.2	4.6
LS-A5	7.2	5.0	5.7	3.8	2.7	3.8	3.7	3.1	4.5	3.1
PC-B5	9.4	9.7	6.5	7.4	3.8	7.4	6.4	6.1	3.6	6.1
FA-B5	15.0	17.4	11.4	13.3	6.7	13.3	11.0	10.9	8.1	10.9
GS-B5	16.8	18.9	12.2	14.4	8.5	14.4	12.8	11.9	9.6	11.9
LS-B5	13.3	12.6	11.2	9.6	3.9	9.6	7.1	7.9	5.2	7.9
PC-C5	7.9	7.2	6.5	5.5	3.0	5.5	4.6	4.5	4.0	4.5
FA-C5	12.7	15.6	10.4	11.9	6.3	11.9	9.7	9.8	6.9	9.8
GS-C5	11.1	11.3	9.3	8.6	5.6	8.6	11.1	7.1	8.8	7.1
LS-C5	9.8	7.9	7.5	6.0	2.7	6.0	7.0	4.9	3.7	4.9
PC-D5	6.1	8.2	6.2	6.2	3.9	6.2	4.4	5.1	3.7	5.1
FA-D5	12.5	15.7	11.0	12.0	6.5	12.0	9.4	9.9	7.7	9.9
GS-D5	11.4	14.6	11.0	11.1	7.3	11.1	8.3	9.2	6.7	9.2
LS-D5	9.3	10.4	8.1	7.9	4.3	7.9	6.5	6.5	4.8	6.5
PC-A6	8.6	6.2	6.7	4.7	2.5	4.7	6.7	3.9	4.2	3.9
FA-A6	12.7	15.4	12.0	11.8	8.2	11.8	10.2	9.7	9.6	9.7
GS-A6	11.8	9.8	10.1	7.5	7.0	7.5	9.6	6.2	8.0	6.2
LS-A6	10.4	5.3	8.4	4.0	5.2	4.0	9.2	3.3	6.7	3.3
PC-B6	15.7	15.1	12.2	11.5	5.5	11.5	9.1	9.5	6.4	9.5
FA-B6	23.4	24.4	18.6	18.6	11.2	18.6	12.8	15.3	11.1	15.3
GS-B6	20.4	25.8	18.4	19.7	11.6	19.7	15.0	16.2	12.7	16.2
LS-B6	14.4	17.1	11.8	13.1	7.3	13.1	10.9	10.7	8.1	10.7
PC-C6	11.5	9.0	10.0	6.9	4.3	6.9	7.6	5.7	6.0	5.7
FA-C6	16.1	16.6	13.9	12.6	8.6	12.6	11.9	10.4	10.1	10.4
GS-C6	19.4	17.8	13.9	13.6	9.8	13.6	14.2	11.2	11.4	11.2
LS-C6	14.2	12.9	10.5	9.8	6.5	9.8	10.4	8.1	9.5	8.1
PC-D6	11.7	12.2	9.9	9.3	5.3	9.3	6.5	7.6	5.7	7.6
FA-D6	19.6	21.8	17.1	16.7	10.8	16.7	10.4	13.7	10.3	13.7
GS-D6	20.1	20.0	11.1	15.2	10.9	15.2	14.2	12.5	9.5	12.5
LS-D6	12.9	12.9	10.4	9.9	6.0	9.9	10.7	8.1	8.6	8.1

Table D.17 Carbonation depth (mm) after 1000 days of exposure - Measured and Model Prediction (using Equation (5.18), based on ToW concept))

Mix Designation	Carbonation depth (mm) after 1000 days of exposure - Measured and Model Prediction (based on ToW concept)				
	Actual time of exposure (t)	TOW	Effective exposure time (te= t - ToW)	Measured	Predicted (based on ToW concept)
PC-A4	1000	203	797	0.0	0.0
FA-A4	1000	209	791	2.6	6.1
GS-A4	1000	214	786	0.5	0.0
LS-A4	1000	212	788	0.5	0.0
PC-B4	1000	203	797	2.6	4.8
FA-B4	1000	209	791	4.5	7.8
GS-B4	1000	214	786	6.8	8.6
LS-B4	1000	212	788	2.3	5.4
PC-C4	1000	203	797	0.5	0.0
FA-C4	1000	209	791	4.2	6.1
GS-C4	1000	214	786	3.1	6.3
LS-C4	1000	212	788	2.1	3.8
PC-D4	1000	199	801	3.1	5.1
FA-D4	1000	199	801	4.2	7.5
GS-D4	1000	203	797	3.7	7.4
LS-D4	1000	203	797	3.2	6.4
PC-A5	1000	209	791	1.4	3.7
FA-A5	1000	211	789	4.7	8.0
GS-A5	1000	214	786	4.4	4.9
LS-A5	1000	212	788	2.7	3.4
PC-B5	1000	209	791	3.8	6.6
FA-B5	1000	211	789	6.7	11.8
GS-B5	1000	214	786	8.5	12.8
LS-B5	1000	212	788	3.9	8.6
PC-C5	1000	209	791	3.0	4.9
FA-C5	1000	211	789	6.3	10.5
GS-C5	1000	214	786	5.6	7.7
LS-C5	1000	212	788	2.7	5.3
PC-D5	1000	199	801	3.9	5.6
FA-D5	1000	199	801	6.5	10.8
GS-D5	1000	203	797	7.3	9.9
LS-D5	1000	203	797	4.3	7.1
PC-A6	1000	214	786	2.5	4.2
FA-A6	1000	214	786	8.2	10.4
GS-A6	1000	212	788	7.0	6.7
LS-A6	1000	212	788	5.2	3.6
PC-B6	1000	214	786	5.5	10.2
FA-B6	1000	214	786	11.2	16.5
GS-B6	1000	212	788	11.6	17.5
LS-B6	1000	212	788	7.3	11.6
PC-C6	1000	214	786	4.3	6.1
FA-C6	1000	214	786	8.6	11.2
GS-C6	1000	212	788	9.8	12.1
LS-C6	1000	212	788	6.5	8.7
PC-D6	1000	199	801	5.3	8.3
FA-D6	1000	199	801	10.8	14.9
GS-D6	1000	203	797	10.9	13.6
LS-D6	1000	203	797	6.0	8.8

Table D.18 Carbonation depth (mm) after 1000 days of exposure - Measured and Model Prediction (using Equation (5.19) & (5.30), based on drying wetting cycles concept))

Mix Designation	ME-Modified		WE-Modified	
	Measured	Predicted	Measured	Predicted
PC-A4	0.0	2.3	0.0	2.4
FA-A4	2.6	4.1	2.7	4.6
GS-A4	0.5	2.8	0.0	3.0
LS-A4	0.5	1.9	0.5	2.0
PC-B4	2.6	3.4	2.6	3.7
FA-B4	4.5	5.2	4.3	5.8
GS-B4	6.8	5.6	4.7	6.4
LS-B4	2.3	3.8	3.3	4.1
PC-C4	0.5	2.9	0.0	3.1
FA-C4	4.2	4.2	3.4	4.6
GS-C4	3.1	4.4	4.1	4.8
LS-C4	2.1	2.7		2.9
PC-D4	3.1	3.5	2.3	3.8
FA-D4	4.2	5.0	4.3	5.6
GS-D4	3.7	4.9	5.9	5.5
LS-D4	3.2	4.4	3.3	4.9
PC-A5	1.4	2.6	0.0	2.8
FA-A5	4.7	5.2	5.6	5.9
GS-A5	4.4	3.4	4.2	3.7
LS-A5	2.7	2.4	4.5	2.6
PC-B5	3.8	4.5	3.6	5.0
FA-B5	6.7	7.5	8.1	8.7
GS-B5	8.5	7.9	9.6	9.3
LS-B5	3.9	5.7	5.2	6.4
PC-C5	3.0	3.5	4.0	3.8
FA-C5	6.3	6.9	6.9	7.8
GS-C5	5.6	5.2	8.8	5.8
LS-C5	2.7	3.7	3.7	4.1
PC-D5	3.9	3.8	3.7	4.2
FA-D5	6.5	6.8	7.7	7.9
GS-D5	7.3	6.3	6.7	7.3
LS-D5	4.3	4.8	4.8	5.3
PC-A6	2.5	3.0	4.2	3.2
FA-A6	8.2	6.5	9.6	7.6
GS-A6	7.0	4.4	8.0	5.0
LS-A6	5.2	2.6	6.7	2.8
PC-B6	5.5	6.7	6.4	7.6
FA-B6	11.2	9.8	11.1	11.8
GS-B6	11.6	10.1	12.7	12.3
LS-B6	7.3	7.5	8.1	8.6
PC-C6	4.3	4.3	6.0	4.7
FA-C6	8.6	7.2	10.1	8.3
GS-C6	9.8	7.7	11.4	8.9
LS-C6	6.5	5.9	9.5	6.6
PC-D6	5.3	5.5	5.7	6.2
FA-D6	10.8	8.9	10.3	10.6
GS-D6	10.9	8.2	9.5	9.7
LS-D6	6.0	5.8	8.6	6.6

D.14 EXPERIMENTAL DETAILS (ALHASSAN (2014))

Table D.19 Concrete mix proportions (Alhassan (2014))

Mix Designation	Binder			Aggregate		Water content	Water/ binder ratio
	CEM I	FA	GGBS	Coarse	Fine		
	(kg/m3)						
PC-40	450	-	-	990	800	180	0.4
PC-50	400	-	-	990	877	200	0.5
PC-60	350	-	-	1015	869	210	0.6
PC-75	300	-	-	1050	810	225	0.75
FA-40	315	135	-	990	800	180	0.4
FA-50	280	120	-	990	877	200	0.5
FA-60	245	105	-	1015	869	210	0.6
FA-75	210	90	-	1050	810	225	0.75
SL-40	225	-	225	990	800	180	0.4
SL-50	200	-	200	990	877	200	0.5
SL-60	175	-	175	1015	869	210	0.6
SL-75	150	-	150	950	900	225	0.75

Table D.20 CH measured using TGA (Alhassan (2014))

Mix Designation	CH content in the concrete		
	(% by mass of cement content)		
	3 days	7 days	28 days
PC-40	17.9	21.3	23.8
PC-50	15.5	19.0	22.5
PC-60	14.7	17.3	21.3
PC-75	13.1	14.9	18.2
FA-40	15.2	14.7	13.8
FA-50	14.5	14.0	13.0
FA-60	13.9	13.2	12.7
FA-75	13.1	12.7	11.9
SL-40	15.1	12.4	11.9
SL-50	14.0	10.5	9.5
SL-60	13.8	9.6	8.7
SL-75	13.1	9.2	8.0

Table D.21 Curing regimes, oxygen permeability and carbonation depth (Alhassan (2014)) and Model Prediction (using Equation (5.19)&(5.30))

Curing Regime	Mix Designation	Oxygen permeability coeffiecient (k) at 28 days	Carbonation depth (mm) - Measured and Model Prediction							
			Exposure Period							
			0.5 Year		1 year		1.5 year		2 year	
			Measured	Predicted	Measured	Predicted	Measured	Predicted	Measured	Predicted
1 day in mould, then 2 days in water curing tank at 22±1 °C, then in air inside lab (till 28 day after casting at 23±2 °C and 60±5% RH)	PC-40	1.20E-10	1.1	1.7	1.5	2.4	1.7	2.9	2.3	3.4
	PC-50	1.90E-10	1.3	2.3	1.7	3.2	2.1	3.9	2.8	4.5
	PC-60	2.50E-10	2.5	2.7	3.5	3.8	3.8	4.7	4.5	5.3
	PC-75	6.50E-10	3.3	4.3	4.9	6.0	5.5	7.3	6.5	8.3
	FA-40	1.00E-10	2.3	2.1	3.3	2.9	4.2	3.5	4.5	4.1
	FA-50	1.70E-10	3.4	2.7	4.8	3.8	6.3	4.6	6.8	5.3
	FA-60	2.40E-10	4.9	3.3	7.3	4.6	8.1	5.6	9.5	6.4
	FA-75	6.10E-10	7.1	5.0	9.8	7.0	11.7	8.4	13.4	9.5
	SL-40	1.70E-10	2.5	2.9	4.1	4.1	4.7	5.0	5.3	5.7
	SL-50	2.70E-10	4.3	3.8	6.4	5.3	7.6	6.4	8.7	7.3
	SL-60	5.00E-10	5.6	5.0	7.9	6.9	9.8	8.3	11.4	9.5
	SL-75	1.20E-09	7.7	7.4	11.3	10.1	12.7	12.1	13.5	13.6
1 day in mould, then 6 days in water curing tank at 22±1 °C, then in air inside lab (till 28 day after casting at 23±2 °C and 60±5% RH)	PC-40	1.20E-10	0.5	1.6	0.8	2.2	1.0	2.7	1.3	3.1
	PC-50	1.50E-10	1.1	1.9	1.5	2.7	1.8	3.2	2.1	3.7
	PC-60	2.40E-10	1.8	2.5	2.5	3.5	3.0	4.2	3.5	4.9
	PC-75	5.80E-10	2.9	3.9	3.9	5.4	4.5	6.6	5.7	7.5
	FA-40	8.00E-11	1.4	2.0	2.3	2.7	2.9	3.3	3.4	3.8
	FA-50	1.20E-10	2.5	2.4	3.8	3.4	4.9	4.2	5.6	4.8
	FA-60	2.40E-10	3.7	3.4	5.4	4.7	6.7	5.7	8.3	6.5
	FA-75	5.20E-10	6.5	4.8	9.1	6.7	11.4	8.1	12.7	9.2
	SL-40	1.20E-10	2.1	2.9	3.0	4.0	3.8	4.9	5.2	5.6
	SL-50	2.70E-10	3.2	4.3	4.4	6.0	6.0	7.3	7.5	8.2
	SL-60	4.70E-10	4.0	5.8	6.1	8.0	7.5	9.6	9.1	10.8
	SL-75	6.50E-10	6.5	7.1	10.0	9.7	11.2	11.5	12.9	12.9
1 day in mould, then 27 day in water curing tank at 22±1 °C	PC-40	1.00E-10	0.2	1.4	0.4	2.0	0.6	2.4	0.8	2.8
	PC-50	1.30E-10	0.8	1.7	1.2	2.3	1.4	2.8	1.7	3.3
	PC-60	2.30E-10	1.6	2.2	2.1	3.1	2.7	3.8	3.1	4.3
	PC-75	3.40E-10	2.4	2.9	3.1	4.1	3.8	5.0	4.8	5.7
	FA-40	5.00E-11	0.8	1.7	1.5	2.4	2.0	2.9	2.3	3.4
	FA-50	1.00E-10	2.2	2.4	3.3	3.3	4.1	4.0	4.7	4.6
	FA-60	2.30E-10	3.4	3.4	4.8	4.7	6.2	5.7	7.5	6.6
	FA-75	3.50E-10	5.5	4.3	7.7	6.1	10.0	7.3	12.8	8.3
	SL-40	1.20E-10	1.1	2.9	1.5	4.1	2.3	5.0	2.9	5.7
	SL-50	2.60E-10	2.1	4.5	3.3	6.2	4.2	7.5	4.7	8.5
	SL-60	4.30E-10	2.8	5.9	4.2	8.1	5.3	9.7	6.1	10.9
	SL-75	6.40E-10	5.3	7.5	7.9	10.3	9.3	12.1	10.2	13.5

APPENDIX E: RAINFALL DATA OF EXPOSURE SITES

Table E.1 Three year daily rainfall data from weather station around five kilometres from the site ME and MS

	2010												2011												2012											
Day	Jan	Feb	Mar	Apr	May	Jun	Jul	Aug	Sep	Oct	Nov	Dec	Jan	Feb	Mar	Apr	May	Jun	Jul	Aug	Sep	Oct	Nov	Dec	Jan	Feb	Mar	Apr	May	Jun	Jul	Aug	Sep	Oct	Nov	Dec
1									24.0				8.6						20.4		29.6				7.2				0.2		1.0		0.2			
2	0.3											13.2	1.0				6.4	0.2	6.0		1.6				5.2				40.8		0.8		0.4	0.2		
3	0.4				4.2	0.2					27.4	2.0		6.8				0.8	0.2			0.6	1.0				5.6		9.2		28.6			12.0		
4					43.4	0.4					1.0	0.6					0.4	1.0		34.6	0.2	0.4	1.4				0.2		4.8		1.2	1.2		4.4		
5					11.2		6.4		7.8		0.2						5.2	6.6		0.6			0.2			0.6			0.2	6.4		16.2				
6					29.4		0.6		0.2		0.8						0.2	9.4						4.6				9.6		6.8	44.0	5.0		6.0		0.6
7		3.0			0.2	56.0		22.0		18.6											4.0		0.4	10.4				45.2		87.2	21.6			0.8		1.0
8				7.6	23.4	8.6		15.2		0.2	19.6										31.4		20.6					14.2		8.4	73.8		0.4	0.2		
9		1.1	0.2	19.6	31.2		15.0	1.8	0.8		0.4						3.0				1.6		10.2					0.2		0.2	9.2		28.2			
10			3.8		16.6		25.8			39.8				5.2			5.0							2.2		4.6			0.2		28.8	67.4				
11					69.0		0.4			1.0	21.2						0.2			16.4				2.0		0.8					13.2			0.6	
12					18.4	24.2					0.2									25.6	8.4		24.4			0.2			0.4	0.6	5.4	0.2	1.0		3.8	
13			1.6		32.8	23.2	10.6				0.4									2.0	21.0		3.8	22.4	13.6				14.4		1.6	0.6	6.6		0.2	
14	3.5			0.2	19.6	22.2	39.8		9.4	0.8							0.4	5.4			4.6	17.0		9.2				5.4	0.4		1.0	24.6				
15		7.0				17.0			5.2	0.2				2.8			0.2	40.4			4.2							5.0			12.0	21.6				
16		0.2				0.2	5.8						0.2					16.8									9.6				0.2	5.8			5.0	
17					0.2																					0.2		20.0	1.8			2.2			
18				2.8				5.6		3.6								18.6		10.4	40.2	10.8		3.6					3.8				1.2	10.8		
19				5.2					19.0	0.2	3.6		3.0					4.6		14.2	0.2		0.8	0.2	0.8				4.2			33.8	0.2	14.0		
20								5.4	4.4	21.0	30.2					19.0				25.2	0.2		25.8		0.6	2.6			0.6		50.6		24.8		5.8	
21				2.4		15.0		24.6	8.6	3.4	4.4				1.0					22.2			0.4	0.4				0.6		1.4	25.6	11.4	11.4			
22				0.2	0.2		24.0	7.0	0.2	1.0					2.2		19.8	52.6				1.4	0.2	17.0	1.4	13.6		0.2		2.8	2.0	0.2	0.8			
23		1.2			0.6			0.2	5.2						3.8		19.0	15.2		9.8			2.2		8.4				1.0	1.6			32.0		20.0	
24		0.8	2.6							2.2		0.4			0.2	28.6	11.4	2.4											8.6	30.2		20.4			3.0	
25	0.1				0.4			3.6								39.0				3.2								0.2	33.4	0.2	0.4	21.0			0.2	
26			0.4				0.2	1.2	16.0		0.6					10.0				2.0		0.4						9.2	2.6	40.8	16.0	7.4	26.6	4.4		
27			6.4		73.2			7.6	0.2		0.8					3.6			8.8			5.0						1.2				19.2			0.2
28						0.2		18.0								0.2	5.6	3.6	18.8			2.8				1.4		8.6	0.2	9.0			0.6			
29						30.6				0.2						0.2	19.6	13.6				2.4					33.2		14.6	6.8			0.4			
30						0.2	0.8	0.2							8.4		29.0	3.0		32.6		6.4	6.4		0.2		5.2	35.2		2.2	5.2	3.0				
31								3.6				3.8			0.2		2.8														2.6	40.8				
Days with rainfall	1	2	3	4	17	13	12	14	13	13	14	5	4	3	6	7	16	16	5	13	13	10	14	10	8	7	6	13	19	16	21	18	17	9	8	3
	Total number of days with rainfall = 111												**Total number of days with rainfall = 117**												**Total number of days with rainfall = 145**											
	Average number of days of rainfall per annum = 124																																			

Table E.2 Three year daily rainfall data from weather station around seven kilometres from the site WE and WS

	2010												2011												2012											
Day	Jan	Feb	Mar	Apr	May	Jun	Jul	Aug	Sep	Oct	Nov	Dec	Jan	Feb	Mar	Apr	May	Jun	Jul	Aug	Sep	Oct	Nov	Dec	Jan	Feb	Mar	Apr	May	Jun	Jul	Aug	Sep	Oct	Nov	Dec
1	7.8	1.6		10.6	0.6						6.4		13.0	8.8			0.2					19.6			0.2											0.2
2	25.0	2.0	11.0	1.2	6.4							2.4	3.0	2.2								1.6				1.8										6.6
3	3.8	4.6		0.2	21.2							1.2	11.2			6.8						0.4			0.2	0.2										5.6
4	32.2	2.8	0.2		0.2								3.8			3.2									2.4	1.8										20.6
5	1.2		27.8	18.0							4.2		26.2			0.6									3.8	9.0							5.4			
6				1.2	0.4											3.0	0.2																4.2			3.2
7	20.6	0.2		0.2	1.6					0.4							6.6	34.2							1.2	0.2	3.0								0.2	
8	59.8			20.2	1.0	0.8					0.4	31.6		39.8				11.8						42.8	9.2	1.2		0.4						0.4	17.8	
9	0.6			2.2	5.8					0.4	18.4	19.6	2.4	0.4				0.4						11.0	2.6	1.2	17.8							2.6	0.2	13.6
10					0.6							10.2					14.4								7.2	2.4	3.0								2.8	6.6
11												25.6												0.2												0.4
12	15.6											3.0		8.0	0.4									0.2	8.6									0.8		
13	0.8	1.0								11.4		2.4			29.0						2.2			20.8	26.0				0.4							
14		3.4								6.6		23.4	2.8		4.6											0.2	2.0									18.4
15		1.8													1.4					3.2												0.6	1.6	1.6	9.6
16	0.8	10.0									9.8	12.6	21.8		3.8		1.4									18.8								0.2	3.8	
17	30.4										10.0		14.8		0.2										0.2	0.2								1.8		
18	0.2			11.2							1.6	4.6	0.4		0.4								0.2									0.4			8.4
19	28.4			0.4							0.8	18.8	0.4	7.4	20.8							4.0				0.4									1.2
20	1.2			5.8											25.0	4.6								5.4		1.6									8.8
21	35.0			4.4								3.6		7.4		0.6						0.2			1.4	0.6	0.2	0.6				3.6	2.2	0.6	0.6
22													0.2	4.6		5.4								1.4	1.2	7.0						0.2			
23	21.4			29.4								2.0		2.6		0.6								1.0	6.6			0.6		1.6				1.0	
24	0.6			2.4						1.6		2.6		0.2		0.2																		0.4	
25	6.4			0.4									3.4	0.6	65.2											1.2								0.8	30.6
26	4.0	37.6		3.6									7.8		6.6	1.0																		1.4		6.8
27	2.8			3.2						14.8					0.2																		0.4	0.6		
28										0.2		13.4										6.2		0.8	0.8			2.8						0.2	1.0	0.2
29	50.4											2.4										8.0			5.4									17.4		4.6
30				15.4								0.2				1.8											0.4									0.6
31										0.2		6.6												0.2												0.2
Days with rainfall	22	10	3	18	9	1	0	0	0	8	8	19	14	11	12	11	5	3	0	1	1	7	1	10	16	16	6	4	1	1	0	0	8	10	11	20
	Total number of days with rainfall = 98												**Total number of days with rainfall = 76**												**Total number of days with rainfall = 93**											
	Average number of days of rainfall per annum = 89																																			

APPENDIX F: RH PROFILE OF CONCRETE SPECIMENS

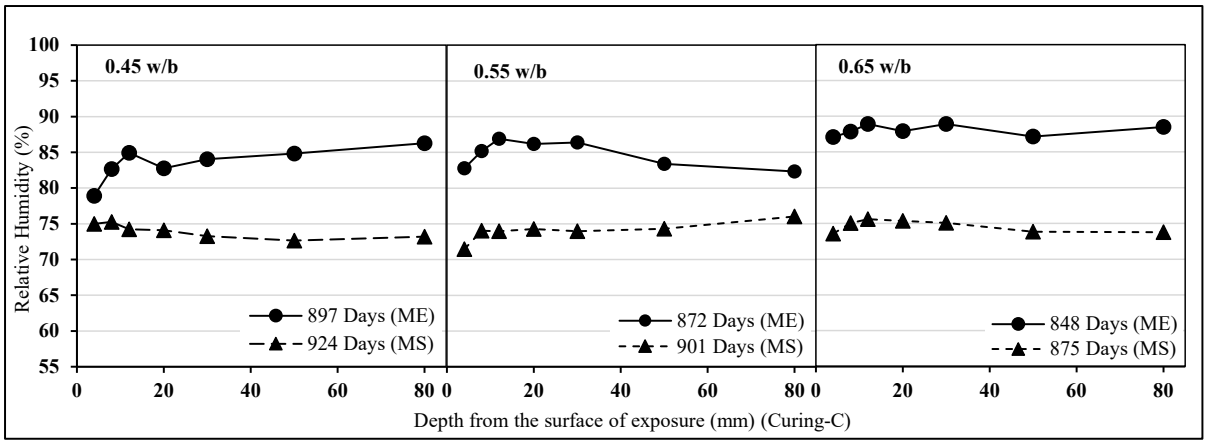

Figure F.1 RH profile of PC concrete specimens exposed to site ME and MS (Curing-C)

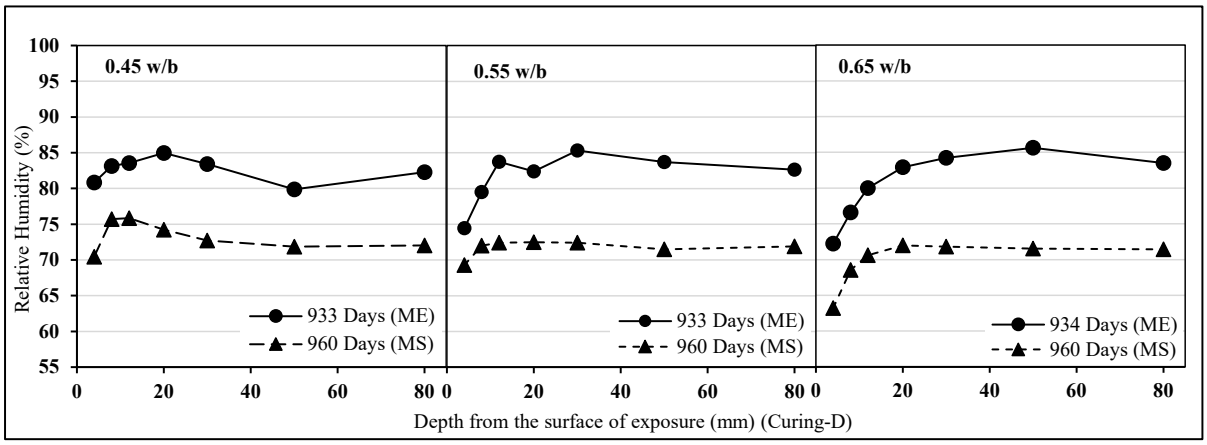

Figure F.2 RH profile of PC concrete specimens exposed to site ME and MS (Curing-D)

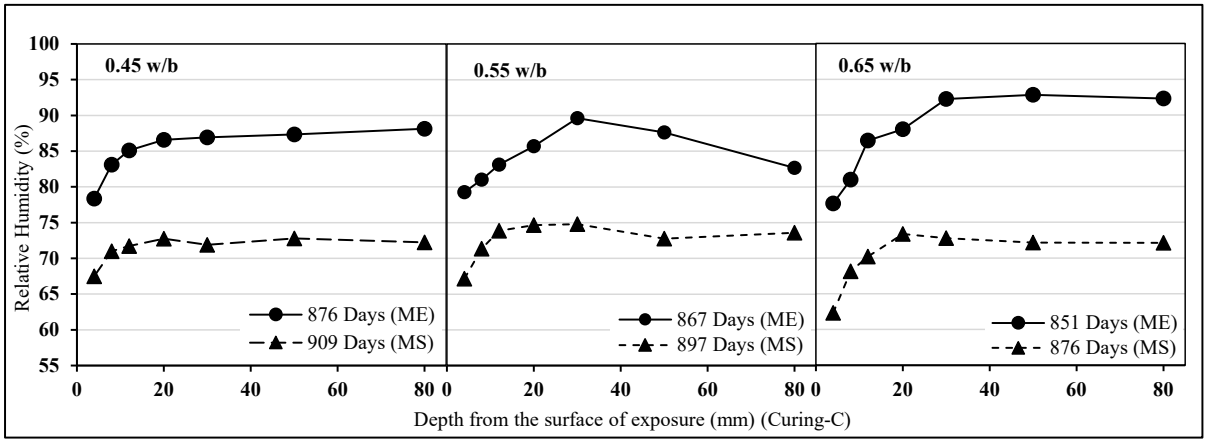

Figure F.3 RH profile of FA concrete specimens exposed to site ME and MS (Curing-C)

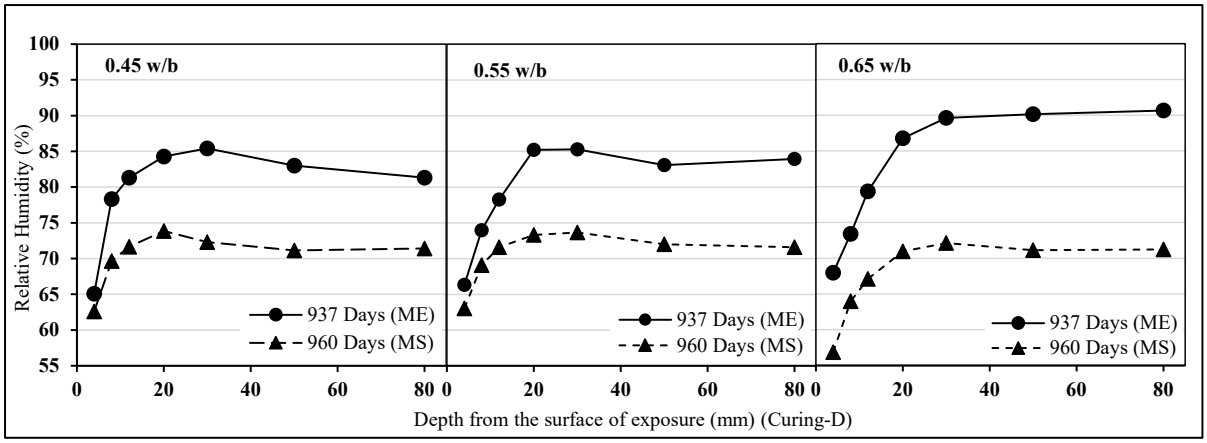

Figure F.4 RH profile of FA concrete specimens exposed to site ME and MS (Curing-D)

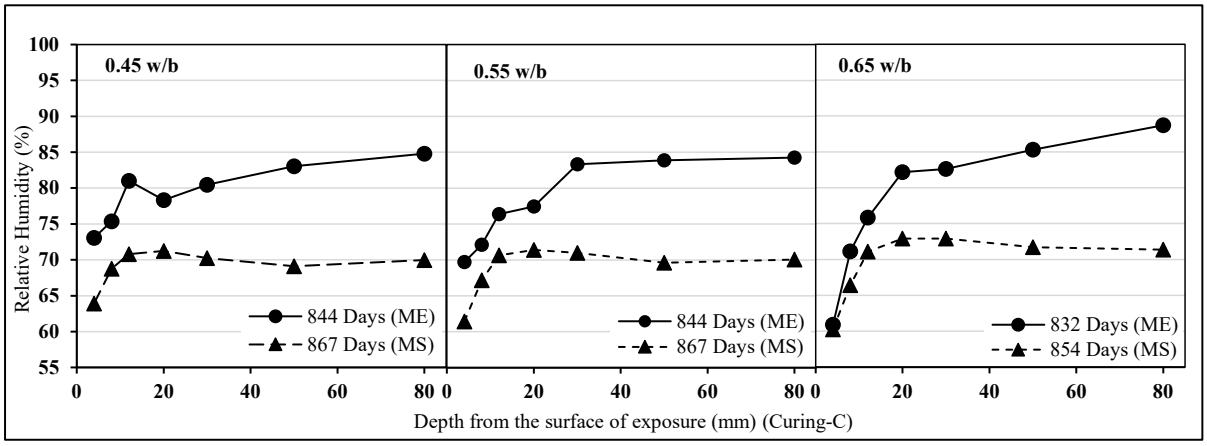

Figure F.5 RH profile of GS concrete specimens exposed to site ME and MS (Curing-C)

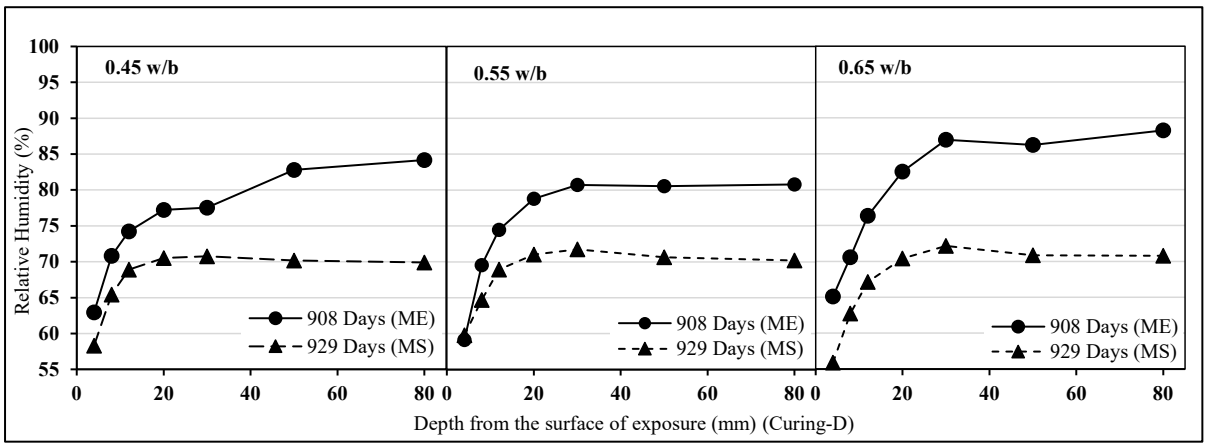

Figure F.6 RH profile of GS concrete specimens exposed to site ME and MS (Curing-D)

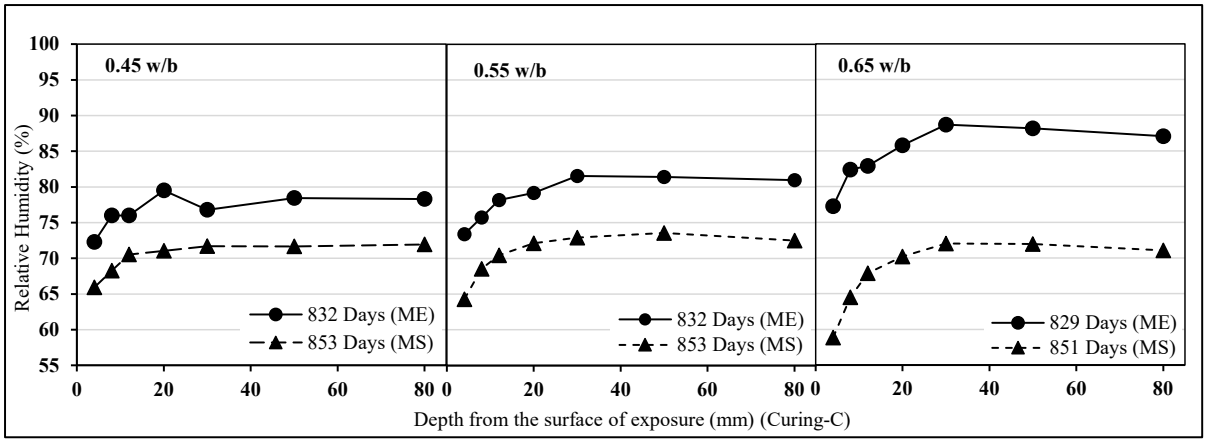

Figure F.7 RH profile of LS concrete specimens exposed to site ME and MS (Curing-C)

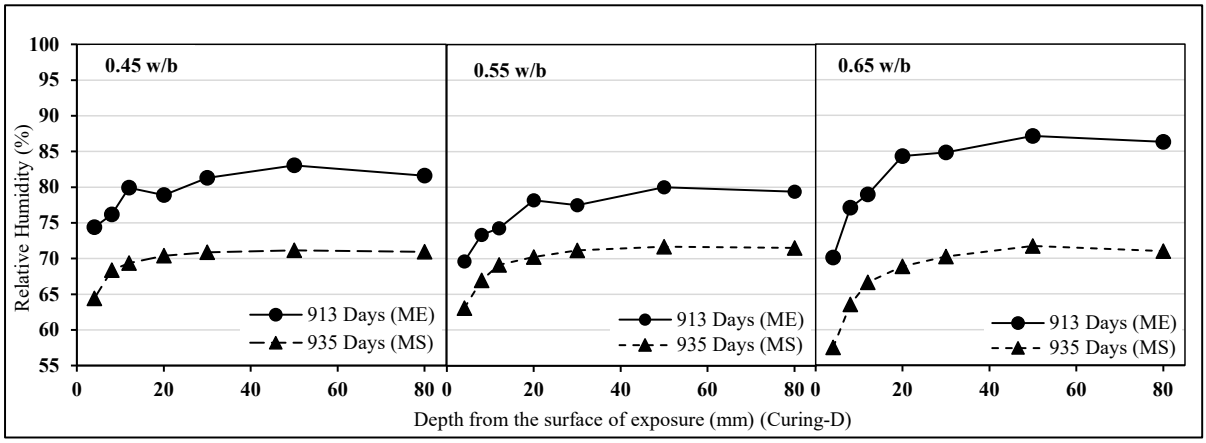

Figure F.8 RH profile of LS concrete specimens exposed to site ME and MS (Curing-D)

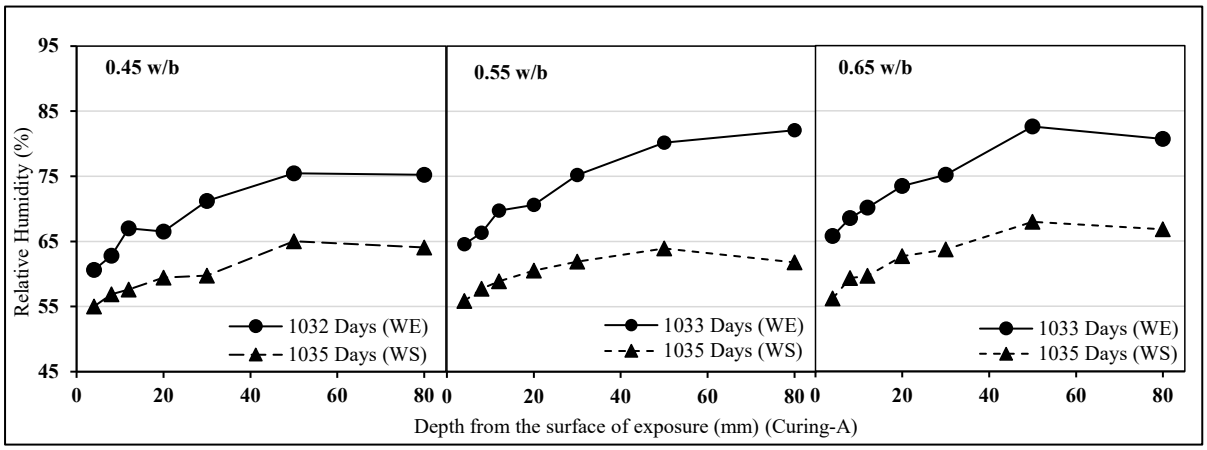

Figure F.9 RH profile of PC concrete specimens exposed to site WE and WS (Curing-A)

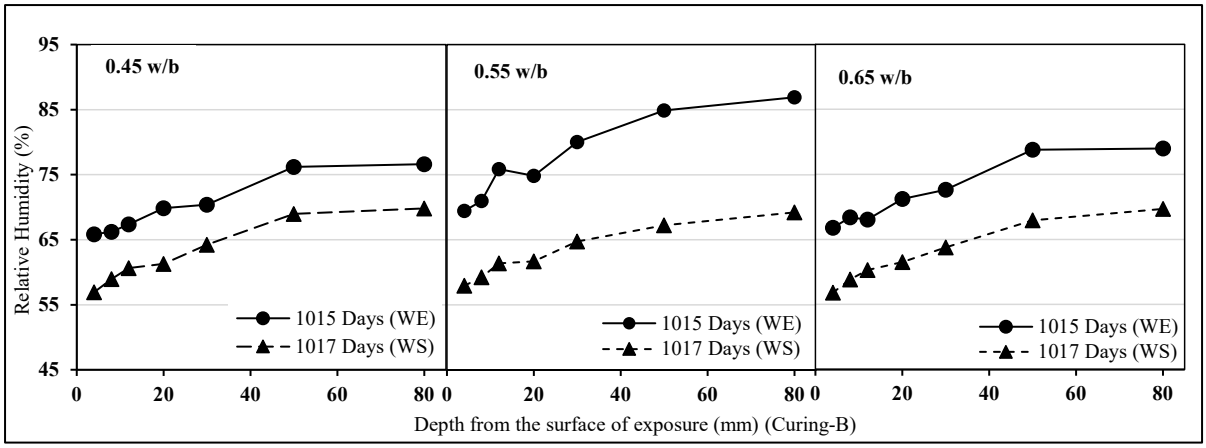

Figure F.10 RH profile of PC concrete specimens exposed to site WE and WS (Curing-B)

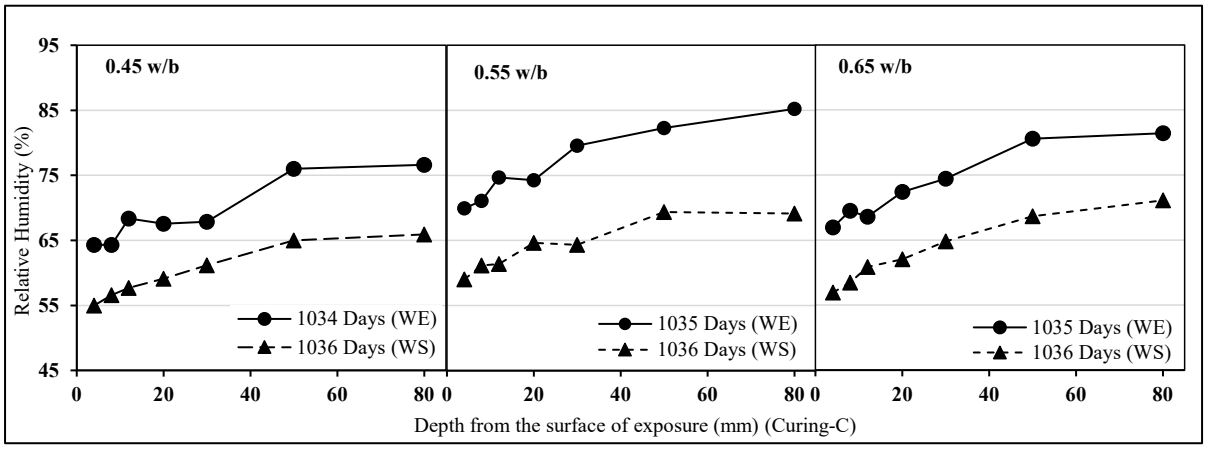

Figure F.11RH profile of PC concrete specimens exposed to site WE and WS (Curing-C)

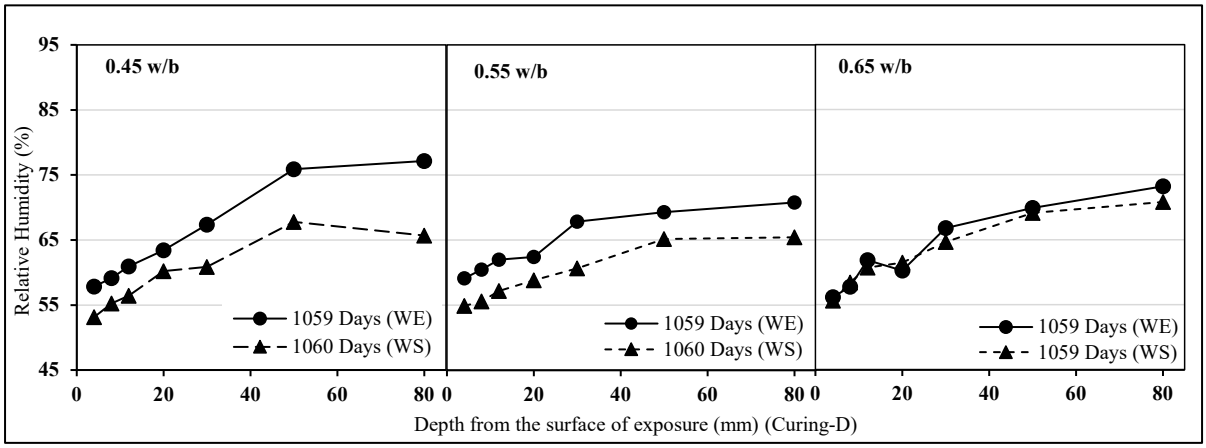

Figure F.12 RH profile of PC concrete specimens exposed to site WE and WS (Curing-D)

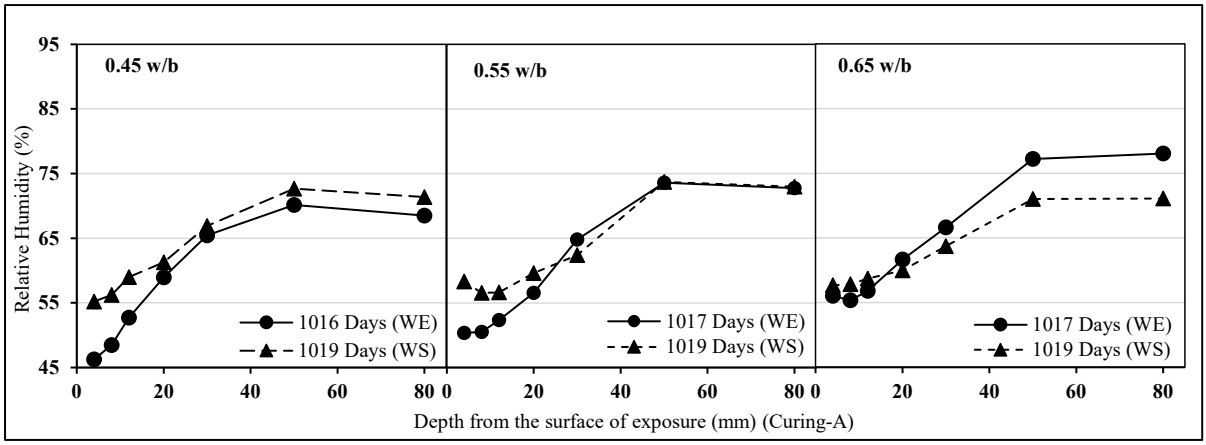

Figure F.13 RH profile of FA concrete specimens exposed to site WE and WS (Curing-A)

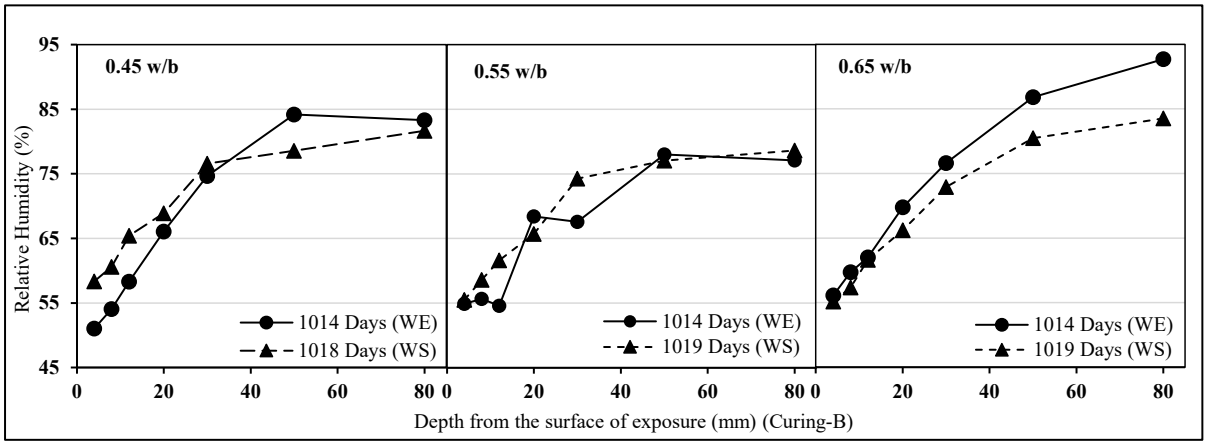

Figure F.14 RH profile of FA concrete specimens exposed to site WE and WS (Curing-B)

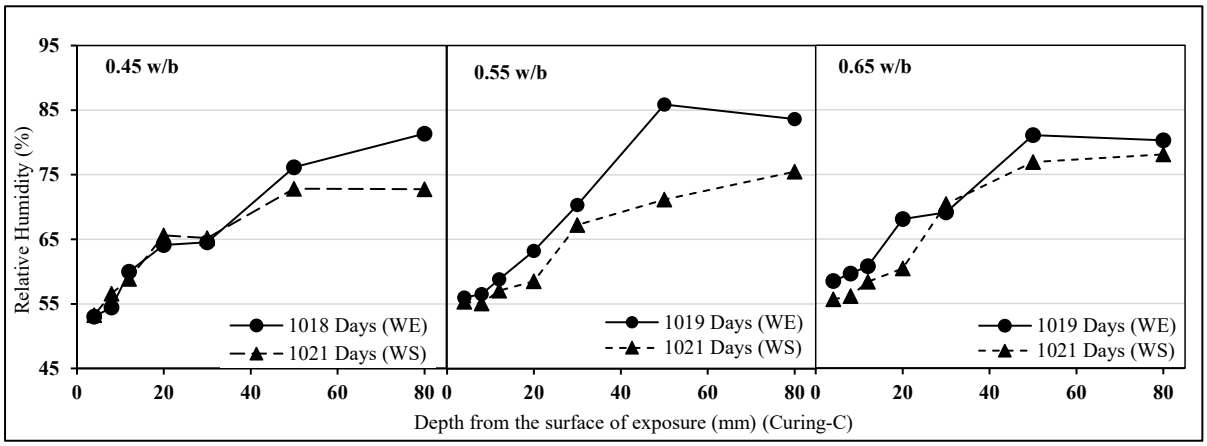

Figure F.15 RH profile of FA concrete specimens exposed to site WE and WS (Curing-C)

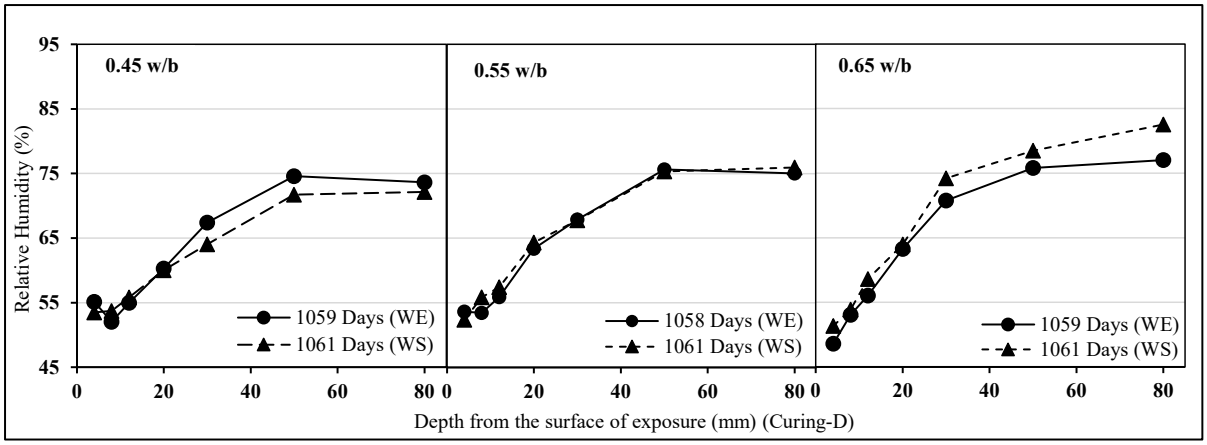

Figure F.16 RH profile of FA concrete specimens exposed to site WE and WS (Curing-D)

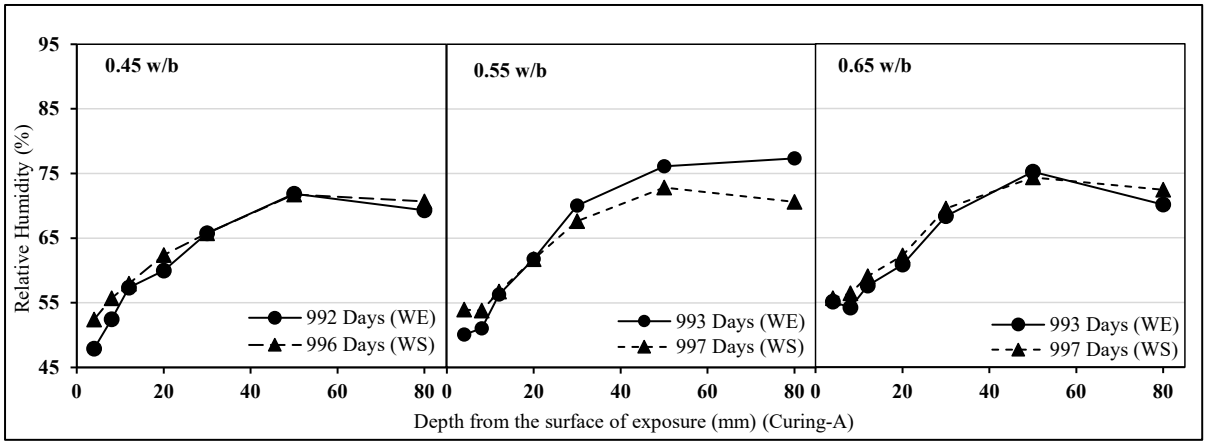

Figure F.17 RH profile of GS concrete specimens exposed to site WE and WS (Curing-A)

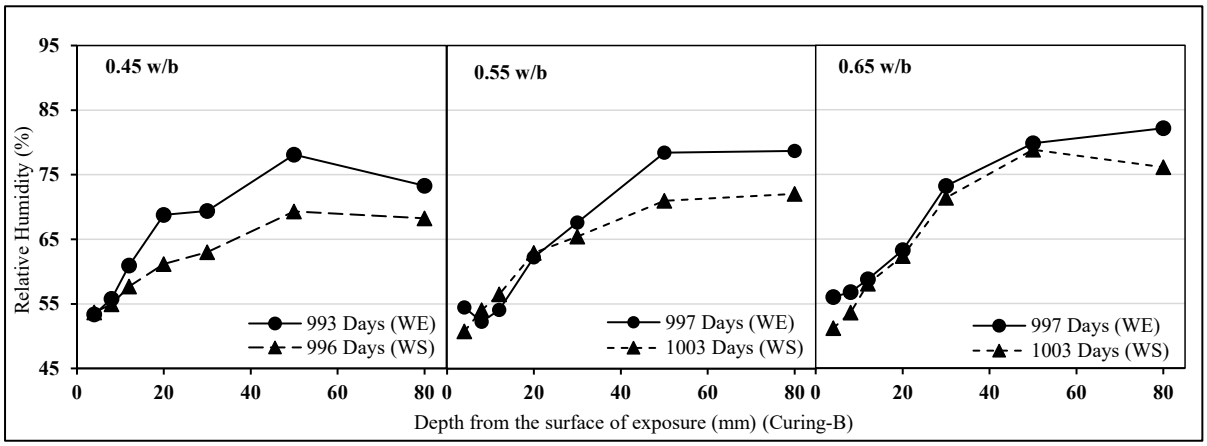

Figure F.18 RH profile of GS concrete specimens exposed to site WE and WS (Curing-B)

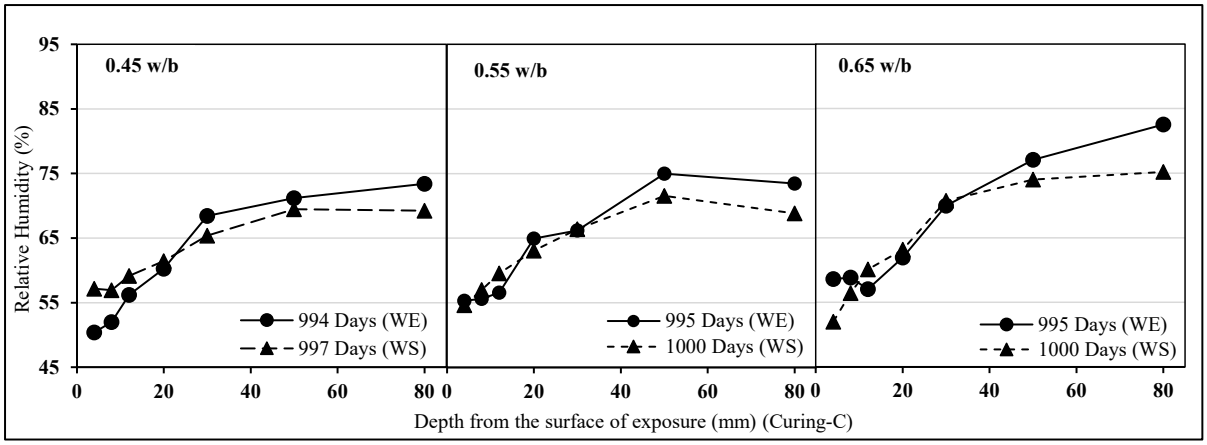

Figure F.19 RH profile of GS concrete specimens exposed to site WE and WS (Curing-C)

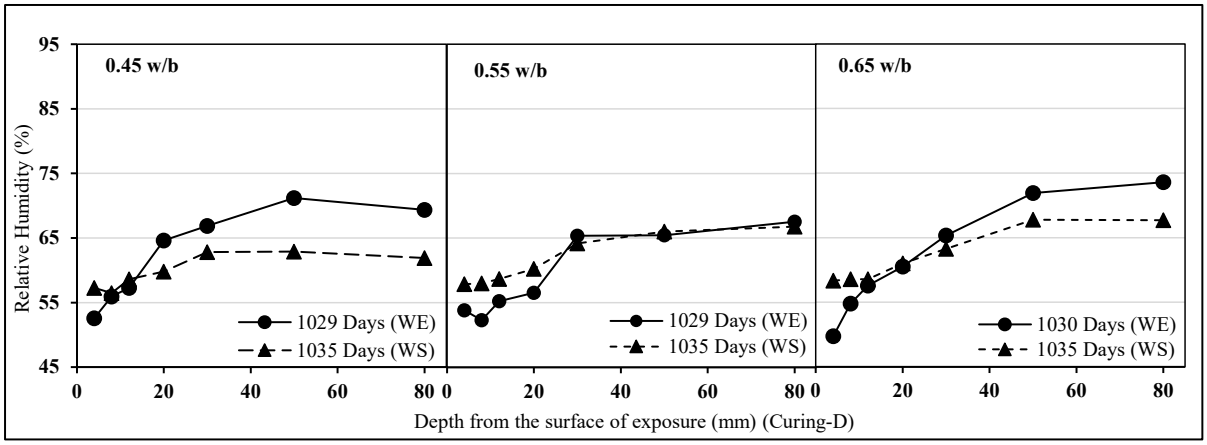

Figure F.20 RH profile of GS concrete specimens exposed to site WE and WS (Curing-D)

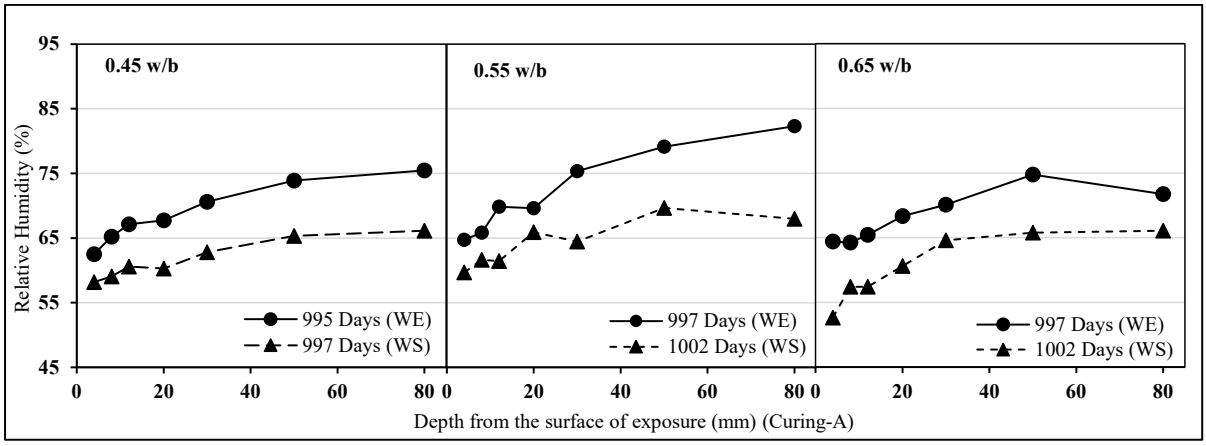

Figure F.21 RH profile of LS concrete specimens exposed to site WE and WS (Curing-A)

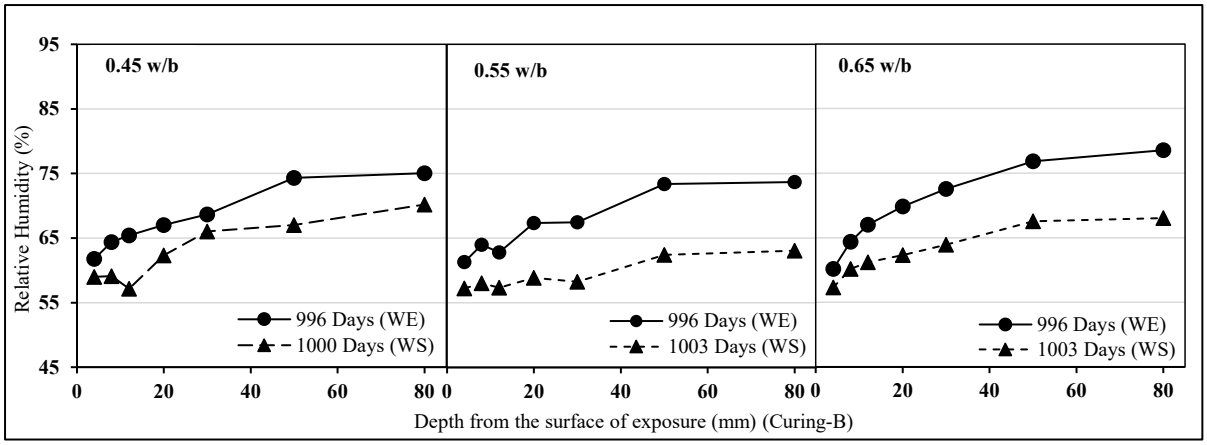

Figure F.22 RH profile of LS concrete specimens exposed to site WE and WS (Curing-B)

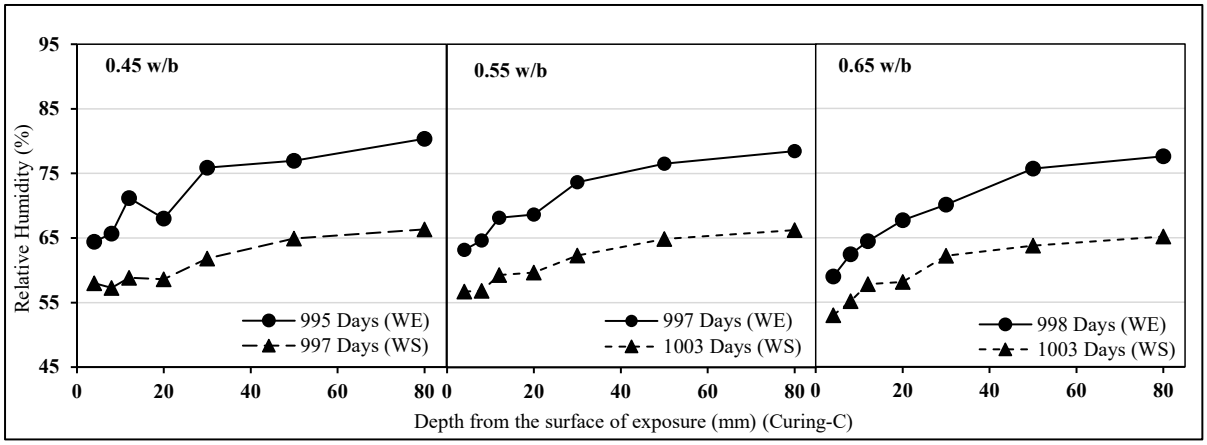

Figure F.23 RH profile of LS concrete specimens exposed to site WE and WS (Curing-C)

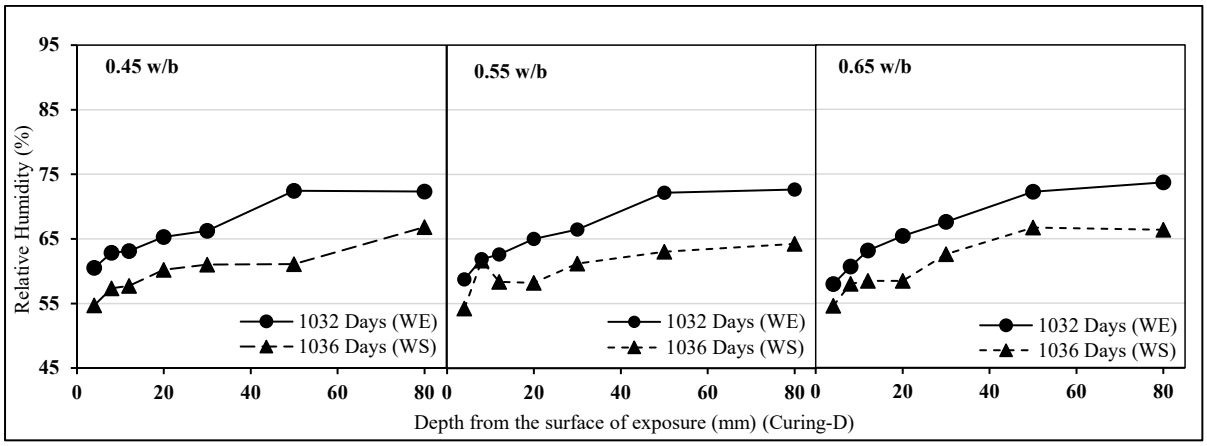

Figure F.24 RH profile of LS concrete specimens exposed to site WE and WS (Curing-D)

APPENDIX G: DERIVATIONS AND CALCULATIONS

G.1 EFFECTIVE DRY DIFFUSION COEFFICIENT CALCULATION

Natural carbonation data of PC-55 concrete specimen subjected to curing Curing-Aand exposed at site CD is as follows:

Carbonation depth (x) = 3.2 mm

Time of exposure (t) = 570 days

CO_2 concentration at site CD (c)= 550 ppm (0.023 mol/m^3)

Carbonatable material (a) based on Equation (5.5) = 1158.48 mol/m^3

Average annual relative humidity at site CD (RH) = 60%

RH modification factor (H_S) can be calculate using Equation (5.13)

$$H_S = 23.32\left(1-\frac{RH}{100}\right)^2\left(\frac{RH}{100}\right)^{2.6} \qquad 5.13$$

$$H_S = 23.32\left(1-\frac{60}{100}\right)^2\left(\frac{60}{100}\right)^{2.6}$$

$$H_S = 0.99$$

Effective dry diffusion coefficient (D_{de}) can be calculated using Equation (5.15) as follows

$$x=\sqrt{\frac{2\times D_{de}\times H_S\times c}{a}}\times\sqrt{t} \qquad 5.15$$

$$3.2=\sqrt{\frac{2\times D_{de}\times 0.9\times 0.023}{1158.48}}\times\sqrt{570}$$

$\underline{D_{de} = 5.33 \times 10^{-9}\ m^2/s}$

G.2 EVAPORATION-DIFFUSION PROCESS FOR DRYING – MODELLING

The modelling of moisture transport during drying as one dimensional evaporation–diffusion process as present in Li et al. (2009) is given below.

The concrete is considered to be saturated at the initial stage. Considering a one dimensional evaporation–diffusion process, at time t = 0, the porous material is saturated by liquid water. At time t > 0, the material is exposed to a lower humidity and hence $h_0 < 100\%$ at the position $x' = 0$. The gas phases in material pores during the drying process are composed of dry air and vapour. Therefore, the mass conservation of vapor can be expressed as follows.

$$\frac{\partial C_v}{\partial t} = \mathrm{div}(D_v \mathrm{grad} C_v) \qquad \text{G.1}$$

Where C_v = the molar concentration of vapour in the gas phases (mol/m^3); D_v = vapour diffusion coefficient in concrete pore structure (m^2/s). The vapour concentration (C_v) can be expressed in terms of its partial pressure (p_v) in gas phases using Claperon's equation and further in terms of relative humidity (h) ash shown in Equation (G.2) and Equation (G.3)

$$p_v = RTC_v \qquad \text{G.2}$$

$$h = \frac{p_v}{p_{vs}} \qquad \text{G.3}$$

Where, R = gas constant (J/K/mol); T = the absolute temperature (K); p_{vs} = saturated vapour pressure (Pa). Therefore Equation G.1 can be written in terms of RH as shown below.

$$\frac{\partial h}{\partial t} = \mathrm{div}(D_v \, \mathrm{grad}\, h) \qquad \text{G.4}$$

The increase in evaporation near the gas–liquid interface, increases the local vapour concentration, as a result the local liquid water content in pores by condensation increases. Assuming this condensation as a local one, the vapour diffusion coefficient can be assumed to be constant between the material surface $x' = 0$ and the evaporation interface $x' = x$. The boundary conditions in term of relative humidity can be expressed as follows.

$$\begin{cases} h(x' = x, t) = h_s = 100\% \\ h(x' = 0, t > 0) = h_0 < 100\% \end{cases} \qquad \text{G.5}$$

The vapour molecules then escape from the gas–liquid interface ($x' = x$) by evaporation and transport to the surface ($x' = 0$) by diffusion. Assuming the evaporation rate to be infinitely large in comparison with the diffusion rate, the moisture mass conservation across the interface is as given in Equation (G.6)

$$\rho_l \left(\frac{dX}{dt}\right) = M_v \, D_v \left(\frac{\partial C_v}{\partial x'}\right)_{x'=x} \qquad \text{G.6}$$

Where, M_V = molar mass of vapour (kg/mol); p_{vs} = saturated vapour pressure (kPa); ρ_l = water density (kg/m^3). Equation (G.6) can be expressed in term RH based on Equation (G.3) as shown below.

$$\rho_l \left(\frac{dX}{dt}\right) = p_{vs} \times \frac{M_v}{RT} \times D_v \left(\frac{\partial h}{\partial x'}\right)_{x'=x} \qquad \text{G.7}$$

The moisture transport process described by Equation (G.4), (G.5) and (G.7) establish a Stefan-like moving boundary problem. In order to solve the Stefan-like moving boundary problem, an intermediate variable η was introduced

$$\eta = \frac{x'}{2 \times \sqrt{D_v \times t}} \qquad \text{G.8}$$

The general solution for the moving boundary problem as per Geebhart (1993) can be in the form as shown in Equation (G.9)

$$h = A \ \mathrm{erf}(\eta) + B \qquad \text{G.9}$$

Where, erf = error function; A and B are constant. Considering the second boundary condition in Equation (G.5)

$$h\,(\eta=0) = h_0 \implies B = h_0 \qquad \text{G.10}$$

Substituting Equation (G.10) in Equation (G.9)

$$h - h_0 = A \ \mathrm{erf}(\eta) \qquad \text{G.11}$$

Substituting the first boundary condition of Equation (G.5) in Equation (G.11)

$$h_s - h_0 = A \ \mathrm{erf}\left(\frac{x}{2 \times \sqrt{D_v \times t}}\right) \qquad \text{G.12}$$

Here,

$$\lambda = \frac{x}{2 \times \sqrt{D_v \times t}} \qquad \text{G.13}$$

Rearranging Equation (G.13)

$$x = 2 \times \lambda \times \sqrt{D_v} \times \sqrt{t} \qquad \text{G.14}$$

Substituting Equation (G.14) in Equation (G.12)

$$A = \frac{h_s - h_0}{\text{erf}(\lambda)} \qquad \text{G.15}$$

Substituting Equation (G.15) in Equation (G.11)

$$h - h_0 = \frac{\text{erf}(\eta)}{\text{erf}(\lambda)} \ (h_s - h_0) \qquad \text{G.16}$$

The solution of λ can be resorted to the moving boundary condition (Equation (G.7)) and the differential terms in Equation (G.7) can be expressed as follows

$$\left(\frac{dX}{dt}\right) = \lambda \times \sqrt{\frac{D_v}{t}} \qquad \text{G.17}$$

$$\left(\frac{\partial h}{\partial x}\right) = \left[\frac{h_s - h_0}{\text{erf}(\lambda)}\right] \times \text{erf}'(\lambda) \times \frac{1}{2 \times \sqrt{D_v \times t}} \qquad \text{G.18}$$

Therefore Equation (G.7) can be written as

$$\rho_l \ \lambda = \frac{1}{2} \times p_{vs} \times \frac{M_v}{RT} \times \left[\frac{h_s - h_0}{\text{erf}(\lambda)}\right] \times \text{erf}'(\lambda) \qquad \text{G.19}$$

However,

$$\text{erf}(\lambda) = \frac{2}{\sqrt{\pi}} \times \int_0^{\lambda} \exp(-y^2)\, dy \qquad \text{G.20}$$

$$\text{erf}'(\lambda) = \frac{2}{\sqrt{\pi}} \times \exp\left(-\lambda^2\right) \qquad \text{G.21}$$

Substituting Equation (G.20) and Equation (G.21) in Equation (G.19) the one variable equation for λ as given below

$$\lambda \ \text{erf}(\lambda) \ \exp\left(\lambda^2\right) = \frac{1}{\sqrt{\pi}} \times \frac{p_{vs}}{\rho_l} \times \frac{M_v}{RT} \times (h_s - h_0) \qquad \text{G.22}$$

Once λ is known, the drying front position 'x' can be calculated using Equation (G.14) and humidity profile can be calculated based on Equation (G.16)

G.3 DERIVAION OF EQUATION (5.19)

The influence of drying/wetting cycles is explained in section 5.5.2 based on Bakker (1998) and Thiery (2005). A drying/wetting cycles will have a consecutive drying period (t_d) and a wetting period (t_w). During the drying period t_d of the drying/wetting cycle, the concrete will carbonate and during the wetting period t_w, the concrete is assumed to be saturated instantaneously and the carbonation ceases completely for the entire duration of t_w. Hence at the end of the first cycle the effective time of carbonation is equal to the total drying time as given in Equation (5.20)

$$t_{e(1)} = t_d \qquad 5.20$$

When there are more than one drying/wetting cycles, carbonation take place during the drying period and stops during the wetting period of the first cycle. Thereafter during the drying period of the second cycle, the carbonation continuous. However, the carbonation will only proceed once the drying depth of the concrete reaches the depth of carbonation which took place at the end of the first cycle. Thereafter, the concrete will continue to carbonate for the rest of the drying period of the second cycle and then during the wetting period the carbonation ceases, and the process continues with the next cycle. Therefore the effective time of carbonation at the end of the second cycle will be

$$t_{e(2)} = 2\times t_d - \begin{pmatrix}\text{time taken for the drying front to reach}\\ \text{the depth of carbonation at the end}\\ \text{of first drying/wetting cycles}\end{pmatrix} \qquad G.23$$

Idealising carbonation as a square root-time relationship as per Equation (5.21);

$$x = A\times\sqrt{t_e} \qquad 5.21$$

Therefore the carbonation depth at the end of the first drying/wetting cycles can we written as

$$x_{c1} = A\times\sqrt{t_{e(1)}} \qquad G.24$$

Idealising the drying of concrete as a one-dimensional evaporation-diffusion process, and assuming the evaporation rate to be infinitely large in comparison with the diffusion rate, the drying front position (x) can be written from Li et al. (2009) as follows

$$x=2\times \lambda\times\sqrt{D_v}\times\sqrt{t} \qquad 5.23$$

Equation (5.23) can be deduced in the form of a square root-time relationship for concrete drying as shown in Equation (5.25). .

$$x = B \times \sqrt{t} \qquad 5.25$$

Therefore the time taken for the drying front to reach the depth of carbonation at the end of first drying/wetting cycles can be obtained by substituting Equation (G.24) in Equation (5.25) as shown in Equation (G.25)

$$A \times \sqrt{t_{e(1)}} = B \times \sqrt{t} \qquad G.25$$

Rearranging Equation (G.25) gives,

$$t = \left(\frac{A}{B}\right)^2 \times t_{e(1)} \qquad G.26$$

Substituting Equation (G.26) in Equation (G.23)

$$t_{e(2)} = 2 \times t_d - \left[\left(\frac{A}{B}\right)^2 \times t_{e(1)}\right] \qquad G.27$$

Therefore, if there are three drying/wetting cycles, Equation (G.27) can be written as

$$t_{e(3)} = 3 \times t_d - \left[\left(\frac{A}{B}\right)^2 \times t_{e(1)}\right] - \left[\left(\frac{A}{B}\right)^2 \times t_{e(2)}\right] \qquad G.28$$

When there are ‘n’ drying/wetting cycles,

$$t_{e(n)} = n \times t_d - \left[\left(\frac{A}{B}\right)^2 \times t_{e(1)}\right] - \left[\left(\frac{A}{B}\right)^2 \times t_{e(2)}\right] \ldots\ldots\ldots\ldots\ldots - \left[\left(\frac{A}{B}\right)^2 \times t_{e(n-1)}\right] \qquad G.29$$

Therefore, the total effective time of carbonation at the end of ‘n’ drying/wetting cycles $t_{e(n)}$ is presented as follows

$$t_{e(n)} = n\, t_d - m \sum_{i=1}^{n-1} t_{e(i)} \qquad (n > 1) \qquad 5.19$$

Where, $m = \left(\frac{A}{B}\right)^2$

APPENDIX H: LIST OF PUBLICATIONS BASED ON THIS RESEARCH

- Rakesh Gopinath and Mark Alexander, (2019) "A Correlation between Vapour Diffusion Coefficient and Oxygen Permeability Coefficient of Concrete", RILEM Spring Convention and Sustainable Materials, Systems and Structures Conference (SMSS2019), Rovinj, Croatia.

- Rakesh Gopinath and Mark Alexander, (2018) "A Modified Carbonation Model for Concrete Subjected to Varying Humidity Conditions", International Symposium on Concrete Modelling (CONMOD2018), Delft, The Netherlands.

- Rakesh Gopinath and Mark Alexander, (2018) "Experimental Investigation and Modelling of Natural Carbonation of Concrete", The 4th International Conference on Service Life Design for Infrastructures (SLD4), Delft, The Netherlands.

- Rakesh Gopinath, Mark Alexander and Hans Beushausen, (2017) "Predicting Depth of Carbonation of Concrete for Varying Climatic Conditions", 2nd International *RILEM/COST Conference on Early Age Cracking and Serviceability in Cement-based Materials and Structures,* Brussels, Belgium.

- Rakesh Gopinath, Mark Alexander and Hans Beushausen, (2014) "Predicting Depth of Carbonation of Concrete – A Performance- based Approach", *RILEM International Symposium on Concrete Modelling,* Beijing, China.